

Through the Looking Glass: Exploration of the Synthesis and Design of Glass-Forming Metal Complexes

Exploration de la Conception et de la Synthèse de Complexes de Coordination Vitreux

A Thesis Submitted to the Division of Graduate Studies
of the Royal Military College of Canada
by

Michael Jonathon James Cherry, BSc
Second Lieutenant

In Partial Fulfillment of the Requirements for the Degree of Masters of Science

September 2018

©This thesis may be used within the Department of National Defence but copyright for open
publication remains the property of the author.

Acknowledgements

First, I would like to thank my supervisors, Dr. Olivier Lebel and Dr. Jennifer Scott for their guidance, encouragement and insight throughout my journey in completing this master's thesis. With their support, I have learned lessons that extend far beyond the field of chemistry. Patience, personal motivation and how to persevere in the face of challenges are but a few of the things that I will bring with me through the rest of my life.

Thank you to the many technologists and departmental staff, particularly Neda Bavarian, Bob Whitehead and Jenn Snelgrove, for the help, guidance, training and time spent with me in the lab. Without the insight and expertise of these individuals, the analysis phase of this project would have been fruitless.

I would also like to acknowledge the postgraduate on scholarship program through Defence Research and Development Canada (DRDC). This program was instrumental in providing the funding and opportunity for me to pursue this Masters degree. As well, thank you to the staff and faculty of the Royal Military College of Canada (RMC) for facilitating and educating me during my time at the college.

To my friends Logan Morris, Jaden Rook and David Patch, thank you for the guidance, time spent editing my work and the feedback you all provided. Most importantly, thank you for joining me on this journey, the time spent together laughing was invaluable in making research and our continued education more enjoyable.

Finally, I would like to express my thanks and gratitude to my family and Laura, whose encouragement and understanding were vital. The support and love offered by you all kept me going through some of the most challenging moments of the research and writing process. Without your unconditional support and encouragement, I would not be able to be successful in this endeavour. Thank you!

Abstract

Molecular glasses are a novel class of chemical compounds that have gained an increasing amount of attention in the development of functionalized thin film materials. The small size, low molecular weight, and monodisperse nature of these compounds lead to easier purification and characterization compared to traditional materials. Our research group has designed a class of compounds based on a mexylaminotriazine core that can readily adopt glassy phases and incorporate glass-forming properties into other molecular functionalities. The development of molecular glass coordination complexes could be used to form amorphous thin films for solid-state applications such as opto-electronics and heterogeneous catalysis. The goal of this research thesis is to develop a viable strategy for incorporating glass-forming properties into coordination complexes. Herein, the synthesis of a number of mexylaminotriazine-functionalized ligands and the subsequent preparation and characterization of a variety of corresponding coordination complexes is presented.

Glass-forming salen derivatives incorporating mexylaminotriazine glass-forming moieties were synthesized. Symmetric and asymmetric glass-forming salen ligands were synthesized with ethylene and cyclohexane backbones, while, a mono-functionalized version was synthesized with a phenylene backbone. A number of first-row transition metal complexes were prepared from the asymmetric ligands and incorporate Mn(III), Fe(III), Co(II), Ni(II), Cu(II), and Zn(II) metal centres. Differential scanning calorimetry (DSC) demonstrated the glass-forming properties of most complexes, with the Co(II) complex being the only complex without a clear glass transition. As expected, the glass transition temperatures (T_g) of the coordination complexes were found to be higher than that of their respective ligands. The proposed cause is the loss of molecular mobility associated with the coordination of metal centres to these ligand structures. In addition, T_g values varied between metal complexes incorporating analogous ligands.

An acetylacetonate ligand incorporating a mexylaminotriazine substituent was also successfully synthesized. DSC was used to demonstrate the glass-forming properties and determine the T_g of this ligand. Attempts to prepare a variety of homoleptic and heteroleptic transition metal complexes with Zn(II), Ni(II), and Cu(II) metal centres were unsuccessful. Subsequent experiments suggest that the ligand was too labile, resulting in hydrolysis during the purification of the coordination complexes.

Lastly, a mexylaminotriazine-functionalized phenanthroline ligand was synthesized. This ligand was subsequently used to prepare a number of heteroleptic lanthanide complexes from lanthanide(III) metal salts and two different β -diketones. The ligand and all corresponding complexes demonstrated glass transition temperatures and glass-forming properties *via* DSC. A lower T_g was observed amongst the resulting coordination complexes. The loss of hydrogen bonding interactions formed from the heteroaromatic nitrogen atoms of the phenanthroline moiety are the proposed cause. The T_g values were consistent amongst most complexes; however, the lanthanum(III) complexes in both series demonstrated higher T_g values. The optical properties of these complexes were found to be consistent with crystalline analogues. Furthermore, the two europium(III) complexes were observed to luminesce when irradiated by UV light. Similar properties have been reported in non-glass forming europium(III) complexes. This project has demonstrated that a library of mexylaminotriazine-functionalized ligands and their respective homoleptic and heteroleptic coordination complexes can be synthesized to incorporate novel glass-forming properties while maintaining the properties of their non-glassy analogues.

Résumé

Les verres moléculaires organiques sont une famille de composés chimiques qui ont suscité un intérêt croissant pour le développement de matériaux fonctionnels en couches minces. La petite taille, la basse masse moléculaire, et la nature monodisperse de ces composés facilitent leur purification, leur caractérisation et leur mise en oeuvre par rapport aux matériaux traditionnels. Notre groupe de recherche a conçu, synthétisé et caractérisé une classe de composés chimiques à base de mexylaminotriazine qui peut facilement adopter des phases vitreuses et induire la formation de verres dans d'autres composés. Le développement de complexes de coordination vitreux pourrait être utilisé pour fabriquer des couches minces amorphes pour certaines applications à l'état solide comme l'optoélectronique et les catalyseurs hétérogènes. Le but de cette thèse de recherche est de proposer une stratégie pour concevoir et synthétiser des complexes de coordination capables de former des phases vitreuses. Dans cette thèse sont présentées la synthèse de divers ligands contenant des groupes mexylaminotriazine, ainsi que la préparation et la caractérisation de divers complexes de coordination correspondants.

Des ligands salen incorporant le groupe mexylaminotriazine ont été synthétisés et leur capacité à former des verres a été confirmée. Des ligands symétriques et asymétriques possédant des propriétés de formation du verre ont été synthétisés avec des ponts éthylène et de cyclohexyle, tandis qu'une version mono-fonctionnalisée a été synthétisée avec un pont phénylène. Plusieurs complexes de métaux de transition de la première rangée ont été préparés à partir des ligands asymétriques et comprennent des centres de métaux Mn(III), Fe(III), Co(II), Ni(II), Cu(II) et Zn(II). Les propriétés de formation de verre ont été démontrées par calorimétrie différentielle à balayage (DSC), le complexe de Co(II) étant le seul complexe sans signal apparent de transition vitreuse. Comme attendu, les températures de transition vitreuse (T_g) des complexes de coordination sont plus élevées que celles des ligands respectifs. La perte de mobilité moléculaire associée à la coordination des centres métalliques est une cause possible. De plus, les mesures de T_g ont varié entre les complexes métalliques de ligands analogues.

Deuxièmement, un ligand acétylacétone incorporant un substituant mexylaminotriazine a également été synthétisé. La T_g du ligand et ses propriétés de formation du verre ont été démontrées par DSC. La préparation de plusieurs complexes de coordination homoleptiques et hétéroleptiques a été tentée avec des centres de métaux Zn(II), Ni(II) et Cu(II) mais les tentatives se sont avérées futiles. Des expériences subséquentes ont suggérées que les complexes s'hydrolysent en présence d'eau lors du procédé de purification.

Enfin, un ligand de phénanthroline contenant une chaîne mexylaminotriazine a été synthétisé. Par la suite, plusieurs complexes de coordination hétéroleptiques ont été préparés à partir de sels métalliques de lanthanides(III) et de deux β -dicétones différentes. Le ligand et tous les complexes correspondants ont montré la capacité à former des verres par DSC. Une transition vitreuse inférieure a été observée parmi les complexes de coordination. La perte d'interactions de liaison hydrogène associées au fragment phénanthroline est la cause la plus plausible. Les températures de transition vitreuse étaient constantes parmi la plupart des complexes, à l'exception des complexes de lanthane(III) qui présentaient des valeurs de T_g plus élevées. Les propriétés optiques de ces complexes de lanthanides étaient compatibles avec des analogues cristallins. Les deux complexes d'euporium(III) présentent une luminescence lorsqu'ils sont irradiés par une lumière UV. Des propriétés similaires ont été rapportées dans des complexes d'euporium(III) qui ne forment pas de verre.

Ce projet a démontré qu'une classe de ligands fonctionnalisés par la mexylaminotriazine et leurs complexes de coordination homoleptiques et hétéroleptiques respectifs peuvent être synthétisés pour incorporer de nouvelles propriétés de formation de verres tout en maintenant les propriétés de leurs analogues cristallins.

Table of Contents

ACKNOWLEDGEMENTS	II
ABSTRACT	III
RÉSUMÉ	IV
LIST OF SCHEMES	IX
LIST OF TABLES	XII
LIST OF FIGURES	XIII
LIST OF SYMBOLS, ABBREVIATIONS, ACRONYMS, AND NOMENCLATURE	XVII
1. INTRODUCTION	1
1.1. Scope of Research	1
1.2. Objectives of Research	2
1.3. Thesis Organization	3
2. LITERATURE REVIEW	4
2.1. Glasses	4
2.1.1. Amorphous Solids	4
2.1.2. Glass Transition and Properties	6
2.1.3. Molecular Glasses	8
2.1.3.1. Design of Molecular Glasses	8
2.1.3.2. Star-Shaped π -Conjugated Molecular Glasses	9
2.1.3.3. Mexylaminotriazine Molecular Glasses	12
2.1.3.3.1. Influence of the Head-Group	13
2.1.3.3.2. Influence of the Tail Groups	15
2.1.3.3.3. Mexylaminotriazine Functionalized Compounds	19
2.1.4. Application of Molecular Glasses	22
2.1.4.1. Pharmaceuticals	22
2.1.4.2. Electronic and Optoelectronic Applications	23
2.1.4.2.1. Molecular Glasses in Organic Light-Emitting Diodes	23
2.1.4.2.2. Molecular Glasses in Organic Field-Effect Transistors	25

2.1.4.2.3.	Molecular Glasses in Organic Photovoltaics	26
2.1.4.2.4.	Molecular Glasses in Photochromic Technologies.....	27
2.1.4.2.5.	Molecular Glasses in Lithography	28
2.1.4.3.	Catalysis	29
2.2.	Coordination Chemistry.....	30
2.2.1.	Molecular Glass Metal Complexes	32
3.	METHODS	34
3.1.	Thermogravimetric Analysis (TGA)	34
3.2.	Differential Scanning Calorimetry (DSC)	34
3.3.	Spin Coating	35
3.4.	UV-Vis Spectroscopy (UV-Vis).....	35
3.5.	Fourier-Transform Infrared Spectroscopy (FTIR).....	36
3.6.	Magnetic Measurements	36
3.7.	Nuclear Magnetic Resonance Spectroscopy (NMR)	39
3.8.	Mass Spectrometry	39
4.	SALEN-FUNCTIONALIZED MOLECULAR GLASS COMPLEXES.....	41
4.1.	Introduction.....	41
4.2.	Results and Discussion	47
4.2.1.	Synthesis and Characterization of Ligands	47
4.2.2.	Coordination with First-Row Transition Metals and Characterization	51
4.2.3.	Optical Properties	56
4.3.	Experimental.....	58
4.3.1.	Materials and Equipment	58
4.3.2.	Physical Measurements	58
4.3.3.	Synthesis	59
4.4.	Summary	74
5.	ACETYLACETONATE FUNCTIONALIZED MOLECULAR GLASS COMPLEXES .	75
5.1.	Introduction.....	75
5.2.	Results and Discussion	79
5.2.1.	Synthesis and Characterization of Ligand.....	79

5.2.2.	Coordination with Metals and Characterization.....	81
5.3.	Experimental.....	84
5.3.1.	Materials, Equipment, and Physical Measurements.....	84
5.3.2.	Synthesis	84
5.4.	Summary	89
6.	PHENANTHROLINE FUNCTIONALIZED MOLECULAR GLASS COMPLEXES.....	90
6.1.	Introduction.....	90
6.2.	Results and Discussion	97
6.2.1.	Synthesis and Characterization of Ligand.....	97
6.2.2.	Coordination with Metals and Characterization.....	98
6.2.3.	Optical Properties.....	101
6.3.	Experimental.....	106
6.3.1.	Materials and Equipment	106
6.3.2.	Physical Measurements	106
6.3.3.	Synthesis	107
6.4.	Summary.....	115
7.	CONCLUSION AND RECOMMENDATIONS.....	116
8.	REFERENCES	119
	APPENDICES.....	131

List of Schemes

Scheme 1: Examples of aryl hydrazone (1-3) ³⁶ , triphenylamine (4-5), triphenylbenzene (6-7), ^{37,38} and triphenylborane (8-11) ³⁹ based star-shaped molecules synthesized by Shirota <i>et al.</i>	9
Scheme 2: Examples of tetrahedral (12-14) ⁴⁰ and spirocyclic (15-19) ⁴¹ star-shaped molecular glasses.	11
Scheme 3: Example of a mexylaminotriazine molecular glass, 2-methylamino-4,6-bis(mexylamino)-1,3,5-triazine (20). ⁴³	13
Scheme 4: Mexylaminotriazine derivatives synthesized for the evaluation of the head group's role in glass formation. ¹⁴ All functional groups were further varied by synthesizing derivatives with varying alkyl chain lengths.	14
Scheme 5: Synthesis and general structure of some molecular glasses synthesized by Eren <i>et al.</i> ¹¹	16
Scheme 6: Procedure for the synthesis of some molecular glasses with di-substituted tail groups. ¹³	17
Scheme 7: Graphical representation of the interactions between molecules, preventing ordered close-packing of the mexylaminotriazine molecules. ¹⁴	19
Scheme 8: Synthesis of a tetraphenylporphyrin derivative functionalized with mexylaminotriazine moieties. ⁶	20
Scheme 9: Examples of mexylaminotriazine glasses containing functional groups to permit covalent bond linkages to other compounds. ¹¹	21
Scheme 10: Synthesis of Azo DR1 compound functionalized with a mexylaminotriazine derivative. ¹⁷	21
Scheme 11: Structures of star-shaped molecular glass compounds (25-31) synthesized as charge carrier materials. ⁵¹⁻⁵⁸	24
Scheme 12: Triphenylamine star-shaped molecular glasses incorporating carbazole (32) and fluorene (33) groups for OFET technologies. ⁶²	26
Scheme 13: Glass-forming spiropyran compound 34 and the photochromic changes induced by treatment with 365 nm light to produce a coloured compound 34a and the thermally reversed ring closure to 34 . ^{74,75}	28
Scheme 14: Molecular glass compounds (35-37) used for nanolithographic applications. ^{77,79}	29
Scheme 15: Structures of two biological coordination complexes, chlorophyll (38) and heme B (39).	31
Scheme 16: General synthetic route and molecular structure of salen ligands.	42
Scheme 17: Molecular structure of Jacobsen's catalyst (40).	46
Scheme 18: Synthesis of mexylaminotriazine functionalized salicylaldehyde 45	47
Scheme 19: Synthesis of symmetrical salen ligands 46a and 46b . The attempted condensation of 1,2-phenylenediamine with compound 45 to afford the proposed compound 47 is also shown, with the desired ligand 46c shown at the side for reference.....	48

Scheme 20: Synthesis of asymmetric salen-glass ligands 48a-c	49
Scheme 21: Attempted synthesis of a <i>t</i> -butyl monotriazine ligand to afford products 46a and 50 . The desired compound ligand 49 is shown below the reaction scheme for reference.	50
Scheme 22: Preparation of Mn(III), Fe(III), Co(II), Ni(II), and Cu(II) coordination complexes from ligand 48a . The preparation of the Co(II) complex, 48a•Co(II) was carried out in the presence of an inert N ₂ atmosphere.	52
Scheme 23: Preparation of Zn(II) complexes from ligands 48a , 48b , and 48c	55
Scheme 24: Structures of common β-diketones: acetylacetone (51), 2-thenoyltrifluoroacetone (52), 1,1,1-trifluoro-5,5-dimethyl-2,4-heptanedione (53), and 3-benzyl-2,4-pentanedione (54).....	76
Scheme 25: Keto-enol tautomerism of β-diketones.	76
Scheme 26: General scheme of the Claisen condensation.	77
Scheme 27: Synthesis of acetylacetone from ethyl acetate, acetone, and sodium ethoxide <i>via</i> a Claisen condensation reaction. ¹⁶³	77
Scheme 28: Molecular structure of curcumin, 1,7-bis(4-hydroxyl-3-methoxyphenyl)-1,6-heptanediene-3,5-dione (55), a naturally occurring β-diketone.	78
Scheme 29: Synthesis of 2-mexylamino-4-methylamino-6-[(3-bromomethylphenyl)amino]-1,3,5-triazine 58 and “glacac” ligand 59	80
Scheme 30: Attempted preparation of complex 59a•Zn(II) . Additional attempts were made using NiCl ₂ and CuCl ₂ •2H ₂ O to prepare complexes 59a•Ni(II) and 59a•Cu(II)	81
Scheme 31: Attempted procedures for the preparation of mixed ligand complexes 59b and 59c . M denotes Zi(II), Ni(II), and Cu(II) metal centres.....	82
Scheme 32: Molecular structure of 1,10-phenanthroline 60	90
Scheme 33: Skraup condensation for the preparation of 1,10-phenanthroline (60) from 8-aminoquinoline and glycerol. ¹⁷⁹	91
Scheme 34: Friedländer condensation for the preparation of 1,10-phenanthroline derivatives from 8-aminoquinolinecarbaldehyde. ^{183–185}	91
Scheme 35: Molecular structure of 1,10-phenanthroline derivatives: 5,6-Epoxy-5,6-dihydro-[1,10]phenanthroline (61), 5-hydroxy-1,10-phenanthroline (63), and 1,10-phenanthroline-5,6-dione (63).	92
Scheme 36: Molecular structure of Ferroin, an iron phenanthroline coordination complex, <i>tris</i> (1,10-phenanthroline)iron(II) (64).	93
Scheme 37: Molecular structure bathocuproine (65).	94
Scheme 38: Molecular structure of (4-[(9-methyl-1,10-phenanthrol-2-yl)methyl]-1,4,7-triazaheptane-1,1,7,7-tetraacetic acid) (66). ²²²	95
Scheme 39: Chemical structure of heteroleptic europium(III) phenanthroline complex 67	95
Scheme 40: Synthesis of the mexylaminotriazine functionalized phenanthroline ligand 68	97
Scheme 41: Preparation of heteroleptic La(III), Pr(III), Nd(III), Eu(III), Tb(III), and Er(III) complexes 68a and 68b from corresponding metal salts, diketones 52 or 53 , and ligand 68 .	

$\text{MX}_3 \cdot n\text{H}_2\text{O} = \text{LaCl}_3 \cdot 6\text{H}_2\text{O}, \text{Pr}(\text{NO})_3 \cdot 6\text{H}_2\text{O}, \text{NdCl}_3 \cdot 6\text{H}_2\text{O}, \text{EuCl}_3 \cdot 6\text{H}_2\text{O}, \text{TbCl}_3 \cdot 6\text{H}_2\text{O},$
 $\text{Er}(\text{NO})_3 \cdot 5\text{H}_2\text{O} \dots\dots\dots 99$

List of Tables

Table 1: Glass transition (T_g), crystallization (T_c), and melting (T_m) temperatures of star-shaped compounds 1-19 . ³⁷⁻⁴¹	12
Table 2: Summary of the reaction types catalyzed by salen complexes. ⁹⁵ Many of these reactions can be made enantioselective using chiral ligands.	44
Table 3: Glass transition temperatures (T_g) of compounds 45 , 46a-b , and 48a-c	51
Table 4: Decomposition temperatures and glass transition temperatures (T_g) for complexes prepared from ligands 48a-c	56
Table 5: UV-Vis absorbance values of salen-functionalized molecular glass complexes 48a-c in CH_2Cl_2 solution.	58
Table 6: Glass transition temperatures (T_g) of compounds 24 and 68 . The T_g of compound 24 is reported from literature values. ¹¹	98
Table 7: Decomposition temperatures and glass transition temperatures (T_g) for complexes of 68a and 68b	100
Table 8: UV-Vis absorbance values of phenanthroline-functionalized molecular glass complexes 68a-b in both CH_2Cl_2 solution and in the solid state.....	104

List of Figures

Figure 1: Microscopic Arrangement of Crystalline and Amorphous Solids. ²¹	4
Figure 2: Heat flow as a function of temperature in an amorphous material.	6
Figure 3: Graphical representation of the general structure and mechanism of function for OLED devices.....	23
Figure 4: Graphical representation of OFET devices employing organic semiconductors.....	25
Figure 5: UV absorption spectra of complexes of ligands 48a , 48b , and 48c in CH ₂ Cl ₂ solution.....	57
Figure 6: ¹ H NMR spectra comparison demonstrating the changing peaks of the keto and enol tautomers in a sample of 59c•Zn(II) , before and after work-up. Top: ¹ H NMR of the unpurified fraction; Middle: reaction mixture following washing with water; Bottom: reference spectrum of ligand 59	83
Figure 7: UV-Vis absorption spectra of complexes 68a in CH ₂ Cl ₂ solution (Top) and in solid-state as thin films (Bottom).	102
Figure 8: UV-Vis absorption spectra of complexes 68b in CH ₂ Cl ₂ solution (Top) and in solid-state as thin films (Bottom).	103
Figure 9: Comparison of the UV-Vis absorption spectra of europium(III) complexes 68a•Eu(III) and 68b•Eu(III) in both solution and in the solid state.	104
Figure 10: Fluorescent behaviour of spin coated samples of the two europium(III) complexes <i>via</i> irradiation with UV light. From left to right: untreated substrate, Htta europium(III) complex, 68a•Eu(III) , Htta praseodymium(III) complex, 68a•Pr(III) , and Hfdh europium(III) complex, 68b•Eu(III)	106
Figure 11: ¹ H NMR of compound 45 in DMSO- <i>d</i> ₆ , 300 MHz at 363K.....	1
Figure 12: ¹³ C NMR of compound 45 in DMSO- <i>d</i> ₆ , 75 MHz.	1
Figure 13: ¹ H NMR of ligand 46a in DMSO- <i>d</i> ₆ , 300 MHz at 363K.....	2
Figure 14: ¹³ C NMR of ligand 46a in DMSO- <i>d</i> ₆ , 75 MHz.	2
Figure 15: ¹ H NMR of ligand 46b in DMSO- <i>d</i> ₆ , 300 MHz at 363 K.	3
Figure 16: ¹³ C NMR of ligand 46b in DMSO- <i>d</i> ₆ , 75 MHz.	3
Figure 17: ¹ H NMR of ligand 48a in DMSO- <i>d</i> ₆ , 300 MHz at 363K.....	4
Figure 18: ¹³ C NMR of ligand 48a in DMSO- <i>d</i> ₆ , 75 MHz.	4
Figure 19: ¹ H NMR of ligand 48b in DMSO- <i>d</i> ₆ , 300 MHz at 363K.	5
Figure 20: ¹³ C NMR of ligand 48b in DMSO- <i>d</i> ₆ , 75 MHz.	5
Figure 21: ¹ H NMR of ligand 48c in DMSO- <i>d</i> ₆ , 300 MHz at 363K.....	6
Figure 22: ¹³ C NMR of ligand 48c in DMSO- <i>d</i> ₆ , 75 MHz.....	6
Figure 23: ¹ H NMR of complex 48a•Fe(III) in DMSO- <i>d</i> ₆ , 300 MHz at 363K.....	7
Figure 24: ¹³ C NMR of complex 48a•Fe(III) in DMSO- <i>d</i> ₆ , 75 MHz.....	7

Figure 25: ^1H NMR of complex 48a•Co(II) in DMSO- d_6 , 300 MHz at 363K.....	8
Figure 26: ^{13}C NMR of complex 48a•Co(II) in DMSO- d_6 , 75 MHz.....	8
Figure 27: ^1H NMR of complex 48a•Ni(II) in DMSO- d_6 , 300 MHz at 363K.....	9
Figure 28: ^{13}C NMR of complex 48a•Ni(II) in DMSO- d_6 , 75 MHz.	9
Figure 29: ^1H NMR of complex 48a•Cu(II) in DMSO- d_6 , 300 MHz at 363K.....	10
Figure 30: ^{13}C NMR of complex 48a•Cu(II) in DMSO- d_6 , 75 MHz.	10
Figure 31: ^1H NMR of complex 48a•Zn(II) in DMSO- d_6 , 300 MHz at 363K.....	11
Figure 32: ^{13}C NMR of complex 48a•Zn(II) in DMSO- d_6 , 75 MHz.....	11
Figure 33: ^1H NMR of complex 48b•Zn(II) in DMSO- d_6 , 300 MHz at 363K.....	12
Figure 34: ^{13}C NMR of complex 48b•Zn(II) in DMSO- d_6 , 75 MHz.	12
Figure 35: ^1H NMR of complex 48c•Zn(II) in DMSO- d_6 , 300 MHz at 363K.	13
Figure 36: ^{13}C NMR of complex 48c•Zn(II) in DMSO- d_6 , 75 MHz.....	13
Figure 37: ^1H NMR of ligand 59 in DMSO- d_6 , 300 MHz.	14
Figure 38: ^1H NMR of complex 59a•Zn(II) in DMSO- d_6 , 300 MHz.....	14
Figure 39: ^1H NMR of complex 59b•Zn(II) in DMSO- d_6 , 300 MHz.	15
Figure 40: ^1H NMR of complex 59b•Zn(II) in DMSO- d_6 , 300 MHz.	15
Figure 41: ^1H NMR spectrum of complex 56c•Zn(II) in DMSO- d_6 , 300 MHz, before purification by precipitation from water.	16
Figure 42: ^1H NMR of complex 59c•Zn(II) in DMSO- d_6 , 300 MHz, after purification by precipitating from water.	16
Figure 43: ^1H NMR of ligand 68 in DMSO- d_6 , 300 MHz.	17
Figure 44: ^{13}C NMR of ligand 68 in DMSO- d_6 , 75 MHz.	17
Figure 45: HSQC NMR of ligand 68 in DMSO- d_6	18
Figure 46: ^1H NMR of complex 68a•La(III) in DMSO- d_6 , 300 MHz.	18
Figure 47: ^{13}C NMR of complex 68a•La(III) in DMSO- d_6 , 75 MHz.	19
Figure 48: ^{19}F NMR of complex 68a•La(III) in DMSO- d_6 , 376 MHz.....	19
Figure 49: HSQC NMR of ligand 68a•La(III) in DMSO- d_6	20
Figure 50: ^1H NMR of complex 68a•Pr(III) in DMSO- d_6 , 300 MHz.....	20
Figure 51: ^{13}C NMR of complex 68a•Pr(III) in DMSO- d_6 , 75 MHz.....	21
Figure 52: ^{19}F NMR of complex 68a•Pr(III) in DMSO- d_6 , 376 MHz.	21
Figure 53: HSQC NMR of ligand 68a•Pr(III) in DMSO- d_6	22
Figure 54: ^1H NMR of complex 68a•Nd(III) in DMSO- d_6 , 300 MHz.....	22
Figure 55: ^{13}C NMR of complex 68a•Nd(III) in DMSO- d_6 , 75 MHz.....	23

Figure 56: ^{19}F NMR of complex 68a•Nd(III) in $\text{DMSO-}d_6$, 376 MHz.	23
Figure 57: HSQC NMR of ligand 68a•Nd(III) in $\text{DMSO-}d_6$	24
Figure 58: ^1H NMR of complex 68a•Eu(III) in $\text{DMSO-}d_6$, 300 MHz.	24
Figure 59: ^{13}C NMR of complex 68a•Eu(III) in $\text{DMSO-}d_6$, 75 MHz.	25
Figure 60: ^{19}F NMR of complex 68a•Eu(III) in $\text{DMSO-}d_6$, 376 MHz.	25
Figure 61: HSQC NMR of ligand 68a•Eu(III) in $\text{DMSO-}d_6$	26
Figure 62: ^1H NMR of complex 68a•Tb(III) in $\text{DMSO-}d_6$, 300 MHz.	26
Figure 63: ^{13}C NMR of complex 68a•Tb(III) in $\text{DMSO-}d_6$, 75 MHz.	27
Figure 64: ^{19}F NMR of complex 68a•Tb(III) in $\text{DMSO-}d_6$, 376 MHz.	27
Figure 65: HSQC NMR of ligand 68a•Tb(III) in $\text{DMSO-}d_6$	28
Figure 66: ^1H NMR of complex 68a•Er(III) in $\text{DMSO-}d_6$, 300 MHz.	28
Figure 67: ^{13}C NMR of complex 68a•Er(III) in $\text{DMSO-}d_6$, 75 MHz.	29
Figure 68: ^{19}F NMR of complex 68a•Er(III) in $\text{DMSO-}d_6$, 376 MHz.	29
Figure 69: HSQC NMR of ligand 68a•Er(III) in $\text{DMSO-}d_6$	30
Figure 70: ^1H NMR of complex 68b•La(III) in $\text{DMSO-}d_6$, 300 MHz.	30
Figure 71: ^{13}C NMR of complex 68b•La(III) in $\text{DMSO-}d_6$, 75 MHz.	31
Figure 72: ^{19}F NMR of complex 68b•La(III) in $\text{DMSO-}d_6$, 376 MHz.	31
Figure 73: HSQC NMR of complex 68b•La(III) in $\text{DMSO-}d_6$	32
Figure 74: ^1H NMR of complex 68b•Pr(III) in $\text{DMSO-}d_6$, 300 MHz.	32
Figure 75: ^{13}C NMR of complex 68b•Pr(III) in $\text{DMSO-}d_6$, 75 MHz.	33
Figure 76: ^{19}F NMR of complex 68b•Pr(III) in $\text{DMSO-}d_6$, 376 MHz.	33
Figure 77: HSQC NMR of complex 68b•Pr(III) in $\text{DMSO-}d_6$	34
Figure 78: ^1H NMR of complex 68b•Nd(III) in $\text{DMSO-}d_6$, 300 MHz.	34
Figure 79: ^{13}C NMR of complex 68b•Nd(III) in $\text{DMSO-}d_6$, 75 MHz.	35
Figure 80: ^{19}F NMR of complex 68b•Nd(III) in $\text{DMSO-}d_6$, 376 MHz.	35
Figure 81: HSQC NMR of complex 68b•Nd(III) in $\text{DMSO-}d_6$	36
Figure 82: ^1H NMR of complex 68b•Eu(III) in $\text{DMSO-}d_6$, 300 MHz.	36
Figure 83: ^{13}C NMR of complex 68b•Eu(III) in $\text{DMSO-}d_6$, 75 MHz.	37
Figure 84: ^{19}F NMR of complex 68b•Eu(III) in $\text{DMSO-}d_6$, 376 MHz.	37
Figure 85: HSQC NMR of complex 68b•Eu(III) in $\text{DMSO-}d_6$	38
Figure 86: TGA thermogram for complex 48a•Mn(III)	1
Figure 87: TGA thermogram for complex 48a•Fe(III)	1
Figure 88: TGA thermogram for complex 48a•Co(II)	2

Figure 89: TGA thermogram for complex 48a•Ni(II)	2
Figure 90: TGA thermogram for complex 48a•Cu(II)	3
Figure 91: TGA thermogram for complex 48a•Zn(II)	3
Figure 92: TGA thermogram for complex 48b•Zn(II)	4
Figure 93: TGA thermogram for complex 48c•Zn(II)	4
Figure 94: TGA thermogram for ligand 59	5
Figure 95: TGA thermogram of ligand 68	6
Figure 96: TGA thermogram for complex 68a•La(III)	6
Figure 97: TGA thermogram for complex 68a•Pr(III)	7
Figure 98: TGA thermogram for complex 68a•Nd(III)	7
Figure 99: TGA thermogram for complex 68a•Eu(III)	8
Figure 100: TGA thermogram for complex 68a•Tb(III)	8
Figure 101: TGA thermogram for complex 68a•Er(III)	9
Figure 102: TGA thermogram for complex 68b•La(III)	9
Figure 103: TGA thermogram for complex 68b•Pr(III)	10
Figure 104: TGA thermogram for complex 68b•Nd(III)	10
Figure 105: TGA thermogram for complex 68b•Eu(III)	11
Figure 106: DSC thermograms of the synthesized mexylaminotriazine-functionalized salen complexes. For reference, the exotherm is oriented down in this chart.	1
Figure 107: DSC thermogram for compound 58	2
Figure 108: DSC thermograms of the synthesized mexylaminotriazine-functionalized phenanthroline complexes 68a . For reference, the exotherm is oriented down in this chart.	3
Figure 109: DSC thermograms of the synthesized mexylaminotriazine-functionalized phenanthroline complexes 68b . For reference, the exotherm is oriented down in this chart.	4

List of Symbols, Abbreviations, Acronyms, and Nomenclature

Symbol, Abbreviation, Acronym	Definition
Ad(tBuSSB) ₄	Tetrakis(4- <i>tert</i> -butylstyrylstilbenyl)adamantine
ASITPA	4,4',4''-tris(allylsuccinimido)triphenylamine
BM	Bohr Magneton
CCDC	Cambridge Crystallographic Data Centre
CDI	Carbonyldiimidazole
C(tBuSSB) ₄	Tetrakis(4- <i>tert</i> -butylstyrylstilbenyl)methane
DMF	Dimethylformamide
DPP	Diketopyrrolopyrrole
DR1	Disperse Red 1
DSC	Differential Scanning Calorimetry
ϵ	Extinction coefficient
e.e	Enantiomeric Excess
ESI	Electrospray Ionization
EtOH	Ethanol
FTIR	Fourier Transform Infrared Spectroscopy
Hacac	Acetylacetone
Hbpd	3-benzyl-2,4-pentanedione
Hfdh	1,1,1-trifluoro-5,5-dimethyl-2,4-hexanedione
Htta	2-thenoyltrifluoroacetone
HRMS	High resolution mass spectrometry
HSQC	Heteronuclear single quantum coherence spectroscopy
ITO	Indium Tin Oxide
MALDI	Matrix-Assisted Laser Desorption/Ionization
NEt ₃	Triethylamine
NIR	Near Infrared
NMR	Nuclear Magnetic Resonance
OAc	Acetoxy group/Acetate
OFET	Organic Field-Effect Transistors
OLED	Organic Light-Emitting Diodes
OPV	Organic photovoltaic
PDI	Perylene diimide
Phen	1,10-Phenanthroline
PMHS	polymethylhydrosiloxane
ppm	Parts per million
Rpm	Revolutions per minute
Salen	Salicylidene diimine
Si(tBuSSB) ₄	Tetrakis(4- <i>tert</i> -butylstyrylstilbenyl) silane
SQ	Squarylium Cyanine
T _c	Temperature of crystallization
T _g	Glass Transition Temperature
TGA	Thermogravimetric Analysis

Symbol, Abbreviation, Acronym	Definition
T_m	Melting Transition Temperature
THF	Tetrahydrofuran
TLC	Thin Layer Chromatography
TPP	Tetraphenylporphyrin
TsOTPB	1,3,5-tris[4-(4-toluenesulfonyloxy)phenyl]benzene
μ_{eff}	Magnetic Moment
UV-Vis	Ultraviolet-visible

1. Introduction

1.1. Scope of Research

Coordination compounds often possess a diverse range of properties normally unachievable by organic compounds. This is the result of the intricate structure of the organic ligands and the electronic nature of the metal atoms. This interplay allows chemists to tune and exploit the properties, such as magnetism, conductivity, and luminescence, in these coordination complexes.¹ Many of the properties of coordination complexes are desirable for various solid-state applications, such as opto-electronics, sensors, solid-state catalysis, and pharmaceuticals. However, for effective use in many solid-state applications, these compounds require some form of support.

Amorphous materials lack the predictable and defined molecular structure that is characteristic of crystalline solids while still possessing a higher degree of intermolecular connectivity than liquids. This fundamental difference results in the two materials exhibiting very different properties. Amorphous materials exhibit what is known as isotropic behaviour. This means that the materials' physical properties, such as electrical and thermal conductivity, do not depend on orientation. For example, electrical current will move in all directions of the material at the same speed.² In addition, some amorphous solids, called glasses, exhibit a unique phase transition known as the glass transition. This reversible transition describes the change in a material's properties as it transforms from a rigid or glassy solid into a flexible or rubbery solid as the temperature increases beyond the glass transition temperature (T_g).³ This phenomena can be exploited to fabricate nanometer to micrometer scale thin film materials that are hard and strong below their T_g .⁴ The incorporation or support of functionalities on thin films is a desirable strategy for the development of materials destined for various solid-state applications such as optical storage devices, optical coatings, magnetic storage materials, and other electronic components.⁴

One of the most common ways of producing thin films for solid-state applications is by generating functionalized polymers. Both inorganic and organic polymers are capable of forming high quality thin films. However, the large molecular size and polydisperse nature of these materials present problems concerning synthesis, purification, and characterization. In addition, polymer materials exhibit variations in composition from one sample to the next.⁴ Small organic molecules present an alternative type of material and exhibit a number of advantages. Their small size makes these materials easier to purify and characterize, while their monodisperse nature leads to behaviour that is more homogeneous between different samples. Furthermore, small molecules are less sensitive to the effects of chain entanglement and other rheological phenomena associated with polymer based thin films.⁵ However, most small molecules possess the disadvantage of crystallizing more rapidly than polymers because of their unhindered mobility.⁶ For this reason, it is difficult for small molecular materials to access the glassy state outside of special processing techniques such as quenching with liquid nitrogen. Even in amorphous samples, crystallization readily occurs upon heating, or on standing over long periods of time.

Small molecules designed for thin-film applications must therefore possess molecular structures specifically engineered to resist crystallization. Such compounds are called molecular glasses, or amorphous molecular materials. Molecular glasses are small organic compounds that are capable of forming solid amorphous phases.⁷ The Lebel group has published a class of compounds based on the mexylaminotriazine core that are capable of adopting amorphous glassy phases and exhibit a high resistance to crystallization.⁸⁻¹¹ Through various studies, structural

parameters have been identified that facilitate the formation of glassy phases while resisting crystallization. Examples of these structural characteristics include irregular shapes, non-planarity, and conformational equilibria.^{10,12-16} The synthesis of these compounds is relatively straightforward and the step-wise substitution steps allow for a high level of synthetic control and tailorability. Subsequently, the synthesis of mexylaminotriazines incorporating reactive groups led to the functionalization of compounds such as chromophores and semiconductors in order to introduce glass-forming properties to novel compounds.^{2,6,11,17}

Despite a great deal of development in the field of molecular glasses, several knowledge gaps have been identified. At present, there is limited information regarding the synthesis of glass-forming coordination complexes with low molecular weights and discrete structures. In some of these cases, the complexes themselves are capable of glass formation, but not the ligands.¹⁸ Lastly, there is currently no strategy for the synthesis and introduction of glass-forming abilities in metal complexes. It is proposed that a family of glass-forming ligands could be synthesized for the purposes of introducing glass-forming properties to their respective coordination complexes. The mexylaminotriazine class of glass formers represents the best strategy for introducing glass-forming properties across a wide range of ligand systems.

1.2. Objectives of Research

The mexylaminotriazine class of glass formers represents an appealing strategy for introducing glass-forming properties across a wide range of coordination complexes. The goal of this project is to prepare coordination complexes bearing the mexylaminotriazine glass former that maintain the chemical and structural properties of both parent compounds while demonstrating novel glass-forming capabilities. To achieve this goal, this project will consist of three objectives.

1. The first objective is to design and synthesize several novel glass-forming derivatives of established ligand frameworks. Mexylaminotriazine glass formers will be covalently bound to candidate ligands in order to incorporate novel glass-forming properties. The ligands selected to be functionalized with the glass former have been well-researched, possess the ability to be altered sterically or electronically, are capable of supporting a number of metal centres, and possess some value in terms of proposed application in which the properties of both parent components, the glass former and chelating ligand, complement each other.
2. The second objective of the project is the preparation of coordination complexes from glass-forming ligands. Various metal centres will be used to generate libraries of coordination complexes from first-row transition and lanthanide metals. It is expected that the preparation of these complexes will be closely related to that of the parent ligands.
3. The final objective will be the characterization and investigation of the structural, thermal, and optical properties of the aforementioned ligands and complexes. The structures of the synthesized ligands and respective complexes will be characterized using nuclear magnetic resonance spectroscopy (NMR), high-resolution mass spectrometry (HRMS), Fourier-transform infrared spectroscopy (FTIR), and magnetic susceptibility. Following these characterization techniques, thermal properties will be measured in order to determine the glass-forming abilities of the complexes by thermogravimetric analysis (TGA), differential scanning calorimetry

(DSC), as well as their ability to form thin films. Ultraviolet-visible spectroscopy (UV-Vis) will also be used to investigate the optical properties of several complexes.

1.3. Thesis Organization

Herein, we report the synthesis of salicylaldehyde diimine, acetylacetonone and phenanthroline derivatives incorporating mexylaminotriazine moieties, along with the preparation of their respective complexes with a variety of metals. These common ligands have been identified as ideal candidates for an initial study of molecular glass coordination complexes according to the criteria outlined above. This thesis will contain seven chapters, as listed below. The three chapters dealing with the formation of novel glassy ligands and their complexes (chapters 4-6) are written in a manuscript style and include their own introduction, results and discussion, and experimental sections.

Chapter 2 will cover the relevant background information on amorphous molecular materials, the design of molecular glass materials, their application as an emerging class of compounds in materials sciences, as well as the necessary information regarding coordination complexes, and the current state of development for molecular glass coordination complexes.

Chapter 3 outlines the theory, selection, and procedures for major experimental procedures.

Chapter 4 will examine the synthesis of glass-forming salicylaldehyde diimine (salen) ligands, the subsequent complexation of these ligands to select first row transition metals followed by their characterization, and lastly, the determination of these complexes' glass-forming and optical properties.

Chapter 5 will discuss the synthesis and characterization of an acetylacetonone (Hacac) ligand functionalized with mexylaminotriazine glass-forming substituents, the preparation of the corresponding metal complexes, and their characterization.

Chapter 6 will describe the synthesis of a phenanthroline ligand incorporating a mexylaminotriazine glass-forming moiety, preparation of heteroleptic lanthanide coordination complexes, and their subsequent characterization.

Chapter 7 will summarize the findings and outcomes of this research project. Future work and recommendations for the application of this research will also be presented in this chapter.

2. Literature Review

2.1. Glasses

2.1.1. Amorphous Solids

Solid materials can be subdivided into two classes, crystalline, and amorphous solids. Crystalline solids possess a definite and ordered arrangement that consists of predictable, repeating structures, thereby giving them well-defined structures at the molecular level.¹⁹ Amorphous solids display a high degree of intermolecular connectivity like crystalline solids; however, they lack the predictable and defined long-range positional and directional order characteristic of crystalline solids.²⁰ Figure 1 shows the organizational differences between crystalline and amorphous solids at the molecular level.²¹ The nature of these two forms of solid materials is vital for the development of specific materials.

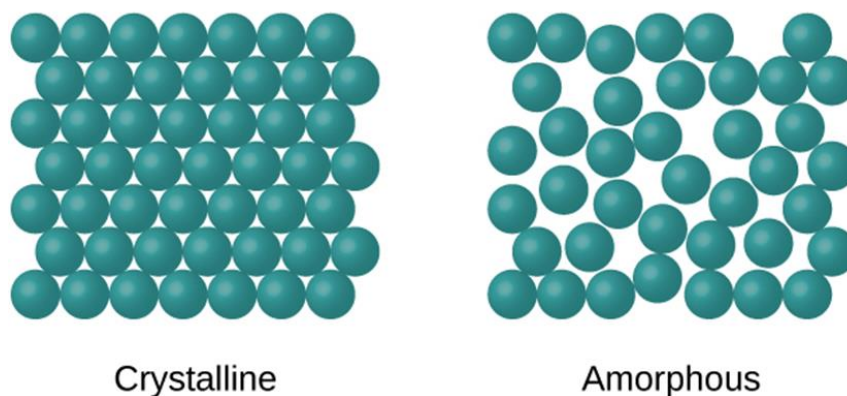


Figure 1: Microscopic Arrangement of Crystalline and Amorphous Solids.²¹

The structures of crystalline and amorphous materials lead to distinct properties in terms of the hardness, density, conductivity, solubility, and transparency of the material.² Amorphous solids may appear to possess similar characteristics on a larger scale; however, their unique undefined supramolecular structure gives them many fluid-like properties.⁴ Amorphous materials combine many desirable properties of both solids and liquids leading to their widespread use in industry.²² Understanding the structural and organizational differences between crystalline and amorphous solids aids in understanding the other differences in their properties and ultimately their application. The differences between these two types of solids can be illustrated by the production of candy.²³ Candies are typically made from supersaturated solutions of sucrose. When the solution is cooled slowly, the molecules of sucrose have time to arrange in an ordered crystalline fashion, producing many types of hard candies. Alternatively, if the solution is cooled quickly, the molecules will have less time to organize, leading to a disordered structure and the formation of an amorphous solid. Faster cooling produces softer and more malleable candies. By manipulating the cooling process the same compound, sucrose, can be manipulated to form either crystalline or amorphous solids with very different properties. For example, these two types of solid materials exhibit drastically different conductive properties. This is because crystalline solids are anisotropic whereas amorphous materials are isotropic. This relates directly to the orientation of the atoms in the materials. The ordered supramolecular structure of crystalline solids leads to differences in the

conductivity as charges can travel faster in certain directions than others. In amorphous materials, the absence of an ordered structure results in charges moving at equal speeds in all directions. As a result, amorphous materials are often prized for conductive materials in a number of applications as they exhibit more homogeneous behaviour. Other properties such as refractive index and thermal conductivity also exhibit this behaviour. Similarly, amorphous and crystalline solids possess different dissolution rates. While the solubility of similar materials in the contrasting phases may be the same, amorphous materials have increased molecular mobility, permitting them to dissolve more readily. In addition, amorphous materials are more kinetically favoured. As such, the free energy of dissolution is often more favourable for the individual molecules rather than the bulk material, so dissolution happens quickly. The unique properties of amorphous compounds have led to their widespread use as building materials, decorations, components in electronics like cellphones, computers, and other technological products, and in pharmaceuticals.

Many polymers, nanostructured materials, gels, and thin films are classified as amorphous solids. Interestingly, some amorphous solids can be further sub-divided into a class of materials called glasses, glassy materials, and are frequently described as a “frozen liquid”.² In a broad sense, glass is a term used to describe all solids that are amorphous and exhibit a glass transition. Many examples of glasses exist in natural forms, such as proteins, peptides, and some sugars.²⁴ Among the many natural materials capable of adopting a glassy state, sugars have received the most attention. Sugars such as sucrose and trehalose are capable of adopting glassy phases that can serve as protective materials when organisms experience particularly dry or cold environmental conditions over an extended period of time.²⁵ These glasses are effective at preventing the denaturation of proteins as well as the formation of crystalline aggregates that can damage and destroy cells.²⁵ Disaccharides can also be used as glassy matrices to stabilize proteins and cellular components for spectroscopic studies and research.²⁶ The study of the glass transition temperature and degree of crystallinity of sugar mixtures is also important for the food industry. The texture of many food products, such as candies and cookies, depends on the behaviour and state of sugars used in their production.²⁷

Glasses are also found in other natural forms such as mineral-based glasses. Mineral glasses, such as the volcanically formed obsidian and pumice, as well as thin glass tube fulgurites that are formed from sand melted by lightning, are commonly found in nature.²⁸ In fact, the use of glassy materials such as these predates human fabrication of glasses themselves.²⁸ Many examples of glass artifacts from early humans have survived because of the robust nature and corrosion resistant properties of these particular glasses. Obsidian, a glassy material formed from granite melted by volcanic activity, has been found as sharpened shards in the shapes of arrowheads and knives. Examples of obsidian tools have been found in early human settlements as early as 75,000 B.C.²⁸ Human production of glasses is a bit of an ambiguity. Some of the oldest dated glass artifacts come from Egypt around 2600 B.C; however, stories placing the fabrication of glass to 5,000 B.C. have been suggested.²⁸ Regardless, humans have been producing glasses for a variety of purposes for thousands of years and today they still find novel use in a myriad of industries.

Generally, the glassy state in synthetic materials is induced by one of several methods, such as vapour condensation, super-cooling, or precipitation from solution. The most commonly found glasses are primarily fabricated from silica compounds like silicon dioxide and additives like soda (Na_2CO_3) and lime (CaO) for use in windows, glazed glasses, and containers.²⁸ These applications are often related to their distinct optical properties such as their ability to transmit, reflect, and refract light. Additionally, glasses are quite strong and durable to corrosion and other stressors

despite being brittle. As a result, they have been employed as various household objects and can even be used as additives for polymers to increase their structural strength. Many other materials that fit the definition of a glass exist such as inorganic glasses and polymers. Inorganic glasses include materials such as silicate glasses, which can be doped with various metals such as aluminum and lead.²⁸ Polymers are large molecules composed of many repeating subunits.²⁹ Many polymers can adopt glassy phases, crystalline phases, or semi-crystalline phases. Polyethylene and polypropylene for example, often form semi-crystalline phases, which contain both amorphous and crystalline domains. Polymer glasses of acrylic, polycarbonate, and polyethylene terephthalate in particular are frequently used as glassy materials.²⁸ The commonality of all glassy materials is what is known as the glass transition.

2.1.2. Glass Transition and Properties

Under certain conditions, glasses will undergo a reversible transition, called the glass transition, from a rigid or glassy solid into a flexible or rubbery solid as the temperature increases beyond their glass transition temperature.³ The T_g describes the nature of an amorphous material at various temperatures. At the glass transition, the material does not melt but it does experience a change in heat capacity as well as different structural properties. At temperatures below the glass transition temperature, the molecules do not possess enough energy to move, and are locked into a rigid structure. As heat is applied and the temperature rises above the glass transition, the molecules gain enough energy and begin to move around freely in a flexible state. Figure 2 depicts an example of a glass transition of an amorphous material. It can be seen that the material heats at different rates depending on whether it is above or below its glass transition. Understanding glass transition is important for determining a material's viability in different industries and applications. Below the T_g , the material has a lower heat capacity, a rigid structure, and strong physical properties. In this solid or "glassy" state, materials possess higher strength in resisting compressive, tensile, and shearing forces. Above the glass transition, materials are said to be in the rubbery or viscous state and are softer, more elastic, and exhibit higher flexibility. This is useful for applications such as epoxy and silicone materials which need to maintain mobility when stress is applied.³⁰

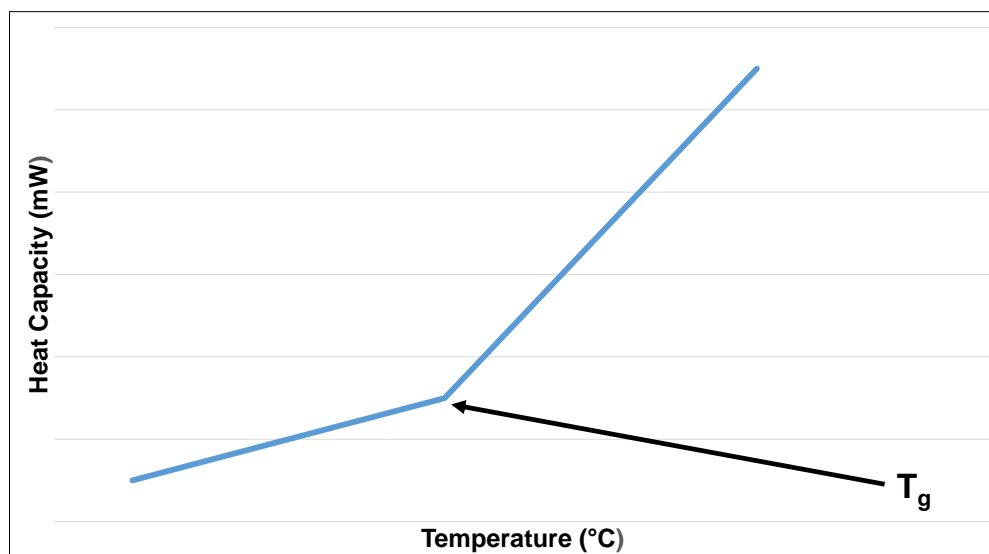


Figure 2: Heat flow as a function of temperature in an amorphous material.

The glass transition is a reversible transition and as glassy materials are cooled, they transition from the viscous state back to a glassy state.³⁰ This shift must be fast enough that the standard first order phase transition toward a crystalline phase is circumvented.³⁰ Compared to the first-order phase transition demonstrated when a material melts, the glass transition appears to exhibit a “pseudo” second-order nature. The transition itself is a complex process that is affected by numerous factors, including the material’s heat capacity, expansion coefficients, heating rate, aging history, morphology, and molecular weight. The glass transition is not a strictly thermodynamic transition as it is defined simply as “the temperature below which the material has become too viscous to flow on a ‘reasonable’ time scale.”³¹ The precise mechanics of the glass transition are not fully understood and several theories exist which attempt to explain this question. For example, kinetic-based theories consider the glass transition to be dynamic in nature. The vitrification of the material occurs as the molecular movements slow to the point that they are effectively frozen. According to these theories, when a material is heated from its glassy state it will eventually reach its glass transition where the molecules receive enough energy to begin moving again. This increase in the speed of molecular movements brings with it a number of properties that are different from those exhibited in the glassy state. While many theories attempt to describe the glass transition, none have adequately explained or modeled the properties and behaviour exhibited by the many types of glass materials.

The nature of the glass transition is important for researchers and those that work with glasses and amorphous materials. As described, materials exhibit very different properties whether they are above or below the glass transition. Being highly viscous, soft, and rubber-like above T_g , while hard, strong, and glassy below T_g , each of these states is of interest in different fields.³⁰ Neither higher nor lower glass transitions are better as the suitability of the transition is subjective to the application of the material. For example, a high T_g may be sought when the materials are used in electronics and technologies such as a cellphone. In these applications, the material must remain below its glass transition to resist crystallization or transitioning to a rubbery state when subjected to the heat produced by these devices. Alternatively, some polymer products require a very low glass transition. Rubber gloves for example, are glassy amorphous materials with a low T_g . These materials need to be flexible and malleable in order to properly cover and protect the wearer’s hands while working. Below T_g , these materials would not function properly and would break due to their increased brittleness. Each field and industry will have appropriate standards for the glass transition that is necessary for a material to function properly according to the operating temperature to which it will be subjected. Understanding the glass transition is vital to the development and function of amorphous materials for each application.

In terms of accessing the glassy phase, several general rules can be used to determine what makes the characteristics of a good glass former. A better or worse glass can be determined by measuring the crystallization kinetics of the material. The critical cooling rate of a material is one such measurement. The critical cooling rate of a glass-forming material is the slowest rate at which a compound can be cooled without demonstrating crystallization. Glasses that can be formed with slower rates are said to have better glass-forming ability. Alternatively, differential scanning calorimetry (DSC) can be used to measure or quantify the glass-forming properties by determining if a compound or material crystallizes upon heating past its T_g . This is because a material is more mobile above its T_g and will reorganize more easily, leading to crystallization. Lastly, the crystallization of a material on standing or sustained heating can be monitored using polarized light optical microscopy. The development of crystalline aggregates from prolonged periods of time or sustained heating can also be observed visually. The ability for a material to resist

crystallization while resting or from heating is known as the glass stability. Connecting these terms to the glass transition, a glass with a higher T_g is generally observed to crystallize more slowly if not resist it completely. This is because of the large difference between ambient temperatures and the material's T_g ; however, the two are not necessarily related due to the complex nature of the glass transition.

2.1.3. Molecular Glasses

Molecular glasses, also known as low molar mass glasses or amorphous molecular materials, are small, low molecular weight organic compounds that are capable of forming solid amorphous phases. A small molecule has a discrete structure in which there are no iterations of repeating units. What is classified as a “small molecule” is incredibly subjective and relative to independent fields. For example, in pharmaceutical applications, molecules below 900 daltons are classified as small. This criterion is accepted, as molecules below this size are generally considered capable of diffusing across cell membranes. Regardless, this range is highly subjective between types the fields and even across various applications within a field.^{32,33} Compared to many other glass materials, molecular glasses offer the advantages of greater synthetic control and purity. As a result, the development and application of these materials has grown greatly.

2.1.3.1. Design of Molecular Glasses

The study of molecular glasses has grown considerably in the past several years. Researchers have dedicated their energy towards the design of molecular glass materials and the enhancement of a material's propensity to adopt glassy phases. This research is of particular interest due to the potential to produce thin films from these materials.⁴ A thin film is a layer of material ranging from the nanometer to the micrometer in scale.⁴ Thin films have current as well as proposed applications in fields including photonics, electronics, and sensors. The amorphous state is ideal for the production of thin films due to the ability to easily apply a homogeneous layer to an entire surface.⁴

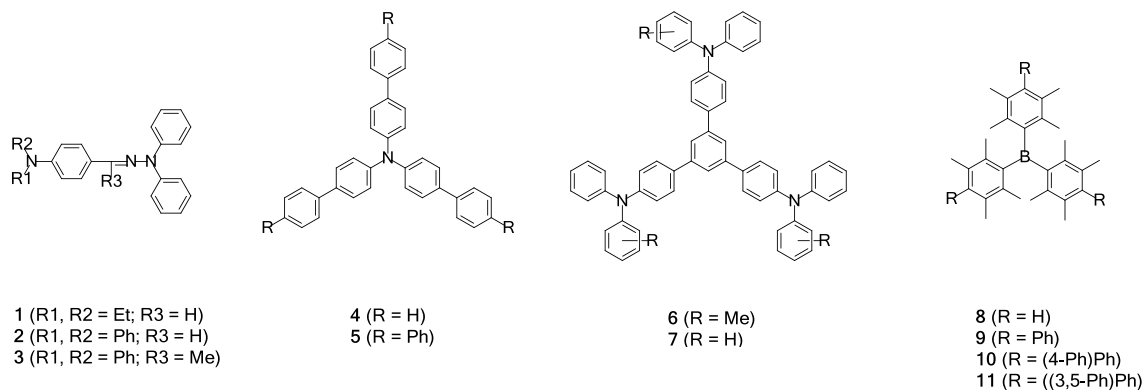
While polymers can be used to form thin films, their polydisperse molecular structures can yield inconsistent behaviour and properties between different samples. Moreover, adding selected functional groups on polymers can also be challenging, especially with partial functional group loading.⁴ Small molecules, on the other hand, are easier to purify, characterize, and process because of their discrete structure and small size. The precise and detailed synthesis of small molecules allows for control over many structural factors and subsequent control of a wide range of properties.⁵ The ability to tailor and readily alter the molecular structure for various applications is of great benefit for many fields. Furthermore, molecular glasses form thin films that are more consistent and possess fewer imperfections. Minimizing the occurrence of imperfections is particularly important as these can hinder the effectiveness and lifetime of thin films.⁴ However, not all small molecules can readily form amorphous thin films under ambient conditions. Furthermore, these materials have a tendency to crystallize with time and exposure to stressors such as heat.^{6,34}

In recent years, studies have been conducted on the design of glass-forming small molecules and the induction of glassy phases. The results found that the greatest factor in favouring the formation of glassy phases was the shape of the molecule, with irregularly shaped molecules having a greater propensity to form glasses. As such, substituents with specific characteristics that promote these irregular shapes and prevent crystallization must be introduced into the molecular

structures of proposed glass-forming materials.³⁵ The strategy adopted in the design of glass-forming molecules relies on the synthesis of molecules that pack inefficiently and crystallize more slowly. Factors such as integrating long and branched alkyl chains, increasing the number of structural conformations, designing globular shapes, and reducing molecular symmetry allow chemists to more predictably synthesize compounds that form glasses.¹⁰ Developments in the field of molecular glass research will be outlined in the following sections.

2.1.3.2. Star-Shaped π -Conjugated Molecular Glasses

Star-shaped molecules are a class of amorphous molecular materials that have been pioneered by Shirota *et al.*³⁶⁻³⁹ Shirota *et al.* incorporated conjugated arms in order to impede the close packing of molecules, consequently inducing the formation of amorphous phases.³⁶⁻⁴¹ The symmetrical shape that gives star-shaped molecular glasses their name induces the ability to adopt glassy phases in the new compounds. Either substitution reactions or coupling reactions were employed to synthesize the star-shaped molecular glasses from simple precursors. These materials can be classified into families based on structural components that are characteristic to each of the series synthesized. Derivatives based on components such as aryl hydrazones,³⁶ triphenylamine, 1,3,5-triphenylbenzene,^{37,38} and triphenylborane³⁹ are examples of sub-classes of these star-shaped molecules. The central structural components on which these molecules are based, N,N-diphenylhydrazine, triphenylamine, 1,3,5-triphenylbenzene, and triphenylborane, are not capable of forming glassy phases and readily crystallize. Scheme 1 depicts examples from several series of compounds synthesized and described by Shirota *et al.* Table 1 shows the thermal properties and phase changes of a number of star-shaped molecules based on aryl hydrazones (**1-3**), triphenylamine (**4-5**), triphenylbenzene (**6-7**), and triphenylborane-based compounds (**8-11**) synthesized by Shirota *et al.*³⁶⁻³⁹

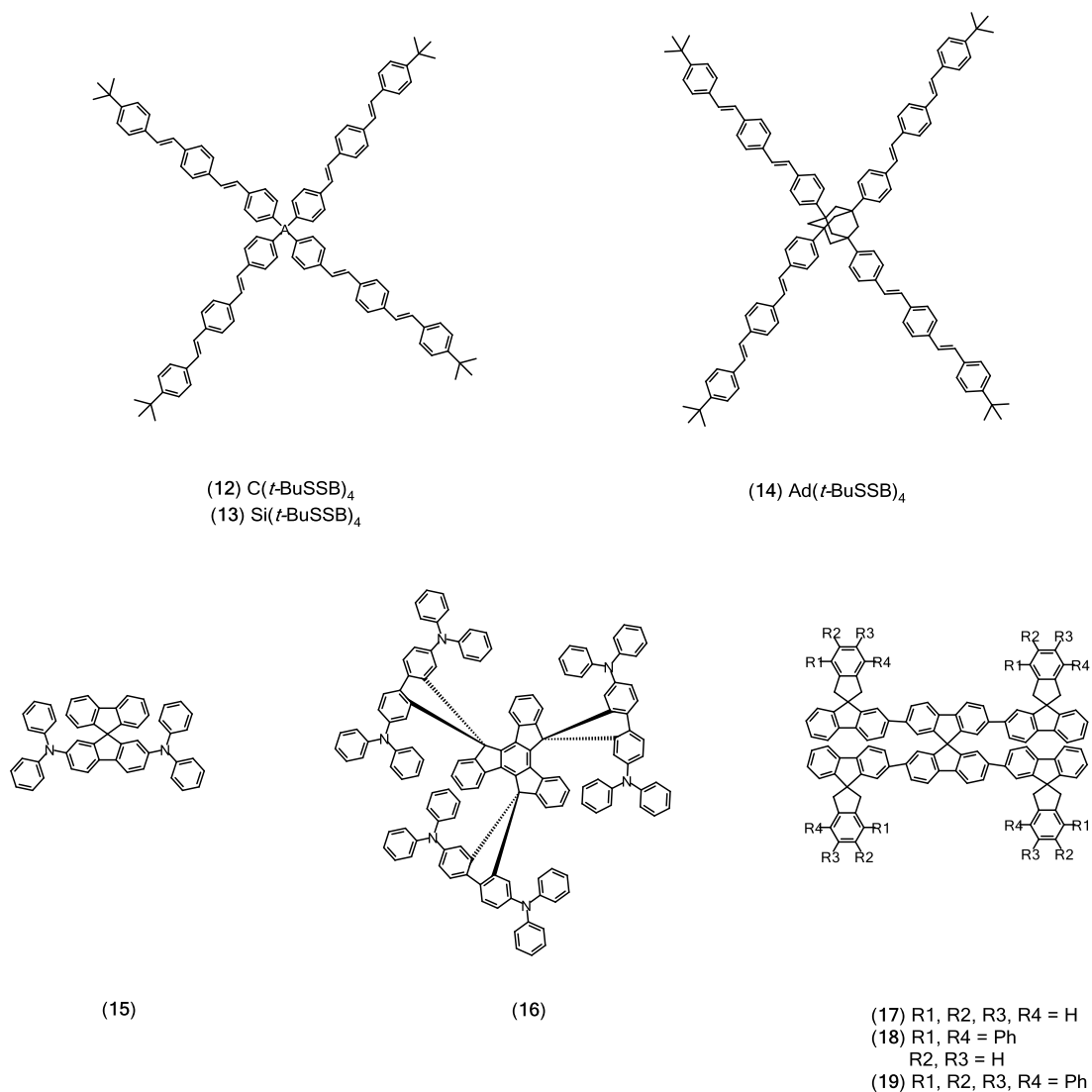


Scheme 1: Examples of aryl hydrazone (**1-3**)³⁶, triphenylamine (**4-5**), triphenylbenzene (**6-7**),^{37,38} and triphenylborane (**8-11**)³⁹ based star-shaped molecules synthesized by Shirota *et al.*

The aryl hydrazine-based compounds exhibited the lowest T_g values followed by the triphenylamine, triphenylbenzene, and triphenylborane compounds, respectively. The addition of small π -conjugated systems around a molecular core that is incapable of forming glassy phases on its own, as is the case in compounds (**1-3**), results in compounds capable of glass formation. However, such glasses demonstrate low T_g values and are not morphologically stable, as they will crystallize over time. In the case of compound **1**, an amorphous phase is only formed if the compound is cooled from its melted form with liquid nitrogen. Furthermore, the resulting glass will crystallize within one week if left at ambient temperature.³⁶ The functionalization of non-glass

forming central cores with longer π -conjugated functional groups, capable of rotating around their axis, resulted in more stable glasses with higher T_g (**4-11**).³⁷⁻³⁹ The increase in T_g and glass stability is the outcome of the greater number of possible conformations that the molecules can adopt. In addition, the geometry of the arms around the central core minimizes cohesion between molecules and improves glass formation.³⁶⁻³⁹ This leads to less efficient and more disorganized packing, greatly increasing the glass-forming ability and stability of these compounds.

While the conjugated arms are a common feature in this family of materials, they are not limited to trigonal geometries. Rather, many central components can be used and attached to the conjugated arms in various geometries. Shirota *et al.* also investigated the effects of replacing the trigonal central cores with larger cores. Several examples of tetrahedral and spirocyclic terfluorene compounds were synthesized (Scheme 2).^{40,41} Table 1 also depicts the thermal properties and phase changes of these compounds. The authors hypothesized that this would increase the size, volume, and steric demand of the compounds by adding an additional branch, further decreasing the propensity to crystallize.⁴⁰ This factor was explored and demonstrated in compounds **12-14**, which incorporated tetrahedral core moieties. The tetrahedral core geometry in compounds **12-14**, led to higher T_g , particularly in compounds with longer conjugated arms, which were shown to be more stable in glassy states and have higher T_g values. This because the tetrahedral central cores changed the geometrical conformations and subsequently affected the T_g . Although changing the core modifies the T_g , the main factor affecting glass formation appears to be the number of conformations as well as length of the conjugated substituents around the core.⁴²



Scheme 2: Examples of tetrahedral (**12-14**)⁴⁰ and spirocyclic (**15-19**)⁴¹ star-shaped molecular glasses.

Among the compounds synthesized by Shirota *et al.*, those functionalized with spirocyclic derivatives **15-19** formed the most stable glasses with the highest T_g values (above 200 °C).⁴¹ The integration of π -conjugated substituents and spiro-shaped structures led to an increased propensity of compounds to form glasses and greatly increased their stability in the glassy state. Spiro derivative **19** possessed the highest T_g (296 °C) of the entire series as a result of several factors: its large molecular weight, bulky center, globular molecular shape, and the configuration of aromatic rings. It was determined that incorporation of rigid moieties led to the formation glassy phases, with greater stability, and higher glass transitions. This observation contrasted a commonly accepted guideline for the design of amorphous molecular glasses. Increasing the degrees of freedom of a molecule generally improved glass formation; however, in this case the rigid central component possesses an irregular shape that prevents the close packing of the molecules. As a result, the molecules cannot converge towards a closely packed and regular arrangement that

would yield a crystalline material. Alternatively, greater molecular size of the central moiety was linked to the ability of these compounds to resist crystallization and remain in stable glassy phases.³⁵ The incorporation of rigid and sterically demanding spirocyclic groups into the core of the star-shaped compounds became one of the most effective strategies adopted by the Shirota group for inducing glass formation. In general, larger, more complex molecular structures correlate with a higher T_g and greater glass stability. However, these benefits come at the expense of complex and costly synthetic procedures. Furthermore, the introduction of large, bulky groups results in large increases in molecular weight due to redundant groups that may be superfluous.

Table 1: Glass transition (T_g), crystallization (T_c), and melting (T_m) temperatures of star-shaped compounds **1-19**.³⁷⁻⁴¹

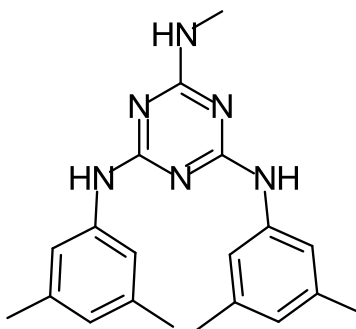
Compound	T_g (°C)	T_c (°C)	T_m (°C)	Compound	T_g (°C)	T_c (°C)	T_m (°C)
1	8	60	90	11	183	261	298
2	50	-	162	12	190	-	246
3	35	103	171	13	165	-	-
4	76	117	260	14	191	-	-
5	132	168	-	15	112	-	-
6	109	154	279	16	170	-	427
7	121	196	269	17	225	-	-
8	63	-	-	18	275	328	452
9	127	174	264	19	296	-	-
10	163	-	-				

The work done by Shirota *et al.*³⁷⁻⁴¹ was key in developing the field of molecular glass design. By incorporating substituents with specific characteristics such as irregular shapes to prevent crystallization, it is possible to induce glass-forming properties into a number of compounds.³⁵ Furthermore, they demonstrated that the incorporation of such substituents was a viable strategy for the design of glass-forming compounds that pack inefficiently and thereby crystallize more slowly.¹⁰ A number of structural components and factors can thus be exploited to frustrate the packing of molecules and prevent crystallization. Exploiting these factors allowed Shirota to propose the design of a number of amorphous molecular materials, ultimately pioneering the star-shaped class of polyaromatic compounds.³⁵

2.1.3.3. Mexylaminotriazine Molecular Glasses

Mexylaminotriazine molecular derivatives synthesized by the Lebel group are another class of long-lived glass-forming compounds. Scheme 3 shows 2-methylamino-4,6-bis(mexylamino)-1,3,5-triazine (**20**), a representative mexylaminotriazine glass.⁴³ Compound **20** has been shown to be one of the most stable glass-forming organic compounds synthesized by the group. This compound has been shown to withstand heating above T_g for 3 weeks as well as shear forces up to 60000 rpm at temperatures above T_g without signs of crystallization.¹² These molecules have been cleverly designed to be smaller and structurally simpler than previously reported molecular glasses by taking advantage of numerous intermolecular forces to enhance glass formation.¹² Intermolecular interactions such as hydrogen bonding allow these compounds to form glassy aggregates which interact poorly with each other.¹² The mexylaminotriazine structure hinders crystallization through a number of mechanisms: 1) it prevents the close and efficient packing of molecules through 3,5-disubstituted aryl groups, 2) hydrogen bonds limit the molecular mobility

of molecules, and 3) several different conformations of the mexylaminotriazine core exist, each with similar energies and high energy barriers that impede interconversion.¹² These compounds have been ingeniously synthesized to take advantage of these factors for the formation of stable glassy phases.



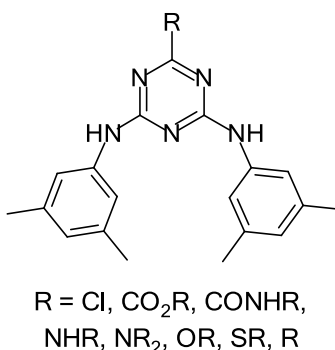
Scheme 3: Example of a mexylaminotriazine molecular glass, 2-methylamino-4,6-bis(mexylamino)-1,3,5-triazine (**20**).⁴³

The impact and role of the mexylaminotriazine structure on glass formation and stability has been further investigated to develop a clear picture of the mechanisms at work in these compounds. Mexylaminotriazine compounds consist of three major functional units, one head unit and two tail groups, one of which is usually a mexylamino group. It has been shown that the nature of these various elements within the structure of the molecule play a role in the glass-forming properties of this class of compounds by altering intermolecular non-covalent interactions. These forces in turn help to prevent the efficient packing of molecules and lead to the formation of glassy phases. For example, the incorporation of mexylamino tail moieties has been shown to produce some of the most stable mexylaminotriazine glasses, giving way to its respective use in the naming of these compounds.¹⁴ Factors that are generally associated with the promotion of crystallization in small, rigid molecules can also be exploited to promote the formation of glasses.¹⁰ The incorporation of nonplanar elements has traditionally been cited as a major factor promoting glass formation and incorporation of nonplanar elements is often used as a strategy to increase the glass-forming ability of various compounds. However, mexylaminotriazine compounds can adopt planar geometries, seemingly in conflict with previously held beliefs. Similarly, hydrogen bonding often promotes crystallization; however, in mexylaminotriazine molecules, hydrogen bonds formed between the mexylamino groups and the head-groups contribute greatly to favour glass formation and inhibit crystallization. The hydrogen bonds promote the formation of many small aggregates which pack poorly and cannot easily reorganize, a process necessary for crystallization.¹⁰ In order to develop the use of mexylaminotriazines as glass-forming moieties, the structure and impact of a number of structural components has been investigated.

2.1.3.3.1. Influence of the Head-Group

Each component of the mexylaminotriazine structure plays a role in the compound's ability to adopt the glassy state. The functional group at the 2-position of the triazine ring (the head-group), has the most pronounced effect on the compound's thermal properties.^{12,13} This functional group was identified as a key component in numerous molecular phenomenon such as hydrogen bonding, conjugation with the triazine ring, and tautomerism; all of which in turn influence the molecule's rotation, symmetry, planarity, and subsequently its glass-forming properties. The use

of various head groups at the 2-position and their impact on glass formation was studied by synthesizing a series of compounds, in which mexylamino groups were substituted at both the 4- and 6-positions. The mexylaminotriazine was then substituted using a variety of functional groups at the head position. Additionally, many of these functional groups were further altered using a variety of linear and branched alkyl chains as well as aryl groups. For example, several mexylaminotriazines were synthesized with carboxyl functional groups at the 2-position. These carboxyl groups were substituted with hydrogen, methyl, ethyl, propyl, *iso*-propyl, butyl, and *iso*-butyl alkyl chains. The resulting library of mexylaminotriazine compounds were then investigated for their propensity to form stable glassy phases.¹³ Scheme 4 depicts the general structure of the mexylaminotriazine compounds synthesized to investigate the role of the head group on glass-forming properties.¹⁴



Scheme 4: Mexylaminotriazine derivatives synthesized for the evaluation of the head group's role in glass formation.¹⁴ All functional groups were further varied by synthesizing derivatives with varying alkyl chain lengths.

The thermal properties of these compounds were determined and measured using DSC. Thermal analysis demonstrated that most of the synthesized compounds were capable of glass formation and resisted crystallization, with most demonstrating T_g values ranging from 26-97 °C.¹⁴ Of the compounds synthesized in this study, the highest T_g values were measured for the amine-functionalized compounds for their respective chain lengths. For example, the compounds substituted with secondary amines demonstrated glass transitions ranging from 65 °C to 94 °C. Comparatively, the series with tertiary amines exhibited a range of T_g values between 26 °C and 65 °C, the carboxamide-functionalized series demonstrated a glass transition range of 59 °C to 84 °C, the ether series exhibited glass transitions from 43 °C to 58 °C, and the ester-functionalized compounds had T_g values measuring from 34 °C to 75 °C. Interestingly, the symmetric tris(mexylamino) substituted compound did not form a glassy phase, further highlighting the unique role of the head-group in frustrating crystallization. Several other head-groups did not promote glass formation, including an unsubstituted hydrogen, chloro, hydroxyl, thiol, primary carboxylic acid and carboxamide group.¹⁴ These head-groups are believed to promote the close packing of molecules and subsequently crystallization of the materials by way of their small size (H, Cl), strong hydrogen bonding (CO₂H, CONH₂, OH, SH), high molecular symmetry (mexylamino), or tautomerism (OH, SH).¹³ The head-group was determined to be necessary for the formation of short-range aggregates that do not pack well with each other and prevent crystallization of the material. It is observed that functional groups that participate in hydrogen bonding facilitate glass formation. This is supported by the amine and amide functionalized series, which exhibit the highest T_g ranges compared to compounds containing functional groups that do

not partake in these interactions. Contrarily, several functionalized compounds that participate in hydrogen bonding interactions did not form a glass. It is suggested, that the hydrogen bonding in these compounds is too strong. The role of the attached alkyl chain has been suggested as a factor, providing necessary steric forces that serve to compete with hydrogen bonding interactions, optimizing the propensity of certain compounds to pack poorly and adopt glassy phases. Enthusiastically, it should be emphasised that nearly all of the functional groups could be incorporated into mexylaminotriazine glass formers, with 31 of the 43 compounds synthesized for this experiment forming glassy phases. This highlights the suitability and versatility of the mexylaminotriazine core as a structure for promoting glass formation.

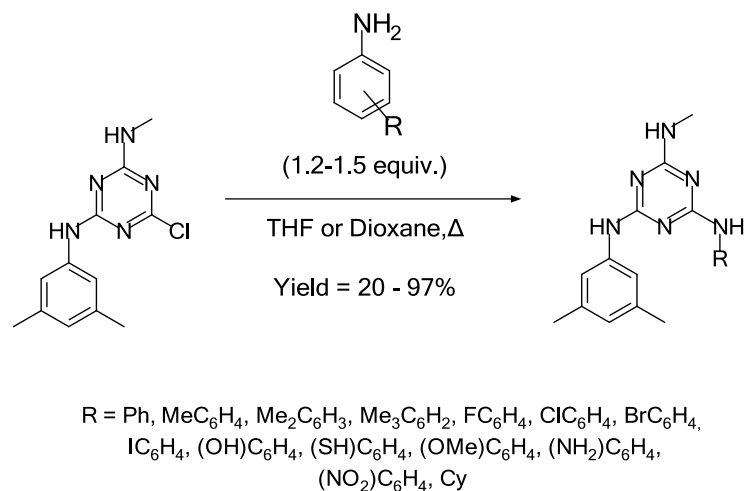
As suggested in the previous paragraph, the length of the head group's alkyl chain can also influence the thermal properties of the glassy compounds. For each respective functional group, there is an optimal chain length. Depending on the head group, alkyl chains that are too short or too long demonstrate poorer glass-forming ability and lack the stability necessary to resist crystallization compared to other compounds. For example, of the mexylaminotriazines functionalized with alkyl chains, the highest glass transition was exhibited by the methyl-substituted chain at 59 °C.¹⁴ Alternatively, the unsubstituted mexylaminotriazine did not exhibit a glass transition at all, while it was observed that increasing the alkyl chain length caused a decrease in T_g relative to the methyl derivative.¹⁴ For example, increasing the alkyl chain length from a methyl to an ethyl resulted in a T_g of 41 °C, a decrease of 18 °C.¹⁴ Furthermore, with the exception of the ester-functionalized mexylaminotriazines, branched alkyl chains of the same size tend to show T_g values 8-12 °C higher than corresponding linear chains. The alkyl chains affect glass-forming properties because of their contribution of weak London forces. Chains that were too short led to crystallization by not contributing the necessary steric forces, while chains that are too long result in stronger London forces, which can become strong enough to promote the reorganization of molecules into more ordered configurations also leading to the crystallization of the material.¹⁴ This outlines the role as well as the need to optimize the length of alkyl chains in the head group in order to facilitate glass formation.

2.1.3.3.2. Influence of the Tail Groups

The chemical and structural properties of the functional groups at both the 4- and 6-positions of the triazine ring (the tail groups or ancillary groups of the triazine structure) have a profound influence on the properties of the molecule. Similar to the head groups, altering one of the ancillary groups can affect the polarity, symmetry, non-covalent interactions, and molecular weight of the molecule, subsequently altering the glass-forming properties. In order to understand the impact of the tail group, the Lebel group performed a number of studies that sought to identify the effects of modifying these substituents on T_g , glass formation, and glass stability. This was done in two studies, the first investigated the glass-forming properties of singly substituted ancillary groups, the second observed the effects of replacing both tail groups.

One study conducted by Eren *et al.* sought to establish the effect of various functional groups in tail positions on the properties of the molecule.¹¹ Subsequently, they aimed to predict the glass-forming ability of mexylaminotriazine analogues from the presence of various functionalized tail groups. A series of derivatives were synthesized in which the head group and one of the two tail groups were kept constant as methylamino and mexylamino groups, respectively. The remaining ancillary group was functionalized using various arylamino and cycloalkylamino groups.¹¹ The mexylaminotriazine derivatives were synthesized by a series of substitution reactions from

cyanuric chloride and the amine groups were added in succession in order to control the directing effects and final configuration of the molecule (Scheme 5).

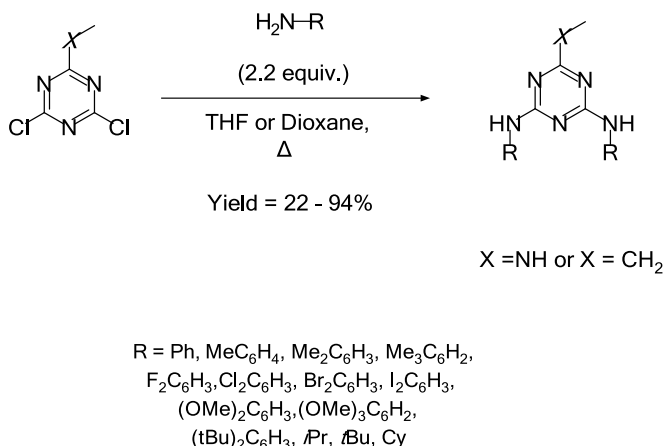


Scheme 5: Synthesis and general structure of some molecular glasses synthesized by Eren *et al.*¹¹

This study led to a number of conclusions regarding the effects of functionalized aryl tail groups on the glass-forming ability and T_g of mexylaminotriazine compounds. All derivatives synthesized for this experiment were able to form amorphous glass phases and demonstrated T_g values from 52-131 °C. Furthermore, all compounds synthesized for this experiment remained stable in a glassy phase, with the exception of one derivative substituted with a 2,4,6-trimethylphenyl group, which crystallized when subjected to heating at a rate of 5 °C/min. Functional groups on the various substituted ancillary groups affected the T_g of the compounds. Functional groups on the aryl moieties with the ability to participate in hydrogen bonding such as OH, NH₂, CONH₂, and CO₂H tended to be associated with higher T_g values. The position of substituents on substituted aryl tail groups also affected the T_g of derivatives. The presence of substituents affected the T_g in the following order, *ortho* < *meta* < *para*. The researchers hypothesized that the *para*-substituted compounds exhibit higher symmetry whereas *ortho* substituents obstruct hydrogen bonding. Lastly, it was observed that symmetrical tail groups were not required and that arylamino or alkylamino groups could replace one of the mexylamino groups without inhibiting the glass-forming properties of the mexylaminotriazine core. This is an interesting and exciting observation that suggests one tail group can be functionalized for a number of purposes while maintaining glass-forming properties.

A subsequent investigation was performed by the Lebel group to investigate the substitution of both mexylamino groups and the subsequent effects on glass-forming ability and stability.¹³ Two series of compounds were synthesized, one series possessing a methylamino head group and another series with an ethyl head group. Earlier work identified that the methylamino head group resulted in extremely stable glasses whereas the ethyl head group was only associated with mediocre glass-forming ability.¹¹ The two series were identical with the only exception being the varied head groups. These series consisted of a number of tail groups that were both substituted. Tail groups selected for this study included alkyl chains, as well as a number of functionalized arylamino groups. Synthesizing two series of compounds allowed for conclusive analysis

regarding the precise effects of the tail groups on glass-forming ability. Both series of compounds were synthesized by reacting either 2-methylamino-4,6-dichloro-1,3,5-triazine or 2-ethyl-4,6-dichloro-1,3,5-triazine with an excess of two equivalents of the respective aniline substituent under reflux conditions in THF (Scheme 6).¹³

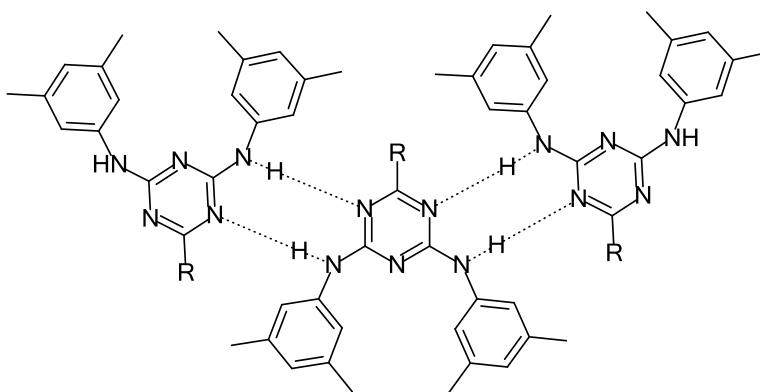


Scheme 6: Procedure for the synthesis of some molecular glasses with di-substituted tail groups.¹³

It was determined that compounds bearing identical tail groups exhibited very similar thermal behaviour when compared to analogues with asymmetric tail groups.¹³ As such, one of the tail groups could be substituted without inhibiting glass formation. Additionally, it was observed that methylamino tail groups were not necessary for glass formation. Although, among those utilized for this study, the 3,5-disubstituted aryl moieties, particularly the methylamino substituent, were identified as being the best tail groups in terms of glass-forming properties. For example, iodide or bromide 3,5-disubstituted aryl moieties also demonstrated glass formation, with T_g values of 94 °C and 128 °C, respectively, and good glass stability. This study was useful in determining which tail groups produced the most stable glasses. The study further highlighted the influence played by the head group at the 2-position on the glass-forming ability, and glass stability of methylaminotriazine compounds. The entire series of compounds synthesized with an NHMe head group were capable of adopting glassy-phases with T_g values ranging from 22 to 129 °C. Furthermore, several of these compounds formed very stable glasses and resisted crystallization despite being subjected to a number of stressors. Alternatively, the series containing an ethyl head group had a much poorer capacity for glass formation with 6 of 21 compounds being unable to form glasses. Of those that did demonstrate glass transitions, T_g values ranged between 19 °C and 96 °C. Additionally, all compounds consisting of ethyl head groups were shown to be significantly less stable. The majority of compounds possessing the ethyl head group crystallized within 1-3 days of standing at room temperature in the laboratory. The systematic differences between the two series is due to the nature of the head groups. The NHMe functional group aids glass formation and stability for a number of reasons: 1) it can participate in hydrogen bonding interactions, and 2) it is conjugated with the triazine ring, limiting the motion of the molecule and preventing crystallization.¹³ In conclusion, this study highlighted which tail groups were most effective for producing stable methylaminotriazine glasses. The report also demonstrated that the methylaminotriazine compounds could accommodate a high degree of tailorability, with regards to the ancillary groups, while maintaining glass-forming properties.

Another factor that was explored was the effect of aryl and alkyl tail groups on the glass-forming abilities of mexylaminotriazine compounds.⁶ Aryl ancillary groups were linked to compounds exhibiting glass formation with the highest T_g values. This is due to the rigidity of the aryl groups, leading to poor molecular mobility and an inability to pack in an ordered fashion. Compounds bearing alkyl tail groups at both positions showed poor glass formation. Those compounds with alkyl groups that could demonstrate glass transitions also had the lowest T_g when compared to the arylamino-substituted compounds. In the case of this particular study, compounds with alkyl ancillary groups only formed glassy phases in the series using the methylamino head group. The planar nature of arylamino groups compared to the alkyl and cyclohexyl groups was suggested as one factor that could facilitate glass formation by causing the molecules to pack more poorly. Furthermore, it was suggested that weak π - π interactions, which occur with aryl-substituted compounds, could play a role in the glass formation of mexylaminotriazines.

In 2017, an additional study by the Lebel group sought to uncover the role of these π - π interactions.¹⁶ Also known as donor-acceptor interactions, these non-covalent interactions play a key role in the design of many materials.^{44,45} Two types of π - π interactions exist, weaker edge-to-face π - π interactions and stronger face-to-face π - π interactions. In order to investigate how these π - π interactions affect glass formation in mexylaminotriazines, two series were synthesized, one incorporating 2,3,4,5,6-pentafluorostilbene and the other possessing the non-fluorinated derivative. The 2,3,4,5,6-pentafluorostilbene moieties are known for their propensity to form face-to-face π - π interactions with electron-rich non-fluorinated aryl groups. Of the synthesized compounds, all demonstrated the ability to form glasses; however, those compounds incorporating 2,3,4,5,6-pentafluorostilbene demonstrated crystallization whereas the non-fluorinated derivatives could not be crystallized. This study subsequently found that face-to-face π - π interactions favoured crystallization. These interactions were shown to display a competition with the strong hydrogen bonding interactions that increase a compounds propensity to form glassy phases. The π - π interactions were found to utilize a higher van der Waals surface of the molecules, subsequently forcing the molecules into specific conformations, while hydrogen bonds use a smaller van der Waals surface that extends laterally, permitting many conformations of the molecules.¹⁶ Contrarily, edge-to-face π - π interactions are believed to contribute similarly to hydrogen bonds. These interactions are weaker, use a smaller proportion of the molecules' van der Waals surface, and permit a number of directional conformations.¹⁶ This hypothesis could not be confirmed in the study as the compounds could not be crystallized and subsequently analyzed. Interestingly, the star-shaped molecular glasses (**1-19**), described in section 2.1.3.2, also contain groups that enhance weak π - π interactions similar to the Lebel group's mexylaminotriazines. The aromatic functional groups in these molecular systems may interact across a number of planes and orientations. As a result, the π - π interactions do not arrange themselves in uniform directions and can exist in a multitude of planes, contributing to the formation of glassy phases.¹⁴ The presence of aryl groups in these systems is not coincidence, rather they are vital to the ability to form and remain in a glassy phase among these series of chemicals. This study ultimately highlighted the selection of substituents as an important factor for balancing the myriad of competing intermolecular forces. The relationship between these interactions along with the rigid irregular molecular structure prevents the ordered close packing of molecules leading to the formation of amorphous materials (Scheme 7).



Scheme 7: Graphical representation of the interactions between molecules, preventing ordered close-packing of the mexylaminotriazine molecules.¹⁴

2.1.3.3.3. Mexylaminotriazine Functionalized Compounds

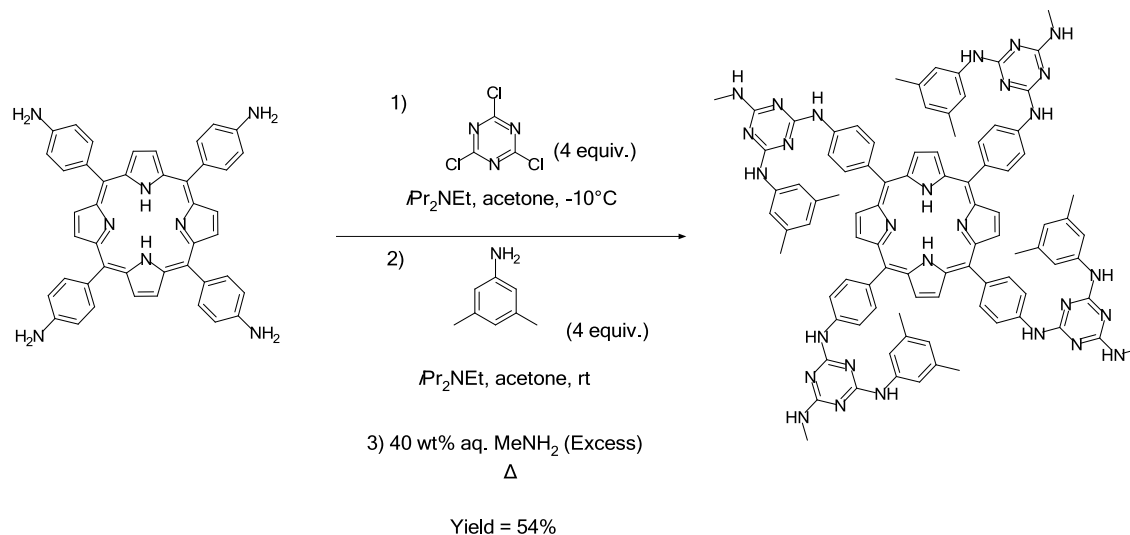
The previous sections have described a number of the interactions and phenomenon that imbue various small organic molecules with the ability to adopt and remain in a glassy phase. The synthetic routes and structure of mexylaminotriazine compounds allow for a greater degree of variability, and control over the properties of this class of chemical compounds. Furthermore, these sections have alluded to several advantages that the mexylaminotriazine glasses have over star-shaped molecular glasses:

- 1) Head and tail groups can be substituted in succession by exploiting the synthetic procedures;
- 2) The sequential synthesis allows for the easy introduction of asymmetric ancillary groups (relative to the star-shaped class of glass formers); and
- 3) A large variety of ancillary groups can be used while maintaining glass-forming ability.

In short, the mexylaminotriazine class of glass-forming compounds can be easily altered and tailored. The tailorability allows researchers to study the compounds to develop a better understanding of the interactions that result in propensity of mexylaminotriazine compounds adopting such stable glasses. Understanding the roles of π - π interactions, hydrogen bonding, and conformational equilibria in the glass formation of mexylaminotriazines allows chemists to optimize materials for various applications. Furthermore, the ability to alter the ancillary groups suggests that mexylaminotriazine derivatives may be used to impart glass-forming properties to compounds that would not exist in the glassy state on their own. Compounds that are used for applications such as semiconductors, dyes, fluorophores, or ligands for transition metals may effectively be functionalized using a mexylaminotriazine group in order to form molecular glasses.⁶

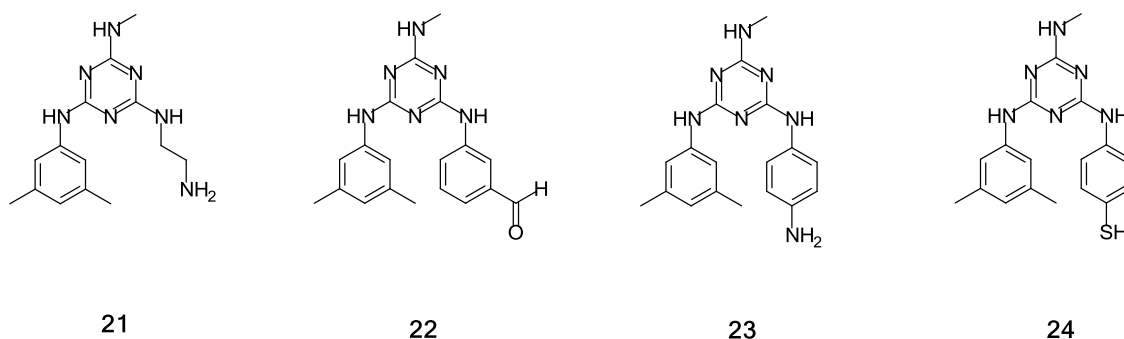
An example of a compound functionalized with a mexylaminotriazine unit is that of tetraphenylporphyrin (TPP). The Lebel group synthesized this compound in order to establish whether glass formation of the TPP core could be induced, despite the parent compound readily crystallizing.⁶ The compound was prepared by the reaction of tetrakis(4-aminophenyl)porphyrin with cyanuric chloride, 3,5-dimethylaniline, and methylamine. The reaction was conducted as a

one-pot procedure and obtained the desired compound in a yield of 54% (Scheme 8). The product was analyzed using DSC in order to determine if the compound exhibited a glass transition. Excitedly, the T_g was measured and found to be 205 °C. Furthermore, despite heating above the T_g , the compound did not crystallize and remained stable. These observations for the thermal behaviour of the product are in stark contrast with that of the parent TPP compound which crystallizes readily and melts at 444 °C.⁶



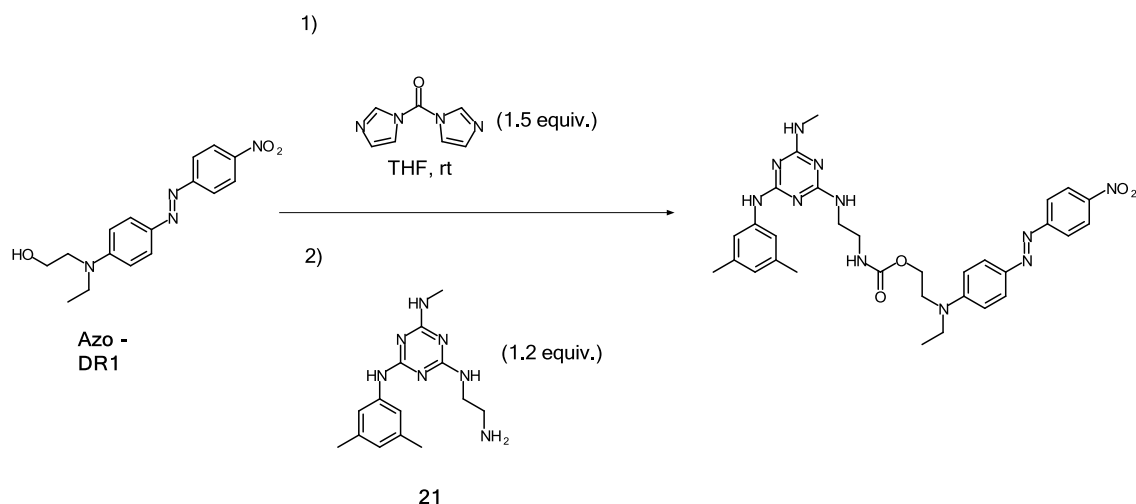
Scheme 8: Synthesis of a tetraphenylporphyrin derivative functionalized with mexylaminotriazine moieties.⁶

Despite these exciting results, the product contained four mexylaminotriazine groups, which unproductively increased the compound's molecular weight and decreased the compound's solubility in many solvents.^{8,9} This research ultimately established that mexylaminotriazine moieties could be used to imbue glass-forming properties to compounds that are typically unable to access the glassy state. Subsequently, a number of mexylaminotriazine glasses were synthesized to include reactive functional groups capable of being used as covalent linkers to other compounds. A sample of mexylaminotriazine glasses capable of being reacted and covalently bonded with other compounds are depicted below in Scheme 9.¹¹ Compounds **21** – **24** are mexylaminotriazines functionalized with reactive groups. These compounds are vital to establishing straightforward, single-step methods for introducing mexylaminotriazine components, and therefore glass-forming abilities to a variety of compounds.



Scheme 9: Examples of methylaminotriazine glasses containing functional groups to permit covalent bond linkages to other compounds.¹¹

In order to demonstrate the use of these functionalized methylaminotriazine derivatives,¹¹ a novel glass-forming azobenzene was synthesized. Disperse Red 1 (DR1), an azo-dye that is unable to adopt a glassy phase, was covalently linked to a methylaminotriazine functionalized with an alkylamino linker (**21**). The glass-forming azobenzene was synthesized by the reaction of Disperse Red 1 (DR1) with *N,N*-carbonyldiimidazole (CDI), the intermediate product was then reacted with the functionalized glass precursor to obtain the desired product in a high yield (94%) (Scheme 10). Despite a significant departure from the structure of the DR1 parent compound, the glassy DR1 derivative maintained the photomechanical and photophysical properties of the parent complex while possessing new thermal properties such as glass transition.¹⁷



Scheme 10: Synthesis of Azo DR1 compound functionalized with a methylaminotriazine derivative.¹⁷

Methylaminotriazines are a particularly exciting class of molecular glasses. As discussed, these compounds readily and predictably form stable, long-lived glasses. Furthermore, when compared to the star-shaped molecular glasses, these compounds present greater opportunity to control and tailor the structure and properties of the molecules. The high degree of synthetic control and modular approach to the synthesis of methylaminotriazines has allowed researchers to better

understand the factors and phenomena that make mexylaminotriazines such great glass formers. Lastly, it has been shown that glass-forming abilities can be imparted to other chemical compounds by the introduction of mexylaminotriazine functional groups. As a result of these characteristics, mexylaminotriazines offer one of the most promising strategies for the induction of glass-forming abilities to a number of compounds for the fabrication of thin film materials.

2.1.4. Application of Molecular Glasses

Molecular glasses have caught the attention of researchers in many fields. Their unique thermal properties, simple production, ease of purification, low cost, low molecular weight, and ability to be processed into a wide array of devices and thin films are but a few of the characteristics that have made this class of chemicals so attractive. With applications in pharmaceuticals and electronics, the use and application of molecular glasses is steadily growing.⁴⁶ The utility of molecular glass materials and their application to several fields will be explored in the following sections.

2.1.4.1. Pharmaceuticals

The role of amorphous molecular glasses in pharmaceutical developments and research is of particular importance due to properties such as their solubility, and molecular stability. For example, amorphous solids have increased molecular mobility, resulting in faster dissolution rates compared to crystalline solids. The solubility and associated kinetics of amorphous materials is of particular interest, as the dissolution of medications in the gastrointestinal system is often the limiting step for many medications to be absorbed and become biologically available to the body.^{47,48} It is these unique properties of amorphous materials that make them desirable in the pharmaceutical industry. A great deal of research effort is devoted to improving the mechanism of action of pharmaceuticals. Improved dissolution rates are one factor that can be improved upon. The development of glassy materials and the induction of glass-forming properties is one strategy that could be employed to achieve better dissolution. As such, research is devoted to better understanding the mechanisms of glass formation in a myriad of small molecules.⁴⁸ Unfortunately, the incorporation of desirable properties can also be accompanied by many undesirable properties, such as the compound's stability in a glassy state.

The second factor of molecular glass that is of great interest for those in the field of pharmacology is the stability of the compounds. Pharmacology is a highly regulated field, which requires medications to be highly stable, both chemically and morphologically, in a number of environmental conditions in order to remain effective and safe despite potentially long-term storage in pharmacies, homes, and warehouses. While enjoying higher dissolution rates, amorphous solids typically exhibit much lower stability, both chemically and physically, relative to crystalline solids.⁴⁷ The nature of amorphous solids leads to a greater degree of molecular mobility. Many molecular glasses are obtained through methods such as liquid cooling, condensation, or evaporation of solvents. As a result, the materials are kinetically frozen as they are cooled below the T_g and the molecular motions slow. The problem lies in the thermodynamic properties of the material, in which molecular glasses are thermodynamically pushed towards crystallization.⁴⁹ The synthesis of compounds with a high degree of stability, both physically and chemically, is vital for applications in the pharmaceutical industry. As such, the observations obtained through the study of mexylaminotriazine glasses could be used to further the development of other glass-forming compounds in other fields.

2.1.4.2. Electronic and Optoelectronic Applications

In recent years, amorphous organic compounds have found numerous applications in the fields of electronics and optoelectronics. Known as amorphous organic charge transport materials, these compounds have been employed as semiconducting materials in electronic and optoelectronic devices. Applications of these materials include organic light emitting diodes (OLEDs), organic field-effect transistors (OFETs), organic photovoltaic cells (OPVs), in photochromic materials, and nanolithography.⁴⁶

2.1.4.2.1. Molecular Glasses in Organic Light-Emitting Diodes

Organic light-emitting diodes (OLEDs) are one technology that depend greatly on amorphous organic materials. OLEDs consist of a number of organic materials layered between electrodes and subsequently sealed. The use of organic materials is necessary for the charge transporting or conductive layer, as well as the hole transporting or emission layer.⁴⁶ When a current is passed through the system, a potential develops and is distributed between the conduction and emission layers. Ultimately, excitons, molecules in an electronically excited state, are formed from the combination of electrons and holes. During the process of deactivation, these excitons must lose energy. This is done through the emission of light by fluorescence or phosphorescence.⁵⁰ Figure 3 depicts the structured layers and their interaction in an OLED device.

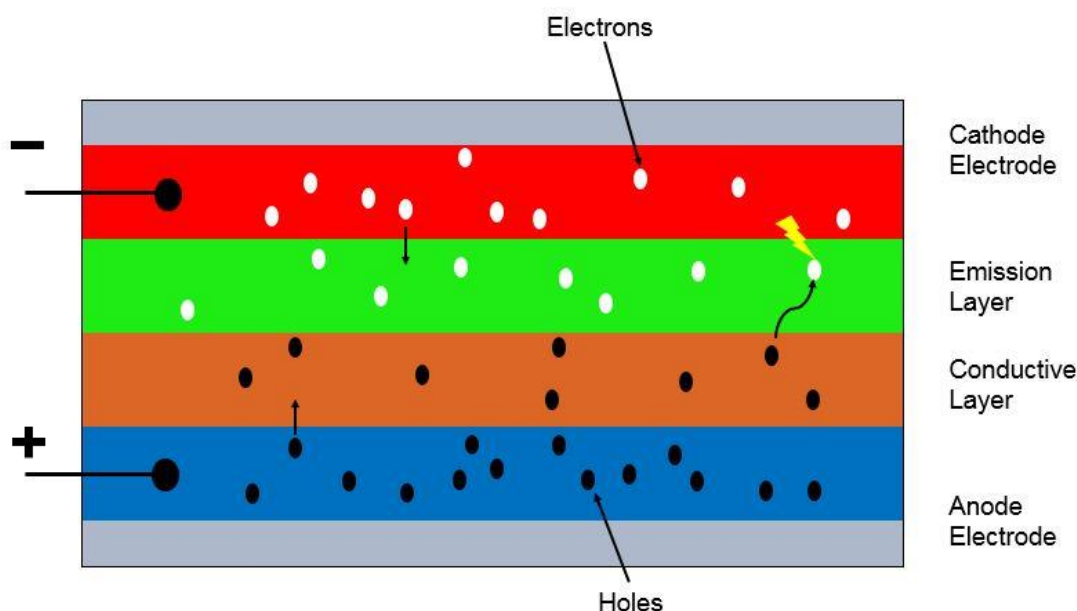
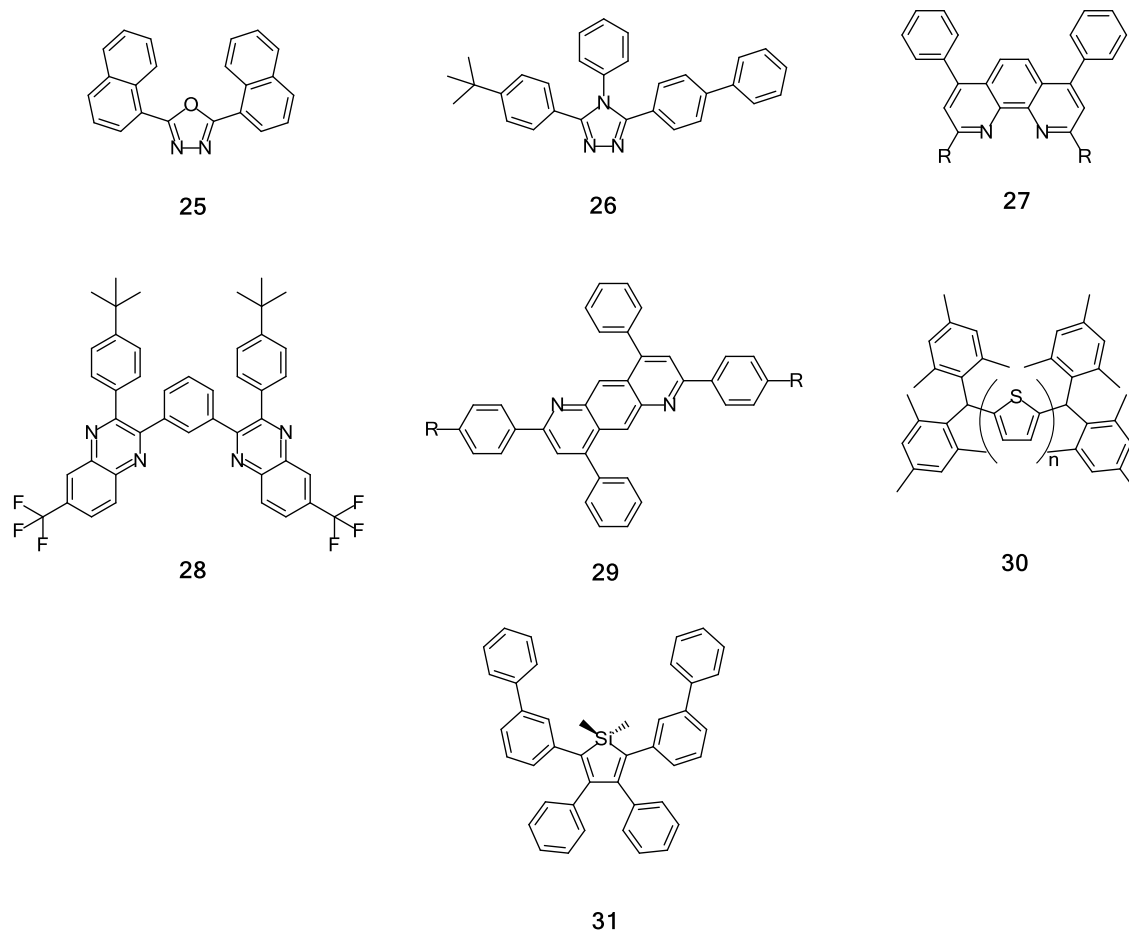


Figure 3: Graphical representation of the general structure and mechanism of function for OLED devices.

When designing materials for OLEDs, several properties are required. First, the materials must be capable of being processed into uniform homogeneous thin films. Secondly, the materials must be physically and thermally stable to maintain performance and function. Lastly, they must have appropriate electronic properties such as electron affinity and ionization potentials in order to allow the passage of charge carriers from the electrodes to adjacent layers. Furthermore, in addition to these general requirements, materials need to possess other characteristics or

tailorability in order for them to be utilized in specific roles such as hole transport, electron transport, charge blocking, and light emission.⁴⁶ Possessing, or permitting the facilitating the incorporating of the necessary properties, molecular glasses are ideal for the synthesis of compounds for these applications. In fact, molecular glasses have already been developed to serve as candidates in OLED technologies, specifically as charge carrying layers, allowing electrons and holes to flow through the devices.⁵⁰ Several of the star-shaped molecular glass compounds described earlier possess these abilities and have been utilized in OLEDs. Star-shaped derivatives used for OLED applications include triphenylamines (**4-7**), tetraphenylmethanes (**12, 13**), spirobifluorene (**15-19**), triazines, triphenyltriazines, benzenes, triphenylbenzenes, tetraphenylsilane, 1,3,4-oxadiazoles (**25**),⁵¹ triazoles (**26**),⁵² phenanthrolines (**27**),^{53,54} quinoxalines (**28**),⁵⁵ anthrazolines (**29**),⁵⁶ boron-containing oligothiophenes (**30**),⁵⁷ and silole derivatives (**31**).⁵⁸ Several of these charge carrying star-shaped compounds are shown below in Scheme 11.



Scheme 11: Structures of star-shaped molecular glass compounds (**25-31**) synthesized as charge carrier materials.⁵¹⁻⁵⁸

2.1.4.2.2. Molecular Glasses in Organic Field-Effect Transistors

While primarily incorporating crystalline materials, organic field-effect transistors (OFETs), are another potential electronic application of molecular glasses. These devices are used in flexible integrated circuits and displays as charge carrier devices. OFETs consist of three electrodes (a source, drain, and gate), an insulator, and an organic semiconducting or channel layer. These transistors function according to the conductivity of the channel layer, which is dependent on the potential applied to the gate electrode. A small insulator also exists between the source electrode and the semiconducting layer in order to create a polarization between these two components. In the “on” configuration, a potential is applied to the gate creating a depletion layer in the channel. This also increases the conductivity of the layer and allows the transfer of electrons between the source and channel. As electrons are injected from the source, they are transported through the organic semiconductor and into the drain electrode. In the “off” state, no potential is applied to the gate, the conductivity of the semiconductor is diminished, and no injection of electrons from the source electrode is possible. Subsequently, no current is passed between the source and drain electrodes.⁴⁶ Figure 4 shows the structure and orientation of the components in an OFET device. Generally, organic compounds such as oligothiophene derivatives,⁵⁹ tetracene,⁶⁰ pentacene,⁶⁰ and fullerenes⁶¹ are used in OFETs. These compounds exist in a crystalline state; however, promising results have also been reported using triphenylamine star-shaped glass-forming compounds possessing carbazole or fluorene functionalized conjugated arms (**32**, **33**).⁶² These glass-forming compounds are depicted below in Scheme 12.

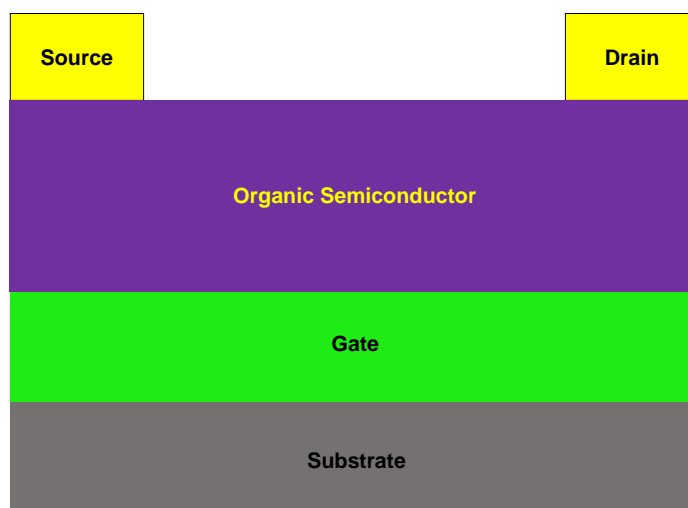
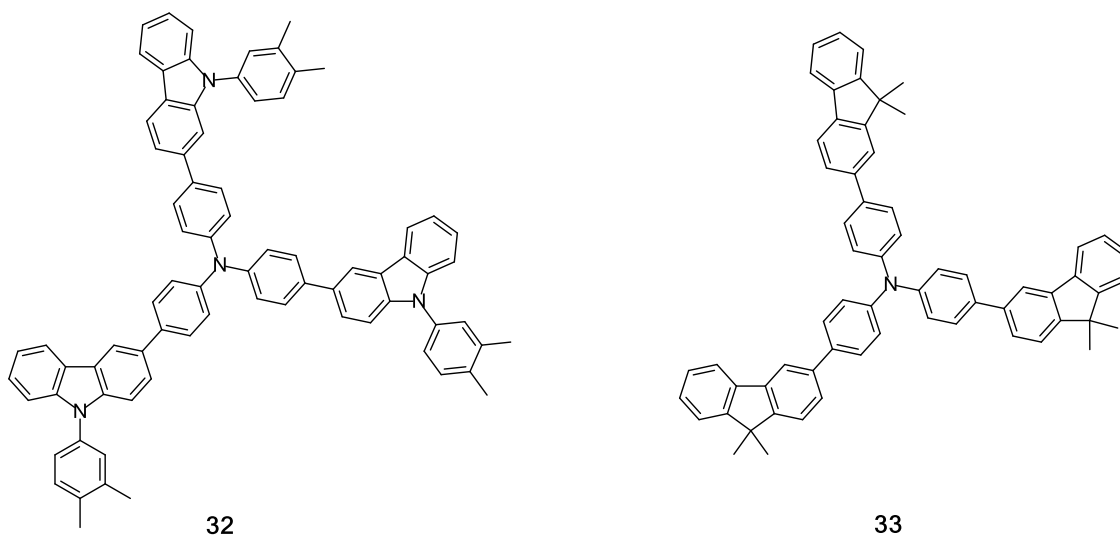


Figure 4: Graphical representation of OFET devices employing organic semiconductors.



Scheme 12: Triphenylamine star-shaped molecular glasses incorporating carbazole (**32**) and fluorene (**33**) groups for OFET technologies.⁶²

2.1.4.2.3. Molecular Glasses in Organic Photovoltaics

An organic photovoltaic (OPV) is a device that is capable of converting solar light energy into electrical energy.⁵⁶ The first step in the functioning of an OPV is the absorption of light by a photoactive layer. This absorption results in the production of excitons in the material, which then diffuse. The diffusion generates charge carriers, electrons and holes, which are carried through the material towards their respective electrodes, ultimately separating the carriers and generating an electrical potential.⁵⁰ Two main types of OPV devices are in existence, Schottky-type and *bulk* heterojunction-type. The Schottky-type OPV utilizes a single organic layer between the two electrodes. In this system, the absorption, production of excitons, diffusion of excitons, and transport to electrodes occurs in the same material. Alternatively, the most effective type of these devices are called bulk heterojunction OPVs, consisting of a nanometer scale blended layer of donor and acceptor materials. Drop casting or spin coating of the blended materials is used to form an interpenetrating network of the materials connecting the two electrodes. In the active layer, either the donor material or both the donor and acceptor materials may capture photons. From these materials, the charge carriers are passed through the device to the corresponding electrodes. Due to the double duty played by this single organic layer, the thickness and dispersion of the materials of the organic layer must be carefully controlled. This is to ensure adequate photon absorption while allowing for the rapid diffusion of excitons to their respective electrodes. Most examples of these blended materials are composed of two compounds, a conjugated compound for donor components and fullerene compounds for acceptor materials, although several other compounds have been explored as acceptor materials.^{63–65} Additionally, ternary blends incorporating additional compounds have been used for either charge transfer, energy transfer, or parallel linkage interfaces.⁶⁶

Organic materials are attractive to those in the field of photovoltaics due to the tailorability of the compounds as well as the subsequent ability to tune the properties of the material.⁵⁶ Compounds such as copper phthalocyanine and C₆₀,^{67,68} tetracene,⁶⁹ and pentacene⁷⁰ have been used as semiconductors in OPV devices; however, these compounds are incapable of adopting

glassy phases. The use of molecular glass compounds would be ideal for the design of OPV technologies due to their low cost, low molecular weight, high purity, ease of purification and the ability to produce thin films. Several types of molecular glasses have been used in OPV technologies. Star-shaped molecular glass **32** was employed as the organic layer between indium tin oxide (ITO) and aluminum electrodes in a Schottky-type device.⁷¹ Compound **32** has also been applied for electron donor layers with tris(8-hydroxyquinolato)aluminium as the electron acceptor.⁷²

Additionally, mexylaminotriazines have been synthesized to incorporate a number of compounds for use in OPV technologies, such as diketopyrrolopyrrole (DPP),⁶³ perylene diimide (PDI),⁶⁴ and squarylium cyanine (SQ)⁶⁵ derivatives. DPP and PDI derivatives are promising as non-fullerene acceptor materials while the SQ derivatives serve as donor materials.^{64,66} These compounds were also investigated for use in a number of blended materials. While early attempts to produce molecular glass derivatives of these compounds yielded modest efficiencies, they did demonstrate much more consistent behaviour and efficiencies comparable to some non-glass forming organic compounds used for OPV devices.^{63,64,66} For example, the novel DPP-mexylaminotriazine was compared to a crystalline analogue and subsequently shown to consistently yield higher efficiencies.⁶⁴ The greater efficiencies obtained were attributed to the fewer defects and higher homogeneity of amorphous thin films.⁶⁴ These reports highlight the advantages of glass-forming small-molecules for the production of acceptor materials for OPV devices. Thin films of these materials can be more easily processed and prepared in comparison to their crystalline counterparts while inducing fewer defects. As a result, mexylaminotriazines functionalized for acceptor materials are promising compounds for the fabrication of high-performance OPV devices.⁶⁴

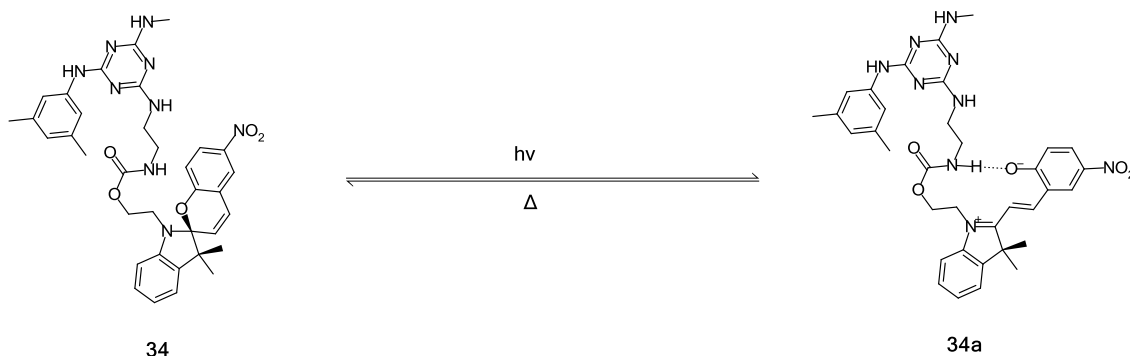
2.1.4.2.4. Molecular Glasses in Photochromic Technologies

Another application of molecular glasses is in the design of photochromic materials. Photochromism describes the reversible transformation of a chemical species on exposure to electromagnetic radiation. The change results in two different forms of the material, each possessing different absorption spectra and subsequently displaying different colours.⁷³ A common example of a photochromic material is in eyeglasses that change tint according to lighting conditions. Photochromic materials are utilized for other applications in image formation, optical data storage, and optical switching.⁵⁰ The nature of these applications requires the materials to be processed into thin films. While photochromic materials have been successfully dispersed and bound to polymer mediums capable of forming thin films, this strategy has its challenges, including ensuring dispersal, purity, and molecular control.³⁵ Amorphous molecular glass materials functionalized with photochromic groups are an excellent alternative for the formation of photochromic thin films. In fact, the synthesis of star-shaped photochromic molecular glasses has been demonstrated, including compounds based on azobenzene chromophores such as 4,4'-bis[bis(4'-*tert*-butylbiphenyl)amino]azobenzene.³⁵ It was shown that this glass-forming azobenzene derivative exhibited reversible photoisomerization from *trans*- to *cis*-isomers when irradiated with alternating 450 and 550 nm light. Despite significant alterations to the molecular structure, the presence of glass-forming substituents did not affect the photochromic behaviour of the azo dye.³⁵

Dithienylethene-based compounds are another series of compounds which have been studied for their photochromic properties in solution.⁷⁴ While dithienylethene compounds do not readily form thin films, several star-shaped compounds have been synthesized by Shirota *et al.* to

include diarylamino substituents that can form a glassy phase.³⁵ One compound of these star-shaped molecules was subsequently shown to exhibit both the photochromic and glass-forming properties of the two parent compounds. Excitedly, these new compounds exhibited photochromic properties similar to the parent compound in both solution and thin film phases.⁷⁴ Irradiation with 360-580 nm light gives the photocyclized form, leading to a coloured product. Contrarily, the colourless product can be restored by treatment with visible light above 580 nm, thereby causing the opening of the ring.⁷⁴

Mexylaminotriazines have been used to synthesize glass-forming photochromic compounds. First reported in 1952, spiropyrans are a class of photochromic materials that have been employed for applications such as optical memory, sensors, photoswitches, and holography because of their reversible photoisomerization. Irradiating spiropyrans with UV light breaks the C-O bond, resulting in a ring opening and rearrangement to a coloured product.⁷⁵ The Leibel group successfully synthesized and characterized a novel spiropyran that incorporated a mexylaminotriazine glass-forming moiety (**34**).⁷⁵ Similar to other mexylaminotriazine analogues, the resulting compound was shown to form stable glassy phases that resisted crystallization when subjected to both heating and long periods at ambient conditions. The mexylaminotriazine-functionalized spiropyran was further shown to undergo the reversible ring-opening to the coloured product (**34a**).⁷⁵ Scheme 13 depicts compound **34** and its photochromic transformation to **34a**.

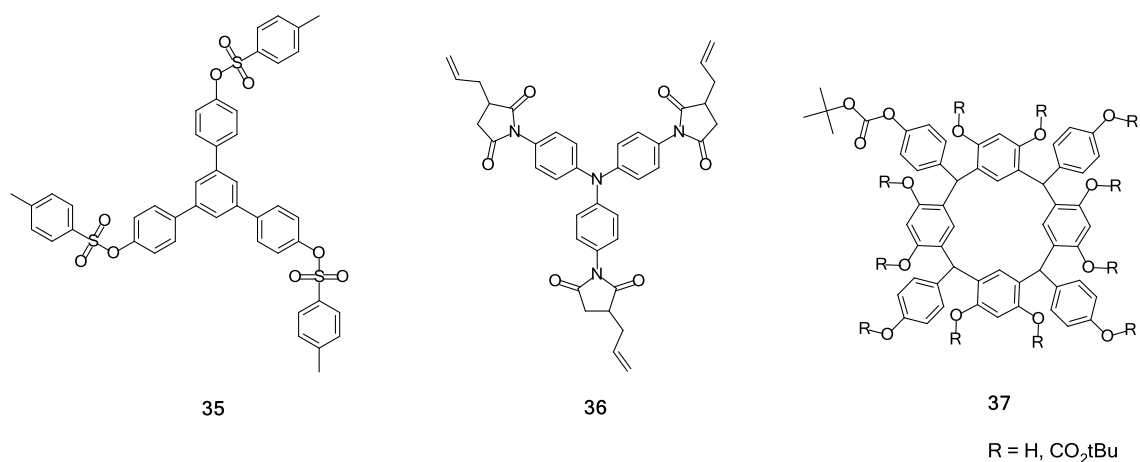


Scheme 13: Glass-forming spiropyran compound **34** and the photochromic changes induced by treatment with 365 nm light to produce a coloured compound **34a** and the thermally reversed ring closure to **34**.^{74,75}

2.1.4.2.5. Molecular Glasses in Lithography

Lithography is a printing technique in which three-dimensional images are formed from the transfer of patterns of media from one surface onto a substrate.⁷⁶ Nanolithography simply refers to lithographic patterning methods used to generate features smaller than 100 nm.⁷⁶ In semiconductor lithography, the patterns are traditionally made using light-sensitive polymers. When exposed to light, a cross-linking reaction occurs, transferring the media to the substrate. The use of a mask blocks regions from being exposed to the light treatment, subsequently generating areas where no media is transferred, and hence the intended patterns.⁷⁶ Molecular glasses are a viable alternative to the polymer media traditionally used. Glass-forming compounds that do not crystallize within the time scale of the application's use can be used to generate patterns with higher quality resolution.⁷⁷ The nature of the synthetic procedures employed to produce polymers results in materials that consist of a range of molecular weights and thus many physical properties of the

polymer are a summation or composite value of the molecular weight distribution. Contrarily, molecular glasses are monodisperse and homogeneous, typically smaller, and have a lower free volume, leading to constant dissolution rates, lower residual stress swelling, and no chain entanglements. Novel low molecular-weight organic materials synthesized for nanolithography are expected to be amorphous molecular compounds for the benefits described above. Like their polymer counterparts, these materials are employed in a mixture with a cross-linking agent and a photoacid generator applied to a substrate. Irradiation of the mixture produces a photoacid in the exposed regions. This acid catalyzes cross-linking reactions between functional groups on the molecular glass molecules and the cross-linking agents, forming a new oligomer in exposed regions. The newly formed cross-linked oligomers typically form insoluble network patterns. Following irradiation, the material is treated with a solvent that is used to develop the resist by removing the un-irradiated mixture, leaving behind the desired patterns.⁷⁸ Several examples of amorphous compounds have been reported and evaluated for nanolithographic application, such as 1,3,5-tris[4-(4-toluenesulfonyloxy)phenyl]benzene (TsOTPB) **35**, 4,4',4''-tris(allylsuccinimido)triphenylamine (ASITPA) **36**,⁷⁷ and C-4-hydroxyphenyl-calix-[4]resorcinarene (**37**)⁷⁹ (Scheme 14). Compounds **35** and **36** were found to produce high resolution features and resists with line patterns smaller than 150 nm.⁷⁷ Compound **37**, in particular, was shown to be capable of forming features around 30 nm in size.⁷⁹



Scheme 14: Molecular glass compounds (**35-37**) used for nanolithographic applications.^{77,79}

2.1.4.3. Catalysis

A promising future application where molecular glasses are not yet used is in the field of catalysis. Catalysis is an acceleration or retardation of the rate of a chemical reaction due to the addition of another substance, known as a catalyst, to the reaction media.⁸⁰ Some catalysts are also capable of influencing the selectivity or specificity of the products from a reaction. These aspects of catalytic activity can translate directly to energy savings, less pollution, fewer side products, lower production costs, and greater overall efficiency.⁸⁰

Catalysts can be described and classified according to their phase relation with the chemical reactants being used. Homogeneous catalysts are present in the same phase as reactants and products (generally in solution), while heterogeneous catalysts are found to be in a different phase (typically a solid catalyst interacting with reactants in a gas or liquid phase).⁸¹ Each class of catalyst possesses its own intrinsic advantages and disadvantages concerning their application and use. As

a whole, homogeneous catalysts provide single active sites generating greater control and selectivity of products, while heterogeneous catalysts are important to industry for their ease of separation and recyclability. Homogeneous catalysts, while typically transition metal complexes, can also be organic compounds.⁸² Many heterogeneous catalysts incorporate organic or inorganic structures, which support various catalytically active sites. Some examples of heterogeneous catalysts include transition metals, transition metal oxides, zeolites, and silica- and alumina-based compounds.⁸³ Despite a great deal of control over the catalysts structure, homogeneous catalysts often require continuous addition to reactions and may be difficult to separate. Alternatively, a challenge associated with many heterogeneous catalysis is the number of wasted active sites. The heterogenization of single-site homogeneous catalysts is of particular interest. This concept allows for the amalgamation of the respective advantages of both types of catalysts: the recyclability, processability, and easy separation of heterogeneous catalysts with the selectivity and structural tunability of homogeneous catalysts. For example, the use of homogeneous catalysts in biphasic systems or by fixation on support systems is technique that is being used to bridge the gap between the two forms of catalysts. This emerging field of research is sometimes known as “semi-heterogeneous” catalysis. Research regarding the ability to attach homogeneous catalysts to a solid support material has been a topic of particular interest for nearly twenty-five years.^{84,85}

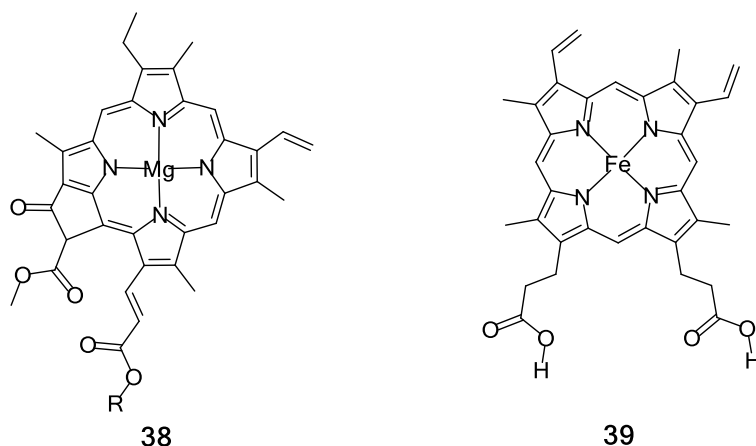
Many heterogenization techniques utilize highly porous materials to bind and support catalysts; however, these techniques often lead to many valuable active sites being isolated within the interior structure of these materials. This can render many sites useless and unable to interact with the reactants of a given reaction or process. While these techniques are suited for packed columns or reactors, they are not suited to produce active coatings on the surface of other substrates. One proposed solution to address this gap is the suspension or dispersion of catalytically active materials onto the surface of the support system to limit waste and cost.⁸¹

Due to the limitations of many current catalytic materials, there is a requirement for a novel class of chemical catalyst capable of a high degree of specificity, while possessing the necessary processability desired for heterogeneous applications. A thin film material is particularly desirable to achieve the processability objectives. By depositing thin layers of catalytic materials onto a surface, thin films can be used to produce catalytic materials that are more flexible, adopt various shapes or forms, and cover a variety of surfaces within reactors. Additionally, these materials can be more cost-effective as they are relatively simple to apply, fabricate, and they minimize the number of active sites lost to the internal structure of many traditional bulk materials. As such, the development of thin film catalytic materials could address the requirements of a heterogeneous catalyst. The design of compounds and materials that adopt stable glassy phases are ideal for the fabrication of thin films. In terms of developing catalytic thin film materials, homogeneous catalysts, such as coordination compounds utilized for a variety of applications, could be functionalized with substituents that promote glass formation. This proposed class of glass-forming catalytically active coordination complexes could help to bridge the gap between homogeneous and heterogeneous catalysis.

2.2. Coordination Chemistry

A coordination complex consists of a central atom or ion (usually a metal), called the coordination centre, and a surrounding array of bound molecules or ions, called ligands. Coordination complexes display interesting properties in terms of electronic absorption spectra, magnetic properties, and many more that would be difficult to achieve with all-organic compounds.¹ Coordination complexes play a vital role in many chemical and biological systems,

an example of which is the green magnesium complex known as chlorophyll. Chlorophyll (**38**), a compound found in plants and vital to the survival of all life on earth, is involved in the process of photosynthesis. In chlorophyll, the coordination of an organic molecule to a magnesium centre allows plants to absorb visible light from the sun and harness its energy to produce other valuable chemicals in the form of sugars used by the plant as energy.¹ The energy converted and stored from the sun is the base of all food energy in ecosystems. All oxygen-breathing organisms also utilize coordination compounds known as cytochromes, which contain a heme-group. Heme is an organic compound containing a porphyrin ring, which binds iron atoms, a few heme analogues exist. Heme-groups are directly responsible for the transport of oxygen throughout the circulatory system. Oxygen is necessary for most organisms to produce their own energy from the molecules and nutrients absorbed from food.¹ The core of these compounds, an Fe(II) center, is capable of performing oxidation and reduction reactions that are central to many processes. Scheme 15 shows the structure of the two aforementioned coordination complexes, chlorophyll (**38**) and heme B (**39**), the most common analogue of heme.



Scheme 15: Structures of two biological coordination complexes, chlorophyll (**38**) and heme B (**39**).

Furthermore, many transition-metal coordination complexes are catalytically important. As discussed earlier, many catalysts possess active sites containing metallic atoms.⁸⁶ These catalysts can activate substrates, accelerate reactions *via* various mechanisms, and are efficient in promoting a number of reactions and processes.⁸⁶ Although many organic-based catalysts exist, these have often been surpassed in efficiency and application by the success of transition-metal complexes.⁸⁷ The nature of many transition-metal complexes and their coordinated ligands allows for a high degree of selectivity, efficiency, and tailorability. Many transition metal complexes are used for catalytic purposes; however, the range of applications for metallic complexes is extremely extensive.¹⁸ The interaction between the organic ligands and the metal centres is important to the application of these complexes. Various ligands have been identified for particular uses and fields. The alteration of these ligands enhances the steric and electronic properties of these complexes, allowing them to adopt many desirable properties and behaviours.

Metals possess the ability to form unique compounds with distinct properties that can be tuned by modifying the chemical groups to which they are bound. These chemical groups, which are known as ligands, can be either neutral or charged, and are generally organic, containing Lewis

base atoms (like N or O). These atoms bind to a metal center by donation of a lone pair of electrons, thereby creating a coordination complex.¹ The formation of a complex results in changes to the steric and electronic properties of both the metal centre and the ligands.⁸⁶ These properties are altered by the presence of groups on the ligand that surround the metal centres and can change the way that electrons are donated or shared between the metal and ligands.

For the purposes of application, a class of ligands for proposed coordination complexes is often selected as the result of a number of factors. First, selecting well-studied ligands is helpful for researchers who wish to develop a well-defined picture of the ligand's properties, coordination chemistry, as well as the applications and capabilities of a class of ligands before investigating further. Additionally, optimization of a complex's structure and electronic properties is frequently required. As such, selecting ligands that permit the variation of a number of substituents can be desired. Next, the ligand's ability to coordinate with a variety of metals, in a myriad of oxidation states, is an important factor for the ligand's utilization in a number of roles. Lastly, the use of ligands that are difficult to procure or synthesize possess more limited use and application. As such, it is ideal to utilize ligands that are relatively simple and straightforward to synthesize from commercially available reagents and starting materials.

2.2.1. Molecular Glass Metal Complexes

Coordination complexes exhibit interesting optical, electronic, and catalytic properties that have proposed applications in many fields. Typically, these materials exist as crystalline solids and while they can be used in solution or supported on substrates such as polymers, the preparation of glass-forming coordination complexes could expand the use of these materials to many novel applications. Despite recent advances in the synthesis of glass-forming organic compounds, only a few glass-forming coordination complexes with discrete structures have been reported. In 2004, the Iida group published a study introducing glass-forming yttrium(III) complexes.¹⁸ The study in question synthesized a number of coordination complexes based on the structure of tris(octadecanoato)lanthanide complexes.¹⁸ These water-insoluble compounds are used in drying, curing, waterproofing, and lubricating processes.⁸⁸ Six complexes were prepared of which two; tris(N-hexanoyl-DL-alaninato)yttrium(III) and tris(N-octanoyl-DL-alaninato)yttrium(III), were described as easily adopting a stable glassy phase through the evaporation of a methanol solution. The remaining complexes demonstrated an array of glass-forming behaviour in which complexes with mixed crystalline-glassy phases were obtained, as well as complexes that were only capable of forming crystalline phases.¹⁸ Additionally, Iida *et al.* recognized the role of ligand structures on the glass-forming properties. Primarily, they noticed that the alkyl chain length of the ligands was a factor and that shorter chain lengths were associated with a higher propensity to form glasses.¹⁸ Ultimately, the work of Iida *et al.* demonstrated the successful preparation of a number of molecular glass metal complexes; however, the ligand structures utilized in this report are unable to adopt glassy phases themselves.¹⁸ While the authors reported the preparation of several metal complexes that exhibited glass formation, the intention of the authors was not to design or develop a strategy to prepare molecular glass complexes.¹⁸ In order to prepare and design molecular glass coordination complexes with any degree of predictability, a strategy must be developed and employed. Instead, a series of ligands that demonstrate a strong propensity to form glassy phases could be synthesized, from which a library of corresponding coordination complexes could be prepared.

At present, there is limited information regarding the synthesis of glass-forming chelating ligands or the preparation of glass-forming coordination complexes. As described in section 2.1.3.3.3, the Lebel group has published a class of compounds based on the mexylaminotriazine core that are capable of reliably adopting amorphous glassy phases.⁴³ The synthesis of these compounds is relatively straightforward and the synthesis *via* step-wise substitution reactions allows for a high level of synthetic control and tailorability. Additionally, it has been demonstrated that the mexylaminotriazine class of glass-forming compounds can be used to functionalize other compounds in order to induce glass-forming properties.^{2,6,11,17} Several compounds were synthesized to include the glass-forming functional group and were shown to maintain the properties of their parent compounds while demonstrating new glass-forming properties and the ability to be processed into thin films.^{2,89} It is thus proposed that this family of glass-forming compounds could be functionalized in such a way as to design compounds that readily form stable glassy phases while possessing novel chelating capabilities.

3. Methods

3.1. Thermogravimetric Analysis (TGA)

TGA measures the mass of a sample as the temperature is increased, the resulting thermogram plots mass as a function of temperature and provides both qualitative and quantitative information. The apparatus for TGA is comprised of a high-precision balance, which suspends a sample pan, a furnace, along with a data recorder and auxiliary equipment to provide the inert atmosphere. By knowing the initial mass of the sample, information about the constituents may be inferred by the resulting decrease in mass as temperature is increased. Primarily, this technique is used to determine the decomposition temperatures of the compounds and can provide additional insight about decomposition mechanisms by monitoring the mass fraction of the gases released at given temperatures. This information is also necessary for safely analyzing the compounds *via* differential scanning calorimetry, which has sensitive sensors and where decomposition must be avoided, especially when it is accompanied by the evolution of gas. Thermogravimetric analysis for glass-forming ligands and their respective complexes were performed on a TA Instruments TGA Q50 thermogravimetric analyzer to determine the decomposition temperatures of the compounds. The temperature was increased from ambient temperature to a maximum temperature of 450 °C to 600 °C at a rate no greater than 10 °C/min.

3.2. Differential Scanning Calorimetry (DSC)

Differential Scanning Calorimetry (DSC) is a thermal analysis technique that looks at how a material's heat capacity (C_p) is altered by temperature. The glass transition temperature (T_g) is the temperature at which amorphous materials undergo a transition from the glassy state to the rubbery (or viscous) state. As a glass is heated, its heat capacity increases and it adsorbs more heat. The apparatus increases the temperature in the chamber at a specific rate, known as the baseline increase. At the glass transition, enough energy is available in the material that it becomes mobile. Unlike a melting transition, which is a first order transition and therefore accompanied by a change in enthalpy, the glass transition is the result of a variation in heat capacity between the glassy state and the viscous state. DSC plots the change in heat flow (W/g) as a function of the temperature (°C) of the system. The glass transition appears as a step change in the instrument baseline. It occurs over a wide temperature range, typically on the order of 10 °C, and is generally reported at half the height of the heat capacity change or the inflection point of the function through this range. In contrast, the melting point will occur very suddenly and appears as either a sharp dip or peak depending on the orientation of exothermic changes in the software. This is because the material will not continue to increase in temperature until all of the molecules have reached the same temperature and melted. This is due to the first order nature of the melting point phase transition.

The apparatus consists of two pans, one containing a sample of known mass to be analyzed and another empty pan as reference. The pans are placed on separate heaters and enclosed in a cell. The apparatus consists of a high precision heating chamber, a computer with special software that controls the furnace, sensors, and auxiliary equipment that provides an inert atmosphere. Analysis is controlled by the software, which begins to increase the temperature of the heaters at a specific rate. More importantly, the computer ensures that the pans are heated at the same rate. As a result of the extra material in the sample pan, the sample pan heats at a different rate. The computer tracks the changing heat capacity and heat flow in the cell. This allows the detection of transitions such as glass transitions, phase changes, and curing. DSC was used in this research project to

measure the glass transition temperature and determine if any other phase changes in the ligands and subsequent complexes occurred. DSC measurements were made using a TA instruments Q20 differential scanning calorimeter. In this experiment, all T_g values reported herein were recorded after an initial heating-cooling cycle in which the materials were melted and residual solvents were removed. Samples were heated at a rate of 5 °C/min to approximately 250 °C, unless otherwise noted. T_g values reported in this report are the average of two runs. Standard deviations for the two runs are noted in parentheses in the appropriate tables. The selected heating rate is slow enough to allow for the monitoring of crystallization processes.

3.3. Spin Coating

Thin films of appropriate samples were prepared by spin-coating samples on pieces of silicate glass. Spin-coating was performed by preparing solutions of the corresponding complexes in CH_2Cl_2 (8 mg of solute in 1 mL solvent). Several drops were placed on a piece of substrate, which was then spin-coated at 1500 rpm for 20 seconds. This process was repeated two additional times for each sample to prepare uniform thin films.

3.4. UV-Vis Spectroscopy (UV-Vis)

UV-Vis spectroscopy measures the absorption in the ultraviolet-visible region of the electromagnetic spectrum. Absorption of visible and ultraviolet radiation is associated with the excitation of electrons from lower to higher energy levels in both atoms and molecules. For example, if the sample is irradiated with the appropriate level of energy, electrons may be excited from a bonding (σ , π), or non-bonding (n) orbital into an empty higher energy anti-bonding orbital (σ^* , π^*). UV-Vis spectrometers measure the absorbance of radiation in this region of the electromagnetic spectrum. A source produces light, which is passed through a sample contained in a quartz cuvette. After passing through the sample, the light is passed through a lens and a small slit. After this, the light is dispersed into a diode array by a holographic grating. The intensity of light from a sample are compared to a blank (I_o), consisting of a quartz cuvette containing the solvent in which the sample will be dissolved. The blank sample is run prior to analyzing the sample solutions. This is done to account for any scattering, reflection, or absorption that can be caused by the cuvette or solvent. Next, the light passing through the sample (I) for each wavelength is also measured. If the light passing through the sample is less than that of the blank, then absorption has occurred. Absorbance of the sample (A) is related to I and I_o by the equation:

$$A = \log_{10} \frac{I_o}{I} \quad (1)$$

The light is then converted by the detector into a current, proportional to the intensity of the light. Typically, a plot of absorbance against wavelength is then generated. The concentration of the analyte (c) can then be related to absorbance according to the Beer-Lambert Law, which is expressed according to the equation:

$$A = \epsilon cl \quad (2)$$

Where A is absorbance, c is the concentration of the analyte in $\text{mol}\cdot\text{L}^{-1}$, l is the optical path length of the cell (cm), and ϵ is the molar extinction coefficient ($\text{L}\cdot\text{mol}^{-1}\cdot\text{cm}^{-1}$), which is constant for a particular substance at a particular wavelength. Consequently, UV-Vis spectroscopy has been employed for a variety of applications. In the present work, it was used to measure the absorbance of the prepared glass-forming metal complexes. UV-Vis spectroscopy measurements were taken

using a Hewlett Packard 8453 UV-Visible spectrophotometer. Spectra were taken from 200 nm to 1100 nm, using a 1.000 cm path length, in quartz cuvettes. Samples were prepared by dissolving 1 mg of solute in the appropriate amount of CH₂Cl₂ required (usually 50 mL) to achieve an absorbance value below two absorbance units. Samples of known concentration were used to calculate an extinction coefficient (ϵ) based on each samples maxima absorbance using equation 2.

3.5. Fourier-Transform Infrared Spectroscopy (FTIR)

The section of the electromagnetic spectrum known as the infrared region comprises wavelengths ranging from 0.78 μm to 1000 μm , or in wavenumbers from 12,800 – 10 cm^{-1} . This section is further sub-divided into near, middle, and far-infrared radiation for the purposes of application and instrumentation. Infrared spectroscopy has been extensively implemented in the identification of pure organic compounds, as the numerous maxima and minima of a spectrum give rise to a theoretically unique spectrum for each compound, barring optical isomers.⁹⁰ The absorbance pattern recorded from infrared spectroscopy correlates to specific resonant frequencies for a molecular structure. Absorbance occurs when the frequency of vibration of a given bond aligns with that of the irradiating radiation. The absorbance at a given frequency is inferred from the measured transmittance. As the energy of a given bond is dependent on its neighbouring atoms, the vibration patterns for bonds found within many common chemical groupings, such as functional groups, have been well documented. For this work, spectra were recorded using a Perkin Elmer FT-IR System Spectrum GX spectrometer (4000-500 cm^{-1}). Samples were prepared for analysis by forming thin films of the respective ligands and complexes from the evaporation of CH₂Cl₂ solutions on KBr windows.

3.6. Magnetic Measurements

Electrons are charged particles, which possess angular momentum coming from both spinning around their axes and orbiting about atoms. A charged spinning object generates a magnetic dipole, where the two poles are of opposite polarity. This means that when an external magnetic field is applied to electrons, torque will be exerted on them; where a competition exists between the thermal tendency towards randomness of the spins and the field's capacity to force alignment. The magnetic dipole moment of an electron is a vector whose directionality is from the "south" to "north" pole of a magnet and whose magnitude is proportional to the magnetic field of the electron. Paired electrons are of equal and opposite spin, and therefore their magnetic moments negate one another, referred to as diamagnetism. However, unpaired electrons lack this inter-electron counter balancing and subsequently act as magnets, referred to as paramagnetism. They may align themselves as parallel or anti-parallel to a magnetic field. A parallel orientation is more energetically favourable; however, the transition to anti-parallel may be observed when an appropriate external electromagnetic frequency is applied to the sample. In the absence of an external field, the individual molecular moments are randomized by thermal motion.

The magnetic field inside a substance that is placed in an external magnetic field will depend not only on the magnitude of the applied field but also upon the ability of that substance to produce its own field, which will add to (paramagnetic) or subtract from (diamagnetic) the applied field. The magnetic induction of the field within the substance, B , is given by equation 3, where H_o is the intensity of the applied field, and I is the intensity of magnetization of the substance.

$$B = H_o + 4\pi I \quad (3)$$

The ratio I/H_o is a measure of the susceptibility of the substance to interact with an applied field and is called the volume susceptibility, X_v .

$$X_v = \frac{I}{H_o} \quad (4)$$

The volume susceptibility is usually converted to susceptibility per gram of substance by dividing by its density, d , in g/cm^3 . This value is called the mass susceptibility, X_g , and can be calculated by equation 5;

$$X_g = \frac{X_v}{d} \quad (5)$$

The magnetic susceptibility per mole of substance, X_m , is of most value for chemical applications. It is obtained by multiplying X_g by the molecular weight, MW , of the compound to obtain the susceptibility per mole. This is shown in equation 6 below;

$$X_m = X_g * MW \quad (6)$$

The molar susceptibility, X_m , is positive if the substance is paramagnetic and negative if it is diamagnetic. The X_m of a compound is the sum of the susceptibilities of both the paramagnetic electrons in the complex and of the diamagnetic contributions of the other groups and ligands present. This concept is summarized and depicted by the relationship in equation 7.

$$X_m = \text{paramagnetic contributions} + \text{diamagnetic contributions} \quad (7)$$

The paramagnetic contributions of the complex are primarily from the metal atom, more specifically the unpaired d electrons, while the diamagnetic contributions originate from the many other components of the complex. As such, a corrected susceptibility of only the unpaired electrons, X'_m , can be determined by using the additive relationship of this phenomenon. Equation 8 demonstrates a rearranged method to calculate for the corrected paramagnetic contributions;

$$X'_m = X_m + X_{m \text{ dia.}} \quad (8)$$

In equation 8, the last term, $X_{m \text{ dia.}}$, is the sum of the diamagnetic contributions of the paired electrons of the inner core of the metal, the ligands, and the counter ions, and is a negative value. Thus, in order to determine the magnetic susceptibility of the unpaired electrons in the complex, it is necessary to correct for the diamagnetism of the other groups. It is known that susceptibilities of diamagnetic groups change very little with their environment; hence, it is possible to calculate the diamagnetism of a molecule by adding the diamagnetic contributions of structural components of the molecule. There are many reports that provide the diamagnetic corrections for some ligands, metal centres, and counter ions.^{91,92}

For a paramagnetic metal ion, it is customary to quote the magnetic moment, μ_{eff} , rather than the corrected molar susceptibility X'_m . This value is reported in Bohr magnetons, a physical constant and natural unit for expressing the magnetic moment of an electron. These two values are related *via* the following equation, equation 9. Where N is Avogadro's number, k is Boltzmann's constant, T is temperature (K), and U_B is Bohr magneton.

$$\mu_{\text{eff}} = \sqrt{\frac{3kTX'_m}{NU_B^2}} = 2.828\sqrt{T * X'_m} \quad (9)$$

In order to correctly calculate μ_{eff} , it is therefore necessary to determine the temperature dependence of X'_m . Temperature has a randomizing effect on the magnetic moments in a compound. A temperature dependence study requires equipment that is more sophisticated. As such, we will assume that X'_m follows the Curie Law, which states that the magnetization of a paramagnetic material is inversely proportional to the temperature of the material for a fixed field. This is a safe assumption and common for this type of analysis as at normal temperatures and in moderate magnetic fields, the paramagnetic susceptibility is small. It is at very low temperatures (<100k) that a more drastic variation would be observed and more likely to influence results. By assuming that all compounds obey Curie's law, the μ_{eff} is independent of temperature, which simplifies the calculation.

The μ_{eff} can then be used to determine the number of unpaired electrons in a complex. In compounds containing unpaired electrons, both the spin angular momentum and the orbital angular momentum of the electrons can contribute to the observed paramagnetism. However, for complexes of transition metal ions, the orbital contribution is largely quenched by the field due to the surrounding ligands. In this case, we can use the spin-only formula, equation 10, to determine the number of unpaired electrons, where n = the number of unpaired electrons and U_B is the bohr magneton. Through a number of calculations, it is possible to determine the number of unpaired electrons in the complex. This allows for the determination of many properties such as the geometry, magnetic properties, and characterization of a particular complex. This information is extremely helpful in characterizing various complexes. Common values of μ_{eff} as a function of n are reported in the literature.⁹¹

$$\mu_{\text{eff}} = \sqrt{[n(n + 2)]} U_B \quad (10)$$

For the present work, magnetic susceptibility measurements were performed on a Johnson Matthey MSB Mk1 magnetic susceptibility balance. Several sources were consulted in order to calculate the diamagnetic contributions by Pascal constants.^{91,92} The diamagnetic contributions for components such as ligands can also be determined using the balance by measuring the magnetic susceptibility of the uncoordinated ligand. Supplier procedures for the preparation of samples and the subsequent measurement of mass susceptibilities is described in the instruments operator manual.⁹² Measurement with a mass susceptibility balance allows one to calculate the mass susceptibility, X_g , through equation 11.

$$X_g = \frac{l}{m} \left(\frac{C_{Bal}}{10^9} * (R - R_0) + X_{v \text{ air}} * A \right) \quad (11)$$

In this equation, C is the constant of proportionality, R is the reading obtained from the sample filled tube, R_0 is the empty tube's reading, l is the length of sample in the tube (cm), m is the mass of the sample (g), A is the cross-sectional area of the tube, and X_v is the volume

susceptibility of the displaced air. For powder samples, the air correction term, $X_{v\ air} * A$, can be ignored. C , the constant of proportionality, is related to the calibration constant of a given balance. This can then be used to solve the equations described earlier in order to calculate the number of unpaired electrons, determine a number of properties, and characterize the metal complexes. In this report, the μ_{eff} will be utilized for characterization of the metal complexes and their geometry, as the number of unpaired electrons depends on the geometry of the metal center and the differential between electronic energy levels of the d orbitals. Several other methods exist for measuring magnetism and determining the structure of metal complexes; however, these analytical techniques typically require crystalline products. Mexylaminotriazine compounds have been specifically designed to resist crystallization and as such, many of these methods are not viable. Rather, a magnetic susceptibility balance such as the one described can analyze the magnetism of both amorphous and crystalline materials. The subsequent μ_{eff} that is calculated can be used as a piece of a larger puzzle to explore, describe, and determine the structure of these metal complexes. This is further validated by comparing the results from the glass-forming complexes to non-glass forming analogues in the literature.

3.7. Nuclear Magnetic Resonance Spectroscopy (NMR)

Nuclear magnetic resonance (NMR) spectroscopy is a widespread characterization technique used in the structural determination of organic and coordination compounds that examines the frequency at which spin state separation of a specific set of nuclei occurs in an externally applied magnetic field. Samples are measured in a solution of a deuterated solvent, such as DMSO- d_6 or CDCl $_3$. This information can then be used to characterize the nature of the chemical environment surrounding that nucleus. ^1H , ^{19}F , heteronuclear single quantum coherence spectroscopy (HSQC), and ^{13}C NMR spectra were recorded at room temperature with a Bruker Avancé 400 MHz spectrometer, unless otherwise noted.

3.8. Mass Spectrometry

High resolution mass spectrometry (HRMS) is a technique frequently used for the identification and quantification of molecules according to their mass-to-charge ratio (m/z). This technique can be employed for determining the molecular weight of compounds which can be then used to elucidate the likely elemental composition. The technique functions by generating charged particles from a chemical substance that can then be analyzed by separating the various ions in an electric or magnetic field according to their mass-to-charge ratio. Although there are many different types of mass spectrometers, all instruments of this type consist of an ion source which ionizes the chemical species to be analyzed, a mass analyzer which separates the ions by mass in an electric or magnetic field, and an ion detector which produces a signal from the separated ions that is used for interpretation. The technique for ionization can vary drastically based on the type of spectrometer, the type of data desired, as well as the physical properties, such as the molecular weight and phase, of the sample to be analyzed. Three common ionization techniques were utilized in the analysis of the complex molecules in this report. Electron ionization (EI) is a technique in which a beam of electrons is passed through a sample in the gas phase. Ions are formed when an electron collides with a neutral analyte molecule, forming molecular ions or fragment ions. This technique is good for small volatile molecules, but the formation of fragment ions can sometimes be undesirable, and occasionally the molecular ion's signal can be weak or absent. Electrospray ionization (ESI) produces ions by spraying a solution of sample across a high potential from a needle to form an ionized aerosol. Heat and gas are used to desolvate the aerosol, leaving the ions behind. This technique is good for producing ions of large compounds that are charged, polar, or

basic without causing fragmentation. Additionally, this technique is frequently employed as it permits the detection of mass-to-charge ratios that are within the capabilities of most spectrometers while producing limited background interference. While this method avoids any fragmentation; however, this technique can produce multiple-charged ions that often require more intensive interpretive and mathematical transformation to analyze. Matrix-assisted laser desorption/ionization (MALDI) is the third technique utilized. MALDI produces ions by irradiating a mixture of the sample in a solid matrix such as sinapinic acid or dihydroxybenzoic acid which absorbs the radiation, forming a plasma that results in vaporization and ionization of the analyte. MALDI is a fast, convenient, and simple technique that produces singly charged ions which can be highly desirable for reporting accurate molecular masses of large, non-volatile molecules. However, the matrix can result in interferences and requires a mass analyzer that is compatible with pulsed ionization techniques. Ionization of the molecules results from the loss or gain of an electron. The charge received enables the mass analyzer to accelerate some ions through the system, separating them based on their mass-to-charge ratio.

In this report, HRMS has been used to confirm the structure of the synthesized ligands and complexes. Samples were sent to an accredited laboratory for analysis. The appropriate techniques were selected by qualified personnel at the analytical laboratory according to the expected molecular weight and chemical properties of each sample. The corresponding technique used for each respective sample is indicated along with mass spectrometry results in the appropriate experimental sections later in this report.

4. Salen-Functionalized Molecular Glass Complexes

4.1. Introduction

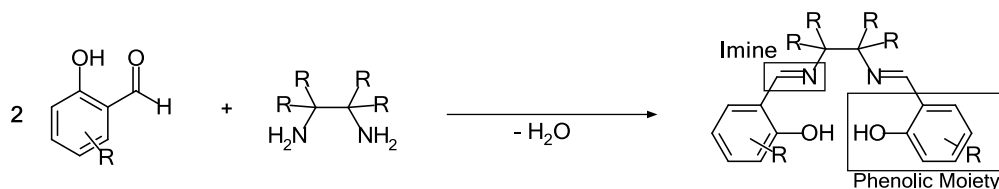
Thin film materials are utilized in a variety of fields for applications such as heterogeneous catalysts, sensors, and various optoelectronic devices.⁴ Compared to the traditional method of using polymers to produce functionalized thin films, small molecules offer easier purification and characterization. Additionally, their homogeneous dispersion leads to more predictable behaviour and properties through the materials and between different samples.⁴ Undesirably, small molecules tend to have difficulty adopting glassy phases without the use of special processing techniques, such as quenching with liquid nitrogen, and exhibit poorer stability in the amorphous phase as they generally crystallize when heated to temperatures above their glass transition, or upon standing for prolonged periods of time.⁶ Molecular glasses, or amorphous molecular materials, are a class of small molecules that have been specifically designed to resist crystallization. Integrating structural characteristics such as irregular shapes, non-planarity, or conformational equilibria allows for the synthesis of compounds that readily form glassy phases and resist crystallization despite stressing the material or allowing it to rest.⁴³

The Lebel group has designed a class of compounds utilizing methylaminotriazine moieties to reliably synthesize small organic molecular materials that readily form glassy phases and exhibit a high resistance to crystallization.^{11,13-15} The formation of various conformers of similar energy with high interconversion barriers and hydrogen bonds that limit the molecular mobility of these compounds in the solid-state increase the propensity of methylaminotriazines to form glassy phases. A number of methylaminotriazine molecular glasses have been further functionalized with reactive groups in order to covalently attach other functionalities, such as chromophores or semiconductors.^{6,9,11,64,75,89} This allows the subsequent compounds to retain the properties and characteristics of both parent compounds. Using this strategy, it is hypothesized that several ligands can be synthesized in order to form corresponding coordination complexes that are capable of glass formation.

First described in 1864, Schiff-bases are ideal for the preparation of libraries of coordination compounds and for many applications because of their tailorability, simple preparation from commercially available starting materials, as well as their ability to stabilize various metals. These factors allow chemists to control the performance of the subsequent coordination complexes for numerous purposes.⁹³ This allows for the extensive study of new classes and derivatives of these compounds, building an understanding of the factors that can alter their properties. The term Schiff base is used to describe imine compounds bearing an alkyl group on the nitrogen atom.⁹⁴ These compounds possess the general chemical formula $R_2C=NR'$.⁹⁴ One of the most important classes of Schiff-bases, based on the structure of the bisimine compound, N,N' -bis(salicylidene)ethylenediimine, are colloquially known as salen ligands or salens.⁹⁵ Salens are derived from the condensation reaction between aromatic aldehydes (typically salicylaldehyde) and either an alkyl- or aryldiamine.⁹³ Salen ligands have been dubbed “privileged ligands”⁹⁶ for their: simple preparation; ability to bind a myriad of metals in various oxidation states; ability to incorporate a variety of substituents for the purposes of altering the chirality, steric, and electronic properties of the complexes; and their application as catalysts for many chemical transformations.^{93,97}

The ability to form transition metal complexes from salens has led to their use across a number of fields as ligands for coordination complexes. With four coordinating sites and space for two additional axial ligands on the metal center, the structure of the salen class of ligands greatly resembles, and in fact was inspired by, the structure of heme-containing enzymes such as the P-450 porphyrin rings found in nature.⁹³ Salens are a class of tetradentate, di-anionic ligands that can bind metal ions through four sites. These ligands coordinate to metal atoms through the two nitrogen atoms of the imine moieties as well as through two functional groups on the aldehyde substituents, usually aryloxides.^{93,98} This results in a ligand that is ideal for the coordination of transition metals with a high level of stability.⁹³ In particular, the catalytic applications of these compounds are of interest because of their chemoselectivity, enantioselectivity, and high catalytic activity.^{93,95,99,100}

Unlike the naturally-occurring porphyrin family, salens are easier to synthesize with significantly higher yields, and tend to display higher solubility in a variety of solvents.⁹⁶ Salen ligands are formed by an uncatalyzed condensation reaction between diamines and salicylaldehydes.⁹⁵ This particular condensation reaction, in which the diamine is converted to two imine groups connecting the salicylaldehydes, can be carried out in numerous reaction conditions and solvents.⁹³ Scheme 16 depicts the general synthetic route used to prepare salen ligands through the condensation reaction between salicylaldehydes and diamines. Furthermore, the structures of salens are much more easily tuned to induce changes in their steric and electronic properties.⁹⁶ This ability is invaluable for designing salen ligands for various applications.⁹³ The steric bulk of the ligand around the metal can be altered by changing the size of the substituents on the phenyl rings, particularly those in the *ortho*-positions. For example, adding *t*-butyl groups to the salicylaldehyde moieties will increase the steric hindrance of the ligand. These changes could affect the catalytic activity of corresponding complexes by blocking coordination sites or making new coordination sites available on the metal. Alterations can also be made by substituting the ethylenediamine group for 1,2-phenylenediamine, or 1,2-diaminocyclohexane groups, changing the planarity of the ligand and therefore altering the geometry around the metal. Additionally, chiral components can be integrated into the structures of salen ligands. This can be achieved by using enantiomerically pure diamines such as 1,2-diaminocyclohexane or 1,2-diphenylethylene-1,2-diamine.⁹⁵ Chiral salens, along with binaphthyls and bisoxazolidines, are the most effective ligands for the synthesis of metal complexes to be used in asymmetric catalytic applications.⁹⁵



Scheme 16: General synthetic route and molecular structure of salen ligands.

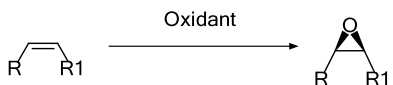
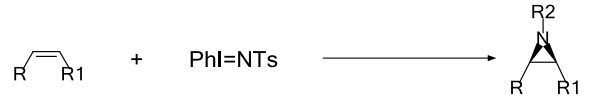

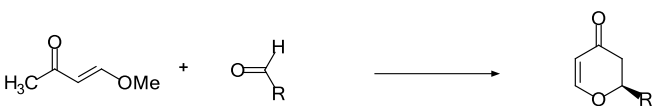




Salen ligands are actively studied for their versatility with many transition metals.⁹⁶ However, the choice of metal centre and reaction conditions during synthesis are particularly crucial for the application of these complexes.⁹³ Salen complexes have been reported for nearly all transition metals.⁹⁵ Coordination of the salen ligands to various metal atoms is typically performed using simple metallic salts.⁹³ There are numerous methods employed to produce salen complexes. For example, many salen metal complexes are prepared by treating the corresponding salen with metal salts containing built-in bases, such as metal acetates, amides, or alkoxides. These


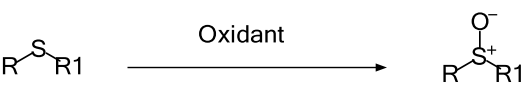
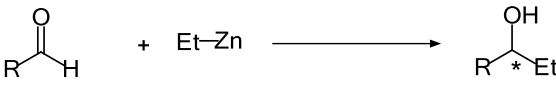
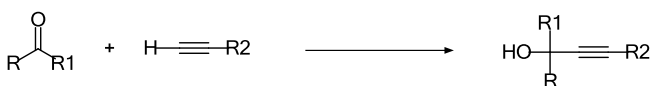

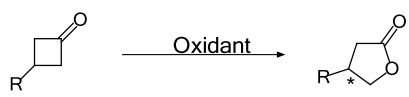
procedures typically involve refluxing a solution of ligand in the presence of a corresponding metal salt. This method is particularly effective for the preparation of Co, Ni, and Cu complexes.⁹³ Salen complexes are also often synthesized through another method involving ligand exchange of the deprotonated salen with metal halides under reflux.⁹³ This permits the use of the salen complexes under a broad array of reaction conditions including wet solvents and aqueous phases.⁹⁵ Although several other methods exist to synthesize salen coordination compounds, these two methods are the most widely employed.

The geometry around the metal of the salen complexes is often described as distorted square planar or square pyramidal depending on the presence of spectator ligands.⁹⁵ Distorted octahedral and trigonal bipyramidal geometries have also been suggested for the intermediates of salen catalysts in various reactions.⁹⁵ The distortion of these geometries is greatly influenced by the nature of the diamine backbone of the compounds. More rigid backbones, like the ones derived from aryl diamines, are associated with square planar, square pyramidal, and octahedral geometries whereas more flexible diamines can give trigonal bipyramidal structures.⁹⁵

The tailorable nature of the salen complexes allows for a great deal of variation in the structure and properties of this class of compounds. This allows for a diverse range of applications for these complexes. In particular, salen complexes have been shown to produce high catalytic turnovers and enantiomeric excesses (e.e.) in many types of chemical reactions.⁹⁵ Table 2 shows a summary of the most common reactions in which salen complexes are employed as catalysts, many of these reactions can also be performed using chiral catalysts to achieve enantioselectivity of the reaction products. It should be noted that this table offers a summary of many common reactions, with the most common metal centres employed for those specific reactions. This table is not intended to be all-encompassing.

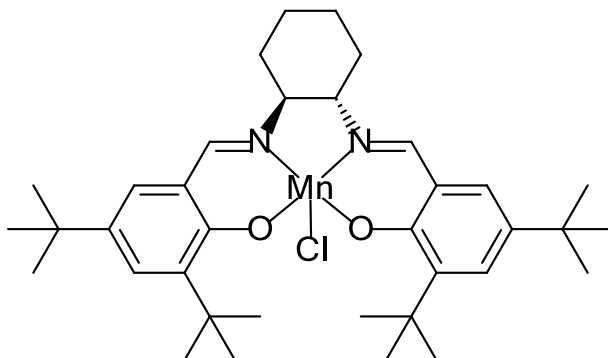
Table 2: Summary of the reaction types catalyzed by salen complexes.⁹⁵ Many of these reactions can be made enantioselective using chiral ligands.

Metal	Reaction
Mn	Alkene epoxidation ¹⁰¹ 
Cu	Alkene aziridination ¹⁰² 
Cr	Epoxide ring opening ¹⁰³ 
Cr	Hetero-Diels-Alder ¹⁰⁴ 
Co	Epoxide kinetic resolution ¹⁰⁵ 
Al	Conjugate addition of cyanide to α,β -unsaturated imides ¹⁰⁶ 
Al	Addition of cyanohydrin acid to imines – Strecker reaction ¹⁰⁷ 
Ru	Sulfimidation ¹⁰⁸ 

Metal	Reaction
Ru	Cyclopropanation ¹⁰⁹ 
Ti	Sulfoxidation ¹¹⁰ 
Zn	Addition of diethylzinc to aldehydes ¹¹¹ 
Zn	Alkyne addition to ketones ¹¹² 
V	Cyanosilylation of aldehydes – cyanohydrin synthesis ¹¹³ 
Zr	Baeyer-Villiger ¹¹⁴ 

Some of the most highly utilized salen complexes are those containing Mn(III) centres. Manganese-containing salen complexes have been extensively studied for their use as catalysts in the epoxidation of alkenes, in a process known as the Jacobsen-Katsuki epoxidation.¹¹⁵ Reports were first published in 1990 by Jacobsen and Katsuki regarding the effectiveness of manganese-based salens in asymmetric epoxidation reactions.^{93,101,116–121} Jacobsen continued to publish work in which the effects of various chiral diamines and modified aldehydes were investigated. Ultimately, N,N'-bis(3,5-di-*t*-butylsalicylidene)-1,2-cyclohexanediaminomanganese(III) chloride (**40**), also known as Jacobsen's catalyst (Scheme 17), was identified as one of the most promising manganese-based salen complex for the asymmetric epoxidation of a library of alkenes.^{93,101,116–121} This catalyst is known for its ability to enantioselectively transform prochiral alkenes into epoxides. Furthermore, Jacobsen was able to demonstrate that a number of unfunctionalized alkenes could be epoxidized by this catalyst. This was a significant breakthrough in the field of asymmetric catalysis at the time. Prior to Jacobsen's research, the epoxidation of alkenes required specific directing groups to be present on substrate molecules.^{122–126} The simple preparation of the ligand and subsequent transition metal complex has allowed Jacobsen's catalyst to become

commercially available and widely used for synthetic preparations. For example, it is used in the synthesis of the anti-cancer drug Taxol.¹¹⁹



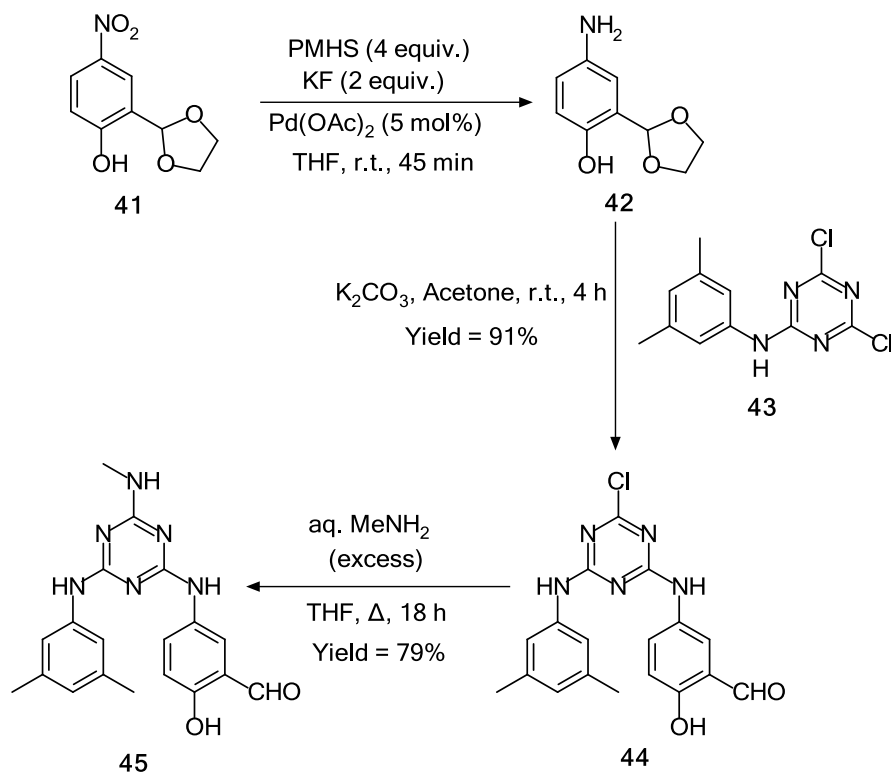
Scheme 17: Molecular structure of Jacobsen's catalyst (**40**).

The commercial production of enantiomerically pure products has grown considerably in recent years.^{127,128} Asymmetric catalysis is one of the most attractive means to generate a single enantiomer; however, the use of asymmetric catalysts in commercial production has not matched the demand for products.⁹⁵ One reason for this is that homogeneous catalysts often require expensive separation techniques in order to remove them from the reaction mixture.⁹⁵ One field that shows great potential for solving this problem and furthering the industrial application of these materials is the heterogenization of enantioselective metal complexes.⁹⁵ One of the simplest methods for the heterogenization of catalysts is to support the active catalysts by binding them onto or into an insoluble support. Salen-functionalized polymers, inorganic solids, and porous solids have been reported in attempts to bridge this divide and heterogenize these complexes.¹²⁹ The fabrication of thin films from amorphous molecular materials as support systems may provide several advantages over other support strategies due to their discrete structure, consistency, and ease of processability. The use of small-molecules to form catalytically active thin film surfaces presents a novel strategy that may address some of the shortcomings of homogeneous catalysts and several other heterogenization techniques alike. The mexylaminotriazine unit developed by our group has been shown to readily form glasses and permit the formation of thin films.¹¹⁻¹⁴ Furthermore, mexylaminotriazines present a method of introducing glass-forming properties to other molecules.^{6,63,64,75,89} In the following sections, we report the synthesis of salicylaldehyde diimine derivatives functionalized with mexylaminotriazine glass-forming substituents as well as the preparation of their respective glass-forming complexes. The salen ligand is an ideal ligand for the study and synthesis of glass-forming ligands due to their propensity to form stable metal complexes and permit a high degree of tailorability. The characterization and determination of glass-forming abilities of the synthesized ligands and corresponding complexes will also be outlined in the following sections.

4.2. Results and Discussion

4.2.1. Synthesis and Characterization of Ligands

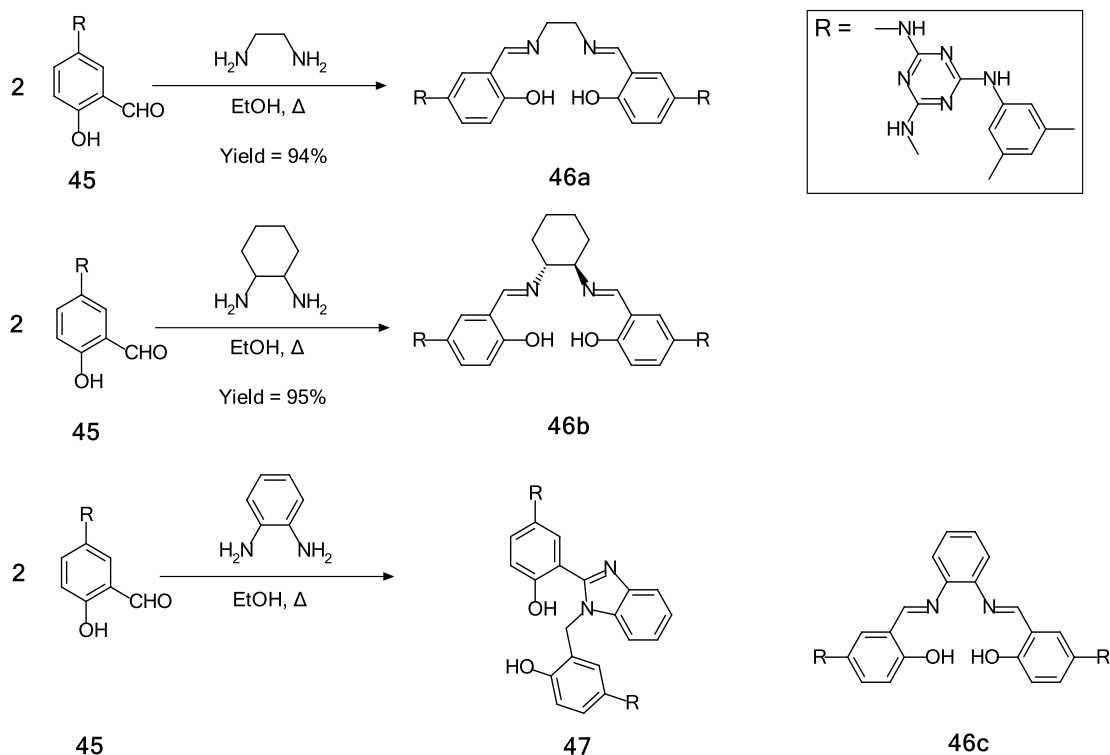
The synthetic routes used to generate salen ligands functionalized with mexylaminotriazines described in the following sections were previously established by Dr. Mahboubeh Jokar during her time with the research group. The glass-forming ligands were synthesized in several steps, beginning with the synthesis of a mexylaminotriazine-functionalized salicylaldehyde. Salicylaldehyde-functionalized glass **45** was synthesized according to Scheme 18. The ethylene acetal of 4-aminosalicylaldehyde **42** was first prepared by the reduction of nitro derivative **41** with polymethylhydrosiloxane (PMHS) and Pd(OAc)₂. As derivative **42** can readily self-condense to yield a polyimine, attempts to react it directly with 2-methylamino-4,6-dichloro-1,3,5-triazine failed. Instead, the intermediate was immediately reacted with 2-methylamino-4,6-dichloro-1,3,5-triazine **43** at ambient temperature in a one-pot procedure in which the acetal was hydrolyzed during purification to give the 6-chlorotriazine intermediate **44** in 91% yield. Substitution of the last chloride with aqueous methylamine yielded salicylaldehyde-functionalized glass **45** in 79% yield (Scheme 18).



Scheme 18: Synthesis of mexylaminotriazine functionalized salicylaldehyde **45**.

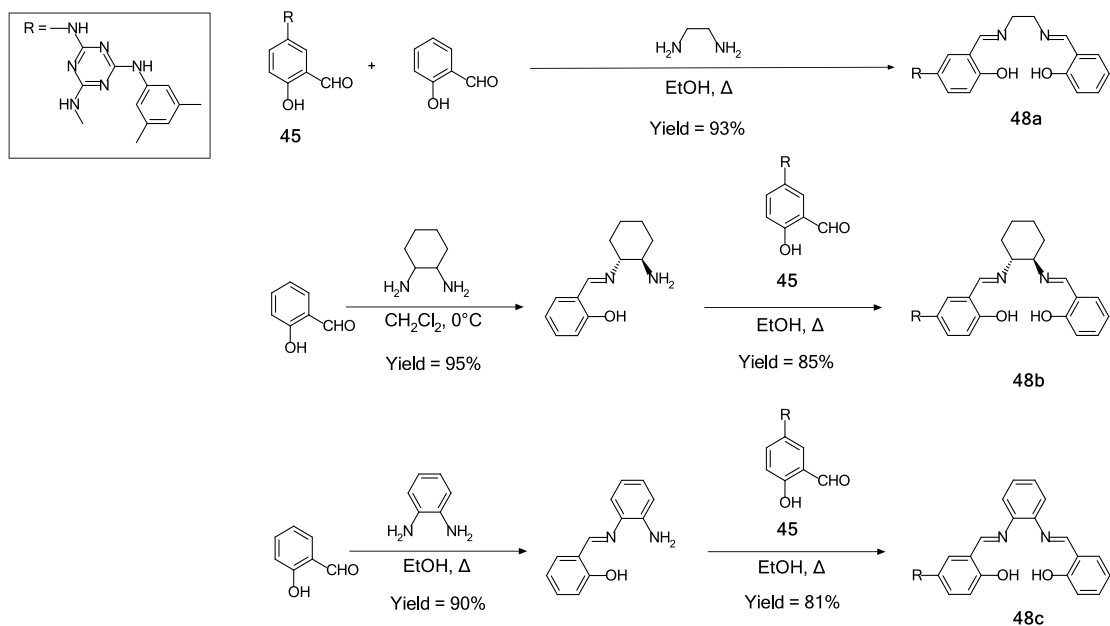
Salicylaldehyde **45** could be directly condensed with ethylenediamine or (1R,2R)-1,2-diaminocyclohexane to yield symmetrical salen ligands **46a** and **46b**, respectively, in 94-95% yields (Scheme 19). However, attempts to condense compound **45** with 1,2-phenylenediamine failed to give the desired symmetrical phenylene based salen, compound **46c**. Instead, an unidentified side product, which is currently under closer investigation, was isolated (Scheme 19).

One possible parasitic reaction would be a cyclization followed by an intramolecular hydrogen transfer to yield a benzimidazole derivative **47**, as supported by the observation of a benzylic CH₂ peak in the ¹H NMR spectrum. Similar condensations have been previously reported in the literature, especially upon condensation of 1,2-phenylenediamine with salicylaldehydes bearing electron-donating groups.^{130,131}



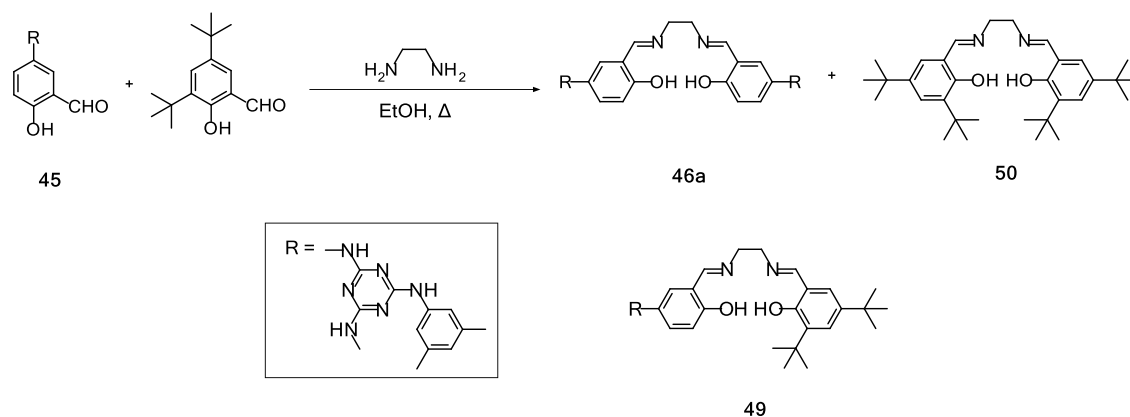
Scheme 19: Synthesis of symmetrical salen ligands **46a** and **46b**. The attempted condensation of 1,2-phenylenediamine with compound **45** to afford the proposed compound **47** is also shown, with the desired ligand **46c** shown at the side for reference.

Although the synthesis and purification of ligands **46a-b** are simple and straightforward, the presence of two methylaminotriazine units results in low solubility, except in polar aprotic solvents such as THF, DMF, and DMSO. Additional methylaminotriazine substituents also cause an undesirable increase in molecular weight with redundant and superfluous chains. As it has already been shown that only one methylaminotriazine unit is required for glass formation, even in polyfunctional compounds,^{6,11} asymmetrically substituted ligands **48a-c**, which contain one methylaminotriazine-functionalized salicylaldehyde and one unfunctionalized salicylaldehyde unit, were synthesized (Scheme 20). While ethylene-bridged ligand **48a** could be synthesized directly in 93% yield from the three components in a one-pot procedure, ligands **48b** and **48c** were produced in two steps. The respective monoimines were prepared from their respective diamines and salicylaldehyde, followed by the condensation of this intermediate with compound **45** to yield the desired products in 95% and 82% yields, respectively. Asymmetric ligands **48a-c** demonstrate solubility in a wide range of solvents ranging from toluene to methanol.



Scheme 20: Synthesis of asymmetric salen-glass ligands **48a-c**.

The highly effective and versatile Jacobsen's ligand possesses *t*-butyl groups on the salicylaldehyde moieties to increase the solubility of the respective complexes in non-polar solvents.¹¹⁶ While other groups may be added to achieve increased solubility in non-polar solvents, incorporating *ortho* and *para t*-butyl groups also play a role in altering the steric properties of the ligand, an important factor in the stereoselectivity of complexes prepared from the Jacobsen ligand.^{95,116} An attempt was made to synthesize an asymmetric glass-forming salen ligand incorporating *t*-butyl groups on the salicylaldehyde. This was sought to achieve similar properties to those observed in the Jacobsen's ligand.^{95,116} However, attempts to condense compound **45** with 3,5-di-*t*-butyl-salicylaldehyde failed to give the desired di-*t*-butyl-monotriazine compound **49**. Instead, a mixture of two symmetrical ligands was achieved, resulting from the double condensation of compound **45** with ethylenediamine, and 3,5-di-*t*-butyl-salicylaldehyde with ethylenediamine to form compounds **46a** and **50**, respectively (Scheme 21). This is likely due to the increased steric bulk of the *t*-butyl groups on this particular salicylaldehyde derivative, which led to a slower condensation reaction. It is proposed that the double substitution of compound **45** occurred first due to the lower steric hindrance until the reagent was expended, giving compound **46a**. The remaining ethylenediamine likely then reacted with the 3,5-di-*t*-butyl-salicylaldehyde to form compound **50**. The initial lack of success using the described one-pot procedure led to several attempts using variations in the reaction conditions. As well, a multi-step route similar to the procedure employed for the synthesis of compounds **48b** and **48c** was attempted in which the respective monoimines were first produced. Unfortunately, all attempts to synthesize compound **49** resulted in the production of a mixture of compounds **46a** and **50**. While several attempts did afford trace amounts of the desired product, it was determined that isolation would be far too difficult and time-consuming.



Scheme 21: Attempted synthesis of a *t*-butyl monotriazine ligand to afford products **46a** and **50**. The desired compound ligand **49** is shown below the reaction scheme for reference.

While the synthesis of a glass-forming salen derivative incorporating *t*-butyl substituents was pursued for increased solubility and steric bulk, there are many other methods to introduce these properties to the corresponding ligand structures. For example, functionalization with linear alkyl groups, such as hexyl groups, could potentially improve the solubility of the ligands. This alternative could strike a balance, offering improved solubility while avoiding the introduction of too much steric hindrance, which prevents the synthesis of the compound altogether. The ability to synthesize relatively large amounts of product and purify these products easily is important for many future applications. This ligand could be revisited in later experiments; however, reasons such as time, current availability of precursors, aim of the project, and the possibility that other ligands may achieve the same results whilst being easier to purify led to the abandonment of the synthesis of the di-*t*-butyl-monotriazine, compound **49**. Attempts to improve the solubility of these ligands will be explored further in future studies.

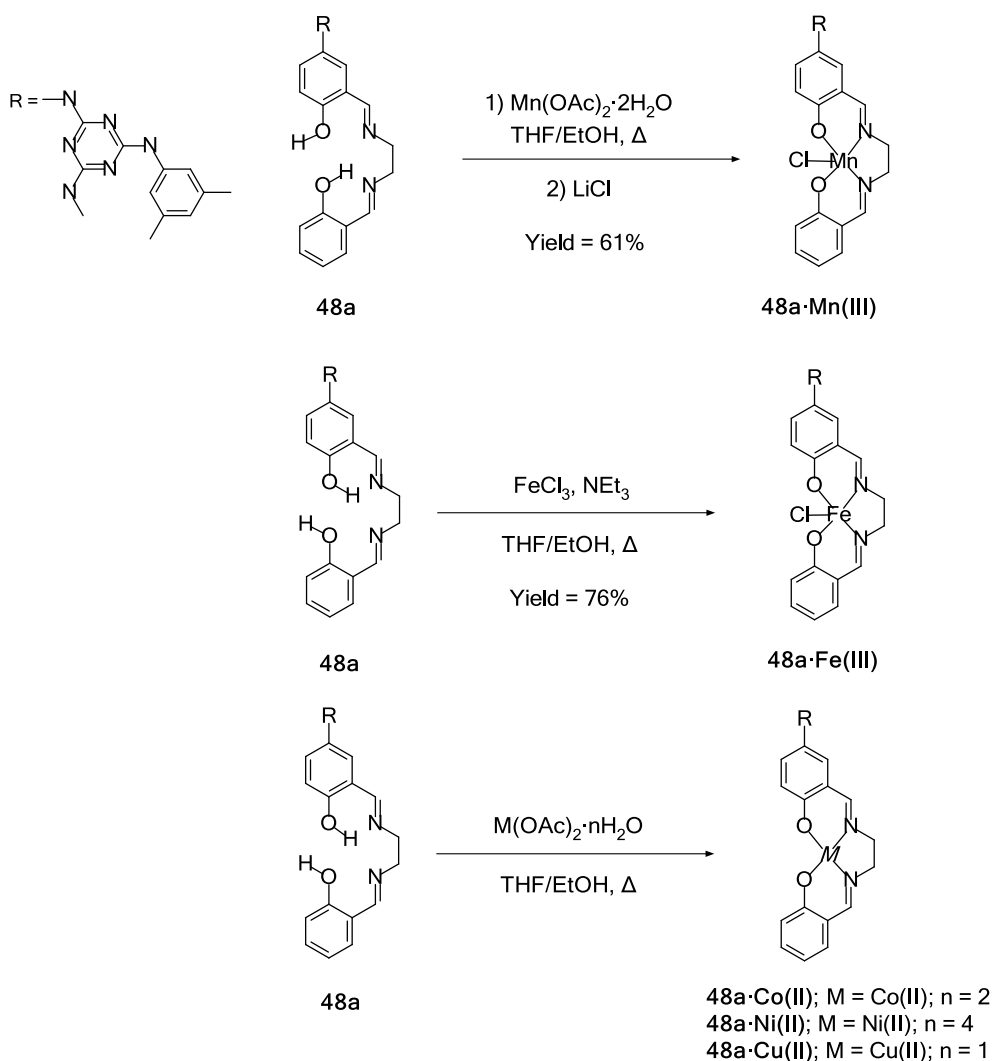
Precursor **45** and ligands **46a**, **46b**, and **48a-c** all readily formed glasses upon evaporation from solution or by cooling from the melt. DSC was used to measure their respective glass transition temperatures (T_g). In all cases, the respective compounds showed a glass transition, and no crystallization was observed upon heating, demonstrating the ability of salen derivatives **46a-b** and **48a-c** to form stable, long-lived glasses. The salicylaldehyde glass **45** shows a T_g of 81 °C, which is similar to analogous mexylaminotriazine compounds.¹¹ While monofunctionalized ligands **48a-c** show similar T_g values ranging from 69 °C to 99 °C, the larger bis(mexylaminotriazine) ligands **46a** and **46b** show higher T_g values of 125 °C and 131 °C, which follows previously observed trends in the glass-forming properties of mexylaminotriazines.¹¹ T_g values for compounds **45**, **46a-b**, and **48a-c** are listed Table 3.

Table 3: Glass transition temperatures (T_g) of compounds **45**, **46a-b**, and **48a-c**.

Compound	T_g (°C)
45	81
46a	125
46b	131
48a	78
48b	99
48c	69

4.2.2. Coordination with First-Row Transition Metals and Characterization

Following established procedures for the preparation of non-glassy salen complexes, ligand **48a** was reacted with various first-row transition metals including Mn(II), Fe(III), Co(II), Ni(II), and Cu(II) to yield the corresponding complexes (Scheme 22). The preparation of the Mn(III) complex, **48a•Mn(III)**, was performed from $\text{Mn}(\text{OAc})_2 \cdot 2\text{H}_2\text{O}$ (2.5 equiv.) and ligand **48a** by refluxing for 3 h in THF/EtOH while bubbling air through the mixture to oxidize the product. An excess of LiCl was added and the crude product was refluxed for an additional hour in order to facilitate a ligand exchange to afford the desired product with an axial chloro ligand. The product was purified by precipitation from H_2O , filtered, and washed with H_2O to give a brown-coloured Mn(III) chloride complex, in 61% yield. The preparation of this complex closely follows the preparation of non-glass forming Mn(III) salen complexes.¹³² Matrix-assisted laser desorption/ionization (MALDI) mass spectrometry of the compound was found to have an actual mass of 563.1696 g/mol, a value that compares to a calculated molecular mass, 563.1710 g/mol, for a complex with no chlorine axial ligands. The axial chlorine ligand was removed in the MALDI matrix in order to produce the charged ions needed for analysis and as such is not included in the measured mass; the expected mass has been adjusted to reflect this. The magnetic susceptibility measurements were performed from which a μ_{eff} of 2.71 BM was calculated. This value is a little lower than expected for Mn(III) complexes with two unpaired electrons.⁹² Alternatively, one explanation could be that the complex was not completely oxidized to Mn(III); however, the observed μ_{eff} is far too high for a Mn(II) complex with one unpaired electron. As such, it is most likely that the product is a Mn(III) complex with a d^4 configuration and two unpaired electrons. This information permits either a low spin octahedral or a square pyramidal geometry. A comparative search *via* the Cambridge Crystallographic Data Centre (CCDC) found that a square pyramidal geometry was most frequently reported among non-glass forming analogues.¹³³



Scheme 22: Preparation of Mn(III), Fe(III), Co(II), Ni(II), and Cu(II) coordination complexes from ligand **48a**. The preparation of the Co(II) complex, **48a·Co(II)** was carried out in the presence of an inert N₂ atmosphere.

The Fe(III) complex, **48a·Fe(III)**, which contains an additional chloride ligand, was synthesized in 76% yield from FeCl₃·6H₂O (1.1 equiv.), in EtOH and ligand **48a** in THF. The solutions were added together and triethylamine (2.3 equiv.) was added to deprotonate the ligand. The resulting mixture was then refluxed for 30 minutes. The purified complex was obtained by precipitation from H₂O followed by filtration and washing with H₂O to yield the respective dark-brown-coloured complex in 76% yield (Scheme 22). The preparation of this complex followed methods described in the literature.¹³⁴ MALDI mass spectrometry of the compound found a mass of 564.1690 g/mol, which corresponds to the calculated molecular mass of the complex without the axial chloride ligand. Similar to the Mn(III) complex, the axial chloride ligand is lost during mass spectrometry analysis and the expected mass has been adjusted to reflect this. Magnetic susceptibility of **48a·Fe(III)** was used to determine a μ_{eff} of 3.6 BM. This value is high for the reported magnetic moments of Fe(III) complexes with one unpaired electron.⁹² This value is also

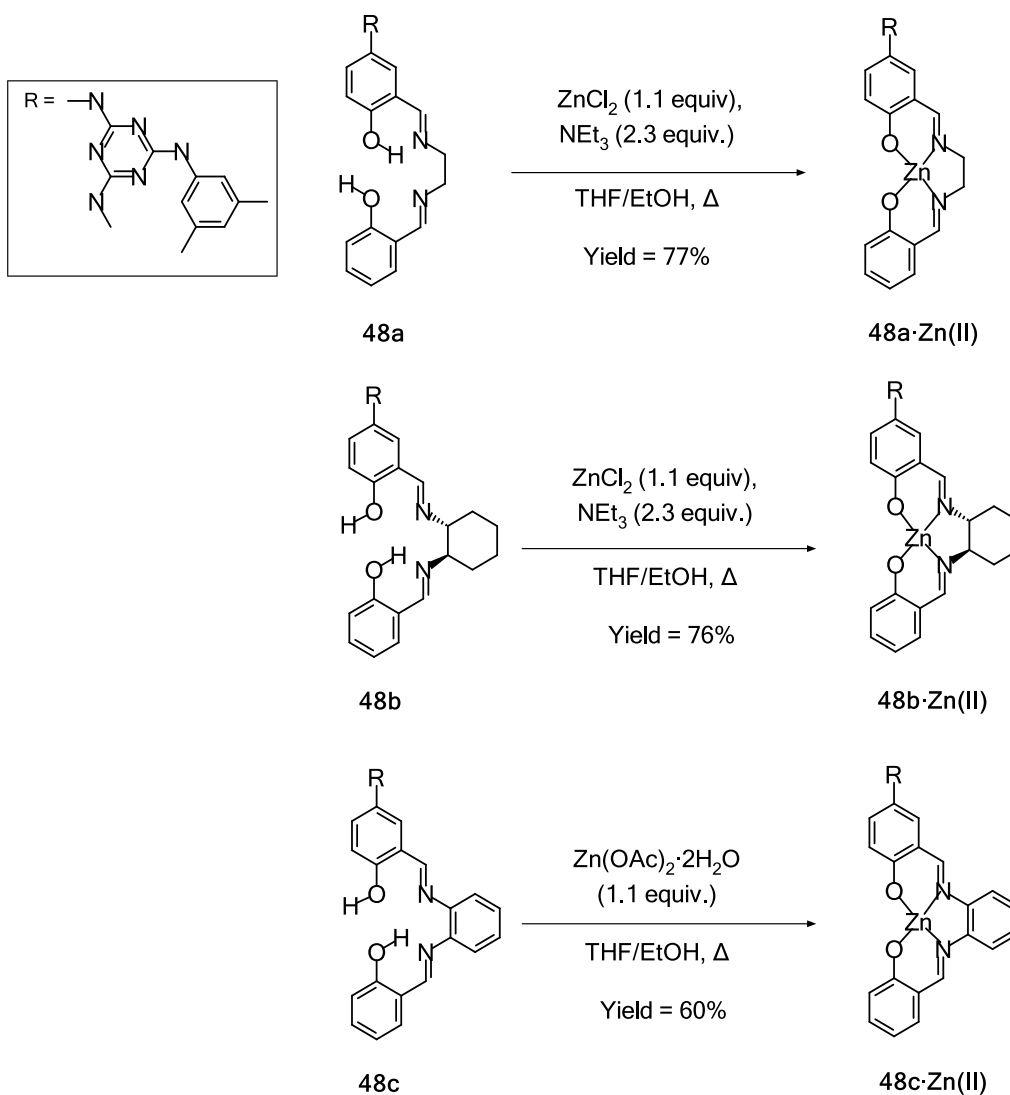
too low compared to reported values for other Fe(III) complexes. One proposed explanation could be the dimerization of the prepared complex and magnetic coupling between the Fe(III) centers. Fe(III) salen dimers have been reported with bridging occurring between the chloride ions, oxo ligands, and the phenoxide of the two salicylaldehyde moieties.^{93,135–138} One such example, a μ -oxo-[Fe(III)salen)] species, was actually shown to be useful as a catalyst for the cyclopropanation of olefins by Nyugen *et al.*¹³⁶ Additionally, the dimerization of Fe(III) salens has been reported in the literature as a side-product during the preparation of Fe(III)(salen)Cl complexes.⁹³ One particular phenoxide-bridged Fe(III) salen derivative was shown to demonstrate antiferromagnetic behaviour.¹³⁹ At room temperature, this complex exhibited a magnetic moment of 4.52 BM, which fell to 2.37 BM at lower temperatures. As such, if the Fe(III) glass-forming salen prepared for this report was also a dimeric species, it could exhibit ferromagnetic or anti-ferromagnetic coupling, producing the unexpected μ_{eff} value observed. At the current time, no further conclusions can be made to explain the observed behaviour in magnetic properties of this complex and more detailed variable temperature magnetic studies are required. A search using the CCDC show that a square pyramidal geometry with a Cl⁻ axial ligand is the most commonly reported geometry for Fe(III) salen complexes.¹³⁴

The Co(II), Ni(II), and Cu(II) complexes of ligand **48a** were synthesized in 66-84% yields by refluxing a mixture of ligand **48a** and the corresponding metal acetates (2 equiv.) in THF/EtOH (Scheme 22). For the Co(II) complex, the reaction was run under an inert atmosphere to prevent oxidation. In all cases, the complexes could be conveniently purified by precipitation with water followed by filtration to remove excess metal salts. The preparation of the dark-brown Co(II) complex, **48a**•Co(II), followed procedures described in the literature.¹⁴⁰ The calculated molecular mass, 568.1740 g/mol, corresponds to the molecular mass of 568.1749 g/mol as analyzed by MALDI mass spectrometry. Magnetic susceptibility measurements indicate a μ_{eff} of 2.04 BM. This measurement corresponds to a single unpaired electron for this complex for a d^7 configuration. This opens many options for geometries; such as low spin octahedral, square pyramidal, or square planar. According to the CCDC, the most frequently reported geometry for analogous complexes is the square planar geometry.¹⁴¹

The orange-brown coloured Ni(II) complex was prepared from Ni(OAc)₂•4H₂O and ligand **48a**, following preparations outlined in the literature for non-glassy analogues (Scheme 22).¹⁴² The expected molecular mass, 567.1761 g/mol, corresponds well with the one measured by MALDI mass spectrometry, 567.1785 g/mol, further confirming the identity of this coordination complex. Magnetic susceptibility calculations indicate that this complex is diamagnetic. Ni(II) complexes exhibit a d^8 configuration and as such, the complex would need to adopt a square planar geometry. The square planar geometry is supported by the reported geometries of non-glass forming analogues in the literature.¹⁴³

The olive green coloured Cu(II) complex was prepared from ligand **48a** and Cu(OAc)₂•xH₂O as starting materials, following methods outlined in the literature (Scheme 22).¹⁴² MALDI mass spectrometry of the compound found an actual mass of 572.1727 g/mol, a value that compares well to the expected molecular mass, 572.1704 g/mol, of the desired complex. The magnetic susceptibility calculations for the Cu(II) complex indicate that this complex has only one unpaired electron, as expected, for Cu(II) complexes with a d^9 configuration. Based on a literature search, most of the corresponding complexes are square pyramidal complexes with solvent or water molecules coordinated to the metal center; however, some square planar geometries have also been reported.¹⁴⁴

The Zn(II) complexes of ligands **48a** and **48b** were not successfully prepared from the corresponding zinc acetate reagent, as was the case for other complexes in this report. This is the most frequently described method for the preparation of non-glassy analogues of these complexes.¹⁴² Attempts using this procedure resulted in an intractable mixture of products. Instead, these complexes were prepared using a modified procedure found in the literature (Scheme 23).⁵⁰ Both **48a•Zn(II)** and **48b•Zn(II)** were prepared by adding a solution of ZnCl₂•2H₂O (1.1 equiv.) in EtOH to a solution of ligand **48a** or **48b**, respectively. Triethylamine (2.3 equiv.) was added and the mixture was refluxed for 30 minutes yielding the respective yellow coloured complexes in 66-84% yields. The orange coloured Zn(II) complex of ligand **48c** followed a similar procedure to that used for the preparation of complexes from ligand **48a** and metal acetates.¹⁴⁵ A solution of Zn(OAc)₂•2H₂O (excess) in EtOH was added to a stirring solution of ligand in THF and was then refluxed for 2 h. Interestingly, complexes **48b•Zn(II)** and **48c•Zn(II)** showed the same solubility as the ethylene-bridged derivative **48a•Zn(II)** despite containing larger diamino substituents. In addition, all three Zn complexes were analyzed by MALDI mass spectrometry and were found to have molecular masses that match their expected values. Magnetic susceptibility confirmed the expected diamagnetic behaviour. The most commonly reported geometries for Zn(II) non-glass forming zinc salen analogues are either distorted square planar or square pyramidal due to the coordination of solvent or water molecules.¹⁴⁵ Mass spectrometry supports the square planar geometry, as the observed mass was consistent to the expected mass of the complexes.



Scheme 23: Preparation of Zn(II) complexes from ligands **48a**, **48b**, and **48c**.

All prepared complexes of ligands **48a**, **48b**, and **48c** were studied by TGA and DSC to explore their thermal behaviour. Decomposition temperatures were measured by TGA and are reported in Table 4. Typically, a mass loss ranging from 2% to 5% was observed around 140 °C, and is the result of loss of residual water trapped in the samples. Most compounds are stable over 300 °C, except for the Co(II) complex **48a·Co(II)**, which decomposes at approximately 225 °C. Like their parent ligands, all complexes studied are capable of forming glassy phases, with T_g values ranging from 133 to 196 °C, as measured by DSC (Table 4), with standard deviations from duplicate measurements less than 1 °C. Only the Co(II) complex of ligand **48a** did not show a glass transition by DSC due to thermal degradation. In this case, the amorphous nature of the compound was confirmed by XRD. No crystallization was observed in any other complex upon heating to 250 °C. It is to be noted that all T_g values reported herein were recorded after an initial heating-cooling cycle in which the materials were melted and residual solvents were removed.

Table 4: Decomposition temperatures and glass transition temperatures (T_g) for complexes prepared from ligands **48a-c**.

Compound	T_{dec} (°C)	T_g (°C)
48a•Mn(III)	290	179
48a•Fe(III)	270	196
48a•Co(II)	225	-
48a•Ni(II)	240	133
48a•Cu(II)	250	159
48a•Zn(II)	250	146
48b•Zn(II)	290	165
48c•Zn(II)	280	167

T_g values for the transition metal complexes were significantly higher than those of their parent ligands, which is to be expected given the loss of degrees of liberty and limited molecular mobility resulting from the presence of the metal atom. For Zn(II) complexes, the T_g values for the larger cyclohexyl and phenylene-bridged ligands, **48b** and **48c**, were similar to each other, and higher than the value for the complex prepared from the ethylene-bridged complex **48a**. Surprisingly, variations in T_g were observed depending on the nature of the transition metal. The Ni(II) complex (133 °C), Zn(II) complex (146 °C), and Cu(II) complex (159 °C) of ligand **48a** showed respective differences in T_g of 13 °C. This observation highlights the metal centre as a factor affecting glass-forming properties. The effect of the metal center on T_g will be investigated in more detail in future studies. Thermograms for TGA and DSC of the metal complexes are provided in appendices B.1 and C.1, respectively.

4.2.3. Optical Properties

The absorption maxima and extinction coefficients are reported in Table 5. The UV-Vis absorption spectra show intense absorption in the ultraviolet region of the spectrum. Samples in solution of the complexes show maximum absorption from $\lambda = 263$ -277 nm. Smaller secondary peaks are observed for the Ni(II) complex, **48a•Ni(II)**, at $\lambda = 305$ nm, and for the phenylene-bridged Zn(II) complex, **48c•Zn(II)**, at $\lambda = 340$ nm. No other secondary peaks are observed; however, the Mn(III), Fe(III), and Co(II) complexes do exhibit what appears to be a trail off of their absorptions extending to $\lambda = 390$ nm, $\lambda = 440$ nm, and $\lambda = 350$ nm, respectively. No pattern appears to exist in accordance with periodic trends and there is only small variations between the complexes. To be noted, the three Zn(II) complexes exhibit absorption maxima that are shifted slightly to longer wavelengths than the other complexes. The absorption maxima for these three complexes are consistent with each other despite variations in their ligand structures. The phenylene-bridged Zn(II) complex does exhibit a second smaller peak as highlighted earlier. This is likely contributed by the aryl-bridge substituent. Of note, the three zinc complexes required additional dilutions in order to obtain absorption spectra within an acceptable range. Unexpectedly, no absorbance peaks were observed within the visible region of the spectra for any samples. It is proposed that the visible metal-based transitions are too weak compared to the ligand-based

transitions in the UV range. The aromatic rings in the ligand, which typically absorb in the UV region, are quite numerous providing a potential explanation for these observations. The preparation of more concentrated samples to be analyzed in the visible range only could be used to visualize peaks in this range. The UV-Vis spectra of glass-forming complexes based on ligand **48a**, **48b**, and **48c** were recorded in CH_2Cl_2 solution. Absorption spectra of the complexes are shown below in Figure 5.

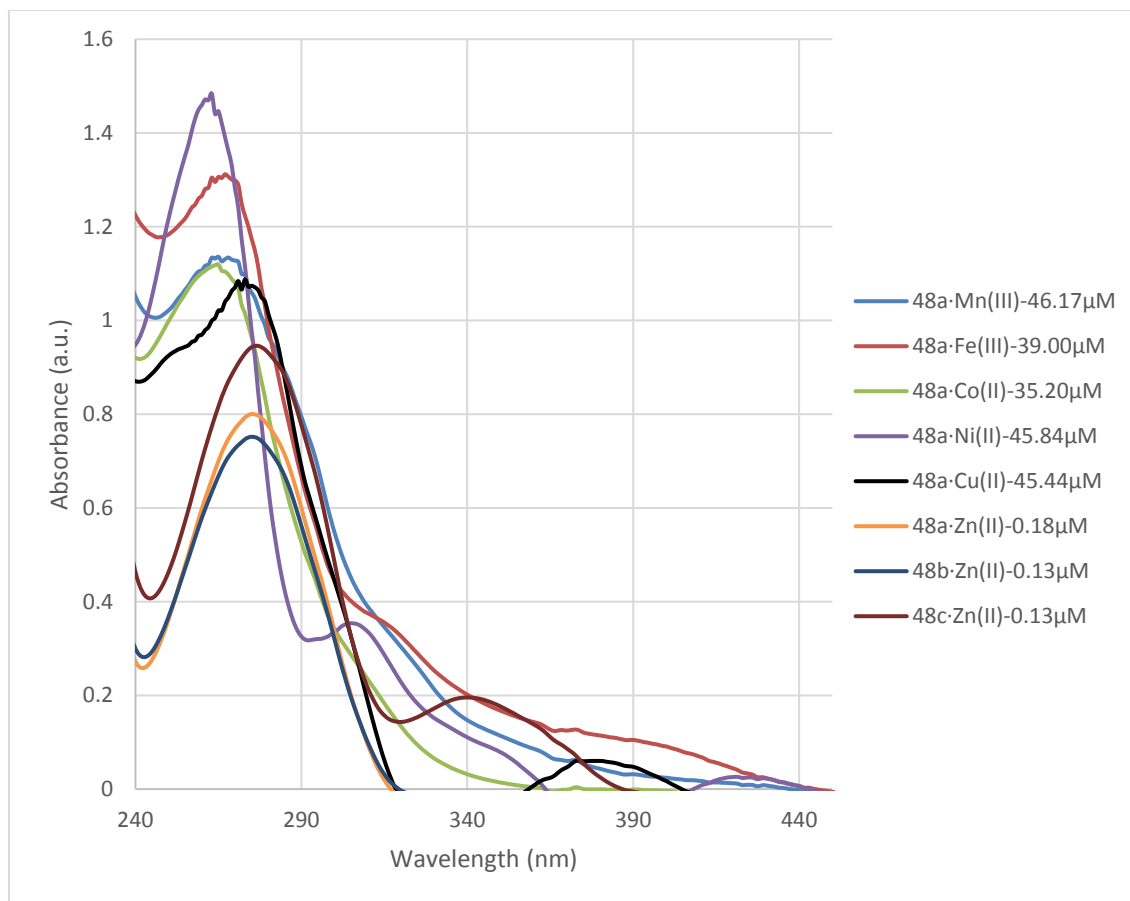


Figure 5: UV absorption spectra of complexes of ligands **48a**, **48b**, and **48c** in CH_2Cl_2 solution.

Table 5: UV-Vis absorbance values of salen-functionalized molecular glass complexes **48a-c** in CH₂Cl₂ solution.

Complex	λ_{max} in solution (nm)	ϵ (extinction coefficient) in solution (cm ⁻¹)
48a•Mn(III)	265	24600
48a•Fe(III)	267	33600
48a•Co(II)	265	31800
48a•Ni(II)	263	32400
48a•Cu(II)	273	23900
48a•Zn(II)	275	440000
48b•Zn(II)	275	587000
48c•Zn(II)	277	727000

4.3. Experimental

4.3.1. Materials and Equipment

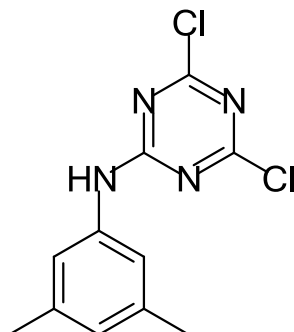
All reagents were purchased from Sigma-Aldrich, AK Scientific or Oakwood Chemicals and were used without further purification. Reagent grade solvents were purchased from Caledon Laboratories, and used without further purification. DMSO-*d*₆ (deuterated dimethyl sulfoxide) and CDCl₃ (deuterated chloroform) were purchased from CDN isotopes. Unless otherwise stated, reactions were performed under ambient atmospheric conditions. Thin film chromatography using SiliCycle products was used to ensure that each reaction had occurred and continued to completion.

4.3.2. Physical Measurements

NMR spectra were recorded using a Bruker Avancé 400 MHz spectrometer at 298K unless otherwise noted. Thermal analysis was obtained by TGA and DSC using a TA Instruments Q50 and Q20, respectively. Ambient temperature magnetic susceptibility measurements were made using an MSB MK1 Magnetic Susceptibility Balance following procedures outlined by the supplier.⁹² Infrared spectra were recorded using a Thermo Scientific Nicolet iS10 spectrometer. Samples were prepared by forming thin films of the respective complexes from the evaporation of CH₂Cl₂ on KBr windows. UV-Vis spectra were obtained using a Hewlett Packard 8453 spectrometer. Samples were prepared by dissolving 1 mg of solute in the appropriate amount of CH₂Cl₂ required to achieve an absorbance value below two.

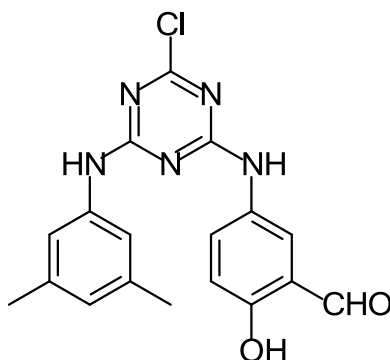
4.3.3. Synthesis

Synthesis of 2-mexylamino-4,6-chloro-1,3,5-triazine (43)



The synthesis of this intermediate compound follows procedures outlined in the literature.^{11,146} To a solution of cyanuric chloride (100 g, 542 mmol) dissolved in acetone (750 mL) in a round-bottomed flask equipped with a magnetic stirrer, K_2CO_3 (74.9 g, 542 mmol) was added. The flask was placed in an ice bath to keep the temperature in the flask under $-10\text{ }^\circ\text{C}$. A solution of 3,5-dimethylaniline (66.4 g, 531 mmol) in acetone (250 mL) was added dropwise while the mixture stirred. The final mixture was allowed to stir for an additional 2 h while warming to room temperature. The mixture was then poured into H_2O (500 mL) and stirred for 20 minutes at room temperature for precipitation to occur. The resulting precipitate was collected by filtration, the crude product was washed with 0.5 M NaOH, H_2O , and hexane. The product was allowed to dry in air to afford the intermediate compound, 2-mexylamino-4,6-dichloro-1,3,5-triazine (**43**) (135 g, 502 mmol, 92% yield).

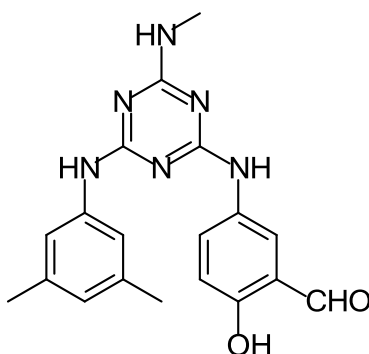
Synthesis of 2-mexylamino-4-[(4-hydroxy-3-formylphenyl)amino]-6-chloro-1,3,5-triazine (44)



The synthetic route used to synthesize this compound were previously established in unpublished work by Dr. M. Jokar. A round-bottom flask was charged with $Pd(OAc)_2$ (11.0 mg, 50.0 μmol), 2-(1,4-dioxo-5-cyclopentyl)-4-nitrophenol (**41**) (211 mg, 1.00 mmol), and freshly distilled THF (5 mL). The flask was sealed and purged with N_2 . While purging the flask with N_2 , an aqueous KF solution (116 mg, 2.00 mmol, in 2 mL degassed H_2O) was added *via* syringe. The N_2 inlet was replaced with a balloon filled with N_2 . Polymethylhydrosiloxane (PMHS) (240 μL , 4.00 mmol) was slowly added dropwise *via* syringe. The reaction was stirred for 45 min or until complete, as judged by TLC. At that time, the reaction flask was opened to the air, then a solution

of 2-mexylamino-4,6-dichloro-1,3,5-triazine (**43**) (268 mg, 1.00 mmol) in acetone (5 mL) was added dropwise to the mixture. K_2CO_3 (138 mg, 1.00 mmol) was then added, and the mixture was stirred for 4h at ambient temperature. The catalyst was removed by filtration and the filtrate was evaporated to dryness *in vacuo*. The residue was purified by adding CH_2Cl_2 (20 mL) and aqueous NaOH (1.0 M). The organic layer was further extracted with aqueous NaOH (1.0 M, 3×30 mL). The basic aqueous washings were recovered, combined, neutralized with concentrated HCl, washed with H_2O , and dried to yield compound **44** (330 mg, 0.910 mmol, 91%) that required no further chromatographic purification. HRMS (ESI) calcd for $\text{C}_{18}\text{H}_{16}\text{ClNaN}_5\text{O}_2$ (m/e): 392.0885, found: 392.0894; FTIR (KBr, cm^{-1}): 3593, 3378, 3295, 3010, 2918, 2955, 2856, 1648, 1626, 1586, 1551, 1536, 1488, 1473, 1438, 1371, 1320, 1292, 1271, 1245, 1175, 1158, 1034, 986, 831, 793, 748, 670, 425; ^1H NMR (300 MHz, $\text{DMSO}-d_6$, 298 K) δ 10.61 (s, 1H), 10.19 (br s, 1.0 H), 10.14 (br s, 1 H), 10.09 (br s, 0.6 H), 10.07 (br s, 0.4 H), 7.82 (br m, 1H), 7.63 (br s, 1 H), 7.33 (br s, 0.5 H), 7.18 (m, 1.5 H), 7.00 (d, $J = 8.7$ Hz, 1 H), 6.66 (s, 1 H), 2.19 (s, 6 H) ppm; ^1H NMR (400 MHz, $\text{DMSO}-d_6$, 363 K) δ 9.44 (br s, 1 H), 7.57 (br s, 1 H), 7.35 (s, 2 H), 6.68 (s, 1 H), 2.86 (s, 3 H), 2.25 (s, 6 H) ppm; ^{13}C NMR (75 MHz, $\text{DMSO}-d_6$) δ 191.2, 168.4, 164.7, 164.1, 158.0, 138.7, 138.1, 131.5, 130.6, 125.4, 125.3, 122.5, 118.7, 21.6 ppm; Spectral data and characterization match those described in the literature.

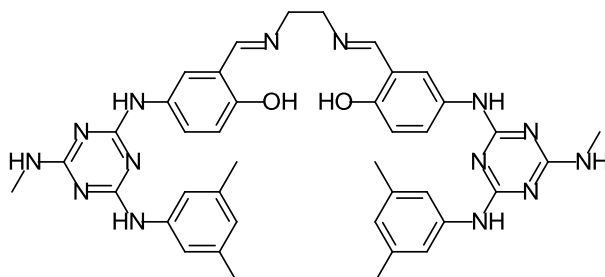
Synthesis of 2-mexylamino-4-methylamino-6-[(4-hydroxy-3-formylphenyl)amino]-1,3,5-triazine (**45**)



The synthetic route used to synthesize this compound were previously established in unpublished work by Dr. M. Jokar. The precursor, 2-mexylamino-4-methylamino-6-[(4-hydroxy-3-formylphenyl)amino]-1,3,5-triazine **5** was synthesized as follows. To a round-bottomed flask equipped with a magnetic stirrer and a water-jacketed condenser were added 2-mexylamino-4-[(4-hydroxy-3-formylphenyl)amino]-6-chloro-1,3,5-triazine **44** (6.03 g, 22.9 mmol) and a solution of aqueous methylamine (40 wt% aqueous, 2.20 mL, 27.4 mmol) in THF (125 mL), then the mixture was refluxed for 18 h. CH_2Cl_2 and aqueous HCl (1.0 M) were added, and both layers were separated. The organic layer was extracted with H_2O and aqueous NaHCO_3 , dried over Na_2SO_4 , filtered, and the volatiles were thoroughly evaporated under vacuum to yield 6.59 g of compound **45** in acceptable purity (18.1 mmol, 79%). HRMS (ESI) calcd for $\text{C}_{19}\text{H}_{21}\text{N}_6\text{O}_2$ (m/e): 365.1721, found: 365.1732; FTIR (KBr, cm^{-1}): 3379, 3274, 3227, 3098, 2950, 2920, 2854, 1661, 1636, 1582, 1561, 1517, 1483, 1429, 1397, 1322, 1272, 1184, 1040, 959, 884, 837, 771, 687, 649 cm^{-1} ; ^1H NMR (300 MHz, $\text{DMSO}-d_6$, 298 K): δ 10.38 (s, 1 H), 10.19 (br s, 1 H), 9.10 (br s, 0.5 H), 8.92 (br s, 1 H), 8.90 (br s, 0.5 H), 7.90 (br m, 2 H), 7.33 (br m, 2 H), 6.91 (d, $J = 8.7$ Hz, 1 H), 6.85 (br s, 1 H), 6.55 (s, 1 H), 2.85 (d, 3 H), 2.18 (s, 6 H) ppm; ^1H NMR (400 MHz, $\text{DMSO}-d_6$, 363 K): δ 9.97 (s, 1 H), 8.98 (br s, 1 H), 8.52 (br s, 1 H), 8.32 (s, 1 H), 8.11 (d, 1 H), 7.49 (m, 2 H), 7.37 (s,

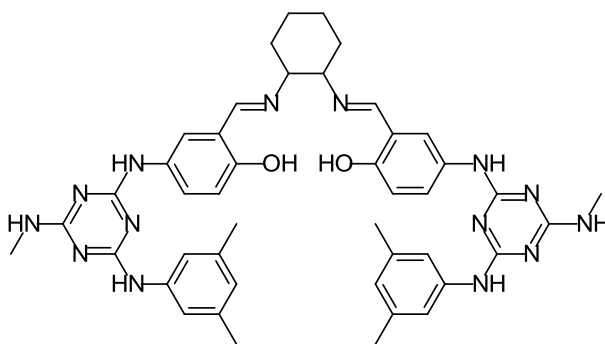
2 H), 6.65 (br s, 1 H), 6.63 (s, 1 H), 2.90 (d, 3 H), 2.25 (s, 6 H) ppm; ^{13}C NMR (75 MHz, DMSO- d_6): δ 192.1, 166.4, 164.6, 164.4, 164.2, 156.5, 140.6, 137.5, 132.9, 130.6, 123.5, 122.1, 121.2, 118.1, 117.5, 108.9, 27.7, 21.7, 21.6 ppm; $T_g = 81\text{ }^\circ\text{C}$.

Synthesis of ligand 46a



The synthetic route used to synthesize this compound were previously established in unpublished work by Dr. M. Jokar. 2-Methylamino-4-methylamino-6-[(4-hydroxy-3-formylphenyl)amino]-1,3,5-triazine **45** (730 mg, 2.00 mmol) was added in a round-bottomed flask which containing 10 mL ethanol. To the reaction mixture, an ethanolic solution (10 mL) of 1,2-ethylenediamine (67.0 μL , 60.0 mg, 1.00 mmol) was added and the mixture was stirred at $80\text{ }^\circ\text{C}$ for 2 h. Then, the reaction mixture was filtered and the residue was washed with ethanol and precipitated from hexane/ethyl acetate to give 710 mg (0.940 mmol, 94% yield) of ligand **46a** as a yellow solid. HRMS (ESI) calcd for $\text{C}_{40}\text{H}_{45}\text{N}_{14}\text{O}_2$ (m/e): 753.3844, found: 753.3867; FTIR (KBr, cm^{-1}): 3397, 3275, 3166, 3012, 2943, 2916, 2863, 1882, 1635, 1579, 1515, 1429, 1395, 1273, 1174, 1129, 1082, 1036, 974, 882, 836, 808, 685, 649; ^1H NMR (300 MHz, DMSO- d_6 , 298 K): δ 12.94 (br s, 2 H), 9.00 (br s, 1 H), 8.91 (br s, 1 H), 8.83 (br s, 1 H), 8.75 (br s, 1 H), 8.48 (s, 2 H), 7.85 (br s, 2 H), 7.55 (br m, 2H), 7.24-7.43 (m, 4 H), 6.70-6.90 (m, 4 H), 6.54 (s, 2 H), 3.91 (s, 4 H), 2.81 (s, 6 H), 2.18 (s, 12 H) ppm; ^1H NMR (400 MHz, DMSO- d_6 , 363 K): δ 9.97 (s, 1 H), 8.98 (br s, 1 H), 8.52 (br s, 1 H), 8.32 (s, 1 H), 8.11 (d, 1 H), 7.49 (m, 2 H), 7.37 (s, 2 H), 6.65 (br s, 1 H), 6.63 (s, 1 H), 2.90 (d, 3 H), 2.25 (s, 6 H) ppm; ^{13}C NMR (75 MHz, DMSO- d_6): δ 172.1, 171.3, 169.4, 160.8, 145.4, 142.3, 136.8, 128.3, 123.1, 122.8, 121.3, 64.3, 32.5, 26.4 ppm; $T_g = 125\text{ }^\circ\text{C}$.

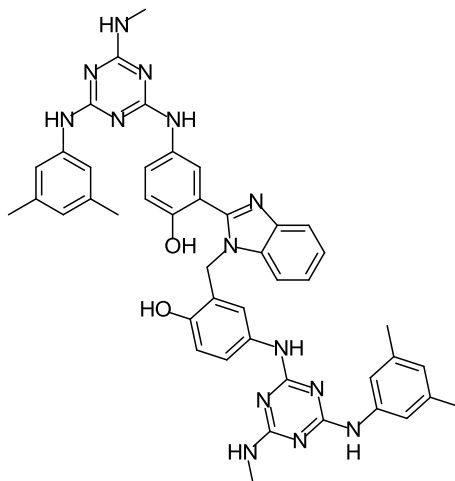
Synthesis of ligand 46b



The synthetic route used to synthesize this compound were previously established in unpublished work by Dr. M. Jokar. To an ethanolic solution (10 mL) of (1R, 2R)-(-)-diaminocyclohexane (220 mg, 2.00 mmol) in a round-bottomed flask equipped with a magnetic stirrer was added dropwise a solution of 2-methylamino-4-methylamino-6-[(4-hydroxy-3-formylphenyl)amino]-1,3,5-triazine (**45**) (1.46 g, 4.00 mmol) in 10 mL of dry ethanol at ambient

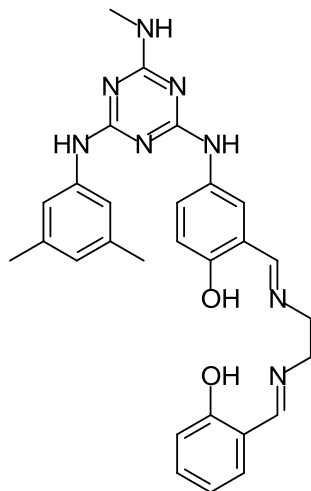
temperature. The mixture was gradually heated to 80 °C and maintained for 3 hours at this temperature. The solvent was then evaporated under vacuum to afford a residue, which was precipitated from hexane/ethyl acetate to give 1.53 g (1.90 mmol, 95%) of the R,R enantiomer of ligand **46b** as a yellow solid. HRMS (ESI) calcd for C₄₄H₅₀NaN₁₄O₂ (*m/e*): 829.4133, found: 829.4160; FTIR (KBr, cm⁻¹): 3733, 3709, 3646, 3564, 3400, 3283, 2926, 2856, 1632, 1579, 1518, 1491, 1430, 1396, 1273, 1184, 1143, 1093, 1039, 879, 837, 808, 783, 687, 651; ¹H NMR (300 MHz, DMSO-*d*₆, 298 K): δ 12.90 (br s, 2 H), 8.94 (br s, 1 H), 8.88 (br s, 1 H), 8.76 (br s, 1 H), 8.72 (br s, 1 H), 8.45 (br s, 2H), 7.80 (br m, 2 H), 733-6.82 (m, 6 H), 6.83-6.76 (m, 2 H), 6.69 (d, 2 H), 6.52 (s, 2 H), 3.31-3.6 (m, 2 H), 2.79 (s, 6 H), 2.18 (s, 12 H), 1.21-1.85 (m, 8 H) ppm; ¹H NMR (400 MHz, DMSO-*d*₆, 363 K): δ 9.97 (s, 1 H), 8.98 (br s, 1 H), 8.52 (br s, 1 H), 8.32 (s, 1 H), 8.11 (d, 1 H), 7.49 (m, 2 H), 7.37 (s, 2 H), 6.65 (br s, 1 H), 6.63 (s, 1 H), 2.90 (d, 3 H), 2.25 (s, 6 H) ppm; ¹³C NMR (75 MHz, DMSO-*d*₆): δ 166.5, 165.5, 164.6, 156.2, 155.9, 141.1, 140.6, 139.6, 137.5, 137.4, 132.1, 123.6, 118.5, 118.3, 118.1, 117.6, 116.4, 72.1, 33.8, 33.4, 33.1, 30.9, 27.7, 25.0, 24.9, 24.6, 24.2, 21.6 ppm; T_g = 131 °C.

Attempted Synthesis of compound **46c** to form compound **47**



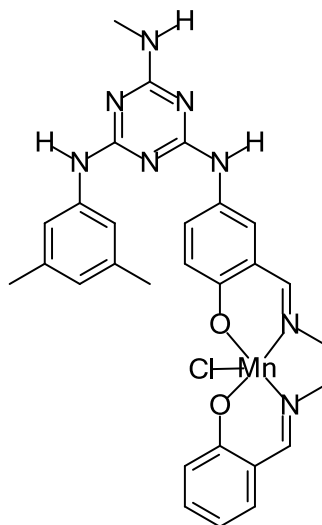
A solution of 2-methylamino-4-methylamino-6-[(4-hydroxy-3-formylphenyl)amino] 1,3,5-triazine **45** (728 mg, 2.00 mmol) and *o*-phenylenediamine (104 mg, 1.00 mmol) in dry ethanol (10 mL) was refluxed for 3 h. The solvent was evaporated under vacuum to afford a residue, which was recrystallized from hexane/ethyl acetate to give 382 mg of product as a red solid. The afforded product was determined to likely be a side product, compound **47** rather than the desired compound **46c**. HRMS (EI) calcd for C₂₅H₂₄N₈O (*m/e*): 425.5149, found 425.5241; FTIR (KBr, cm⁻¹): 3400, 3275, 2954, 2930, 1614, 1557, 1517, 1493, 1429, 1397, 1319, 1273, 1183, 1159, 1142, 1116, 1104, 975, 883, 839, 746, 686, 649; ¹H NMR (300 MHz, DMSO-*d*₆, 298 K): δ 12.9 (br s, 0.2 H), 12.58 (br s, 0.4 H), 12.39 (br s, 0.4 H), 8.7-9.1 (m b, 3 H), 8.10 (br s, 1 H), 7.68 (br m, 1 H), 7.33-7.58 (m, 3 H), 6.61-7.08 (m, 4 H), 6.52 (s, 1 H), 5.04 (s, 1 H), 2.82 (s, 3 H), 2.18 (s, 6 H). ¹H NMR (400 MHz, DMSO-*d*₆, 363 K): δ 9.97 (s, 1 H), 8.98 (br s, 1H), 8.52 (br s, 1H), 8.32 (s, 1H), 8.11 (d, 1H), 7.49 (m, 2H), 7.37 (s, 2H), 6.65 (br s, 1H), 6.63 (s, 1H), 2.90 (d, 3H), 2.25 (s, 6H) ppm; ¹³C NMR (75 MHz, DMSO-*d*₆): δ 166.7, 164.7, 164.4, 152.1, 143.1, 142.8, 141.1, 140.7, 140.6, 137.5, 134.7, 132.5, 128.2, 123.6, 119.7, 119.1, 118.7, 118.2, 117.6, 117.1, 115.7, 112.5, 27.7, 21.6 ppm.

Synthesis of Ligand 48a



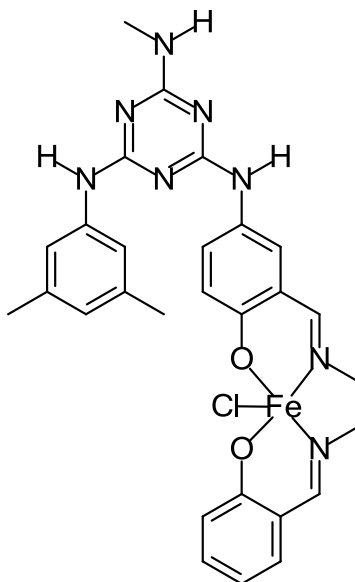
The synthetic route used to synthesize this compound were previously established in unpublished work by Dr. M. Jokar. To a solution of 2-mexylamino-4-methylamino-6-[(4-hydroxy-3-formylphenyl)amino]-1,3,5-triazine **45** (730 mg, 2.00 mmol) and salicylaldehyde (210 μL , 244 mg, 2.00 mmol) in 20 mL absolute ethanol was added dropwise a solution of ethylenediamine (130 μL , 120 mg, 2.00 mmol) in 10 mL absolute ethanol. The solution mixture was refluxed for 2 h, filtered while hot, excess solvent was removed *in vacuo* to afford a residue. The residue was precipitated from hexane/ethyl acetate to give 950 mg of a yellow solid ligand **48a** (1.86 mmol, 93%). HRMS (ESI) calcd for $\text{C}_{28}\text{H}_{31}\text{N}_8\text{O}_2$ (*m/e*): 511.2564, found: 511.2572; FTIR (KBr, cm^{-1}): 3410, 2924, 1632, 1581, 1517, 1492, 1397, 1300, 1275, 1185, 1151, 1128, 1050, 977, 877, 839, 808, 779, 756, 736, 686, 687, 647; ^1H NMR (300 MHz, $\text{DMSO-}d_6$, 298 K): δ 13.34 (b s, 1 H), 12.90 (br s, 1 H), 8.99 (br s, 0.5 H), 8.90 (br s, 0.5 H), 8.82 (br s, 0.5 H), 8.75 (br s, 0.5 H), 8.55-8.57 (m, 1 H), 8.47 (br s, 1 H), 7.83 (br s, 1 H), 7.55-7.58 (m, 1 H), 7.26-7.42 (m, 4 H), 6.76-6.88 (m, 4 H), 6.54 (s, 1 H), 3.90 (s, 4 H), 2.81 (s, 3 H), 2.16 (s, 6 H) ppm; ^1H NMR (400 MHz, $\text{DMSO-}d_6$, 363 K): δ 9.97 (s, 1 H), 8.98 (br s, 1 H), 8.52 (br s, 1 H), 8.32 (s, 1 H), 8.11 (d, 1 H), 7.49 (m, 2 H), 7.37 (s, 2 H), 6.65 (br s, 1 H), 6.63 (s, 1 H), 2.90 (d, 3 H), 2.25 (s, 6 H) ppm; ^{13}C NMR (75 MHz, $\text{DMSO-}d_6$): δ 167.4, 167.3, 167.3, 166.5, 164.6, 161.0, 161.0, 156.1, 140.6, 137.5, 132.8, 132.1, 123.6, 119.0, 118.3, 118.1, 116.9, 116.5, 59.3, 59.2, 27.7, 21.6 ppm; $T_g = 78$ $^\circ\text{C}$.

Preparation of 48a•Mn(III)



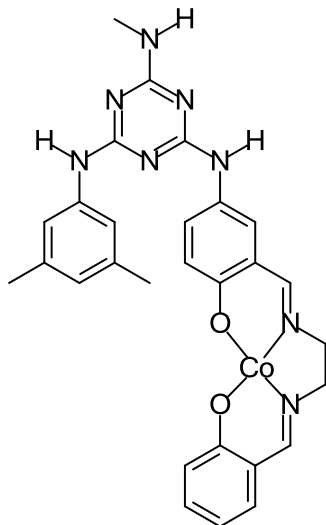
The preparation of this metal complex was performed by adding $\text{Mn}(\text{OAc})_2 \cdot 2\text{H}_2\text{O}$ (2.5 equiv., 296 mg, 1.71 mmol) to a solution of ligand **48a** (1.0 equiv., 350 mg, 0.685 mmol) in 5 mL of THF and 5 mL ethanol. The resulting brown-coloured mixture was refluxed for two hours with an air bubbler. LiCl (3 equiv., 87.0 mg, 2.06 mmol) was added to the mixture and the mixture refluxed for another three hours. The mixture was poured into water to form a precipitate. The precipitate was collected by filtration, washed with H_2O , and allowed to dry to afford 240 mg of a brown complex **48a•Mn(III)** (0.425 mmol, 62% yield). HRMS (MALDI) calcd for $\text{C}_{28}\text{H}_{28}\text{MnN}_8\text{O}_2$ (m/e): 563.1710, found: 563.1696; FTIR (KBr, cm^{-1}) 3384, 2951, 2887, 1767, 1723, 1654, 1619, 1536, 1514, 1461, 1443, 1424, 1378, 1339, 1289, 1239, 1178, 1116, 1057, 1036, 991, 929, 920, 868, 802 cm^{-1} ; ^1H NMR and ^{13}C NMR data are not provided as the spectra were intractable as a result of the paramagnetic properties of this complex; $\mu_{\text{eff}} = 2.71$; $T_g = 176$ °C.

Preparation of 48a•Fe(III)



A solution of $\text{FeCl}_3 \cdot 6\text{H}_2\text{O}$ (204 mg, 0.754 mmol) in anhydrous EtOH (5 mL) was added to a solution of ligand **48a** (350 mg, 0.685 mmol) in THF (5 mL) in a round-bottomed flask equipped with a magnetic stirrer and a water-jacketed condenser. Triethylamine (220 μL , 159 mg, 1.58 mmol) was added, then the brown-coloured mixture was refluxed for 30 min. The mixture was then poured into H_2O , the resulting precipitate was collected by filtration, washed abundantly with H_2O , and allowed to completely dry under air to give 310 mg of a dark-brown coloured complex, **48a•Fe(III)**. (0.520 mmol, 76%). HRMS (MALDI) calcd for $\text{C}_{28}\text{H}_{28}\text{FeN}_8\text{O}_2$ (m/e): 564.1679, found: 564.1690; FTIR (KBr, cm^{-1}): 3390, 2953, 2888, 1766, 1722, 1625, 1536, 1512, 1461, 1444, 1422, 1377, 1340, 1292, 1239, 1179, 1116, 1058, 1036, 990, 929, 920, 870, 801, 759 cm^{-1} ; ^1H NMR (400 MHz, $\text{DMSO}-d_6$, 363 K): δ 9.08 (br d, 2H), 7.55-6.90 (br m, 13 H), 3.3-2.27 (br m, 38 H); ppm; ^{13}C NMR (75 MHz, $\text{DMSO}-d_6$): δ 167.6, 164.9, 163.0, 162.6, 155.3, 139.5, 136.4, 130.4, 122.5, 116.9, 26.7, 20.7 ppm; $\mu_{\text{eff}} = 3.59$; $T_g = 196$ $^\circ\text{C}$.

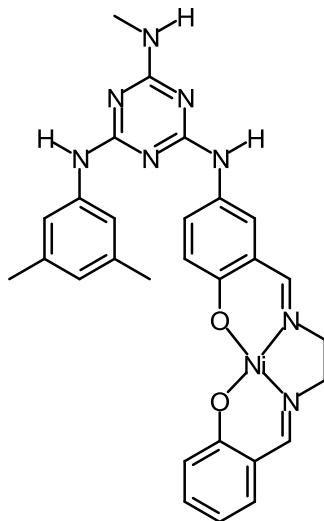
Preparation of 48a•Co(II)



A solution of $\text{Co}(\text{OAc})_2 \cdot 4\text{H}_2\text{O}$ (498 mg, 2.00 mmol) in anhydrous EtOH (5 mL) was added to a solution of ligand **48a** (509 mg, 1.00 mmol) in THF (10 mL) in a round-bottomed flask equipped with a magnetic stirrer and a water-jacketed condenser. The mixture was degassed by sparging with N_2 for 10 min, then the brown-coloured mixture was refluxed for 18 h under N_2 atmosphere. After cooling to ambient temperature, the mixture was poured into H_2O , then the precipitate was collected by filtration, briefly washed with H_2O , and allowed to dry under air to yield 370 mg of the dark-brown coloured complex, **48a•Co(II)** (0.660 mmol, 66%). HRMS (MALDI) calcd for $\text{C}_{28}\text{H}_{29}\text{CoN}_8\text{O}_2$ (m/e): 568.1740, found: 568.1749; FTIR (KBr, cm^{-1}): 3392, 2952, 2888, 1769, 1769, 1723, 1623, 1513, 1460, 1443, 1422, 1376, 1340, 1281, 1262, 1239, 1177, 1116, 1058, 1036, 991, 929, 920, 869, 801, 759 cm^{-1} ; ^1H NMR (400 MHz, $\text{DMSO}-d_6$, 363 K): δ 9.08 (br d, 2H), 7.64 (br m, 6H), 6.73 (br m, 3H), 3.71 (br s, 8.5), 3.02 (br s, 3H), 2.36 (br s, 7H) ppm; ^{13}C NMR (75 MHz, $\text{DMSO}-d_6$): δ 167.4, 166.1, 164.1, 160.4, 140.2, 137.1, 134.2, 129.4, 125.1, 123.0, 122.6, 117.5, 117.2, 114.9, 57.7, 27.2, 21.2 ppm; $\mu_{\text{eff}} = 2.04$; $T_{\text{dec}} = 170$ °C.

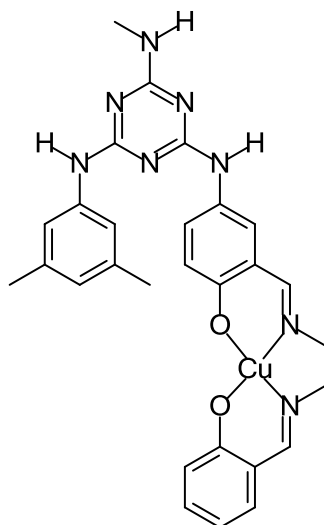
Complexes containing Ni(II) and Cu(II) metal centres were synthesized according to the same procedure as analogue cobalt complex, **48a•Co(II)** from their respective acetates ($\text{Ni}(\text{OAc})_2 \cdot 4\text{H}_2\text{O}$, $\text{Cu}(\text{OAc})_2 \cdot x\text{H}_2\text{O}$) except that the reactions were run under an ambient atmosphere:

Preparation of 48a•Ni(II)



Colour: Orange-brown; Yield: 78%; HRMS (MALDI) calcd for $C_{28}H_{29}N_8NiO_2$ (m/e): 567.1761, found: 567.1785; FTIR (KBr, cm^{-1}): 3375, 2952, 2886, 1765, 1667, 1620, 1535, 1511, 1460, 1424, 1378, 1337, 1311, 1278, 1239, 1179, 1116, 1044, 991, 921, 869, 849, 802, 780, 762 cm^{-1} ; 1H NMR (400 MHz, DMSO- d_6 , 363 K): δ 8.38 (s, 1H), 8.32 (s, 1H), 7.80 - 7.79 (m, 1H), 7.72 - 7.71 (m, 1H), 7.55 (s, 1H), 7.45-7.43 (m, 1H), 7.36 (s, 2H), 7.23-7.21 (m, 1H), 7.16 (t, 1H), 6.73 - 6.71 (m, 1H), 6.69 - 6.66 (m, 1H), 6.59 (s, 1H), 6.49 (m, 1H), 6.44 (m, 1H), 3.42 (s, 3H), 2.87 - 2.86 (m, 3H), 2.24 (s, 6H) ppm; ^{13}C NMR (75 MHz, DMSO- d_6): δ 166.0, 164.1, 163.8, 162.4, 162.2, 160.4, 140.2, 139.1, 137.0, 133.4, 132.7, 129.2, 127.3, 124.8, 122.9, 120.2, 119.6, 119.1, 117.5, 114.2, 57.9, 27.2, 21.1 ppm; T_g = 133. °C.

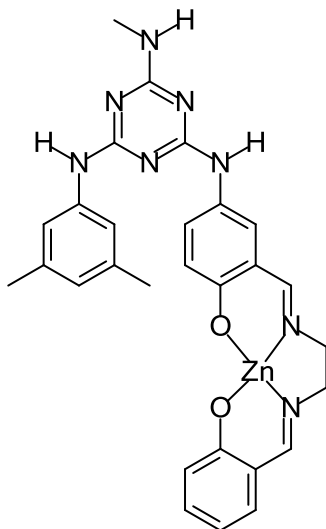
Preparation of 48a•Cu(II)



Colour: Olive-green; yield: 84%; HRMS (MALDI) calcd for $C_{28}H_{29}CuN_8O_2$ (m/e): 572.1704, found: 572.1727; FTIR (KBr, cm^{-1}): 3379, 2949, 2886, 1770, 1722, 1631, 1602, 1521, 1460, 1425, 1379, 1339, 1301, 1239, 1176, 1116, 1057, 1036, 991, 929, 920, 861, 801, 762 cm^{-1} ;

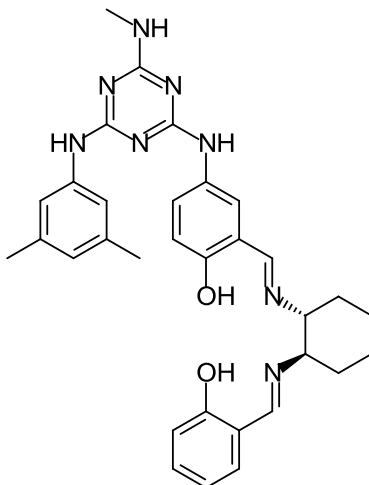
^1H NMR (400 MHz, $\text{DMSO-}d_6$, 363 K): δ 8.29 (br s, 1H), 8.04 (br m, 0.5H), 7.29 (br s, 1H), 6.60 (br s, 1H), 6.35 (br m, 1H), 3.62 (br s, 2H), 2.80 (br s, 3H), 2.26 (br s, 6H) ppm; ^{13}C NMR (75 MHz, $\text{DMSO-}d_6$): δ 165.9, 163.7, 140.2, 137.2, 129.3, 123.2, 117.6, 114.6, 67.0, 27.2, 21.3 ppm; $\mu_{\text{eff}} = 2.25$; $T_g = 159$ °C.

Preparation of **48a**•Zn(II)



A solution of ZnCl_2 (150 mg, 0.110 mmol) in anhydrous EtOH (2 mL) was added to a solution of ligand **48a** (56.0 mg, 0.100 mmol) in THF (2 mL) in a round-bottomed flask equipped with a magnetic stirrer and a water-jacketed condenser. NEt_3 (30.0 μL , 0.230 mmol) was added and the yellow-coloured mixture was refluxed for 30 min under ambient atmosphere. After cooling to ambient temperature, the mixture was poured into H_2O , then the precipitate was collected by filtration, briefly washed with H_2O , and allowed to dry under air to yield 44.1 mg of the yellow solid complex, **48c**•Zn(II) (77 μmol , 77%). HRMS (MALDI) calcd for $\text{C}_{28}\text{H}_{29}\text{N}_8\text{O}_2\text{Zn}$ (m/e): 573.1699, found: 573.1715. FTIR (KBr, cm^{-1}) 3388, 2951, 2887, 2733, 1768, 1723, 1620, 1512, 1485, 1460, 1443, 1422, 1376, 1340, 1278, 1238, 1178, 1116, 1058, 1036, 991, 929, 920, 870, 801, 761 cm^{-1} ; ^1H NMR (400 MHz, $\text{DMSO-}d_6$, 363 K): δ 8.44 (s, 1H), 8.34 (s, 1H), 7.37 (m, 4H), 7.16-7.07 (m, 1H), 6.92-6.81 (m, 1H), 6.61-6.56 (m, 2H), 3.73 (s, 3H), 2.83 (s, 3H), 2.20 (s, 6H) ppm; ^{13}C NMR (75 MHz, $\text{DMSO-}d_6$): δ 171.5, 168.5, 168.3, 166.6, 164.6, 140.9, 137.5, 133.2, 129.1, 127.9, 123.4, 123.2, 122.7, 119.8, 118.3, 117.9, 114.3, 56.3, 29.5, 27.8, 21.7 ppm; $T_g = 146$ °C.

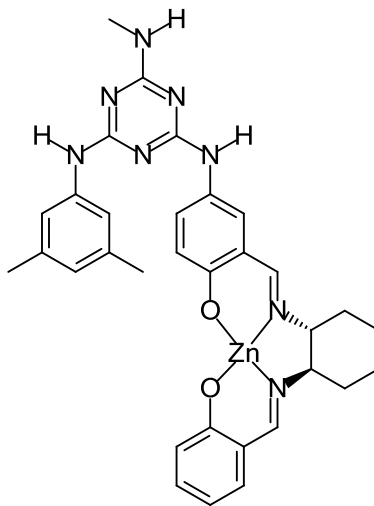
Synthesis of Chiral Ligand 48b



The synthetic route used to synthesize this compound were previously established in unpublished work by Dr. M. Jokar. Salicylaldehyde (710 μL , 830 mg, 6.80 mmol) in CH_2Cl_2 (50 mL) was added dropwise to a vigorously stirred solution of (1R,2R)-diaminocyclohexane (780 mg, 6.80 mmol) in CH_2Cl_2 (150 mL) containing 3 Å molecular sieves at 0 °C. The complete addition took approximately 5 hours, and then the reaction mixture was stirred for 5 h without interruption. Upon filtration, the filtrate was evaporated under vacuum at 60 °C to give a pale-yellow creamy solid, 1.43 g (6.56 mmol, 95%): ^1H NMR (300 MHz, CDCl_3) δ 13.34 (s, 0.3 H), 13.24 (s, 0.7 H), 8.41 (s, 0.6 H), 8.23 (s, 0.4 H), 7.21-7.31 (m, 2 H), 6.77-6.96 (m, 2 H), 3.23-3.31 (m, 0.6 H), 2.83 (q, 1 H), 2.21-2.29 (m, 0.4 H), 1.77-1.91 (m, 2 H), 1.51-1.77 (m, 2 H), 1.11-1.50 (m, 4 H) ppm.

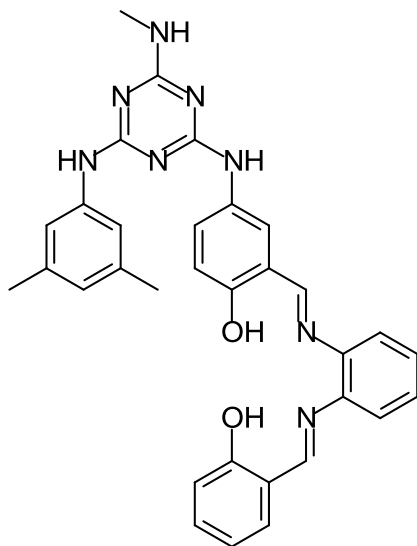
To an ethanol solution (20 mL) of the resulting chiral monoimine intermediate (437 mg, 2.00 mmol) was added dropwise 2-mexylamino-4-methylamino-6-[(4-hydroxy-3-formylphenyl)amino]-1,3,5-triazine (**45**) (728 mg, 2.00 mmol) in 20 mL of ethanol at ambient temperature. The mixture was gradually heated to 80 °C and this temperature was maintained for 4 h. Upon the removal of the solvent and cooling, a yellow precipitate was collected and precipitated from ethanol to give 1.07 g of the yellow chiral ligand **48b**, (1.71 mmol, 85%): HRMS (ESI) calcd for $\text{C}_{32}\text{H}_{37}\text{N}_8\text{O}_2$ (m/e): 565.3034, found: 565.3057; FTIR (KBr, cm^{-1}): 3400, 3279, 3055, 3011, 2930, 2857, 1631, 1579, 1517, 1492, 1430, 1396, 1275, 1185, 1144, 1092, 1041, 976, 940, 881, 837, 808, 783, 756, 736, 687, 663 cm^{-1} ; ^1H NMR (300 MHz, $\text{DMSO}-d_6$, 298 K): δ 13.25 (br s, 1 H), 12.90 (br s, 1 H), 8.93 (br s, 0.5 H), 8.88 (br s, 0.5 H), 8.76 (br s, 0.5H), 8.72 (br s, 0.5 H), 8.47 (d, $J = 5.1$ Hz, 1 H), 8.45 (br s, 1 H), 7.80 (br m, 1 H), 7.33-6.82 (m, 5 H), 6.82-6.70 (m, 4 H), 6.52 (s, 1 H), 3.31-3.38 (m, 2 H), 2.79 (s, 3 H), 2.18 (s, 6 H). 1.21-1.85 (m, 8 H) ppm; ^1H NMR (400 MHz, $\text{DMSO}-d_6$, 363 K): δ 9.97 (s, 1 H), 8.98 (br s, 1 H), 8.52 (br s, 1 H), 8.32 (s, 1 H), 8.11 (d, 1 H), 7.49 (m, 2 H), 7.37 (s, 2 H), 6.65 (br s, 1 H), 6.63 (s, 1 H), 2.90 (d, 3 H), 2.25 (s, 6 H) ppm; ^{13}C NMR (75 MHz, $\text{DMSO}-d_6$): δ 166.5, 165.5, 165.5, 165.5, 164.6, 164.3, 160.8, 155.9, 140.6, 137.5, 132.7, 132.1, 123.6, 119.0, 118.9, 118.3, 118.1, 116.8, 116.4, 71.8, 33.1, 33.0, 27.7, 24.1, 21.6 ppm; $T_g = 99$ °C.

Preparation of 48b•Zn(II)



A solution of ZnCl_2 (20.0 mg, 0.215 mmol) in anhydrous EtOH (2 mL) was added to a solution of ligand **48b** (100 mg, 0.196 mmol) in THF (2 mL) in a round-bottomed flask equipped with a magnetic stirrer and a water-jacketed condenser. NEt_3 (63.0 mL, 0.451 mmol) was added and the yellow mixture was refluxed for 30 min under ambient atmosphere. After cooling down to ambient temperature, the mixture was poured into H_2O , then the precipitate was collected by filtration, briefly washed with H_2O , and allowed to dry under air to yield 93.4 mg of the yellow complex **48c•Zn(II)** (0.149 mmol, 76%). HRMS (MALDI) calcd for $\text{C}_{32}\text{H}_{35}\text{N}_8\text{O}_2\text{Zn}$ (m/e): 627.2169, found: 627.2183; FTIR (KBr, cm^{-1}): 3381, 2948, 2885, 1765, 1723, 1612, 1539, 1516, 1491, 1460, 1443, 1423, 1402, 1377, 1341, 1315, 1299, 1277, 1238, 1178, 1116, 1043, 991, 929, 920, 869, 849, 803 cm^{-1} ; ^1H NMR (400 MHz, $\text{DMSO}-d_6$, 363 K): δ 8.23 (s, 2H), 7.34 (m, 5H), 7.23 (d, 1H), 7.13 (t, 1H), 6.60 (m, 2H), 6.55 (d, 2H), 6.42 (t, 2H), 3.19 (s, 2H), 2.83 (s, 3H), 2.19 (s, 6H), 1.91 (s, 2H), 1.41-1.39 (m, 4H) ppm; ^{13}C NMR (75 MHz, $\text{DMSO}-d_6$): δ 171.3, 167.8, 166.6, 165.1, 164.8, 140.8, 139.7, 137.5, 135.9, 133.2, 129.1, 125.8, 125.4, 123.4, 123.1, 122.6, 119.8, 118.3, 118.0, 112.6, 65.0, 35.0, 30.6, 28.2, 27.7, 24.3, 21.7 ppm; $T_g = 165$ °C.

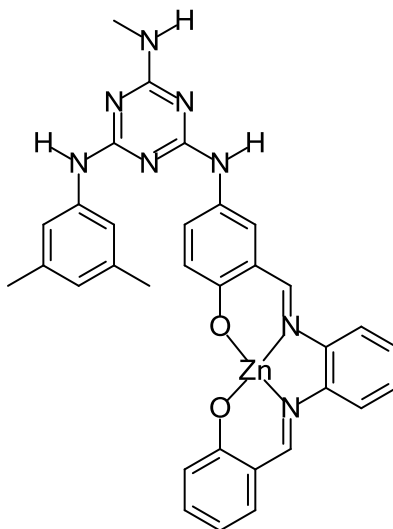
Synthesis of ligand **48c**



The synthetic route used to synthesize this compound were previously established in unpublished work by Dr. M. Jokar. Solutions of salicylaldehyde (1.10 mL, 1.22 g, 10.0 mmol) and *o*-phenylenediamine (1.08 g, 10.0 mmol) in ethanol (20 mL each) were combined. The mixture was then refluxed for 4 h. The reaction mixture was condensed by rotary evaporation and left to cool. The resulting monoimine intermediate precipitated on cooling and then was it filtered off, washed with ethanol and recrystallized from ethanol. The purity of the intermediate was monitored on TLC using ethyl acetate/petroleum ether 1:1 to give a brown solid (90% yield).⁴ ¹H NMR (300 MHz, CDCl₃): δ 12.83 (s, 1 H), 8.63 (s, 1 H), 7.47-6.77 (m, 8 H), 3.79 (br, 2 H) ppm.

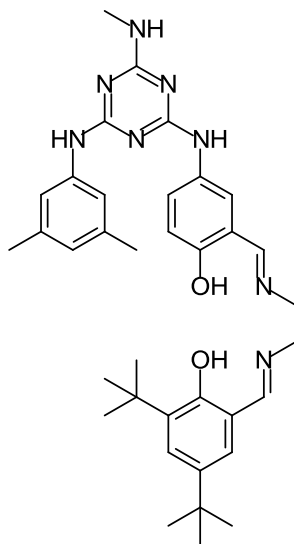
A solution of 2-mexylamino-4-methylamino-6-[(4-hydroxy-3-formylphenyl)amino]-1,3,5-triazine **45** (364 mg, 1.00 mmol) and salicylaldehyde 2-aminophenyl monoimine (212 mg, 1.00 mmol) in dry ethanol (10 mL) was refluxed for 3 h. The solvent was evaporated under vacuum to afford a residue, which was reprecipitated from hexane/ethyl acetate to give 477 mg (0.820 mmol, 82%) of the yellow solid compound, **48c**. HRMS (ESI) calcd for C₃₂H₃₀NaN₈O₂ (m/e): 581.2384, found: 581.2396; FTIR (KBr, cm⁻¹): 3392, 3274, 3221, 3061 2959, 2918, 1614, 1572, 1514, 1487, 1428, 1396, 1320, 1299, 1275, 1213, 1184, 1152, 1130, 1116, 1104, 1035, 976, 939, 907, 883, 840, 750, 685, 646 cm⁻¹; ¹H NMR (300 MHz, DMSO-*d*₆, 298 K): δ 12.9 (br s, 0.6 H), 12.58 (br s, 1H), 12.39 (br s, 0.4 H), 9.07 (br s, 0.5 H), 8.92 (br s, 2 H), 8.74 (br s, 1.5 H), 8.11 (br s, 1 H), 7.45 (br m, 2 H), 7.45-7.21 (m, 6 H), 6.92 (d, 2 H), 6.87 (d, 3 H), 6.51 (s, 1 H), 2.80 (s, 3 H), 2.18 (s, 6 H) ppm; ¹H NMR (400 MHz, DMSO-*d*₆, 363 K): δ 9.97 (s, 1 H), 8.98 (br s, 1 H), 8.52 (br s, 1 H), 8.32 (s, 1 H), 8.11 (d, 1 H), 7.49 (m, 2 H), 7.37 (s, 2 H), 6.65 (br s, 1 H), 6.63 (s, 1 H), 2.90 (d, 3 H), 2.25 (s, 6 H) ppm; ¹³C NMR (75 MHz, DMSO-*d*₆): δ 166.6, 165.9, 164.5, 160.8, 156.1, 142.8, 140.6, 137.5, 133.9, 132.9, 132.4, 128.7, 123.6, 120.20, 119.9, 119.5, 119.1, 118.1, 117.1, 116.8, 150, 27.7, 21.6 ppm; T_g = 69 °C.

Preparation of 48c•Zn(II)



The orange coloured complex, **48c•Zn(II)**, was synthesized according to the same procedure as analogue **48a•Co(II)** from ligand **48c** and $\text{Zn}(\text{OAc})_2 \cdot 2\text{H}_2\text{O}$. Yield: 60%; HRMS (MALDI) calcd for $\text{C}_{32}\text{H}_{31}\text{N}_8\text{O}_2\text{Zn}$ (m/e): 621.1699, found: 621.1702; FTIR (KBr, cm^{-1}): 3389.14, 2950.89, 2886.98, 1767.89, 1722.85, 1613.85, 1513.85, 1484.42, 1460.44, 1443.78, 1422.4, 1377.88, 1340.37, 1317.03, 1278.97, 1238.68, 1177.79, 1116.46, 1058.04, 1036.32, 991.01, 929.82, 920.52, 869.99, 801.38, 761.39 cm^{-1} ; ^1H NMR (400 MHz, $\text{DMSO-}d_6$, 363 K): δ 8.96 (s, 1H), 8.85 (s, 1H), 8.41 (s, 1H), 8.30 (s, 1H), 7.86 (m, 1H), 7.79 (s, 1H), 7.73 (s, 1H), 7.49 – 7.47 (d, 1H), 7.39 (m, 5H), 7.25 (t, 2H), 6.73 (t, 2H), 6.56 (s, 1H), 6.52 (t, 1H), 6.45 (m, 1H), 2.89 (s, 3H), 2.21 (s, 7H) ppm; ^{13}C NMR (75 MHz, $\text{DMSO-}d_6$): δ 172.2, 169.0, 166.0, 164.2, 162.7, 162.1, 140.2, 139.3, 137.0, 136.1, 134.2, 130.5, 127.1, 127.1, 126.0, 124.8, 123.0, 122.9, 122.6, 119.3, 117.9, 117.5, 116.4, 116.2, 112.9, 27.2, 21.1 ppm; $T_g = 167$ °C;

Attempted Synthesis of 3,5-di-*t*-butyl Salen Schiff-base (49)



(Method A) Attempts for the preparation for the synthesis of a 3,5-di-*t*-butyl salen-glass ligand (**49**) followed similar procedures to the synthesis of ligand **48a**. A solution of 2-methylamino-4-methylamino-6-[(4-hydroxy-3-formylphenyl)amino]-1,3,5-triazine (364 mg, 1.00 mmol) **45** and 3,5-di-*t*-butyl-salicylaldehyde (108 mg, 1.00 mmol) in 10 mL absolute ethanol was added drop wise to a solution of 1,2-ethylenediamine (60.0 μ L, 54.1 mg, 1.00 mmol) in 10 mL absolute ethanol in a round bottomed flask equipped with a magnetic stir rod. The resulting mixture was sealed and left stirring for 24 h at room temperature. Overnight a precipitate had formed which was filtered, rinsed with 10 mL of ethanol, and excess solvent was removed under vacuum to afford a residue. The result was an intractable mixture of products.

(Method B) A second series of attempts were made using the same procedures as those employed for **48a**; however, following the complete addition of reactants the mixture was left at reflux for 24 hours. A solution of 2-methylamino-4-methylamino-6-[(4-hydroxy-3-formylphenyl)amino]-1,3,5-triazine (364 mg, 1.00 mmol) **45** and 3,5-di-*t*-butyl-salicylaldehyde (108 mg, 1.00 mmol) in 10 mL absolute ethanol was added drop wise to a solution of 1,2-ethylenediamine (60.0 μ L, 54.1 mg, 1.00 mmol) in 10 mL absolute ethanol in a round bottomed flask equipped with a magnetic stir rod and the mixture was refluxed for 24 h. The precipitate was removed by filtration, washed with 10 mL of ethanol while hot, and the excess solvent removed in vacuum to afford a residue. The result was an intractable mixture of products.

(Method C) Another series of attempts were performed using the procedures for ligands **48b** and **48c**. A mixture of 3,5-di-*t*-butyl-salicylaldehyde (1.60 g, 6.80 mmol) and *o*-phenylenediamine (740 mg, 6.80 mmol) in absolute ethanol (10 mL) was stirred in a round-bottomed flask equipped with a magnetic stir bar at reflux conditions 4 h. The crude intermediate was obtained by removing solvents *via* rotary evaporation to give 1.2 g of a yellow solid. A solution of 2-methylamino-4-methylamino-6-[(4-hydroxy-3-formylphenyl)amino]-1,3,5-triazine **45** (364 mg, 1.00 mmol) and 3,5-di-*t*-butylsalicylaldehyde 2-aminophenyl monoimine (325 mg, 1.00 mmol) in dry ethanol (10 mL) was refluxed for 4 h. The product was precipitated from hexane and allowed to dry in air. The result was an intractable mixture of products.

4.4. Summary

Mexylaminotriazine molecular glasses functionalized with salen ligands were successfully synthesized. A series of successive substitution reactions was utilized to prepare a glass-forming salicylaldehyde **45** in good yield, which could be used as the common precursor to synthesize several glass-forming salen ligands. Mexylaminotriazine-functionalized salicylaldehyde **45** was reacted through a condensation mechanism with salicylaldehyde and ethylenediamine, (1R,2R)-1,2-diaminocyclohexane, or 1,2-phenylenediamine to generate the respective glass-forming salen ligands. The yields obtained were good and the resulting ligands demonstrated the ability to readily form long-lived glasses. From these ligands, a series of transition metal complexes were synthesized and characterized. These ligands were subsequently reacted with transition metal salts under reflux conditions in order to give the corresponding transition metal complexes in good yields. Complexes and ligands were then characterized using NMR spectroscopy, FTIR spectroscopy, and HRMS techniques. The T_g of these complexes was measured by DSC, which was used to demonstrate the glass-forming properties and the ability of most complexes to form uniform thin films. The T_g values for the mexylaminotriazine ligands ranged from 69 °C to 131 °C, while that of the subsequent coordination complexes ranged from 133 °C to 196 °C. It is proposed that the metal complexes exhibit higher glass transition as a result of the decreased molecular mobility caused by the coordination of metal centres. Only one exception was noted, the Co(II) complex decomposed at 225 °C and was the only sample that did not exhibit a glass transition. This research identified two areas of focus for future research. Firstly, the role of the metal centre was identified as a factor that influences glass-forming abilities in these complexes. A range of glass transition temperatures between the synthesized complexes of ligand **48a** indicate that the metal centre has an effect on the thermal properties of these complexes that must be investigated. Secondly, the synthesized complexes were found to have lower solubility compared to their respective ligands. The synthesis of glass-forming salen complexes with increased solubility may be important for the future application of these compounds.

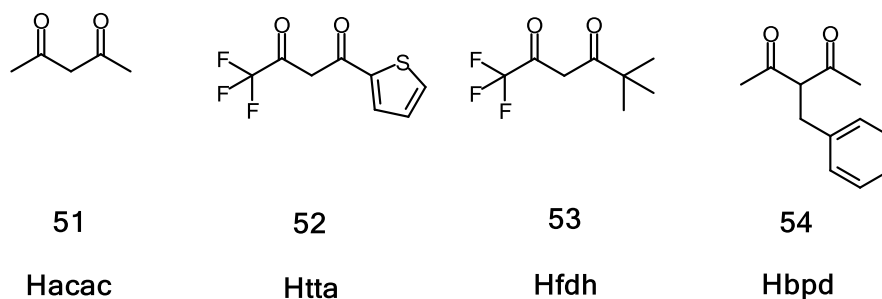
5. Acetylacetonate Functionalized Molecular Glass Complexes

5.1. Introduction

Thin film materials have been instrumental in the development of a number of fields such as optoelectronics, sensors, and solid-state catalysis.^{147–149} Small molecules offer a number of distinct advantages over polymers, the traditional method of incorporating specific functionalities into thin films. Small molecules are easier to purify, characterize, and their monodisperse nature leads to more homogeneous behaviour between different samples. Regrettably, most small-molecule materials have difficulty adopting glassy states without the use of special processing techniques, such as quenching with liquid nitrogen, and most of those that can adopt amorphous phases readily crystallize heated above their glass transition temperature, or on resting for longer periods of time. A class of small molecules, called molecular glasses, or amorphous molecular materials, have been specifically designed to possess structures that resist crystallization. Integrating irregular shapes, non-planarity, and conformational equilibria are several such structural features that can be implemented in order to synthesize compounds that readily form glassy phases and remain amorphous for extended periods of time.

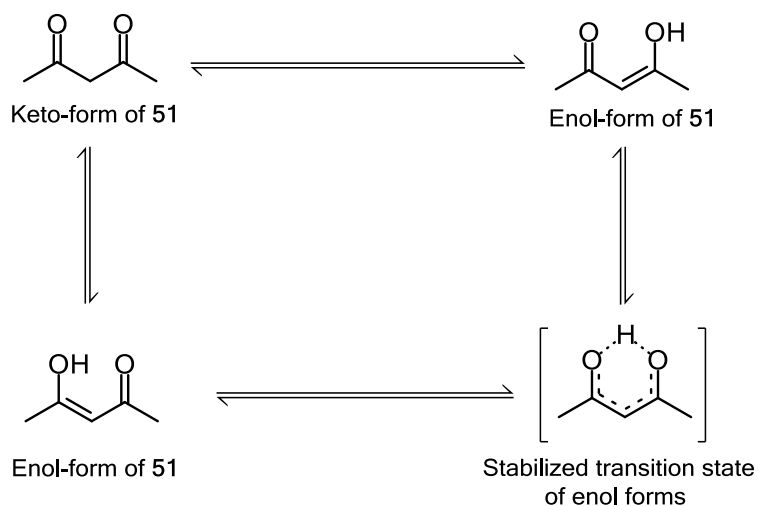
Our group has developed a class of compounds, based on methylaminotriazine units, which can be used to consistently design and synthesize organic materials that spontaneously form glassy phases and exhibit high resistance to crystallization. Exploiting the features listed above, these methylaminotriazine derivatives frustrate crystallization by 1) forming various conformers of similar energy with high interconversion barriers; and 2) through hydrogen bonding interactions that further limit the mobility of the molecules in the solid-state. Furthermore, it has been shown that methylaminotriazine molecular glasses functionalized with reactive groups can be used to incorporate other functionalities, such as chromophores or semiconductors, in order to obtain adducts that retain the properties and characteristics of both parent compounds. Using this strategy, it is hypothesized that several methylaminotriazine-functionalized ligands can be synthesized to generate corresponding coordination complexes that are also capable of glass formation.

β -diketones are a family of compounds possessing two carbonyl functional groups separated by a single carbon atom. They are commonly used as ligands and have been studied for over 100 years.^{150,151} The deprotonated conjugated bases of β -diketones form excellent coordination complexes with transition metals and have been studied for a number of purposes within the field of inorganic chemistry.¹⁵² The α -carbon of these compounds can be deprotonated to yield the respective anionic ligands. The simplest β -diketone is 2,4-pentanedione, commonly known as acetylacetonate (Hacac, **51**). Hacac is a β -diketone with a methyl group substituent on both carbonyls.¹⁴⁷ Many derivatives of β -diketones exist, producing analogues with varying steric and electronic properties resulting from the substituted functional groups at the α and β carbons.¹⁴⁷ Several examples of commonly used β -diketones include; 2-thenoyltrifluoroacetone (Htta, **52**), 1,1,1-trifluoro-5,5-dimethyl-2,4-hexanedione (Hfdh, **53**), and 3-benzyl-2,4-pentanedione (Hbpd, **54**) (Scheme 24).^{147,153}



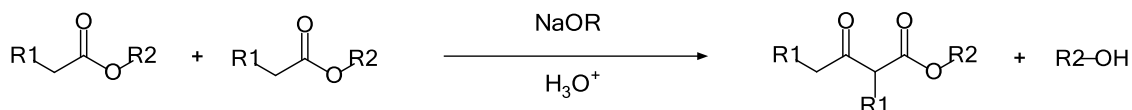
Scheme 24: Structures of common β -diketones: acetylacetone (**51**), 2-thenoyltrifluoroacetone (**52**), 1,1,1-trifluoro-5,5-dimethyl-2,4-heptanedione (**53**), and 3-benzyl-2,4-pentanedione (**54**).

Acetylacetone and its β -diketone derivatives exhibit a characteristic keto-enol tautomerism, a shifting equilibrium between two structural forms, one possessing two ketones, the other a ketone and an enol. Typically, this equilibrium is shifted towards the mono-enol form as a result of stabilization through a six-membered ring that forms *via* intramolecular O-H-O hydrogen bonding (Scheme 25).^{153,154} The keto-enol equilibrium is affected by a number of factors such as the functionalization of the derivative, solvent polarity, temperature, and the presence of other chemicals (in solution).^{147,153} For example, 81% of acetylacetone exists in the mono-enol form at room temperature, whereas a bulky α -alkyl substituent, such as an isopropyl or butyl alkyl group, exhibits an equilibrium shifted almost completely towards the di-keto tautomer.^{147,155} On the other hand, the presence of a chlorine group at the α -position of a β -diketone can shift the proportion of the enol tautomer to 92%. The polarity of solvents and temperature are also important factors in determining the keto-enol tautomer equilibrium. Lower polarity solvents and lower temperatures tend to shift the equilibrium towards the mono-enol form.¹⁴⁷ The ratio of keto and enol tautomers can often be evaluated using ^1H NMR. If the compound exists in an equilibrium of the two tautomers, specific peaks will appear in ^1H NMR that are characteristic of each form. For example, a CH_2 peak will often be seen for the keto tautomer, while, a CH peak will appear for the enol form. The ratio of their integrations can be used to describe the equilibrium of these two forms. This keto-enol tautomerization is critical to the preparation of metal complexes of these ligands.

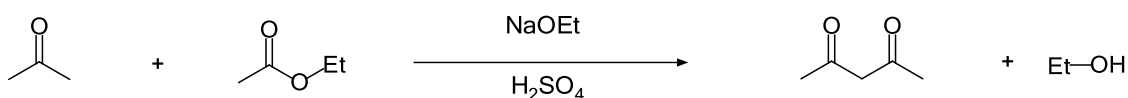


Scheme 25: Keto-enol tautomerism of β -diketones.

Acetylacetone itself, along with various substituted analogues, is commercially available and relatively inexpensive.¹⁴⁷ β -diketones can also be synthesized using a variety of well-established procedures, such as aldol condensations, acylation of ketones, or Claisen condensations.^{147,156–162} The Claisen condensation in particular has been employed for the synthesis of many β -diketones. The general scheme of a Claisen condensation is depicted in Scheme 26. A scheme depicting the synthesis of acetylacetone using the procedures described for the Claisen condensation from ethyl acetate and acetone is shown in Scheme 27. This reaction is performed by the sequential dropwise addition of the starting materials in diethyl ether with a slight excess of base.¹⁵⁶



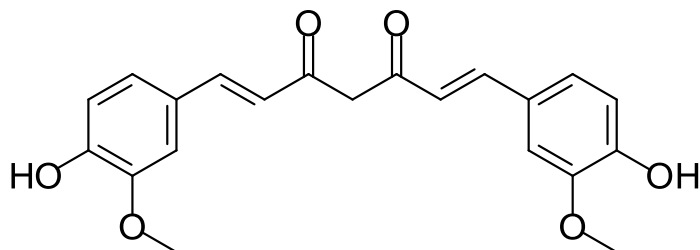
Scheme 26: General scheme of the Claisen condensation.



Scheme 27: Synthesis of acetylacetone from ethyl acetate, acetone, and sodium ethoxide *via* a Claisen condensation reaction.¹⁶³

β -Diketonates are bidentate ligands that are capable of forming metallic complexes with nearly all metal ions.¹⁶⁴ β -diketones can be deprotonated to form an anionic mono-enolate species which may coordinate to metal atoms in a bidentate, chelating fashion *via* the two oxygen atoms, forming a six-membered planar ring.¹⁵³ As the diketones must be deprotonated to form the corresponding monoenolates, a base is generally used *in situ* during the coordination reaction. Due to the presence of two carbonyl groups, the α -carbon's proton is relatively acidic ($\text{pK}_a = 8.99$ at $25\text{ }^\circ\text{C}$)¹⁶⁵ and can be removed by a range of bases.¹⁴⁷ Some complexes can also be prepared *via* a metathesis reaction.¹⁵¹ Typically, two or three acac ligands will be coordinated to a single metal to form either bis-acetylacetonates ($\text{M}(\text{acac})_2$) or tris-acetylacetonates ($\text{M}(\text{acac})_3$) of nearly all metal species.¹⁶⁴ Although less frequently prepared, heteroleptic complexes also exist, particularly with nitrogen-donor Lewis bases such as 1,10-phenanthroline and 2,2'-bipyridine.¹⁵¹

β -diketones can accommodate a wide variety of substituents. Altering the substituents of diketones can modulate the solubility, volatility, acidity, and thermal properties of these compounds and their respective complexes. For example, the inclusion of branched alkyl chains can increase the solubility of complexes in organic solvents whereas aromatic substituents exhibit stronger UV-Vis absorption.¹⁴⁷ Many aromatically substituted β -diketones containing electron-donating groups, such as thiophene, typically exhibit higher luminescence than other β -diketones.¹⁴⁷ The structure of substituents can play a role in the energy levels of the ligands relative to the metal centre, a factor that influences whether a complex will luminesce.¹⁴⁷ Curcumin, 1,7-bis(4-hydroxyl-3-methoxyphenyl)-1,6-heptanedione-3,5-dione (**55**), a naturally occurring β -diketone found as one of the components of turmeric, has been found to possess potential for a variety of medical applications due to anti-cancer, anti-inflammatory, and anti-oxidative properties.^{166–170} In addition, curcumin has also been shown to exhibit luminescent properties when irradiated with UV and visible light.^{166–170}



Scheme 28: Molecular structure of curcumin, 1,7-bis(4-hydroxy-3-methoxyphenyl)-1,6-heptanedione-3,5-dione (**55**), a naturally occurring β -diketone.

β -diketonates and their metal complexes have been utilized for a broad range of applications throughout their history and development.¹⁵³ The application of β -diketonates relies heavily on a number of factors, such as the ability of the ligands to coordinate with a wide array of metal ions, and the ability to tailor and alter the substituents on the ligand.^{147,153} The tailorability of both inorganic and organic components of these complexes allows for the introduction of distinct chemical properties, such as luminescent properties, to the resulting complexes. As a result, acetylacetonate and its derivatives have been utilized for applications ranging from pharmaceuticals, optical devices, and analytical techniques.^{147,152,171} The polymer industry, for example, utilizes the chelating properties of β -diketonates for the production of both homogeneous and heterogeneous catalytic materials.¹⁴⁷ For example, vanadyl(IV) acetylacetonates catalyze the epoxidation of allylic alcohols by peroxides.¹⁴⁹ Alternatively, manganese(II) acetylacetonates have been used for the asymmetric sulfoxidation of sulfides¹⁷² and are currently being investigated as heterogeneous catalysts supported on metal-organic frameworks in alkene epoxidation reactions.¹⁴⁸

Many applications of β -diketonates are a direct result of the propensity for β -diketonates to form metal complexes.¹⁵³ β -diketonates are capable of coordinating to metals in either solution or gas phases, such as effluent or exhaust gases. This behaviour can be exploited for applications in fields like environmental or analytical chemistry. Environmental chemists can use these β -diketonate ligands to remove metals from effluent or exhaust gases, thereby preventing their release into the atmosphere. Alternatively, analytical chemists can use the chelating abilities of β -diketonates to bind with metals in order to analyze the chemical components of samples.¹⁴⁷ These β -diketonates can be used for applications such as chromatography as a component of stationary phases.

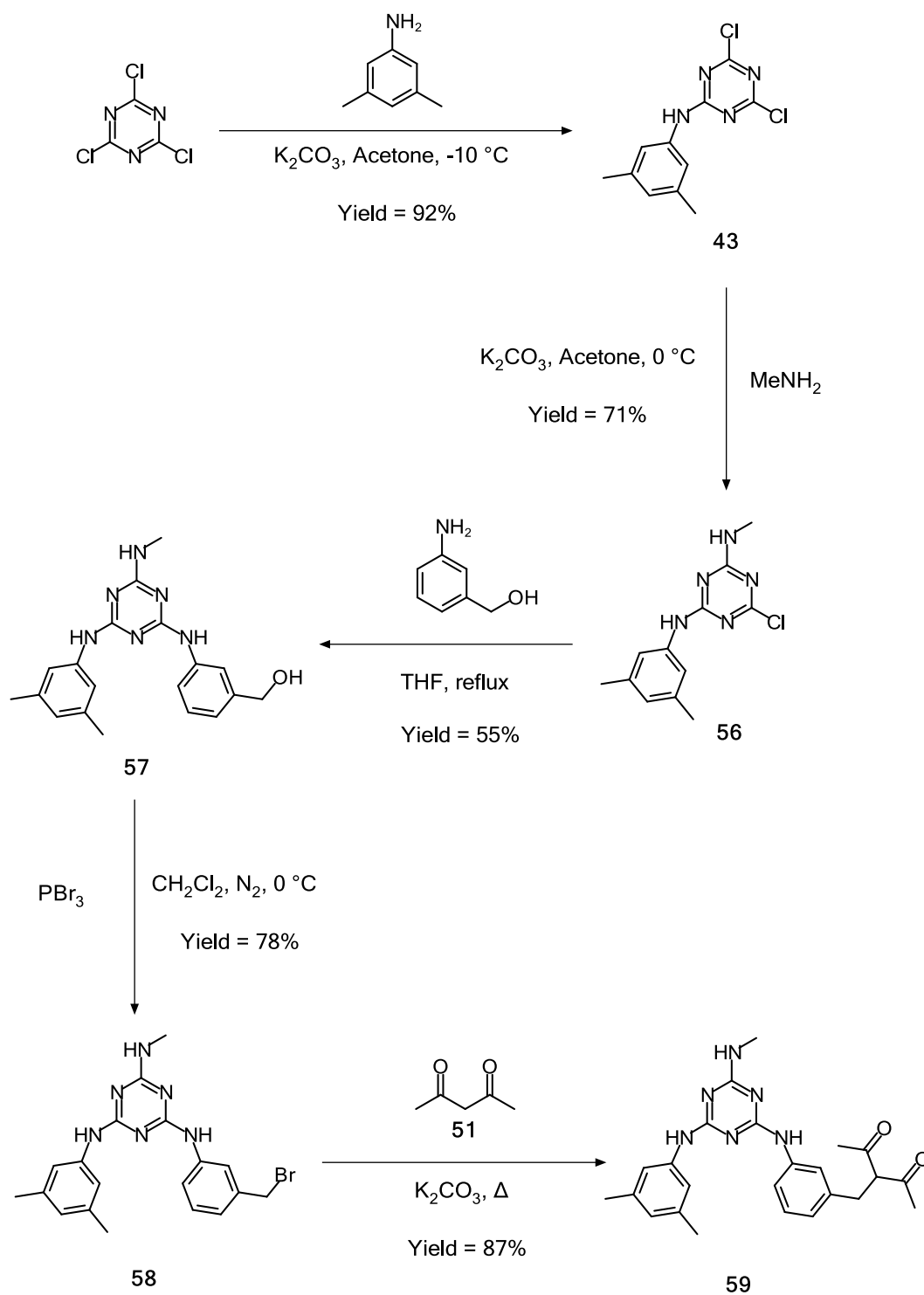
As one of the most versatile classes of ligands, acetylacetonate and its derivatives are model candidates for functionalization with a methylaminotriazine substituent in order to produce a series of highly tailorable, well-defined molecular glass coordination complexes. Functionalization of methylaminotriazine molecular glasses with a β -diketonate group is expected to yield acac ligands that can readily form glasses. Furthermore, as a result of the ability to form metal complexes with many different metals, the preparation of a library of glass-forming metal complexes using a glass-forming β -diketonate could provide an effective method of studying the effects of various metal centres and ligand substituents on the properties and glass-forming abilities of methylaminotriazine materials. Additionally, many applications of β -diketonates could be expanded by the potential for these ligands to adopt amorphous glassy phases and be used for the production of thin films. The incorporation of glass-forming properties *via* the introduction of methylaminotriazine substituents to the structure of acetylacetonate and other β -diketonates may pave the way towards the use of thin films for novel industrial applications. Herein, we report the synthesis and characterization of a

mexylaminotriazine-functionalized acetylacetonate ligand and the attempted preparation of its homoleptic and heteroleptic coordination complexes.

5.2. Results and Discussion

5.2.1. Synthesis and Characterization of Ligand

The synthesis of the bromomethyl precursor **58** was performed in 4 steps from cyanuric chloride according to the method depicted in Scheme 29. The synthesis of precursor **58** was performed according to the literature procedures.¹¹ Through a series of sequential substitutions at different temperatures it is possible to selectively substitute the three chlorides of cyanuric chloride with various alkyl- and arylamines, in the present case, with methylamine, 3,5-dimethylaniline, and 3-hydroxymethylaniline. The three amines can be introduced in any order, though starting with the substitution of 3,5-dimethylaniline has been shown to give higher yields.¹¹ The singly substituted precursor, 2-mexylamino-4,6-dichloro-1,3,5-triazine (**43**) was prepared *via* the dropwise addition of 3,5-dimethylaniline in the presence of K₂CO₃ at a temperature of -10 °C to give the desired intermediate in 90% yield (see Chapter 4), which is then reacted with methylamine under similar conditions but at a higher temperature (0-25 °C) to produce intermediate **56**. Intermediate **56**, the common precursor used to generate most functionalized mexylaminotriazine glasses, was thusly obtained in 69% yield. Compound **56** is then reacted with 3-aminobenzyl alcohol in THF under reflux conditions for 3 h to generate precursor **57** in 84% yield. A base is not required for the third substitution reaction as the product, compound **57**, effectively serves to neutralize the HCl generated during the reaction.¹¹ The hydroxymethyl group of compound **57** is then converted to a bromomethyl substituent by stirring with phosphorus tribromide under an inert atmosphere at 0 °C for 18 h to yield precursor **58** (2-mexylamino-4-methylamino-6-[(3-bromomethylphenyl)amino]-1,3,5-triazine) in 78% yield. Following the synthesis of **58**, it is possible to synthesize the desired ligand (**59**). The acidic proton on the α -carbon of acetylacetonate can be easily removed in the presence of a base (K₂CO₃), generating the reactive enolate carbanion species, which can then react with the bromomethyl group of precursor **58** in a single step *via* an S_N2 substitution reaction. The resulting compound (**59**), which is synthesized in 87% yield, is an acetylacetonate ligand functionalized with a glass-forming mexylaminotriazine at the α -carbon, termed “glacac”. Excess reagents and reaction by-products are easily removed *via* acidic aqueous extractions at the end of each substitution step, leaving the desired product behind. However, while purification was straightforward and did not require additional methods such as recrystallization or chromatography, it should be noted that the complete removal of solvents from the product was difficult. THF generally remained trapped in the material unless it had been melted under vacuum.

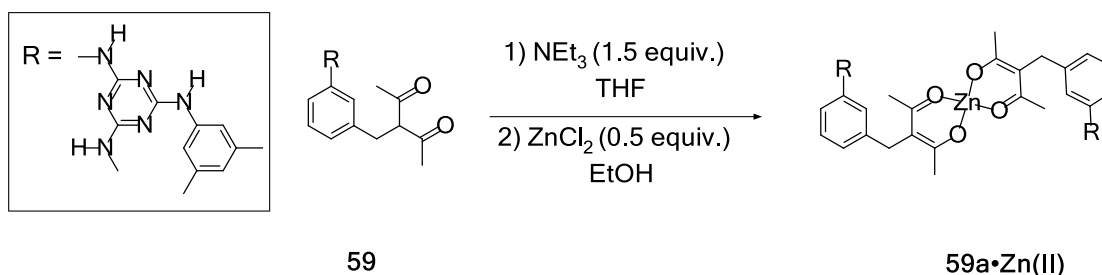


Scheme 29: Synthesis of 2-methylamino-4-methylamino-6-[(3-bromomethyl)phenyl]amino-1,3,5-triazine **58** and "glacac" ligand **59**.

Ligand **59** readily forms glassy phases upon drying from solution or by cooling from its melted phase. The corresponding glass transition temperature was measured using DSC. No crystallization was observed upon heating the compound and the glass transition was measured to be 68 °C, demonstrating the ability of the ligand to adopt a stable glassy phase. Furthermore, this glass transition is similar to the T_g values exhibited by other analogous mexylaminotriazines.¹¹ The measured glass transition of the ligand was only slightly lower than the reported T_g for the hydroxymethyl precursor **57** (69 °C) and was slightly higher than the reported T_g for the bromomethyl precursor **58** (62 °C).¹¹ This variation in T_g is likely the result of the hydrogen bonding interactions formed with these various substituents. The increased T_g relative to bromomethyl-functionalized compound **58** is likely due to the likelihood of the enol tautomer of ligand **59** to participate in hydrogen bonding interactions. The ability for this ligand to participate or not in these interactions likely further frustrates crystallization by adopting a number of conformations and packing in a disordered fashion. The T_g of the ligand, **59**, is comparable to the hydroxymethyl precursor, **57**, likely because these compounds can participate in hydrogen bonding interactions. Thermograms for TGA and DSC of compound **59** are provided in appendices B.2 and C.2, respectively.

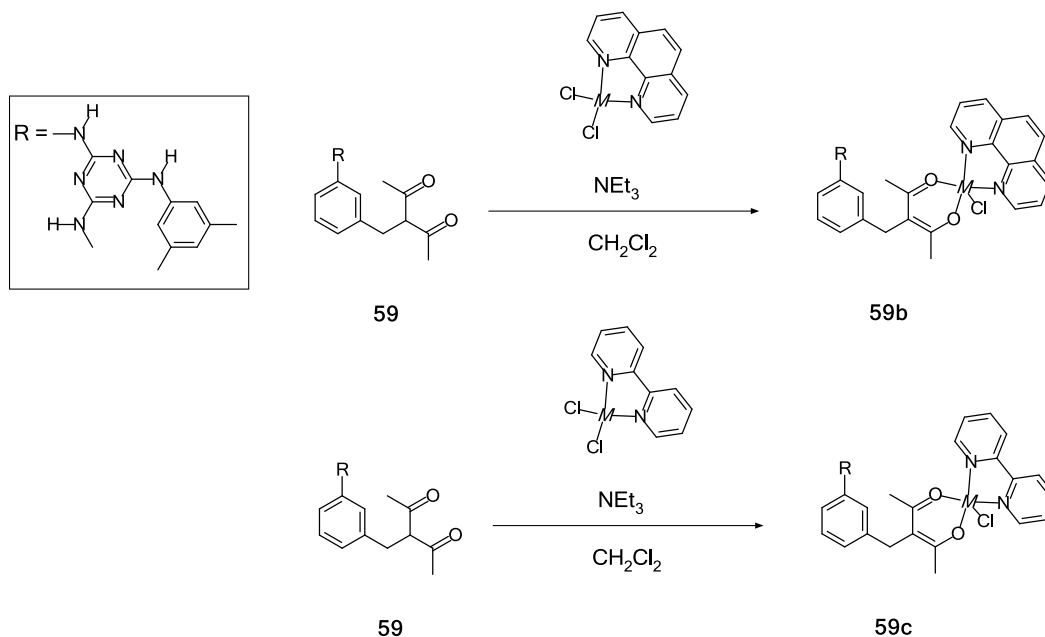
5.2.2. Coordination with Metals and Characterization

The synthetic routes attempted for the preparation of Zn(II), Ni(II), and Cu(II) homoleptic and heteroleptic coordination complexes of *glacac* ligand **59** are presented here and are modified from the preparation of analogous diketonate complexes in the literature.^{147,168,169} The first attempted synthetic route sought to prepare a homoleptic *bis*-*glacac* zinc complex, **59a•Zn(II)**, as is widely reported for other divalent transition metals.¹⁴⁷ A solution of ligand **59** in THF was treated with NEt₃ followed by the addition of a solution of ZnCl₂ in EtOH (Scheme 30). An excess of base was used to deprotonate the enolate and generate an anionic species, which was expected to coordinate to zinc cations. Several attempts were made to yield complex **59a•Zn(II)** by varying the solvents, reagents, and the reaction conditions like temperature, reaction time, and the sequence in which reagents were added. The same procedure was attempted with other metal salts (NiCl₂ and CuCl₂•2H₂O). This method failed to produce zinc(II) complexes of ligand **59**. This was confirmed *via* ¹H NMR in which the peaks for the keto-enol protons were compared. Samples were analyzed by ¹H NMR to demonstrate that the ligand was in fact deprotonated. This was shown by the absence of the peaks associated with the keto-tautomer of the ligand, and the presence of the enol peak. Despite this, the final product depicted both the keto and enol peaks. This suggestion that either coordination did not happen at all, or coordination had occurred but the reaction did not progress to completion, producing a mixture of the starting material and the product.



Scheme 30: Attempted preparation of complex **59a•Zn(II)**. Additional attempts were made using NiCl₂ and CuCl₂•2H₂O to prepare complexes **59a•Ni(II)** and **59a•Cu(II)**.

A second synthetic approach was attempted to prepare heteroleptic mexylaminotriazine-functionalized *glacac* complexes. In most cases, these complexes are prepared using β -diketonates such as curcumin, Htta, Hfdh, and other derivatives. A wide array of heteroleptic β -diketonate complexes are reported in the literature, particularly containing neutral nitrogen-donor ligands such as 1,10-phenanthroline and 2,2'-bipyridine.^{147,166–169,173,174} Similar procedures to those reported in the literature were employed for the preparation of glass-forming analogous complexes (Scheme 6).^{166,167,169,175} Zinc chloride salts were first reacted with 1,10-phenanthroline or 2,2'-bipyridine to form their respective complexes. Next, NEt_3 was added to a mixture of one these intermediate species and *glacac* (**59**) in CH_2Cl_2 to form the desired heteroleptic complexes **59b**•**Zn(II)** and **59c**•**Zn(II)** *via* a metathesis mechanism. The reaction mixtures were then washed with distilled water to remove excess metallic salts and reagents. Unfortunately, these reactions failed to give the desired complexes. A 1:1 ratio of the keto-enol peaks was observed *via* ^1H NMR. As was the case with the attempted preparation of **59a**•**Zn(II)**, the presence of the two tautomers of ligand **59** suggest that either the preparation was not successful or that a mixture of the product and starting material was obtained. Similar attempts were performed using a variety of reaction procedures, metal salts (NiCl_2 and $\text{CuCl}_2\cdot 2\text{H}_2\text{O}$), reagents, and conditions.



Scheme 31: Attempted procedures for the preparation of mixed ligand complexes **59b** and **59c**. M denotes **Zi(II)**, **Ni(II)**, and **Cu(II)** metal centres.

A third synthetic route was attempted involving an initial deprotonation of **59** to form a corresponding sodium salt. Ligand **59** was dissolved in warm *i*PrOH and the resulting solution was treated with sodium methoxide in methanol. This intermediate complex was prepared using a 1:1 stoichiometry and isolated by removing all solvent by rotary evaporation. The intermediate was then re-dissolved in CH_2Cl_2 and a solution of **Zn(II)**, **Cu(II)**, or **Ni(II)** bipyridine or phenanthroline complexes in CH_2Cl_2 was added to prepare the desired complexes *via* a metathesis mechanism. The resulting mixture was then condensed and washed with water to remove excess reagents. A variety of reaction conditions were again attempted for this third procedure. These attempts all resulted in a mixture of starting materials, ligand **59** and the bipyridine or phenanthroline

intermediates. No attempt to prepare heteroleptic compounds **59b** and **59c** were successful using either method described.

During one of the attempts to prepare the heteroleptic products, an aliquot of the unpurified reaction mixture was taken, solvent was removed by rotary evaporation and the resulting crude product was analyzed with ^1H NMR to determine whether the ligand was successfully deprotonated by triethylamine. The test demonstrated that in fact the ligand had been deprotonated, as the ^1H NMR spectrum did not exhibit the characteristic keto peaks. The subsequent failures to produce the desired complexes led to the use of a similar experiment to examine the mechanisms of the reaction. The reactions employed in the attempted preparation of complexes **59b** and **59c** were probed with ^1H NMR at several points of the reaction and work-up. It was determined that the reaction did in fact yield the desired product. A ^1H NMR spectrum of an unpurified solution did not show the peaks associated with the keto tautomer at 4.2 and 2.9 ppm and only exhibited the peaks characteristic of the linking CH_2 for the enol form at 3.6 ppm. However, the use of water for the purification of the product led to the appearance of the keto peaks characteristic of the ligand. Additionally, the enol peak was observed to move to a shift that is more comparable with the ligand's tautomer. This experiment highlighted the water sensitivity of the prepared complexes. Figure 6 shows the region of the ^1H NMR spectra characteristic of the keto and enol peaks and depicts the shifting in the enol peak and the appearance of keto peaks following purification of the product. Additionally, broad low-resolution peaks characteristic of either the phenanthroline or the bipyridine intermediates remained suggesting the presence of the corresponding zinc complexes of these neutral ligands in the product following purification. This suggests that the use of water for the purification of the product hydrolyzed the ligand **59** leaving a mixture of either a zinc phenanthroline or bipyridine complex and the starting material **59**. Regrettably, the work-up of these complexes required the use of water despite the sensitivity of the ligand. Precipitating the compound from water is a necessary step, as the mexylaminotriazines cannot be recrystallized as is normal for non-glass forming analogues.

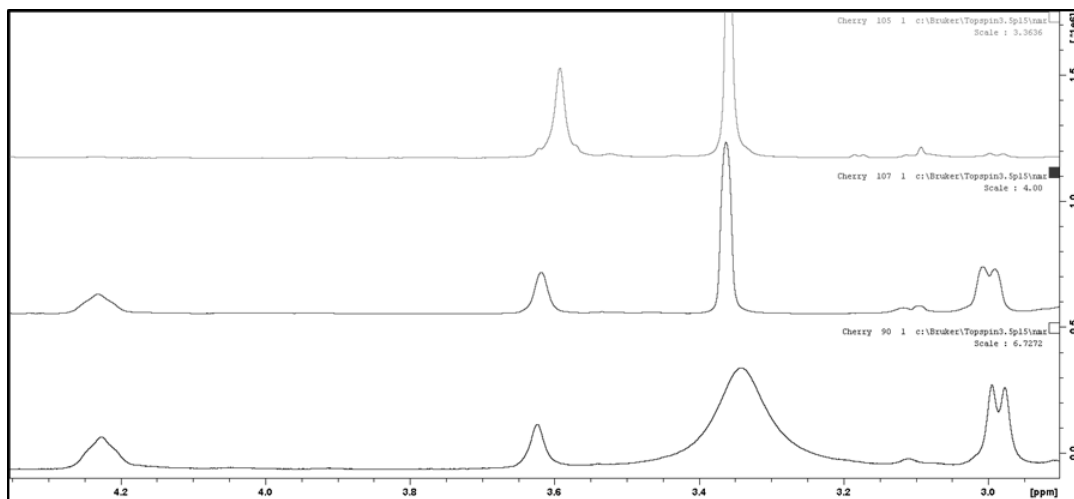


Figure 6: ^1H NMR spectra comparison demonstrating the changing peaks of the keto and enol tautomers in a sample of **59c**•**Zn(II)**, before and after work-up. Top: ^1H NMR of the unpurified fraction; Middle: reaction mixture following washing with water; Bottom: reference spectrum of ligand **59**.

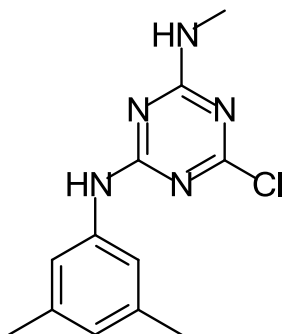
5.3. Experimental

5.3.1. Materials, Equipment, and Physical Measurements

All reagents were purchased from Sigma-Aldrich, AK Scientific or Oakwood Chemicals and were used without further purification. Reagent grade solvents were purchased from Caledon Laboratories, and used without further purification. DMSO-*d*₆ (deuterated dimethyl sulfoxide) and CDCl₃ (deuterated chloroform) were purchased from CDN isotopes. Unless otherwise stated, reactions were performed under ambient atmospheric conditions. Thin film chromatography using SiliCycle products was used to investigate the progress of each reaction. NMR spectra were recorded using a Bruker Avancé 400 MHz spectrometer at 298K unless otherwise noted. Thermal analysis was obtained by TGA and DSC using a TA Instruments Q50 and Q20, respectively

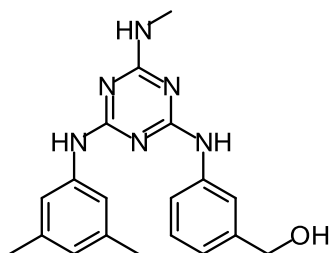
5.3.2. Synthesis

Synthesis of 2-mexylamino-4-methylamino-6-chloro-1,3,5-triazine (56)



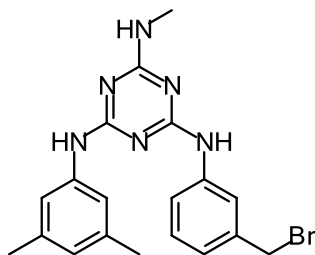
Precursor compound **43** was synthesized according to procedures outlined in section 4.3.3. The synthesis of compound **56** followed procedures outlined in the literature.¹¹ 2-Mexylamino-4,6-dichloro-1,3,5-triazine (**43**) (135 g, 502 mmol) was dissolved in acetone (750 mL) in a round-bottomed flask equipped with a magnetic stirrer. K₂CO₃ (69.4 g, 502 mmol) was added and the flask was placed in an ice bath to keep the temperature below 5 °C. A solution of methylamine (39.0 mL, 40 wt% aqueous, 502 mmol) in acetone (250 mL) was added dropwise to the mixture. The ice bath was removed following the complete addition of the solution. The mixture was stirred at room temperature for an additional hour, at which point the mixture was poured into H₂O (500 mL), and stirring was continued for 30 min until precipitation was completed. The precipitate was collected by filtration, the crude product was washed with H₂O, triturated in hot toluene, filtered, and allowed to dry completely to afford 88.7 g of the pure title compound **56** (336 mmol, 69%): HRMS (ESI) calcd for C₁₂H₁₅N₅Cl m/e: 264.1015, found: 264.1029. Anal. Calcd for C₁₂H₁₄N₅Cl: C, 54.60; H, 5.31; N, 26.54. Found: C, 54.66; H, 5.32; N, 26.46. FTIR (KBr, cm⁻¹) 3264, 3196, 3123, 3007, 2914, 2848, 1634, 1615, 1587, 1542, 1453, 1391, 1373, 1276, 1239, 1157, 1125, 1059, 986, 880, 836, 800, 723, 682, 634 cm⁻¹; ¹H NMR (400 MHz, DMSO-*d*₆, 298 K) δ 9.92, 9.75 (s, 1H), 8.02, 7.92 (s, 1H), 7.40, 7.34 (s, 2H), 6.65 (s, 1H), 2.85, 2.80 (m, 3H), 2.23 (s, 6H) ppm; ¹H NMR (400 MHz, DMSO-*d*₆, 363 K) δ 9.44 (br s, 1H), 7.57 (br s, 1H), 7.35 (s, 2H), 6.68 (s, 1H), 2.86 (s, 3H), 2.25 (s, 6H) ppm; ¹³C NMR (75 MHz, DMSO-*d*₆) δ 168.3, 167.6, 165.9, 165.8, 163.6, 163.1, 138.8, 138.7, 137.37, 137.35, 124.4, 124.3, 117.9, 117.8, 27.3, 27.2, 21.11, 21.08 ppm; Tm = 231 °C. This characterization data matches the data published in the literature.

Synthesis of 2-mexylamino-4-methylamino-6-[3-(hydroxymethyl)phenylamino]-1,3,5-triazine (**57**)



The synthetic route used to synthesize this precursor follows those outlined in the literature and the spectral data are concordant.¹¹ The synthesis of the precursor **56** was performed according to literature procedures.¹¹ The synthesis of this general precursor is provided in section 4.3.3. 2-mexylamino-4-methylamino-6-chloro-1,3,5-triazine (**56**) (11.0 g, 41.8 mmol) and 3-aminobenzoic acid (6.18 g, 50.2 mmol) were added in THF (150 mL) to a round-bottomed flask equipped with a magnetic stirrer and a water-jacketed condenser. The mixture was refluxed for 24 h, at which point a precipitate had formed. The precipitate was collected by filtration, washed with CH₂Cl₂, and re-suspended in MeOH. AcOEt and aqueous NaHCO₃ were added and the mixture was shaken in an extraction funnel. Both layers were separated, the aqueous layer was extracted with a second portion of AcOEt, then the combined organic extracts were washed with H₂O, washed with a brine, dried over Na₂SO₄, filtered, and the volatiles were thoroughly evaporated under vacuum to yield 8.10 g of compound **57** (23.1 mmol, 55%): HRMS (EI) calcd for C₁₉H₂₂N₆O (m/e): 350.1855, found: 350.1848; FTIR (KBr, cm⁻¹) 3401, 3376, 3286, 3021, 2943, 2921, 2869, 1611, 1583, 1565, 1553, 1527, 1514, 1487, 1461, 1434, 1400, 1362, 1321, 1301, 1262, 1245, 1188, 1177, 1166, 1083, 1037, 1012, 998, 973, 956, 890, 842, 808, 784, 736, 693, 650 cm⁻¹; ¹H NMR (300 MHz, DMSO-*d*₆, 298 K): δ 9.01 (br s, 0.5H), 8.97 (br s, 1H), 8.80 (br s, 0.5H), 7.77 (t, 1H), 7.56 (br s, 1H), 7.40 (br d, 2H), 7.20 (t, 1H), 6.92 (d, 1H), 6.89 (br s, 1H), 6.58 (s, 1H), 5.13 (t, 1H), 4.46 (d, 1H), 2.85 (d, 3H), 2.22 (s, 6H) ppm; ¹³C NMR (75 MHz, DMSO-*d*₆): δ 166.1, 164.1, 163.9, 142.6, 140.1, 137.1, 127.9, 123.1, 119.7, 118.3, 118.1, 117.6, 63.1, 27.2, 21.1 ppm; T_g = 69 °C.

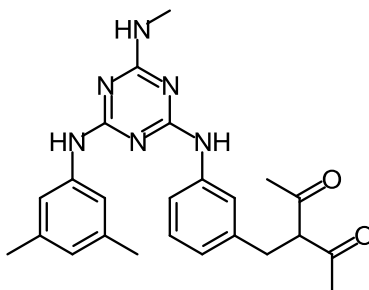
Synthesis of 2-mexylamino-4-methylamino-6-[3-(bromomethyl)phenylamino]-1,3,5-triazine (**58**)



The synthetic route used to synthesize this precursor follows those outlined in the literature and the spectral data is concordant.¹¹ 2-Mexylamino-4-methylamino-6-(3-hydroxymethylphenylamino)-1,3,5-triazine (**57**) (8.10 g, 23.0 mmol) was dissolved in dry CH₂Cl₂ (10 mL) in a dry round-bottomed flask equipped with a magnetic stirrer. The solution was cooled to 0 °C and PBr₃ (2.70 mL, 29.0 mmol) was added dropwise under inert atmosphere. Once the addition was complete, the mixture was stirred under inert atmosphere at ambient temperature for 24 h. A precipitate started forming after 2-3 h. The mixture was poured into aqueous NaHCO₃,

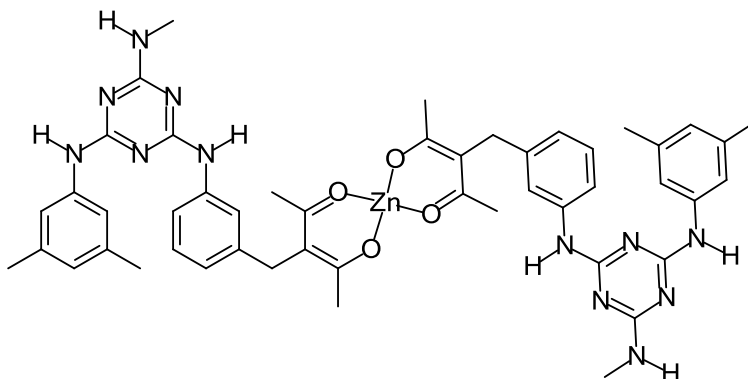
followed by addition of CH₂Cl₂. The aqueous layer was extracted with CH₂Cl₂. Then the combined organic extracts were washed with aqueous NaHCO₃, washed with brine, dried over Na₂SO₄, filtered, and the volatiles were evaporated under reduced pressure to yield 7.40 g of the title compound **58** (18.0 mmol, 78%): HRMS (EI) calcd for C₁₉H₂₁BrN₆ (m/e): 412.1011, found: 412.1003; FTIR (KBr, cm⁻¹) 3399, 3275, 3171, 3137, 3023, 2955, 2921, 2866, 1611, 1583, 1564, 1554, 1515, 1488, 1463, 1432, 1398, 1361, 1320, 1301, 1262, 1245, 1214, 1188, 1168, 1145, 1125, 1084, 1037, 998, 971, 933, 886, 842, 810, 786, 766, 738, 693 cm⁻¹; ¹H NMR (300 MHz, DMSO-*d*₆, 298 K): δ 9.23 (br s, 0.5H), 9.09 (br s, 0.5H), 9.02 (br s, 0.5H), 8.85 (br s, 0.5H), 7.95 (br s, 1H), 7.82 (br m, 1H), 7.41 (br d, 2H), 7.24 (t, 3 J=7.6 Hz, 1H), 7.02 (d, 3 J=7.6 Hz, 1H), 7.01 (br s, 1H), 6.59 (s, 1H), 4.64 (s, 2H), 2.87 (d, 3 J=4.1 Hz, 3H), 2.23 (s, 6H) ppm; ¹³C NMR (75 MHz, DMSO-*d*₆): δ 165.9, 164.0, 163.7, 140.6, 139.9, 137.9, 137.1, 128.5, 123.2, 122.2, 120.4, 119.7, 117.7, 34.9, 27.2, 21.1 ppm; T_g = 62 °C, T_{dec} = 131 °C. The spectral data of this compound matches the literature values.

Synthesis of Glacac Ligand (**59**)



In a round-bottomed flask equipped with a magnetic stir bar, 2-methylamino-4-methylamino-6-[3-(bromomethyl)phenylamino]-1,3,5-triazine (**58**) (7.50 g, 17.4 mmol) and K₂CO₃ (12.1 g, 87.5 mmol) were dissolved in acetylacetone (**51**) (50 mL). The mixture was then heated to 80 °C and stirred for 4 h. The mixture was then poured into 1M aq. NaOH, the resulting precipitate was collected by filtration and washed with H₂O. The crude solid was re-dissolved in CH₂Cl₂ and washed with NaOH. Glacial AcOH (5 mL) was added, the organic layer was separated, washed with brine, dried over Na₂SO₄, filtered, and the solvent was removed by rotary evaporation to yield 6.50 g of ligand **59**. (15.1 mmol, 87% yield). FTIR (KBr, cm⁻¹) 3283, 2921, 2853, 1698, 1582, 1514, 1429, 1358, 1182, 842, 809, 737, 691 cm⁻¹; ¹H NMR (300 MHz, DMSO-*d*₆, 298 K): δ 7.26-7.19 (m, 6H), 7.06 (s, 1H), 6.87-6.84 (m, 2H), 6.72 (s, 2H), 4.03 (t, 1H), 3.67 (s, 2H), 3.17 (d, 2H), 3.03 (m, 6H), 2.32 (s, 12 H), 2.17 (s, 6H), 2.11 (s, 6H) ppm; ¹³C NMR (75 MHz, DMSO-*d*₆): δ 204.1, 191.9, 166.1, 164.2, 163.9, 140.4, 140.1, 138.6, 137.1, 128.3, 123.2, 121.6, 119.9, 117.7, 67.6, 33.3, 30.0, 27.3, 23.1, 21.2 ppm; T_g = 68 °C.

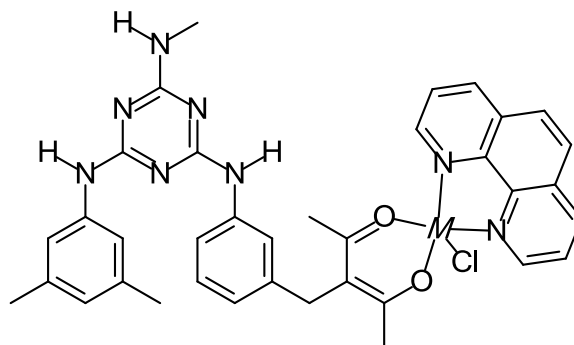
Attempted Preparation of complex **59a**•Zn(II)



NEt₃ (8.80 μ L, 60.0 μ mol) was added to a solution of ligand **59** (21.6 mg, 50.0 μ mol) in THF (2 mL) in a round bottomed flask equipped with a magnetic stir bar. ZnCl₂ (3.41 mg, 25.0 μ mol) in EtOH (2 mL) was added to the resulting solution and the resulting mixture was stirred for 24 h at ambient temperatures. The mixture was precipitated by pouring into water; the precipitate was collected by filtration, washed with H₂O, and allowed to dry under air to afford a yellow solid. Several other attempts were made following variations of this procedure in which the sequence of added reagents, metal salts (NiCl₂ and CuCl₂•2H₂O were also used), the temperature, duration, and other factors were altered. In all attempts, the same yellow solid was afforded and found not to be the desired product *via* ¹H NMR spectroscopy.

Attempted preparations of complexes containing Ni(II) and Cu(II) metal centres of **59a** were synthesized according to the same procedures for the attempted preparation of **59a**•Zn(II). These attempts were unsuccessful.

Attempted preparation of complex **59b** Zn(II), Ni(II), and Cu(II)



(Method A): The attempted synthesis of this compound followed procedures outlined for heteroleptic Zn(II) diketonate analogues and consisted of two synthetic steps.¹⁶⁹ To a solution of 1,10-phenanthroline (880 mg, 4.89 mmol) in CH₂Cl₂ (5 mL) in a round-bottomed flask equipped with a magnetic stir bar was added ZnCl₂ (1.00 g, 7.34 mmol). The resulting mixture was stirred at ambient temperatures for 48 h. The precipitate was removed by filtration, washed with CH₂Cl₂, and the remaining solvent was removed under reduced pressure. The solid was then washed with H₂O and allowed to dry in air to afford 1.24 g of a white solid compound, Zn(phenanthroline)Cl₂ intermediate (3.92 mmol, 78%). ¹H NMR (300 MHz, DMSO-*d*₆, 298 K): δ 8.88-8.86 (d, 4H), 8.28 (d, 2H), 8.04-8.00 (m, 2H) ppm.

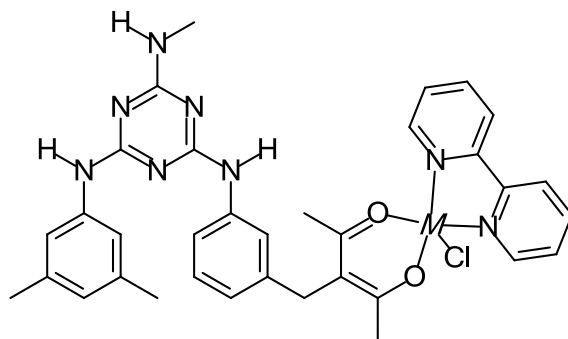
To a solution of the phenanthroline intermediate (72.8 mg, 0.230 mmol) in THF (10 mL) in a round-bottomed flask with a magnetic stirrer was added a solution of ligand **59** (99.5 mg, 0.230 mmol) and NEt₃ (64.4 μ l, 0.460 mmol) in THF (5 mL). The resulting mixture was then stirred at ambient temperature for 5 days. The crude product was poured into H₂O, the precipitate was washed with H₂O, and allowed to dry in air. The resulting yellow coloured solid was determined not to be the desired complex.

(Method B): To a solution of 1,10-phenanthroline (881 mg, 4.89 mmol) in CH₂Cl₂ (5 mL) in a round-bottomed flask equipped with a magnetic stir bar was added ZnCl₂ (1.00 g, 7.34 mmol). The resulting mixture was stirred at ambient temperatures for 48 h. The precipitate was removed by filtration, washed with CH₂Cl₂, and the remaining solvent was removed under reduced pressure. The solid was then washed with H₂O and allowed to dry in air to afford 1.24 g of a white solid compound, Zn(phenanthroline)Cl₂ intermediate (3.82 mmol, 78%). ¹H NMR (300 MHz, DMSO-*d*₆, 298 K): δ 8.88-8.86 (d, 4H), 8.28 (s, 2H), 8.04-8.00 (dd, 2H) ppm.

To a solution of ligand **59** (216 mg, 0.500 mmol) in warm iPrOH in a round-bottomed flask equipped with a magnetic stir bar, was added NaOMe/MeOH (25 wt.%, 115 μ l, 0.500 mmol) in a single portion. The resulting mixture was stirred for 1 hour, during which a colour change to a yellow solution was observed. The solvent was removed by rotary evaporation to afford an orange solid intermediate compound, the sodium salt of ligand **59** (210 mg, 0.460 mmol). In a round-bottomed flask, the intermediate products, the sodium salt of ligand **59** (91.1 mg, 0.200 mmol) and the Zn(phen)Cl₂ intermediate (63.3 mg, 0.200 mmol) were then re-dissolved in CH₂Cl₂ (5 mL). The resulting solution was stirred for 5 days at ambient temperature. The reaction mixture was condensed by rotary evaporation, the condensed solution was washed with H₂O, washed with brine, dried over Na₂SO₄, filtered, and the solvents were removed under vacuum to yield a yellow-coloured solid that was determined to be an intractable mixture of the starting materials, ligand **59** and the phenanthroline intermediate complex by analysis with ¹H NMR. Several other attempts were made following variations of this procedure in which the sequence of added reagents, the temperature, duration, and other factors were altered. In all attempts, a yellow solid was obtained and found not to be the desired product *via* ¹H NMR spectroscopy.

Preparations of complexes containing Ni(II) and Cu(II) metal centres of **59b** were also attempted. These attempts followed the same procedures for both method A and method B for the attempted preparation of **59b**•Zn(II). All attempts with these metal centres were also unsuccessful.

Attempted preparation of complexes **59c** with Zn(II), Ni(II), and Cu(II)



The same procedure was also used to synthesize a 2,2'-bipyridine intermediate of the form, Zn(bipyridine)Cl₂. ¹H NMR (300 MHz, DMSO-*d*₆, 298 K): δ 8.67 (s, 2H), 8.60-8.58 (d, 2H), 8.20 (t, 2H), 7.67 (t, 2H) ppm. Following this, attempted preparations of complexes containing Zn(II), Ni(II) and Cu(II) metal centres of **59c** were synthesized according to the same procedures for both method A and B for the attempted synthesis of **59b•Zn(II)**. These attempts were unsuccessful and yielded solid products that were not the corresponding desired complexes.

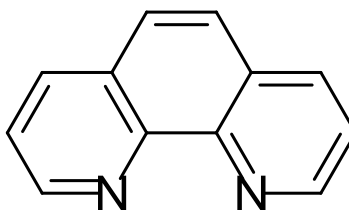
5.4. Summary

The synthesis of a molecular glass functionalized with acetylacetonate was successful. The T_g of ligand **59** was measured by DSC and found to be 68 °C, a value that is compared to other mexylaminotriazine derivatives as well as the precursor compounds **57** and **58**.¹¹ However, the sensitivity of the respective transition metal complexes made the process of purification challenging. As such, attempts to prepare the corresponding metal complexes were unsuccessful and the desired products could not be obtained in pure form. The use of water was employed to remove excess metallic salts from the reaction products. This step resulted in the hydrolysis of the reaction product, creating what is believed to be a mixture of the starting materials, the zinc phenanthroline intermediate complex, and the glass-forming acetylacetonate ligand. The preparation of the desired mexylaminotriazine functionalized acetylacetonate complexes was subsequently abandoned following the discovery of the sensitivity of the complexes towards water. Many of the envisioned applications, particularly potential catalytic applications, for glass-forming complexes of this ligand would likely require the complexes to be more robust and stable in the presence of water, as many applications and devices do not employ inert atmospheres. One proposed strategy is to synthesize a similar acetylacetonate analogue in which the mexylaminotriazine moiety is covalently attached at another position of the β-diketone. The substituents of β-diketones were identified at the beginning of the chapter as a factor influencing the keto-enol tautomerization of these ligands. As such, screening could be conducted, and a new synthetic route could be devised to covalently attach mexylaminotriazines at the 1- or 5-β-carbon positions of the molecule. Alternatively, it may be possible to prepare heteroleptic acetylacetonate complexes by synthesizing glass-forming ligands of the other ligands involved in these reported mixed ligand compounds. For example, synthesizing glass-forming phenanthroline analogues could serve as an alternative strategy for the preparation of complexes that incorporate both β-diketones and neutral N,N ligands given the suitability of these mixed ligand complexes for a number of proposed thin film applications.

6. Phenanthroline Functionalized Molecular Glass Complexes

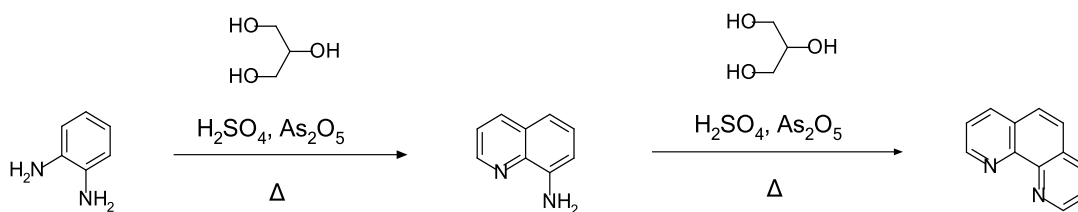
6.1. Introduction

First reported in 1898 by Blau, 1,10-phenanthroline (**60**), colloquially known as phenanthroline and abbreviated as phen, is an N-polyheterocyclic aromatic hydrocarbon (Scheme 32) that has played an important role in the development of many coordination complexes.^{176–178} Phenanthroline is a white solid that is rigid, planar, and hydrophobic.¹⁷⁷ With regards to its coordination properties, phenanthroline is similar to 2,2'-bipyridine, both neutral ligands forming strong complexes with most metal ions.¹⁷⁹ Coordination with metals occurs in a bidentate fashion through the two nitrogen atoms. The first reported complexes of phenanthroline and bipyridine were also reported by Blau, who synthesized a series of iron complexes that demonstrated colorimetric changes in various solutions.¹⁸⁰ However, the central ring of phenanthrolines imposes additional structural properties on it, such as planarity and rigidity.¹⁸¹ The rigidity of the compound holds the two nitrogen atoms in a *syn* conformation, which is optimal for coordination with metal ions. Bipyridine on the other hand, can rotate freely around the linking bonds, and in the most stable conformation, the two nitrogen atoms are *anti* relative to each other. This structural difference results in phenanthroline forming more stable coordination complexes that are more entropically favoured compared to analogous bipyridine complexes.^{177,182}

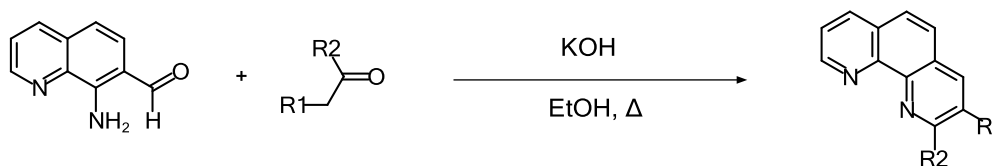


Scheme 32: Molecular structure of 1,10-phenanthroline **60**.

Many phenanthroline-based ligands are commercially available; however, more elaborate analogues often require direct synthesis from a variety of precursors.¹⁷⁹ Traditionally, phenanthroline can be synthesized by the double cyclization of *o*-phenylenediamine with glycerol, sulfuric acid as a catalyst, and As₂O₅ as an oxidizing agent *via* sequential Skraup condensations (Scheme 33).^{179,183–185} This method remains one of the best synthetic routes to prepare some phenanthroline derivatives.¹⁸⁶ Alternatively, a Friedländer condensation can also be used to synthesize phenanthroline derivatives. For example, 8-aminoquinolinecarbaldehyde can be reacted with acetaldehyde and potassium hydroxide in ethanol to synthesize 1,10-phenanthroline derivatives (Scheme 34).^{184,186} Using these condensation reactions, it is possible to synthesize a number of ring-substituted phenanthrolines from functionalized precursors such as *o*-phenylenediamine or aminoquinoline derivatives.^{187–191} Substitution of the hydrogen atoms in any of these positions leads to drastic changes in the properties of the phenanthroline ligand.

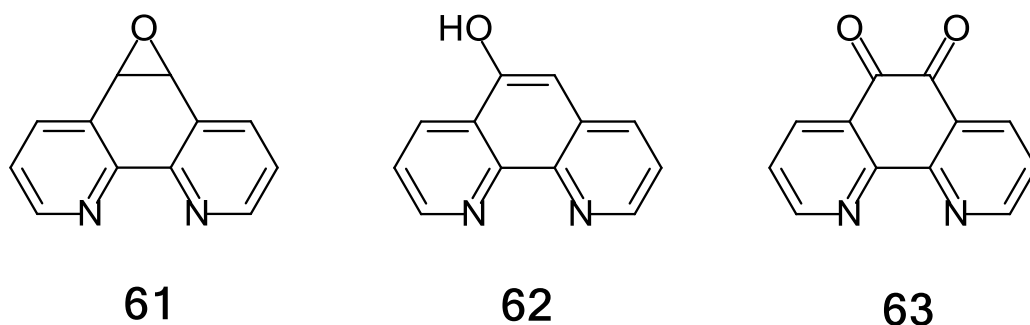


Scheme 33: Skraup condensation for the preparation of 1,10-phenanthroline (**60**) from 8-aminoquinoline and glycerol.¹⁷⁹



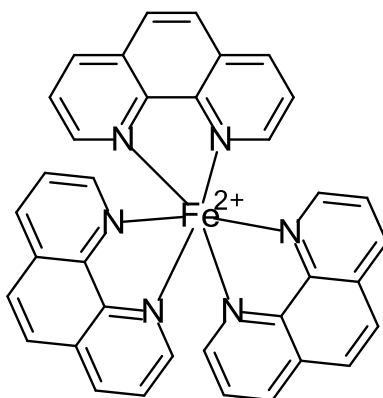
Scheme 34: Friedländer condensation for the preparation of 1,10-phenanthroline derivatives from 8-aminoquinolinecarbaldehyde.^{183–185}

A number of symmetric substitutions can also be used to synthesize phenanthroline derivatives. Positions 2, 4, 7, and 9 on phenanthroline are the most susceptible to nucleophilic attack, while positions 3, 5, 6, and 8 are the most reactive towards electrophiles.¹⁷⁸ Halogenation and oxidation reactions are particularly useful for the synthesis of various phenanthroline derivatives.¹⁷⁹ For example, dichlorinated analogues can be synthesized from phenanthroline and a solution of aqueous hypochlorous acid¹⁹², or phosphorous pentachloride and phosphoryl chloride, depending on the desired position of chlorination. 5,6-Epoxy-5,6-dihydro-[1,10]phenanthroline (**60**), a particularly useful derivative, can be synthesized by the oxidation of phenanthroline using commercial bleach (sodium hypochlorite) and a phase transfer catalyst.^{193,194} Phenanthroline epoxide can be used to prepare a number of versatile and reactive 5-substituted-phenanthrolines, such as 5-hydroxy-1,10-phenanthroline (**62**), or -further oxidized to 1,10-phenanthroline-5,6-dione (**63**). Other functional groups, such as dimethylamino, methoxy, or cyano groups, can also be incorporated. These compounds can be used as building blocks to generate countless other functionalized phenanthroline derivatives.¹⁹⁴ Alkyl and aryl-moieties can be substituted at the 2 and 9-positions of phenanthroline by the addition of organolithium reagents or using catalyzed coupling reactions.¹⁷⁹ The highly varied nature of phenanthroline and its derivatives have led to applications for a number of different purposes. Scheme 35 depicts the structures of several of the substituted phenanthrolines described in this section.



Scheme 35: Molecular structure of 1,10-phenanthroline derivatives: 5,6-Epoxy-5,6-dihydro-[1,10]phenanthroline (**61**), 5-hydroxy-1,10-phenanthroline (**62**), and 1,10-phenanthroline-5,6-dione (**63**).

Phenanthroline reacts readily with many metals as a bidentate ligand, forming a five-membered chelated ring through the two nitrogen atoms.¹⁷⁸ Phenanthrolines have been shown to form a number of *mono*, *bis*, and *tris* metal complexes with transition metals and lanthanides.^{195,196} Phenanthrolines possess relatively poor σ -donor ability compared to ethylenediamine. Despite this, the coordination of phenanthroline ligands to metal centres tends to be quite strong as a result of the electron-deficient nature of the aromatic ring system. This electron deficiency allows these ligands to behave as π -acceptors. This property helps phenanthroline stabilize metals in lower oxidation states by accepting electron density from the metal centres.¹⁷⁷ The general procedure employed for the coordination of phenanthroline ligands is to react stoichiometric equivalents of ligand with metal salts.^{195,197} As a neutral ligand, additional reagents are often unnecessary, a solution of ligand can be treated with a solution of metal salts, such as halides or nitrates, and allowed to mix.^{198,199} The exact reaction conditions, temperatures, solvents, and reaction times vary quite extensively depending on the solubility of the starting materials as well as the structure and presence of functional groups in phenanthroline analogues.²⁰⁰ Stoichiometric control can be exploited to obtain *mono*, *bis*, and *tris*-complexes.²⁰¹ Phenanthroline analogues and their respective complexes have been the focus of many researchers' efforts due to their use as versatile starting materials for the synthesis and development of organic, inorganic, and supramolecular materials.¹⁷⁷ For example, one of the best-known *tris*-phenanthroline complexes is $[\text{Fe}(\text{phen})_3]^{2+}$, colloquially known as ferriox (64) (Scheme 36). The ferriox complex is used for the photometric determination of redox processes in analytical chemistry. The ferriox complex is a chromophore that exhibits a pronounced change in colour when oxidized to $[\text{Fe}(\text{phen})_3]^{3+}$.¹⁹⁵

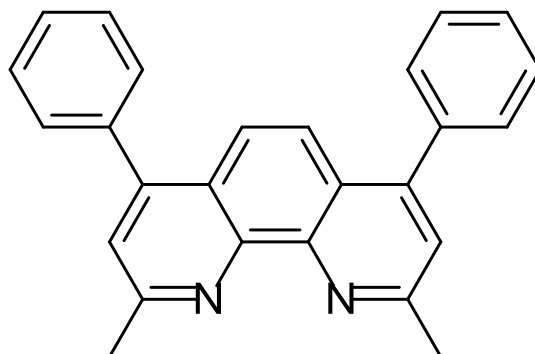


Scheme 36: Molecular structure of Ferrioxamine B, an iron phenanthroline coordination complex, *tris*(1,10-phenanthroline)iron(II) (**64**).

The rigid, planar, and aromatic structure of phenanthrolines coupled with their chelating capability and the photophysical properties makes them appealing for a number of applications.^{197,202} For example, the rigid, planar structure of phenanthrolines have led to their extensive use in the design of supramolecular materials and devices.^{203–205} As an example, Cu(I) complexes of phenanthroline analogues have been used in the synthesis of catenanes, rotaxanes, and knots.²⁰⁶ The chelating properties of phenanthrolines are also widely exploited in many fields. Analytical chemists can exploit phenanthrolines as colorimetric reagents for the determination of metal species.^{179,207} The chelating abilities of phenanthrolines can be exploited for environmental protection as optically active sensors signalling the presence of contaminants, as chelating complexes for the removal of metals from effluent waters, exhausts, and even in nuclear waste treatment.^{182,202} The unique properties of phenanthrolines have led to other applications: such as ligands in transition metal catalysis,^{204,208} directly as chiral catalysts for asymmetric catalysis, or indirectly as stabilizing agents for nanoparticle synthesis;²⁰⁹ in molecular biology as DNA intercalating agents; and various technological applications in materials chemistry.^{210–214}

One of the most promising fields in which phenanthroline and its subsequent complexes have seen diverse use is the field of molecular biology. The rigid, planar structure of phenanthroline analogues enables them to fit in the grooves of DNA's double-helix structure. There, these compounds and their respective complexes can bind, intercalate, and interact with DNA.¹⁸¹ Octahedral phenanthroline complexes formed from Cu²⁺, Co²⁺, Zn²⁺, and Ru³⁺ are specifically known for their interactions with DNA.¹⁷⁷ For example, [Cu(phen)₂]²⁺ complexes are well-recognized for their ability to act as DNA nucleases and cleave specific nucleotide sequences.²¹⁵ Similarly, in 2013, a report was published describing the preparation of a series of mixed ligand Cu(II) complexes with phenanthroline and Schiff base ligands. The authors demonstrated that this series of compounds possessed an extraordinary propensity to bind to DNA. Additionally, they revealed that the compounds functioned as superoxide dismutase mimics and were effective chemotherapeutic compounds for some forms of tumors.²¹⁶ Furthermore, the chelating properties of phenanthrolines are invaluable to the use of these compounds. Subsequently, phenanthroline complexes have been used for a number of other applications because of their luminescent properties. For example, some lanthanide complexes have been employed as fluoroimmunoassays binding to specific DNA sequences as markers.¹⁹⁶

The material sciences have particularly benefited from the properties possessed by phenanthroline and its analogues for the design of photochemically and electrochemically active materials.^{199,203,217} Electronically, phenanthrolines are an interesting class of chemical compounds that can be used for a number of applications. For example, phenanthroline analogue 2,9-dimethyl-4,7-diphenyl-1,10-phenanthroline (bathocuproine, **65**, Scheme 37) is one example employed in OLED technologies as both emissive layers as well as hole-blocking materials used to optimize the charge transport of these devices.¹⁸²

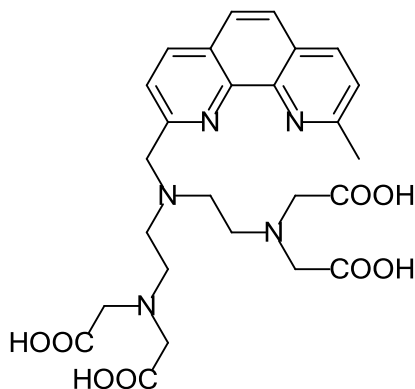


Scheme 37: Molecular structure bathocuproine (**65**).

1,10-Phenanthroline also absorbs radiation in the UV region; however, the structure of the molecule can be altered to shift the absorption towards the visible and near infrared regions.^{204,218} The luminescent behaviour and efficiency of phenanthrolines can be enhanced by the addition of various functional groups, protonation of the nitrogen atoms, and incorporation into conjugated polymers.^{182,204} Additionally, phenanthrolines are prized for their ability to stabilize and photosensitize the triplet state in the respective metal complexes, particularly those formed with *d*- and *f*-block metals, giving way to their use in luminescent materials.^{181,204}

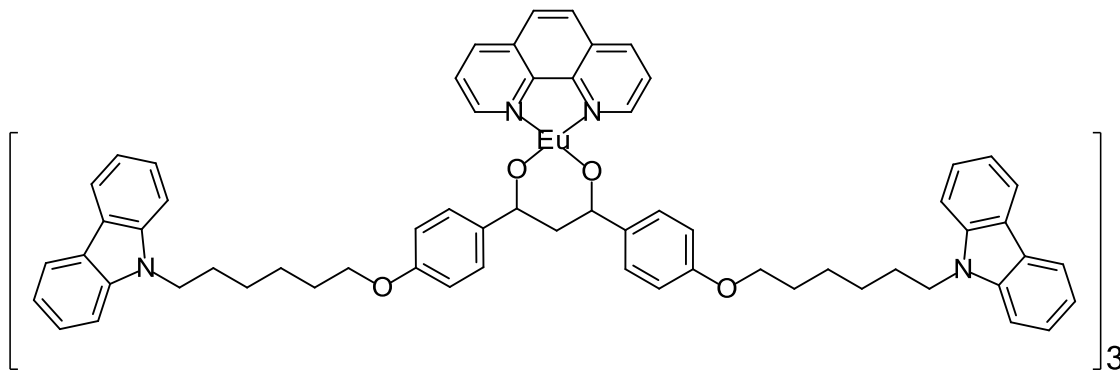
Lanthanide cations demonstrate impressive luminescent and optical behaviour. For example, neodymium doped materials such as ceramics and glasses are frequently employed as gain media for many types of lasers.²¹⁹ The lanthanides exhibit luminescence that is characterized by long decay times, a large difference between excitation and emission wavelengths, and narrow emission bands.¹⁷³ These properties make lanthanide ions the ideal candidates for the preparation of luminescent materials as they show both high optical purity and minimal background interference and scattering.¹⁷³ Unfortunately, the lanthanide ions exhibit low absorption coefficients, making direct excitation difficult and subsequently the luminescence intensity and quantum yields of these cations to be relatively low.^{173,217} Alternatively, coordination complexes of lanthanide metals often demonstrate much more intense luminescence. Acting as harvesting antennae, some ligands sensitize the metal cations towards luminescence by absorbing UV-Vis radiation and efficiently transferring this energy to the metal centre.^{182,214,220} Phenanthrolines are particularly well suited for the coordination of *d*- and *f*-block metals. In addition, the tunability of phenanthrolines allows for the optimization of highly efficient UV light absorption.^{173,182,221} As such, phenanthroline-based compounds and complexes, particularly those incorporating lanthanide metals, have been extensively used in the design of materials that exhibit luminescent and photochemical properties.¹⁸² A number of studies have demonstrated the use of phenanthroline based ligands as sensitizers for lanthanide ions with regards to luminescent properties.^{182,202,221} For example, coordination complexes of 4-[(9-methyl-1,10-phenanthroline-2-yl)methyl]-1,4,7-

triazahaepthane-1,1,7,7-tetraacetic acid] (**66**, Scheme 38) have been prepared with all lanthanide metals.^{182,222} These complexes have been further shown to demonstrate emission spectra across the UV, visible, and near-infrared spectral regions. Additionally, the Eu^{3+} and Tb^{3+} complexes have been further employed as labels for biological immunoassays.¹⁷³



Scheme 38: Molecular structure of (4-[(9-methyl-1,10-phenanthrolyl)methyl]-1,4,7-triazahaepthane-1,1,7,7-tetraacetic acid) (**66**).²²²

Additionally, phenanthrolines also serve as assistant ligands in mixed-ligand octahedral complexes, particularly in conjunction with various photosensitizing β -diketonates.²²³ The presence of coordinated solvent molecules, particularly those containing $-\text{OH}$ groups, play a role in nonradiative deactivation.^{173,182} In highly coordinated lanthanide complexes, neutral chelating ligands like phenanthroline serve the secondary purpose of excluding the coordination of solvent and water molecules, thereby protecting the luminescence of the complexes.¹⁷³ An example of a heteroleptic europium(III) complex (**67**) incorporating a phenanthroline ligand as well as a β -diketonate derivative is depicted in Scheme 39. This compound was used to demonstrate the luminescence of lanthanide coordination complexes in solid-state systems.^{182,224,225}



Scheme 39: Chemical structure of heteroleptic europium(III) phenanthroline complex **67**.

As previously mentioned, many lanthanides and phenanthroline-based compounds exhibit unique optical and electronic properties; however, in order to make many of these materials suitable for use, the complexes must be bound to a matrix or support system. Neodymium for example is often used as a dopant for gain media in lasers. This rare-earth metal is often suspended

in materials such as yttrium aluminum garnet, yttrium vanadate, or silicate and phosphate glasses.^{219,226} Similarly, bathocuproine (**65**), used in amorphous semiconducting materials, exhibits poor morphological stability as the presence of moisture, oxygen, and heat has been shown to cause the crystallization of bathocuproine. Doping bathocuproine with larger compounds such as *tris*-(8-hydroxyquinoline)aluminum has been used to improve the lifetime and efficiency of this material; however, the morphological stability and lifetime of these blended materials are still a challenge for many applications.^{182,227}

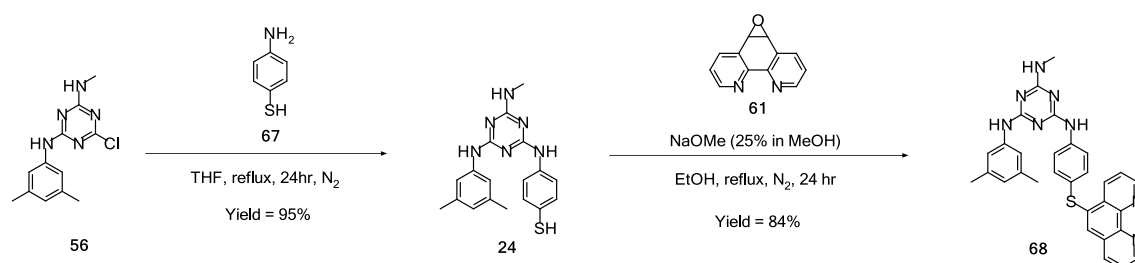
Glass-forming amorphous materials that readily form thin films present an alternative for the production of optoelectronic and electronic materials for a variety of applications. This is because of their ease of use, their improved optical properties, as well as their thermal stability.²²⁸ However, many conventional methods for preparing these materials require high temperatures which can damage some functionalities, such as many organometallic complexes.²²⁸ Polymers are another common method for introducing glass-forming capabilities to various functionalities. Unfortunately, many of these systems are not robust and have a tendency to decompose under thermal and radiative stress. Furthermore, the nature of polymer chemistry makes obtaining a discrete chemical structure challenging and leads to more difficult purification.²²⁸ Small molecules offer greater synthetic control, as well as easier purification and processability. The properties of small molecules address many of the limitations of other materials. Unfortunately, small molecular materials not bound to a support system have a tendency to crystallize quickly and generally do not form stable glassy phases. This leads to limited lifetimes as well as poorer performance.²²⁹ Fortunately, the functionalization of compounds with small molecular glass formers offers a method for introducing or improving glass-forming abilities and the ability to fabricate thin films.^{6,51-58} The incorporation of glass formers, such as mexylaminotriazines, presents an alternative option for developing and designing functionalized thin film materials that possess the advantages and mitigate the failures of other types of solid-state materials.

Herein, we report the synthesis of a phenanthroline derivative functionalized with a mexylaminotriazine glass-forming substituent as well as the preparation of two series of glass-forming lanthanide complexes with different spectator ligands, 2-thenoyltrifluoroacetone (**52**) or 1,1,1-trifluoro-5,5-dimethyl-2,4-hexanedione (**53**). The phenanthroline ligand is an ideal candidate for functionalization with mexylaminotriazine substituents in order to produce a series of highly tailorable, well-defined, molecular glasses possessing photoactive and optical materials. Functionalization of a phenanthroline ligand derivative with a mexylaminotriazine unit is expected to introduce glass-forming properties to the corresponding derivative and the respective complexes. The characterization and determination of glass-forming abilities of the synthesized ligands and corresponding complexes will also be outlined in the following sections.

6.2. Results and Discussion

6.2.1. Synthesis and Characterization of Ligand

Phenanthroline-functionalized glass **68** was synthesized according to the following route (Scheme 40). Precursor thiol **24** was synthesized using a published procedure¹¹ similar to that used for bromomethyl-glass **58** (Chapter 5): 2-mexyl-4-methylamino-6-chloro-1,3,5-triazine (**56**) was refluxed for 24 h in THF with 4-aminothiophenol (**67**) under nitrogen to give 2-mexylamino-4-methylamino-6-(4-mercaptophenylamino)-1,3,5-triazine (**24**) in 89% yield. In both steps, the products could be easily purified by acidic and basic extractions and did not require chromatography, though compound **24** slowly oxidizes to the corresponding disulfide upon exposure to air. Precursor **24** in ethanol was then refluxed for 24 h with phenanthroline epoxide (**61**) under an inert atmosphere in the presence of sodium methoxide to give phenanthroline-functionalized mexylaminotriazine **68** in 84% yield. The final product can be purified by precipitation in H₂O, several washes with H₂O, and allowing the compound to dry in air.



Scheme 40: Synthesis of the mexylaminotriazine functionalized phenanthroline ligand **68**.

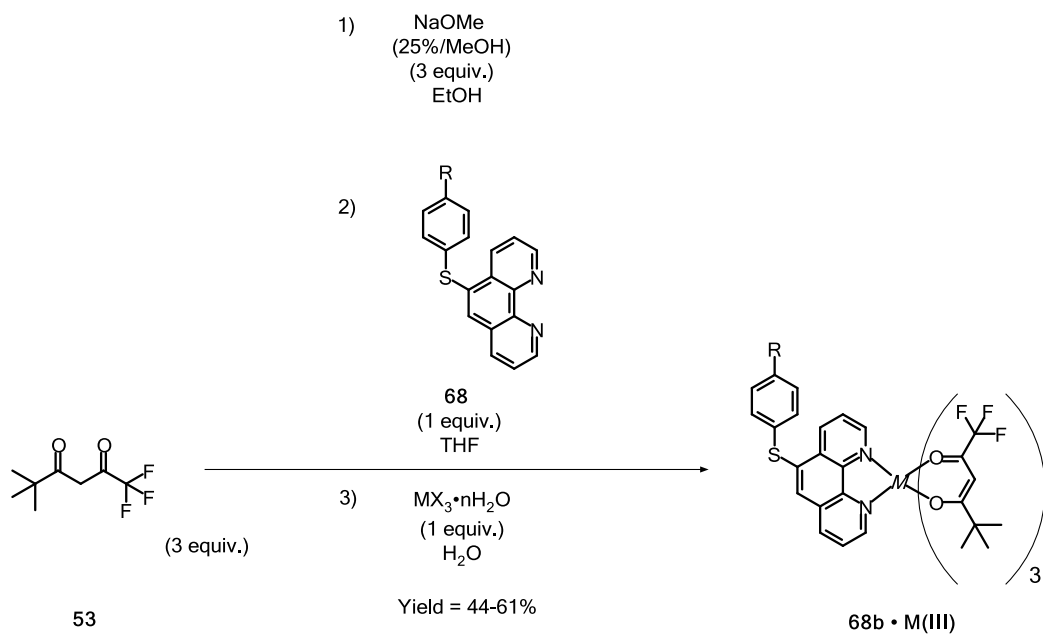
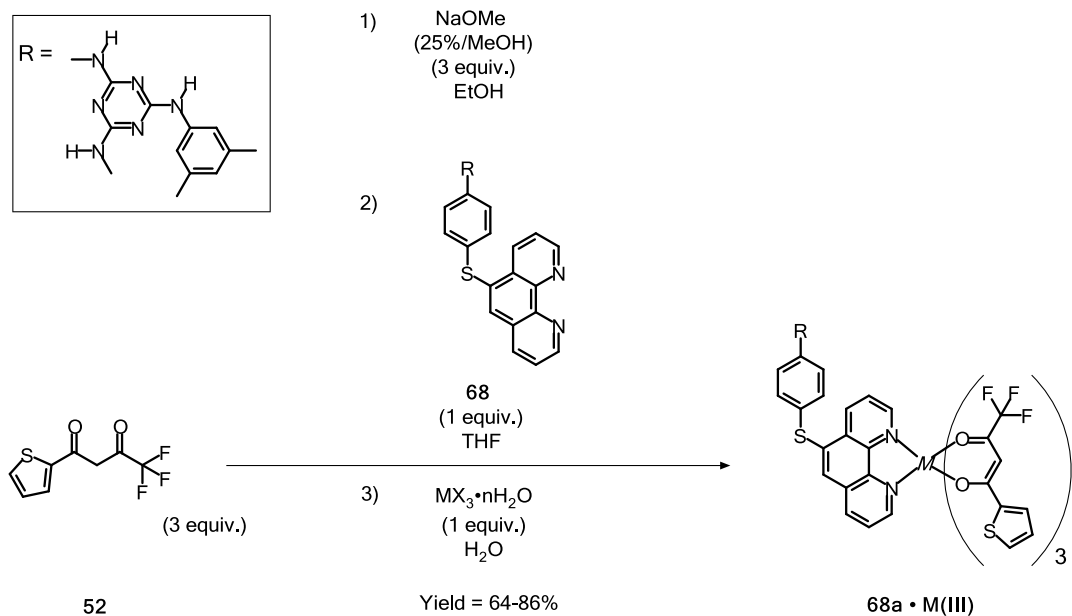
Precursor **24** and ligand **68** both readily formed glasses upon drying from solution or by cooling from the melt. Ligand **68** decomposed around 300 °C, as measured by TGA. T_g values for ligand **68** and precursor **24**, are listed in Table 6. Phenanthroline derivative **68** shows a T_g of 134 °C, which is higher than that of precursor **24**, and no crystallization was observed upon heating. This demonstrates the ability of the phenanthroline derivative **68** to form stable, long-lived glasses. This higher observed T_g is possibly due to the ability of the nitrogen atoms in the phenanthroline moiety to participate in the formation of hydrogen bonds. As explored in Chapter 2, hydrogen bonds form between the various amino groups and the nitrogen atoms of the triazine and now the phenanthroline moieties have been shown to increase T_g in mexylaminotriazines. Thus moieties capable of forming additional hydrogen bonds would likely exhibit higher glass transition temperatures.^{10,11} These hydrogen bonds promote glass formation and an increased T_g by forming aggregates in the material, which pack poorly amongst each other and cannot easily reorganize. The T_g of the glass-forming phenanthroline ligand was also higher than the synthesized glass-forming salen ligands described in Chapter 4. As was the case with the coordination of the salen ligands to metal centres, the greater rigidity, and lower molecular mobility of the glass-forming phenanthroline ligand likely contributes to this higher T_g . Thermograms for TGA and DSC are provided in appendices B.3 and C.3, respectively.

Table 6: Glass transition temperatures (T_g) of compounds **24** and **68**. The T_g of compound **24** is reported from literature values.¹¹

Compound	T_g (°C)
24	84
68	134

6.2.2. Coordination with Metals and Characterization

As trivalent octacoordinated metals, it was necessary to prepare heteroleptic lanthanide complexes that satisfied the metal centres by employing a neutral glass-forming phenanthroline ligand as well as anionic β -diketonate ligands. Ligand **68** was reacted with various lanthanide series metals including La(III), Pr(III), Nd(III), Eu(III), Tb(III), and Er(III) to yield the corresponding complexes **68a** and **68b**. Complexes of the form **68a** were prepared using 2-thenoyltrifluoroacetone (Htta, **52**) as the anionic ligands as well as the corresponding lanthanide chloride or nitrate hydrates. The β -diketone ligand was first deprotonated *in situ* by adding NaOMe in MeOH (3 equiv.) to a solution of ligand **52** (3 equiv.) in EtOH. Solutions of the glass-phenanthroline ligand (**68**) (1 equiv.) in THF, and metal salt (1 equiv.) in H₂O were sequentially added at ambient temperature leading to the immediate formation of a precipitate. A small portion of THF was added to re-dissolve the precipitate and the mixture was allowed to stir for 30 minutes. The complexes were obtained in 65-86% yield by precipitation from H₂O. In all cases, the complexes could be purified by precipitation from water followed by dissolving in CH₂Cl₂, drying with Na₂SO₄, and the thorough removal of solvents by rotary evaporation. For the purposes of comparing various heteroleptic complexes of this type, the glass-phenanthroline ligand (**68**) was also used to prepare a second series of lanthanide metal complexes. Complexes of the type **68b** were prepared following similar procedures; however, 1,1,1-trifluoro-5,5-dimethyl-2,4-hexanedione (Hfdh, **53**) was used instead of 2-thenoyltrifluoroacetone. Initial attempts to prepare compound **68b**•Ln(III) produced low yields (20-30%). This was likely due to the increased steric demands of the Hfdh ligands relative to Htta ligands. Similar yields were reported in the literature using non-glass forming derivatives.²³⁰ As a result, the final mixture was refluxed for 24 h while stirring before the product was precipitated from H₂O. This additional step improved yields slightly and complexes of the form **68b**•M(III) were prepared from La(III), Pr(III), Nd(III), and Eu(III) metal salts in 45-61% yields. Scheme 41 depicts the general method used to prepare lanthanide complexes of the form **68a** and **68b**.



Scheme 41: Preparation of heteroleptic La(III), Pr(III), Nd(III), Eu(III), Tb(III), and Er(III) complexes **68a** and **68b** from corresponding metal salts, diketones **52** or **53**, and ligand **68**.

$\text{MX}_3 \cdot n\text{H}_2\text{O} = \text{LaCl}_3 \cdot 6\text{H}_2\text{O}, \text{Pr}(\text{NO})_3 \cdot 6\text{H}_2\text{O}, \text{NdCl}_3 \cdot 6\text{H}_2\text{O}, \text{EuCl}_3 \cdot 6\text{H}_2\text{O}, \text{TbCl}_3 \cdot 6\text{H}_2\text{O}, \text{Er}(\text{NO})_3 \cdot 5\text{H}_2\text{O}.$

The thermal behaviour of complexes **68a** and **68b** were studied by TGA and DSC (Table 7). Typically, a first mass loss peak ranging from 2 to 4% was observed around 140 °C, attributed to the loss of residual water trapped in the samples. TGA analysis showed most complexes to be stable at temperatures over 200 °C, with some showing stability at temperatures nearing 300 °C. All complexes prepared for this study demonstrated glass-forming properties, with T_g values ranging from 101 to 130 °C, as measured by DSC (Table 7), with standard deviations from duplicate measurements less than 2 °C and typically less than 1 °C. Interestingly, DSC analysis showed small transitions occurring between 140 and 185 °C. These peaks are not large enough to be attributable to melting transitions or crystallization and the exact point seems to change between runs of the same sample. As such, these complexes appear to demonstrate slight decomposition above their T_g . The complexes will need to be kept below temperatures of approximately 140 °C and this minor decomposition should be kept in mind for any potential applications of these complexes.

Table 7: Decomposition temperatures and glass transition temperatures (T_g) for complexes of **68a** and **68b**.

Complex	T_{dec} (°C)	T_g (°C)
68a•La(III)	270	130
68a•Pr(III)	280	108
68a•Nd(III)	250	112
68a•Eu(III)	260	109
68a•Tb(III)	290	112
68a•Er(III)	270	117
68b•La(III)	260	113
68b•Pr(III)	250	101
68b•Nd(III)	250	103
68b•Eu(III)	250	101

In contrast to the glass-forming salen complexes described in Chapter 4, these complexes exhibited a decrease in their T_g upon coordination to metal centres. It was proposed that the salen complexes demonstrated an increase in T_g relative to their respective ligands as a result of their increased rigidity. In the case of phenanthroline, the ligand is already rigid and planar and coordination did not further limit the molecular mobility. Alternatively, the decrease in T_g is likely the result of a loss of hydrogen bonds formed from the heteroaromatic nitrogen atoms. Similar to the salen-mexylaminotriazine complexes, variations in T_g were observed depending on the nature of the metal in each series. In particular, the lanthanum(III) complexes of both series of complexes exhibited higher T_g . For example, the lanthanum complexes showed T_g values 22 °C and 12 °C higher than the corresponding Pr(III) complexes. Comparatively, the glass transitions of the other metal complexes in both series are more consistent. For example, the **68a** complexes of Pr(III), Nd(III), and Eu(III) exhibited glass transitions within 4 °C of each other, while the **68b** complexes incorporating the same metal centres were within 2 °C. The magnetism is the only obvious

difference at this time between the La(III) complexes and the remaining metal complexes. However, at this point no conclusions can be drawn until the role of metal centres on T_g is investigated further in future studies. Thermograms for TGA and DSC are provided in appendices B.3 and C.3, respectively.

6.2.3. Optical Properties

The UV-Vis spectra of glass-forming complexes **68a** and **68b** were recorded in both a CH_2Cl_2 solution and in the solid state as thin films. Given the widely reported luminescent behaviour of phenanthroline-based lanthanide complexes in the solid-state, thin films were prepared for analysis in order to compare the absorption of the chromophores as well as any shifts in absorption as a result of any molecular aggregation in the solid-state. Thin films of the respective complexes were deposited on glass substrates by spin-coating from a CH_2Cl_2 solution. Uniform thin films were formed in all cases as solvent evaporated. Absorption spectra of the Htta series of complexes, **68a**, are shown below in Figure 7, and for the Hfdh complexes, **68b**, in Figure 8, respectively. A comparison of the UV-Vis absorption spectra of the two europium(III) complexes, **68a•Eu(III)** and **68b•Eu(III)** in both solution and solid-state is shown for visible reference in Figure 9. The absorption maxima and extinction coefficients at the primary λ_{max} are reported in Table 8.

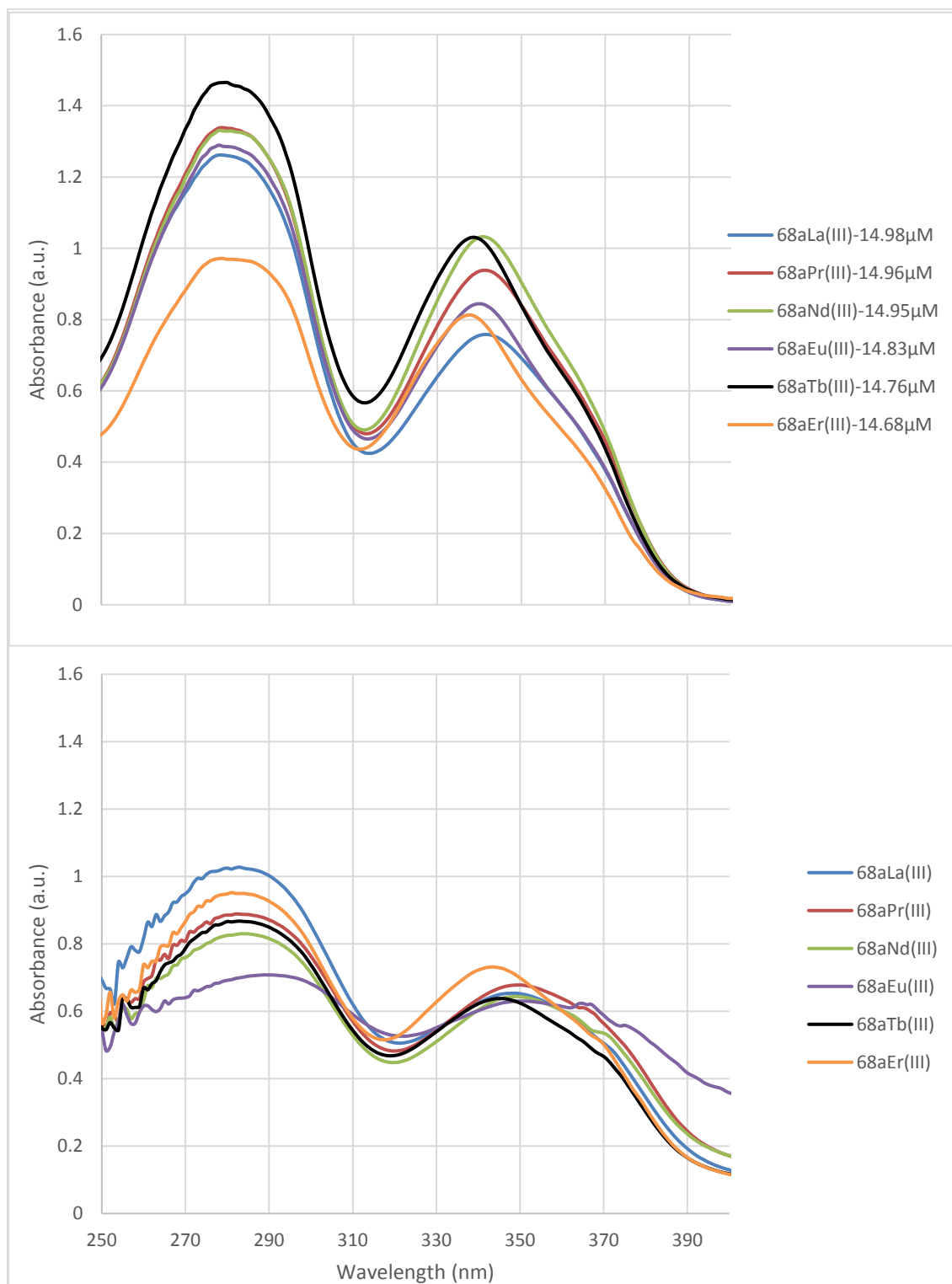


Figure 7: UV-Vis absorption spectra of complexes **68a** in CH₂Cl₂ solution (Top) and in solid-state as thin films (Bottom).

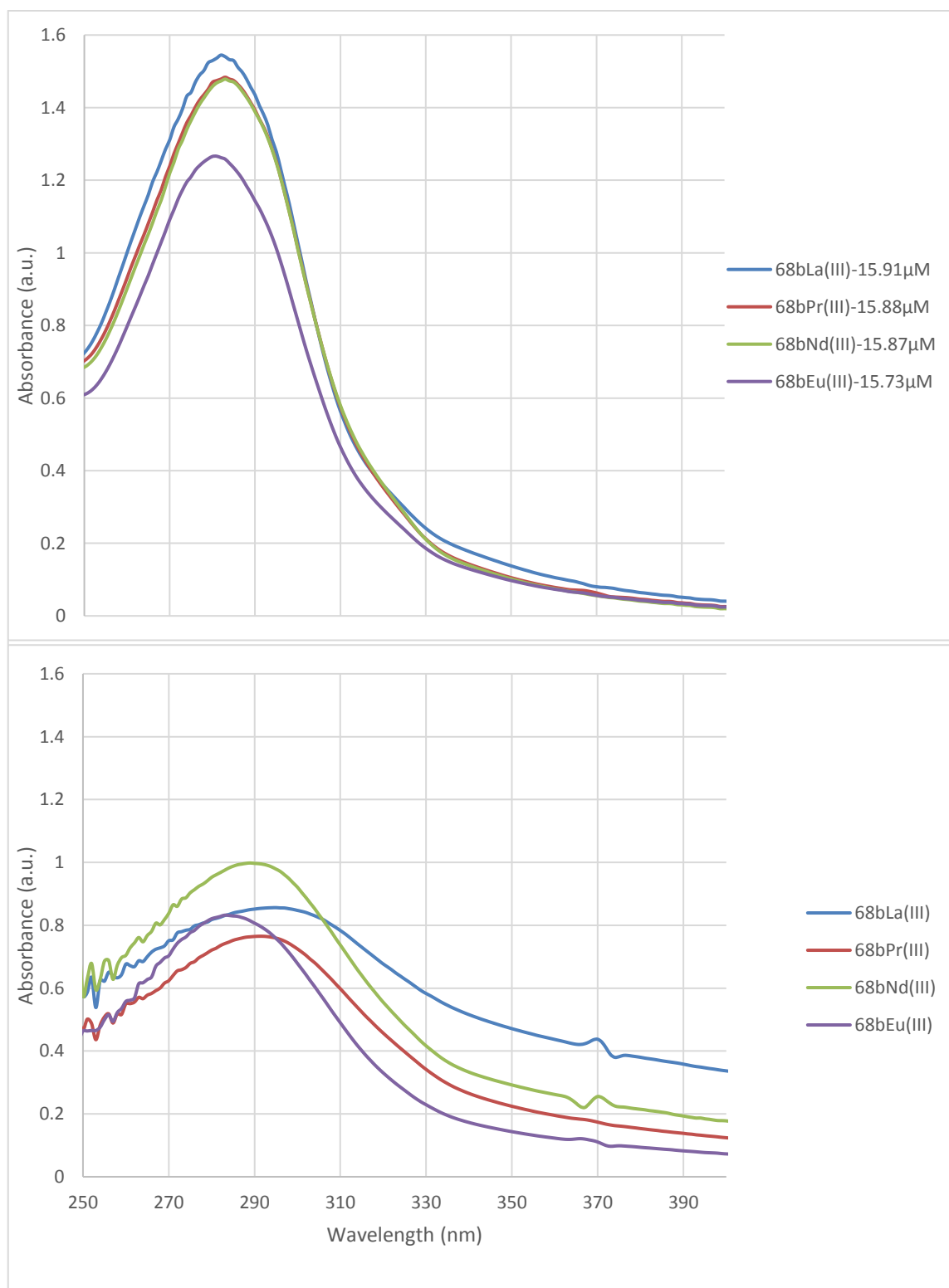


Figure 8: UV-Vis absorption spectra of complexes **68b** in CH_2Cl_2 solution (Top) and in solid-state as thin films (Bottom).

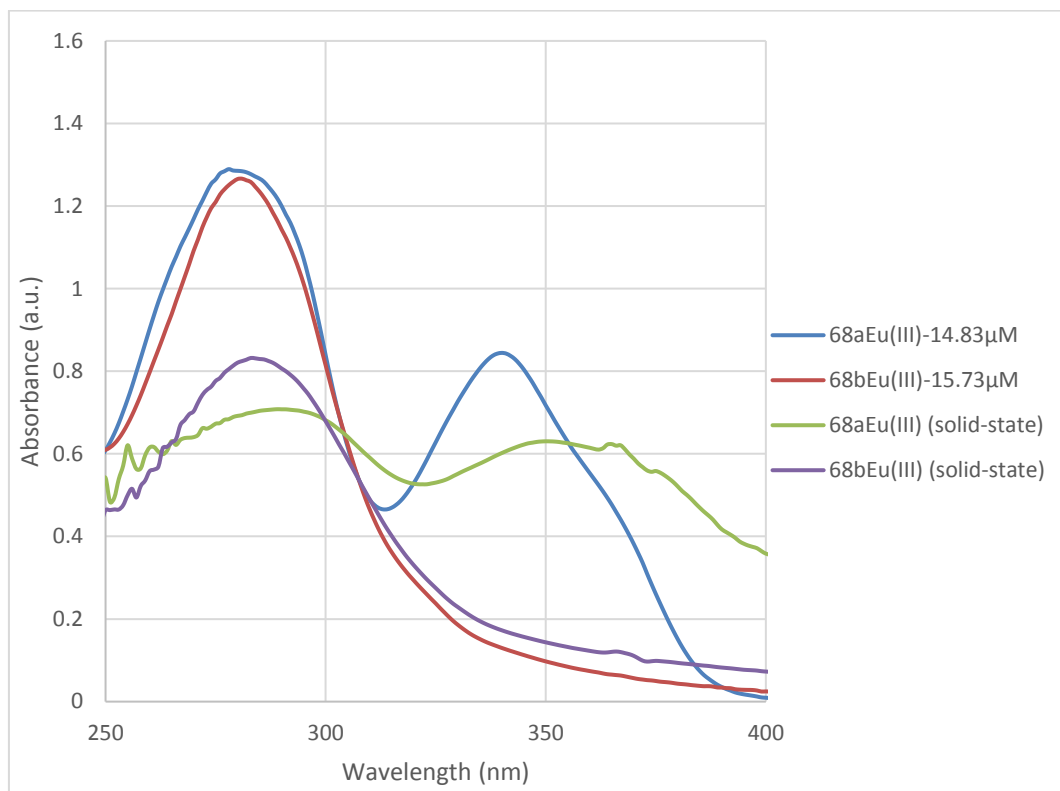


Figure 9: Comparison of the UV-Vis absorption spectra of europium(III) complexes **68a•Eu(III)** and **68b•Eu(III)** in both solution and in the solid state.

Table 8: UV-Vis absorbance values of phenanthroline-functionalized molecular glass complexes **68a-b** in both CH₂Cl₂ solution and in the solid state.

Complex	λ_{\max} in solution (nm)		ϵ (extinction coefficient) in solution (cm ⁻¹ M ⁻¹)	λ_{\max} in solid state (nm)	
	Primary	Secondary		Primary	Secondary
68a•La(III)	278	342	84200	283	349
68a•Pr(III)	279	341	89500	282	350
68a•Nd(III)	278	341	89000	284	349
68a•Eu(III)	278	340	87000	289	350
68a•Tb(III)	280	339	99300	283	345
68a•Er(III)	279	338	66200	281	343
68b•La(III)	282	-	97100	295	-
68b•Pr(III)	283	-	93400	291	-
68b•Nd(III)	283	-	93200	289	-
68b•Eu(III)	281	-	80500	283	-

The UV-Vis absorption spectra of both series of prepared complexes show intense absorption in the ultraviolet region of the spectrum. The complexes of the Htta series appear to show maximum absorption from $\lambda = 278$ - 280 nm. A secondary peak is observed from $\lambda = 338$ to $\lambda = 342$ nm and appears in all Htta series complexes **68a**. No pattern appears to exist in accordance with periodic trends and there is only a small variation between the complexes of different metals within the same series. This indicates that the ligands may be a more significant factor in the absorption of UV-Vis radiation. Ligands are frequently employed in analogous compounds as antennas for exactly this purpose.^{182,214,220} The ligands in analogous complexes have been shown to absorb UV-Vis radiation and transfer the energy to the metal centre for emission. The complexes of the Hfdh series **68b** show maximum absorbance from $\lambda = 281$ - 283 nm. Unlike the Htta series, this series does not show any other absorbance peaks at other wavelengths. This observation suggests that the aromatic thiophene groups on the β -diketonate ligands in series **68a**, 2-thenoyltrifluoroacetone (Htta), are responsible for the high absorbance peak around $\lambda = 340$ nm. The observed absorption maxima are reported in the literature for non-glass forming Htta and phenanthroline based complexes.²³¹ All complexes in the **68a** series also appear to exhibit a shift to slightly shorter wavelengths relative to their corresponding Hfdh series complexes (**68b**). This suggests that the optical properties of these novel coordination complexes could be tailored and altered for a variety of purposes. For example, by altering the diketones, derivatives could be prepared that absorb in different regions and potentially exhibit other varying optical properties.

Given the desired use of these complexes for solid state and thin film applications, the complexes were also analyzed for the absorbance of UV-Vis radiation as thin films. The complexes of the Htta series (**68a**) as thin films demonstrate maximum absorption from $\lambda = 281$ - 289 nm. Secondary absorption peaks were once again observed from $\lambda = 349$ - 350 nm and appear in all solid state Htta complexes. The solid samples of the Hfdh series (**68b**) show maximum absorbance from $\lambda = 283$ - 295 nm. Again, no secondary absorption peak is observed in this series of complexes. This further suggests that the ligands and their respective substituents play an important role in the absorption of UV-Vis radiation. Comparing the samples in solution to those as thin films, a red-shift can be observed. This is expected and due to the increased aggregation observed of the materials in the solid-state relative to solution. This factor will need to be studied further to determine whether this can be exploited or altered in order to design optically active thin films of these glass-forming complexes in the future. Similar to the salen complexes, no absorbance peaks were observed within the visible region of the spectra for any samples. The same explanation could be proposed for these complexes, that the metal-based transitions are too weak relative to the ligand-based transitions in the UV range. Solutions that are more concentrated could be prepared and used to analyze the visible region of the electromagnetic spectrum for absorbance peaks in this region.

Another observation was made regarding the fluorescent properties exhibited by some metal complexes. Both of the europium(III) complexes, **68a•Eu(III)** and **68b•Eu(III)**, exhibit strong luminescence in the visible region. This was noted when the samples were irradiated with a handheld laboratory UV lamp, both in solution and in the solid state. Both complexes fluoresced with a red-orange colour. Figure 10 shows the fluorescent behaviour of these two samples in the solid state as spin-coated thin films. In Figure 10, the two samples are compared to two references, the substrate material without any sample being applied and the Htta series praseodymium(III) complex **68a•Pr(III)**. Lanthanide based complexes, such as those containing Pr, Nd, Er and Tb, are known to exhibit a range of luminescent properties.^{224,232} In particular, Tb(III) and Eu(III) complexes are known for luminescence in the solid state.²²⁴ However, in this study no other

complexes were observed to luminesce. This observation can be explained in a number of ways. First, the quantum yield of many luminescent materials is quite low.^{210,231,233} The other complexes at this point could demonstrate luminescence at intensities too low to be observed qualitatively. Alternatively, other complexes could luminesce at wavelengths that are not in the visible region of the spectrum.^{232,234} For example, Nd is known to luminesce in the IR regions of the spectrum.²³² Lastly, non-glass forming europium(III) analogues of these novel coordination complexes have been shown to exhibit strong visible luminescence.^{182,230,235–237} As such, the observation of this complexes' luminescence is not unexpected while the lack of observed luminescence in other complexes does not necessarily rule out their luminescent properties. Unfortunately, this qualitative observation could not be further studied for this research thesis. Time constraints as well as a lack of access to a fluorescence spectrometer made further characterization of these properties impossible. Nevertheless, this observation is exciting in that it supports one of this report's hypotheses, that novel glass-forming coordination complexes will retain the properties of their parent compounds despite the introduction of mexylaminotriazine moieties. As such, the evaluation and study of the luminescent properties of this series of glass-forming complexes should be pursued in the future.



Figure 10: Fluorescent behaviour of spin coated samples of the two europium(III) complexes *via* irradiation with UV light. From left to right: untreated substrate, Htta europium(III) complex, **68a•Eu(III)**, Htta praseodymium(III) complex, **68a•Pr(III)**, and Hfdh europium(III) complex, **68b•Eu(III)**.

6.3. Experimental

6.3.1. Materials and Equipment

All reagents were purchased from Sigma-Aldrich, AK Scientific or Oakwood Chemicals and were used without further purification. Reagent grade solvents were purchased from Caledon Laboratories, and used without further purification. DMSO-*d*₆ (deuterated dimethyl sulfoxide) and CDCl₃ (deuterated chloroform) were purchased from CDN isotopes. Unless otherwise stated, reactions were performed under ambient atmospheric conditions. Thin film chromatography using SiliCycle products was used to investigate the progress of each reaction.

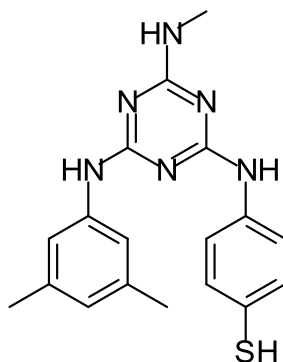
6.3.2. Physical Measurements

Compounds were characterized by nuclear magnetic resonance (NMR) in order to fully identify the compounds obtained. NMR spectra were recorded using a Bruker Avancé 400 MHz

spectrometer at 298K unless otherwise noted. Thermal analysis was obtained by TGA and DSC using a TA Instruments Q50 and Q20, respectively. Ambient temperature magnetic susceptibility measurements were made using a MSB MK1 Magnetic Susceptibility Balance following procedures outlined by the supplier. Infrared spectra were recorded using a Thermo Scientific Nicolet iS10 spectrometer. UV-Vis spectra were recorded using a Hewlett Packard 8453 spectrometer. HRMS analysis was conducted by an analytical party according to the techniques identified for the each specific compound.

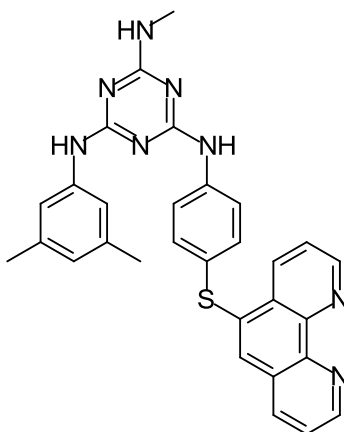
6.3.3. Synthesis

Synthesis of 2-methylamino-4-methylamino-6-(4-mercapto-phenylamino)-1,3,5-triazine (**57**)



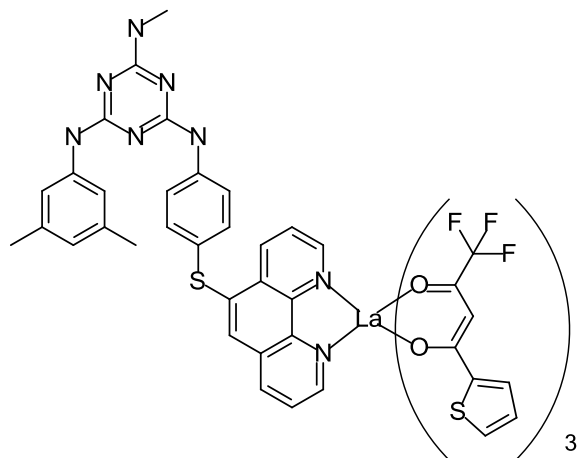
The synthesis of precursor **56** was performed according to literature procedures.¹¹ The synthesis of this general precursor is provided in section 5.3.2. The synthesis of this compound **57** followed literature procedures.¹¹ 2-methylamino-4-methylamino-6-chloro-1,3,5-triazine (**56**) (7.18 g, 27.2 mmol) and 4-aminothiophenol (**67**) (4.09 g, 32.7 mmol) were dissolved in THF (50 mL) in a degassed round-bottomed flask equipped with a magnetic stirrer, a water-jacketed condenser. The reaction mixture was refluxed overnight under a N₂ atmosphere with constant stirring. After allowing to cool to ambient temperature, a small amount of EtOAc and 1 M aqueous HCl were added to the reaction mixture. Both layers were separated. The organic layer was washed with H₂O, extracted with aqueous NaHCO₃, dried over Na₂SO₄, filtered, and the solvent was thoroughly evaporated under reduced pressure to give 4.23 g of the title compound **24** (12.0 mmol). Yield: 95%; HRMS (EI) calcd for C₁₈H₂₀N₆S (m/e): 352.1470, found: 352.1477; FTIR (CH₂Cl₂/KBr) 3448, 3416, 3283, 3054, 2987, 1575, 1556, 1496, 1423, 1400, 1355, 1323, 1266, 1183, 896, 841, 810, 705 cm⁻¹; ¹H NMR (300 MHz, DMSO-d₆, 298 K): δ 9.09 (br s, 0.5H), 8.96 (br s, 1H), 8.81 (br s, 0.5H), 7.66 (br s, 2H), 7.35 (br d, 2H), 7.15 (d, 2H), 6.87 (br s, 1H), 6.57 (s, 1H), 5.15 (br s, 1H), 2.81 (d, 3H), 2.21 (s, 6H) ppm; ¹³C NMR (75 MHz, DMSO-d₆): δ 166.6, 164.7, 140.6, 138.7, 137.7, 129.9, 123.8, 123.3, 121.3, 118.4, 27.9, 21.7 ppm; T_g = 84 °C. This spectral data matches the data published in the literature.

Synthesis of Phenanthroline Ligand (**68**)



2-Methylamino-4-methylamino-6-(4-mercapto-phenylamino)-1,3,5-triazine (**57**) (2.78 g, 7.89 mmol) was added to EtOH (80 mL) in a round-bottomed flask equipped with a magnetic stirrer, and the mixture was degassed by sparging with N₂ for 15 minutes. NaOMe (25 wt% in MeOH, 0.850 mL, 3.94 mmol) was added and the solution was stirred with gentle heating for 5 minutes. 5,6-epoxy-5,6-dihydro-[1,10]phenanthroline (**61**) (1.62 g, 8.28 mmol) was added, the flask was fitted with a water-jacketed condenser, and the mixture was refluxed overnight under N₂. The mixture was poured into H₂O while warm, forming a precipitate. The precipitate was collected by filtration, washed with H₂O, and allowed to dry in air to give ligand **68** as a white solid (3.53 g, 6.65 mmol). Yield: 84%; FTIR (KBr, cm⁻¹): 3270, 2957, 1574, 1504, 1417, 1361, 1286, 1236, 1181, 1141, 1080, 1037, 1012, 939, 874, 836, 808, 738, 624, 543, 522 cm⁻¹; ¹H NMR (300 MHz, DMSO-*d*₆, 298 K): δ 9.34 (d, 1H), 9.11 (d, 2H), 8.93 (d, 1H), 8.85 (d, 1H), 8.41 (d, 1H), 7.96-7.76 (m, 5H), 7.33 (d, 4H), 6.94 (s, 1H), 6.52 (s, 1H), 2.83 (s, 3H), 2.12 (s, 6H) ppm; ¹³C NMR (75 MHz, DMSO-*d*₆): δ 166.5, 164.6, 164.2, 150.8, 146.4, 145.6, 141.1, 140.4, 137.7, 137.6, 136.3, 135.3, 133.7, 132.4, 130.8, 130.0, 128.6, 128.0, 124.3, 124.1, 123.8, 123.5, 121.3, 118.8, 118.3, 115.6, 102.7, 64.6, 27.8, 21.5, 15.1 ppm; T_g = 134 °C.

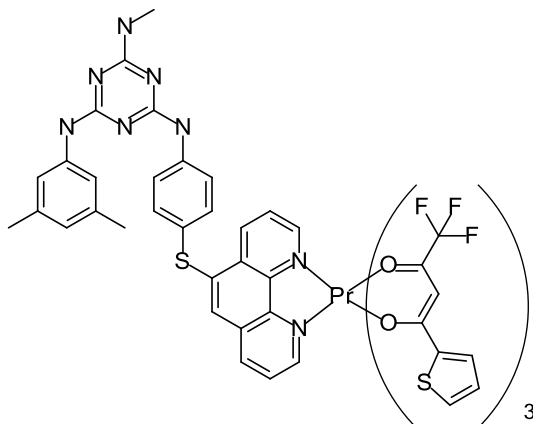
Preparation of 68a•La(III)



To a solution of 2-thenoyltrifluoroacetone (**52**) (333 mg, 1.50 mmol) in EtOH (4 mL) in a round-bottomed flask equipped with a magnetic stir bar was added NaOMe (25% in MeOH, 340 μ L, 1.50 mmol), the mixture was stirred for 5 minutes at room temperature. A solution of ligand **68** (265 mg, 0.500 mmol) in THF (3 mL) was added. A solution of LaCl₃•xH₂O (123 mg, 0.500 mmol) in H₂O (4 mL) was added and a precipitate formed immediately. A small portion of THF (2-3 mL) was added to re-dissolve the precipitate, then the mixture was poured into H₂O. The precipitate was collected by filtration. The precipitate was redissolved in CH₂Cl₂ and the solution was dried over Na₂SO₄, filtered, and the solvent was removed under reduced pressure to afford 431 mg of complex **68a•La(III)** (0.323 mmol, Yield 65%). FTIR (KBr, cm⁻¹): 3404, 2919, 2360, 1608, 1534, 1501, 1412, 1354, 1299, 1242, 1228, 1182, 1139, 1082, 1059, 1012, 932, 883, 859, 837, 807, 783, 736, 718, 679, 640, 604, 578 cm⁻¹; ¹H NMR (400 MHz, DMSO-*d*₆, 298 K): δ 9.34 (s, 1H), 9.21 (m, 2H), 8.96 (d, 1H), 8.79 (d, 1H), 8.45 (d, 1H), 8.45 (d, 1H), 7.99-7.78 (m, 10H), 7.32 (d, 4H), 7.11 (s, 3H), 6.93 (m, 1H), 6.51 (s, 1H), 6.16 (s, 2H), 2.83 (s, 3H), 2.12 (s, 6H) ppm; ¹³C NMR (75 MHz, MSO-*d*₆): δ 179.9, 168.7, 166.6, 164.3, 150.9, 146.4, 145.3, 141.2, 140.4, 137.6, 136.8, 135.3, 134.3, 133.0, 132.3, 130.1, 129.2, 128.7, 128.2, 125.4, 124.4, 124.2, 123.8, 121.3, 121.0, 118.3, 118.1, 115.3, 90.6, 67.5, 30.9, 27.8, 25.6, 21.5 ppm; ¹⁹F NMR (376 MHz, DMSO-*d*₆) δ -74.2 (s, 9H) ppm; T_g = 130 °C.

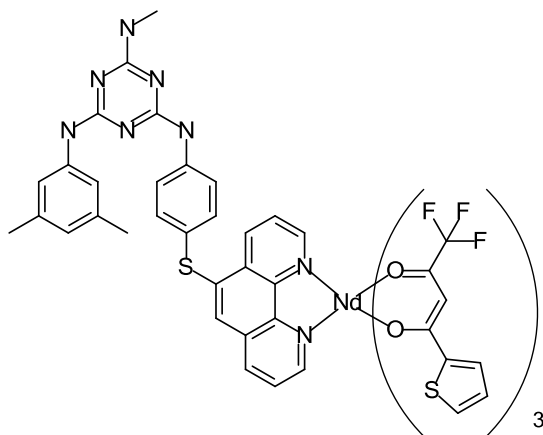
Additional complexes of with the metal centres including; Pr(III), Nd(III), Eu(III), Tb(III), and Er(III) were prepared according to the same procedure as analogue **68a•La(III)** from the respective lanthanide salts (Pr(NO₃)₃•6H₂O, NdCl₃•6H₂O, EuCl₃•6H₂O, TbCl₃•6H₂O, Er(NO₃)₃•5H₂O.) and ligand **68**.

Preparation of 68a•Pr(III)



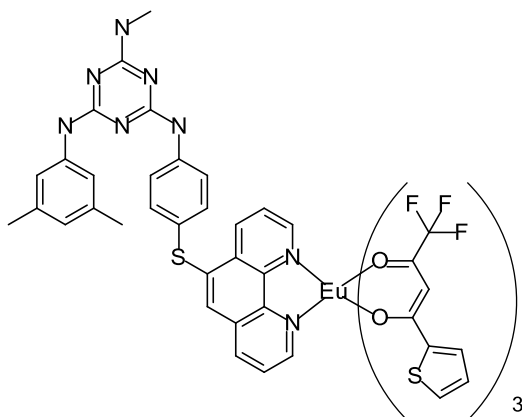
Yield: 80%; FTIR (KBr, cm^{-1}): 3389, 3103, 2956, 2923, 2360, 2342 1601, 1538, 1505, 1412, 1357, 1303, 1245, 1230, 1186, 1141, 1083, 1061, 1035, 1013, 950, 933, 885, 859, 838, 808, 787, 768, 735, 720, 692, 681, 641, 605, 580, 521, 490, 458, 418 cm^{-1} ; ^1H NMR (300 MHz, $\text{DMSO-}d_6$, 298 K): δ 9.14-8.87 (m, 3H), 7.82 (m, 7H), 7.34 (m, 3H), 6.93 (m, 1H), 2.85 (s, 3H), 2.17 (s, 6H) ppm; ^{13}C NMR (75 MHz, $\text{DMSO-}d_6$): δ 166.6, 164.5, 141.0, 140.5, 139.7, 137.7, 135.3, 134.4, 132.6, 131.5, 129.2, 128.5, 125.4, 124.0, 121.0, 118.9, 118.4, 55.4, 34.9, 30.9, 27.8, 25.6, 21.6 ppm; ^{19}F NMR (376 MHz, $\text{DMSO-}d_6$) δ -69.9 (s, 9H) ppm; $\mu_{\text{eff}} = 2.47$; $T_g = 108$ °C.

Preparation of 68a•Nd(III)



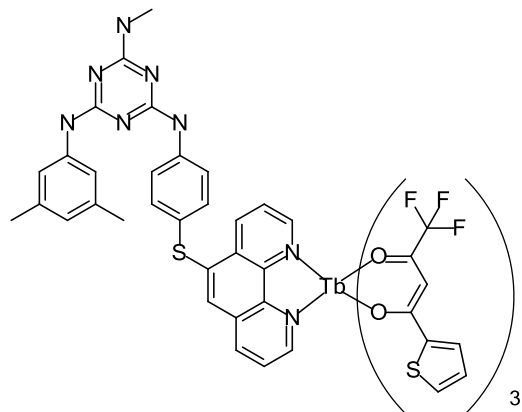
Yield: 77%; FTIR (KBr, cm^{-1}): 3396, 3104, 2957, 2923, 1600, 1558, 1538, 1505, 1412, 1356, 1304, 1246, 1230, 1186, 1141, 1083, 1061, 1035, 1013, 951, 934, 885, 860, 838, 808, 787, 768, 735, 720, 692, 681, 641, 605, 580, 521, 493, 459 cm^{-1} ; ^1H NMR (300 MHz, $\text{DMSO-}d_6$, 298 K): δ 9.95 (s, 3H), 9.31 (s, 3H), 9.18-9.02 (m, 3H), 8.85 (s, 1H), 8.10 (s, 3H), 7.84 (s, 3H), 7.35 (m 4H), 6.91 (m, 1H), 6.56 (s, 1H), 2.84 (s, 3H), 2.10 (s, 6H) ppm; ^{13}C NMR (75 MHz, $\text{DMSO-}d_6$): δ 193.0, 171.2, 166.6, 164.3, 151.9, 150.7, 141.1, 140.4, 137.6, 132.6, 131.8, 131.1, 129.6, 123.8, 121.2, 118.3, 108.6, 30.9, 27.8, 21.5 ppm; ^{19}F NMR (376 MHz, $\text{DMSO-}d_6$) δ -71.1 (s, 9H) ppm; $\mu_{\text{eff}} = 2.655$; $T_g = 112$ °C.

Preparation of 68a•Eu(III)



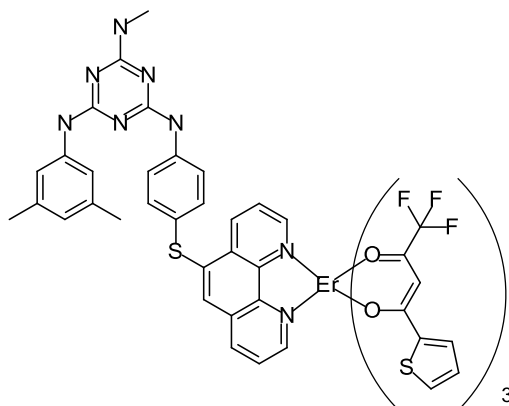
Yield: 67%; FTIR (KBr, cm^{-1}): 3822, 3405, 1601, 1537, 1502, 1412, 1357, 1307, 1246, 1230, 1187, 1141, 1083, 1062, 1035, 1014, 952, 934, 887, 859, 838, 808, 787, 768, 734, 722, 681, 641, 605, 581, 461 cm^{-1} ; ^1H NMR (300 MHz, $\text{DMSO-}d_6$, 298 K): δ 9.33 (d, 1H), 9.10 (d, 2H), 8.96 (d, 1H), 8.73 (s, 1H), 8.42 (s, 1H), 7.96-7.76 (m, 7H), 7.45-7.33 (m, 8H), 6.93 (s, 1H), 6.51 (s, 4H), 6.34 (s, 3H), 2.82 (s, 3H), 2.12 (s, 6H) ppm; ^{13}C NMR (75 MHz, $\text{DMSO-}d_6$): δ 168.5, 166.6, 164.3, 154.1, 150.7, 145.7, 141.2, 140.4, 137.5, 136.0, 132.4, 130.0, 127.1, 125.1, 123.7, 121.4, 118.3, 102.7, 61.6, 31.1, 27.8, 25.7, 21.7 ppm; ^{19}F NMR (376 MHz, $\text{DMSO-}d_6$) δ -78.4 (s, 9H) ppm; $\mu_{\text{eff}} = 2.401$; $T_g = 109$ °C.

Preparation of 68a•Tb(III)



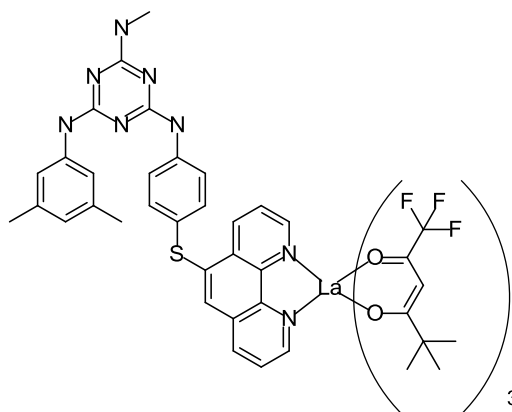
Yield: 77%; FTIR (KBr, cm^{-1}): 3405, 2361, 1627, 1601, 1538, 1504, 1468, 1412, 1357, 1308, 1246, 1230, 1187, 1141, 1062, 1035, 935, 886, 859, 808, 787, 719, 682, 582, 521, 422 cm^{-1} ; ^1H NMR (300 MHz, $\text{DMSO-}d_6$, 298 K): δ 9.40 (d, 1H), 9.21 (d, 2H), 9.06 (s, 1H), 8.90 (s, 1H), 8.46 (s, 1H), 8.04 (m, 3H), 7.85 (s, 1H), 7.73 (s, 1H), 7.51 (s, 3H), 7.07 (s, 1H), 6.62 (m, 3H), 3.01 (s, 3H), 2.29 (s, 6H) ppm; ^{13}C NMR (75 MHz, $\text{DMSO-}d_6$): δ 207.1, 166.9, .41, 133.9, 164.8, 150.9, 141.3, 140.8, 138.0, 136.4, 133.9, 132.6, 130.3, 129.0, 125.8, 124.3, 121.6, 118.7, 103.9, 31.3, 28.2, 21.9 ppm; ^{19}F NMR (376 MHz, $\text{DMSO-}d_6$) δ -43.8 (s, 9H) ppm; $\mu_{\text{eff}} = 7.853$; $T_g = 112$ °C.

Preparation of 68a•Er(III)



Yield: 86%; FTIR (KBr, cm^{-1}): 3406, 2956, 2923, 2360, 2342, 1529, 1604, 1538, 1503, 1469, 1413, 1358, 1311, 1247, 1231, 1187, 1142, 1083, 1062, 936, 860, 808, 787, 769, 734, 720, 682, 669, 642, 605, 583, 522, 421, 409 cm^{-1} ; ^1H NMR (300 MHz, $\text{DMSO-}d_6$, 298 K): δ 9.29 (s, 1H), 9.09 (d, 2H), 8.89 (d, 1H), 7.93 (s, 1H), 7.83 (m, 3H), 7.28 (s, 4H), 6.91 (s, 3H), 6.47 (s, 1H), 4.63 (s, 3H), 2.79 (s, 3H), 2.08 (s, 6H) ppm; ^{13}C NMR (75 MHz, $\text{DMSO-}d_6$): δ 166.5, 164.6, 150.7, 140.3, 137.5, 136.2, 133.7, 132.3, 128.7, 125.3, 123.6, 122.7, 121.2, 118.2, 114.6, 107.3, 30.8, 27.7, 21.5 ppm; ^{19}F NMR (376 MHz, $\text{DMSO-}d_6$) δ -92.0 (s, 9H) ppm; $\mu_{\text{eff}} = 7.719$; $T_g = 117$ °C.

Preparation of 68b•La(III)

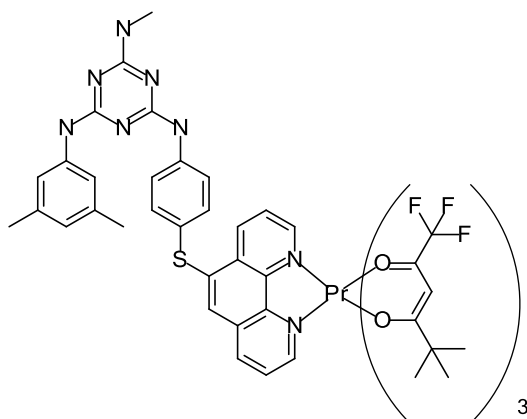


To a solution of 1,1,1-trifluoro-5,5-dimethyl-2,4-hexanedione (**53**) (222 mg, 1.13 mmol) in EtOH (4 mL) in a round-bottomed flask equipped with a magnetic stir bar was added NaOMe (25% in MeOH, 260 μL , 1.13 mmol), the mixture was stirred for 5 minutes at room temperature. A solution of ligand **68** (200 mg, 0.377 mmol) in THF (3 mL) was added. A solution of $\text{LaCl}_3 \cdot x\text{H}_2\text{O}$ (92.5 mg, 0.377 mmol) in H_2O (4 mL) was added dropwise. A small portion of THF (2-3 mL) was added to re-dissolve any precipitate that had formed and the mixture was refluxed for 24 h. The mixture was then poured into H_2O . The precipitate was collected by filtration, redissolved in CH_2Cl_2 , dried over Na_2SO_4 , filtered, and the solvent was removed under reduced pressure to afford 211 mg complex **68b•La(III)** (0.168 mmol, Yield 45%). FTIR (KBr, cm^{-1}): 3289, 2960, 2926, 2869, 1627, 1575, 1511, 1471, 1426, 1364, 1297, 1250, 1183, 1160, 1135, 1107, 950, 882, 846, 808, 794, 737, 688, 567, 520, 475 cm^{-1} ; ^1H NMR (300 MHz, $\text{DMSO-}d_6$, 298 K): δ 9.34 (s, 1H), 9.20 (m, 2H), 9.02-9.85 (m, 1H), 8.79 (s, 1H), 8.46 (s, 1H), 7.98 (m, 1H), 7.87-7.79

(m, 4H), 7.32 (m, 4H), 6.93 (m, 1H), 6.52 (s, 1H), 5.64 (s, 2H), 2.83 (s, 3H), 2.09 (s, 6H) ppm; ^{13}C NMR (75 MHz, DMSO- d_6): δ 203.0, 168.2, 167.9, 167.6, 166.6, 164.6, 164.3, 150.9, 146.2, 145.4, 141.1, 140.4, 137.5, 132.3, 130.1, 128.7, 128.1, 125.4, 124.3, 124.1, 123.8, 121.3, 121.2, 118.3, 118.3, 115.5, 89.5, 55.4, 30.9, 27.7, 26.3, 21.5 ppm; ^{19}F NMR (376 MHz, DMSO- d_6) δ -74.4 (s, 9H) ppm; $T_g = 113$ °C.

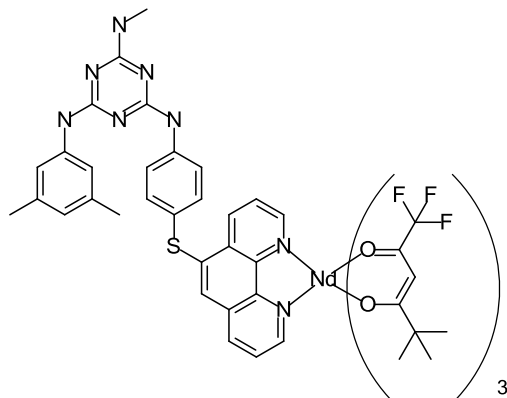
Additional complexes of with the metal centres including; Pr(III), Nd(III), and Eu(III) were prepared according to the same procedure as analogue **68b**•La(III) from the respective lanthanide salts (Pr(NO₃)₃•6H₂O, NdCl₃•6H₂O, and EuCl₃•6H₂O) and ligand **68b**.

Preparation of **68b**•Pr(III)



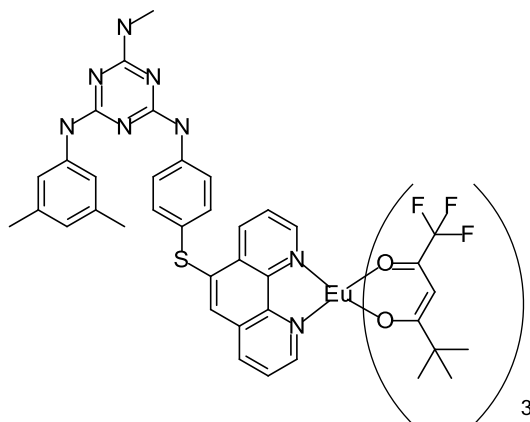
Yield: 56%; FTIR (KBr, cm^{-1}): 3280, 2959, 2925, 2870, 1619, 1593, 1514, 1468, 1427, 1364, 1301, 1251, 1186, 1160, 1139, 1111, 951, 885, 848, 797, 736, 689, 637, 570, 521, 455 cm^{-1} ; ^1H NMR (300 MHz, DMSO- d_6 , 298 K): δ 9.33-8.87 (m, 4H), 8.76 (s, 1H), 8.43 (s, 1H), 8.14-7.66 (m, 4H), 7.35 (m, 3H), 6.84 (m, 1H), 6.56 (m, 1H), 2.85 (s, 3H), 2.24 (s, 3H), 2.15 (s, 3H) ppm; ^{13}C NMR (75 MHz, DMSO- d_6): δ 166.5, 164.3, 153.2, 150.4, 140.4, 137.6, 130.3, 127.9, 125.4, 123.9, 120.7, 118.3, 117.8, 117.1, 70.2, 57.2, 29.1, 27.8, 26.5, 21.6, 21.3 ppm; ^{19}F NMR (376 MHz, DMSO- d_6) δ -68.9 (s, 9H) ppm; $\mu_{\text{eff}} = 2.308$; $T_g = 101$ °C.

Preparation of 68b•Nd(III)



Yield: 61%; FTIR (KBr, cm^{-1}): 3280, 2967, 2360, 1621, 1557, 1515, 1471, 1428, 1365, 1301, 1251, 1186, 1139, 1111, 1038, 952, 885, 848, 797, 762, 736, 689, 638, 570, 521, 478, 458 cm^{-1} ; ^1H NMR (300 MHz, $\text{DMSO-}d_6$, 298 K): δ 9.50 (2H), 9.33 – 9.01 (m, 2H), 8.84 – 8.77 (d, 1H), 8.43 (s, 1H), 7.86 (m, 3H), 7.36 (s, 3H), 6.93 – 6.80 (m, 1H), 6.54 (d, 1H), 2.83 (s, 3H), 2.23 – 2.13 (d, 7H) ppm; ^{13}C NMR (75 MHz, $\text{DMSO-}d_6$): δ 211.6, 182.6, 166.5, 164.6, 150.7, 141.1, 140.4, 137.6, 136.2, 133.7, 132.2, 129.8, 128.3, 123.8, 121.2, 118.3, 117.8, 108.1, 60.2, 27.8, 26.9, 21.7, 21.5, 21.3, 21.2 ppm; ^{19}F NMR (376 MHz, $\text{DMSO-}d_6$) δ -70.8 (s, 9H) ppm; $\mu_{\text{eff}} = 2.398$; $T_g = 103$ °C.

Preparation of 68b•Eu(III)



Yield: 48%; FTIR (KBr, cm^{-1}): 3845, 3279, 2960, 2926, 1620, 1515, 1470, 1427, 1365, 1303, 1251, 1187, 1140, 1114, 953, 886, 849, 796, 735, 689, 571, 521 cm^{-1} ; ^1H NMR (300 MHz, $\text{DMSO-}d_6$, 298 K): δ 9.32 (s, 1H), 9.15 (m, 2H), 8.91 (d, 1H), 8.75 (s, 1H), 8.42 (s, 1H), 7.97 (s, 1H), 7.85 (m, 3H), 7.33 (s, 3H), 6.91-6.79 (m, 2H), 6.59-6.51 (m, 1H), 2.83 (s, 3H), 2.16 (s, 6H) ppm; ^{13}C NMR (75 MHz, $\text{DMSO-}d_6$): δ 203.6, 167.5, 166.6, 164.3, 150.8, 146.4, 145.6, 141.2, 140.4, 137.5, 136.2, 133.7, 132.4, 130.0, 128.6, 124.2, 123.7, 121.3, 118.3, 117.8, 60.6, 55.8, 52.9, 30.9, 29.1, 28.8, 27.8, 27.5, 21.7, 21.5, 21.3, 11.3 ppm; ^{19}F NMR (376 MHz, $\text{DMSO-}d_6$) δ -78.9 (s, 9H) ppm; $\mu_{\text{eff}} = 2.127$; $T_g = 101$ °C.

6.4. Summary

A phenanthroline ligand functionalized with a mexylaminotriazine group (**68**) was successfully synthesized in one pot with high yields. The product shared the ability of its mexylaminotriazine precursor to readily form long-lived glasses. From this ligand, a series of lanthanide metal complexes were prepared and characterized. Mexylaminotriazine-functionalized phenanthroline **68** was prepared from a thiol-substituted mexylaminotriazine precursor (**24**) with 5,6-epoxy-5,6-dihydro-[1,10]phenanthroline (**61**) in the presence of sodium methoxide through a one-pot substitution-elimination sequence. The resulting glass-forming ligand (**68**) was used as the common precursor to prepare two series of glass-forming heteroleptic metal complexes with β -diketonate ligands, 2-thenoyltrifluoroacetone (**52**) or 1,1,1-trifluoro-5,5-dimethyl-2,4-hexanedione (**53**), and various lanthanide salts. This was done by reacting the respective ligands with the corresponding lanthanide metal salts in the presence of sodium methoxide. The ligand and subsequent complexes were then characterized using NMR spectroscopy, UV-Vis spectroscopy, FTIR spectroscopy, and HRMS techniques. The T_g of these complexes was measured by DSC, which was used to demonstrate the glass-forming properties and the ability to form uniform thin films of the ligand and all complexes. The T_g values for the mexylaminotriazine-functionalized phenanthroline ligand (**68**) was found to be 134 °C. A decrease in T_g from the ligand to the coordination complexes was observed as the lanthanide metal complexes exhibit glass transitions ranging 101 °C to 130 °C. The metal complexes exhibited consistent T_g values with the exception of the lanthanum complexes which exhibit higher glass transitions. This highlights the conclusion made in chapter 4 that a study is required to determine the effect of metal centres of glass-forming properties. Variations in the UV-Vis absorption spectra between the two series of these novel coordination complexes suggests that the structure and properties of these complexes can still be tailored for various purposes. As expected, a red-shift was observed in the UV-Vis spectra of solid-state samples. This is the result of increased molecular aggregation in the solid samples. In addition, informal testing demonstrated luminescent properties in some complexes. The europium complexes demonstrated luminescent properties when irradiated with UV light. Unfortunately, the scope of this project, time constraints, and the availability of instruments did not allow for the proper assessment and characterization of these complexes' luminescent properties. This information will be necessary for developing these materials for future applications. Furthermore, not all complexes demonstrated the same behaviour. This could be explained by several factors: the limited range of wavelengths used to irradiate the materials; an inability to measure low intensity luminescence properly or at wavelengths outside of the visible region; or the lack of luminescent properties in some compounds altogether. Further research is necessary to determine the optical and luminescent properties of these complexes. As such, accurate conclusions cannot be made; however, the observation of luminescent Eu(III) complexes indicates that these series of complexes could hold potential value for the production of luminescent materials.

7. Conclusion and Recommendations

The overall objective of this research thesis was to develop a strategy for the preparation of molecular glass coordination complexes. The first objective of this research project was to introduce mexylaminotriazine substituents to an array of chelating ligands. Several novel ligands capable of readily forming glassy phases have been synthesized based on the salen, acetylacetonate, and phenanthroline ligand structures. The synthesis of glass-forming ligands can be synthetically challenging. While a variety of ligands have been synthesized in this report, not all follow the same procedures. Furthermore, the synthesis of some analogous ligands required more drastic variations in their synthetic procedures, while the synthesis of some others was unsuccessful. Nevertheless, it has been demonstrated that a library of glass-forming compounds can be synthesized to incorporate chelating functionalities.

The second objective of this research thesis was to prepare coordination complexes from the synthesized glass-forming complexes. A number of homoleptic and heteroleptic metal complexes were subsequently prepared from transition and lanthanide metals and the newly formed glassy ligands. These mexylaminotriazine-functionalized coordination complexes were shown to exhibit glass transition and the formation of stable glassy phases. In addition, these novel glass-forming coordination complexes were shown to possess many of the same properties as their non-glassy analogues. As such, this preliminary research supports the use, and further development of mexylaminotriazine compounds as a viable strategy for introducing glass-forming properties across a wide-range of ligand systems for the formation of glass-forming coordination complexes.

In Chapter 4, the syntheses of a number of salen derivatives that incorporated the mexylaminotriazine glass-forming moiety were described. The T_g of these complexes was measured by DSC, which was used to demonstrate the glass-forming properties and the ability of most complexes to form uniform thin films. These novel salen complexes hold promise as solid-state catalysts; however, further research will be required. This research will focus on determining which catalytic applications of salen complexes are best suited for heterogenization and subsequently the optimization of their performance. For example, thin film catalysts have been suggested for the development of protective coatings against chemical warfare agents. It has been demonstrated that salen complexes are capable of catalyzing sulfoxidation reactions.¹¹⁰ Thin film salen complexes could be applied to vehicles and equipment to form a protective coating that catalytically decontaminates chemical warfare agents such as sulfur mustard, a chemical vesicant, through its oxidation to a less toxic sulfoxide form.²³⁸ Additionally, this library of glass-forming salen complexes can be expanded by substituting the functional groups on the salicylaldehyde moieties. These complexes are known for their versatility and ability to incorporate a variety of substituents. Many derivatives of the salen ligand exist and lead to wide differences in their steric and electronic properties. This variation is key to their application for a variety of diverse applications and high catalytic activity and stereoselectivity. Altering the molecular structure of these complexes could also be used to improve properties or for the optimization of catalytic activity in various applications. For example, the present study recognized the limited solubility of these complexes. Changing the molecular structure of these complexes in the future could be used to improve their solubility and other physical properties. Ultimately, this information can be used to develop novel heterogeneous salen catalysts as well as the development of other heterogeneous catalysts. One example of a future application could be the use of these complexes

to form thin coatings for sensors or as protective coatings among other traditional uses for heterogeneous catalysts.

Chapter 5 reported the synthetic procedures used to synthesize a glassy acetylacetonone ligand functionalized with a mexylaminotriazine substituent. Subsequently, several attempts were made to prepare a variety of homoleptic and heteroleptic transition metal complexes from glacac with Zn(II), Ni(II), and Cu(II) metal salts. Regrettably, the crude products were shown to be water sensitive and ultimately, the preparation of these complexes was abandoned due to the limited potential for future application. The substituents at both the α - and β -positions of β -diketonates are factors that affect the equilibrium of the keto-enol tautomerization. In this report, acetylacetonone-functionalized with mexylaminotriazines at the 3-position were synthesized. A proposed alternative strategy could be screening various other acetylacetonone derivatives to determine a suitable method for covalently linking mexylaminotriazines at the 1- or 5-positions. An alternative structure could be the solution for synthesizing acetylacetonone ligands that are more suitable for coordination with metals by resisting hydrolysis and lability.

Chapter 6, the final part of this project, described the synthesis of a glass-forming phenanthroline ligand by the incorporation of a mexylaminotriazine moiety. The ligand was subsequently used to prepare a number of heteroleptic lanthanide complexes from lanthanide(III) metal salts and one of two β -diketonates, 2-thenoyltrifluoroacetone or 1,1,1-trifluoro-5,5-dimethyl-2,4-hexanedione. The T_g values of these complexes were measured by DSC, which was used to demonstrate the glass-forming properties and the ability to form uniform thin films from all of the subsequent complexes. The various metal complexes exhibit glass transitions that are consistent with each other, with the exception of the lanthanum(III) complexes of both the **68a** and the **68b** series of complexes, which exhibit higher T_g . This observation further highlights the requirement of studying the effect of metal centres on T_g and glass-forming properties.

These novel glass-forming phenanthroline complexes show promise for a range of optoelectronic applications. This library of glass-forming phenanthroline complexes could be expanded by altering the substituents on the phenanthroline ligand or by incorporating derivatives of the β -diketonate ligands. The β -diketonates in particular offer a great deal of variability in both properties and applications as countless derivatives of these compounds exist. For example, analysis *via* UV-Vis spectroscopy demonstrated variations in optical properties between the two series synthesized for this report. As such, it has been demonstrated that the optical properties of these novel glass-forming coordination complexes can still be altered and tailored despite the introduction of mexylaminotriazine moieties. Given their current and proposed use for solid-state optoelectronic devices, UV-Vis spectra were also obtained for solid-state samples of all lanthanide complexes. Upon comparison of the solid-state samples to those in solution, a red shift was observed as expected. This correlates to the increased molecular aggregation observed for materials in the solid-state. Furthermore, the two europium(III) complexes exhibited luminescent properties similar to their non-glass forming counterparts when irradiated by UV light. These same properties in similar non-glass forming europium(III) complexes have been exploited for a myriad of purposes.^{182,230,235-237} However, a lack of access to the proper instruments prevented the quantitative evaluation of the luminescence of these complexes and those containing other metal centres. Future research will include a full evaluation of the fluorescent properties of these complexes as non-glass forming complexes containing a myriad of metal centres have seen diverse utilization in devices such as emissive layers in OLEDs, as gain media in lasers, and for other applications in luminescent and electronic materials.^{199,203,217} Additionally, development of these

compounds will require investigation to ascertain the optimal glass structure, molecular structure for specific applied purposes, as well as the ideal conditions for synthesis, spin-coating, and device fabrication.

Several areas requiring further research were uncovered in this research project. Firstly, the effect of the metal centre on the glass-forming abilities of these metal complexes was identified. For example, the measured glass transition temperatures varied between the salen metal complexes; however, generally those complexes containing the same metal centre show closer T_g values. This seems to indicate that the metal centre does in fact play a role on the complexes' glass transitions. Secondly, not all ligands are suitable for functionalization with methylaminotriazine glass-forming substituents. The acetylacetonate ligand functionalized with a molecular glass proved to be too labile and demonstrated water sensitivity that prevented the preparation of complexes. Fortunately, in addition to salen, acetylacetonate, and phenanthroline, many other ligands and respective complexes exist. The development of a library of molecular glass ligands and coordination complexes could be further augmented by the synthesis of other methylaminotriazine-functionalized ligands. It is envisaged that this research described in this report will be utilized for the development of novel glass-forming ligands and metal complexes as well as for the use of these compounds in a variety of applications as thin film materials.

8. References

- (1) Shriver, D. F.; Atkins, P. W.; Langford, C. H. *Inorganic Chemistry*, 1st ed.; W.H. Freeman and Co.: New York, 1990.
- (2) Umezawa, H.; Nunzi, J.-M.; Lebel, O.; Sabat, R. G. *Langmuir* **2016**, *32* (22), 5646–5652.
- (3) Roudaut, G.; Simatos, D.; Champion, D.; Contreras-Lopez, E.; Le Meste, M. *Innov. Food Sci. Emerg. Technol.* **2004**, *5*, 127–134.
- (4) Ohring, M. *Materials science of thin films : deposition and structure*; Academic Press, 2002.
- (5) Ley, S.; Baxendale, I. *Supported Catalysts and Their Applications*; Sherrington, D. C., Kybett, A. P., Eds.; Royal Society of Chemistry: Cambridge, 2001.
- (6) Meunier, A.; Lebel, O. *Org. Lett.* **2010**, *12* (9), 1896–1899.
- (7) Plante, A.; Palato, S.; Lebel, O.; Soldera, A. *J. Mater. Chem. C.* **2013**, *1*, 1037–1042.
- (8) Lebel, O. Molecular Glasses with Functionalizable Groups. US. Pat. Appl. 13/714942, 2012.
- (9) Lebel, O. Molecular Glasses with Functionalizable Groups. Can. Pat. Appl. 2,762,434, 2011.
- (10) Lebel, O.; Maris, T.; Perron, M. È.; Demers, E.; Wuest, J. D. *J. Am. Chem. Soc.* **2006**, *128* (32), 10372–10373.
- (11) Eren, R. N.; Plante, A.; Meunier, A.; Laventure, A.; Huang, Y.; Briard, J. G.; Creber, K. J.; Pellerin, C.; Soldera, A.; Lebel, O. *Tetrahedron* **2012**, *68* (49), 10130–10144.
- (12) Plante, A.; Mauran, D.; Carvalho, S. P.; Pagé, J. Y. S. D.; Pellerin, C.; Lebel, O. *J. Phys. Chem.* **2009**, *113*, 14884–14891.
- (13) Laventure, A.; Soldera, A.; Pellerin, C.; Lebel, O. *New J. Chem.* **2013**, *37* (12), 3881–3889.
- (14) Wuest, J. D.; Lebel, O. *Tetrahedron* **2009**, *65* (36), 7393–7402.
- (15) Laventure, A.; De Grandpré, G.; Soldera, A.; Lebel, O.; Pellerin, C. *Phys. Chem. Chem. Phys.* **2016**, *18* (January), 1681–1692.
- (16) Laventure, A.; Maris, T.; Pellerin, C.; Lebel, O. *Cryst. Growth Des.* **2017**, *17* (5), 2365–2373.
- (17) Mazaheri, L.; Bobbara, S. R.; Lebel, O.; Nunzi, J.-M. *Opt. Lett.* **2016**, *41* (13), 2958–2961.
- (18) Iida, M.; Masuda, R.; Naren, G.; Bin, Y.; Kajiwara, K. *Chem. Lett.* **2004**, *33* (11), 1462–1463.
- (19) *Oxford Dictionary of Science*, 7th ed.; Law, J., Ed.; Oxford University Press, 2017.

- (20) Tilley, R. *Understanding Solids*; John Wiley & Sons Ltd: West Sussex, 2004.
- (21) Openstax. The Solid State of Matter <https://courses.lumenlearning.com/suny-mcc-chemistryformajors-1/chapter/the-solid-state-of-matter-2/>.
- (22) Lambert, R. M.; Pacchioni, G. *Chemisorption and Reactivity on Supported Clusters and Thin Films : Towards an Understanding of Microscopic Processes in Catalysis*; Springer Netherlands, 1997.
- (23) Husband, T. *ChemMatters*. pp 5–8.
- (24) Yu, L. *Adv. Drug Deliv. Rev.* **2001**, 48 (1), 27–42.
- (25) Seo, J.-A.; Kim, S. J.; Kwon, H.-J.; Yang, Y. S.; Kim, H. K.; Hwang, Y.-H. *Carbohydr. Res.* **2006**, 341 (15), 2516–2520.
- (26) Crowe, L. M.; Reid, D. S.; Crowe, J. H. *Biophys. J.* **1996**, 71 (4), 2087–2093.
- (27) Slade, L.; Levine, H.; Reid, D. S. *Crit. Rev. Food Sci. Nutr.* **1991**, 30 (2–3), 115–360.
- (28) Kolb, D.; Kolb, K. E. *J. Chem. Educ.* **1979**, 56 (9), 604–608.
- (29) Painter, P. C.; Coleman, M. M. *Fundamentals of polymer science : an introductory text*, 2nd ed.; Technomic Pub. Co: Lancaster, 1997.
- (30) Mckenna, G.; Simon, S. In *Handbook of Thermal Analysis and Calorimetry. Vol 3: Application to polymers and Plastics*; 2002; pp 49–109.
- (31) Biroli, G. *Glass and Jamming Transitions. In Glasses and Grains: Poincaré Seminar 2009*; Bertrand Duplantier, Thomas Halsey, Vincent Rivasseau, Eds.; Birkhauser: Berlin, 2009.
- (32) Dougherty, T. J.; Pucci, M. J. *Antibiotic discovery and development*; Springer, 2012.
- (33) Veber, D. F.; Johnson, S. R.; Cheng, H. Y.; Smith, B. R.; Ward, K. W.; Kopple, K. D. *J. Med. Chem.* **2002**, 45 (12), 2615–2623.
- (34) Berthier, L.; Biroli, G. *Rev. Mod. Phys.* **2011**, 83 (2), 587–645.
- (35) Shirota, Y. *J. Mater. Chem.* **2000**, 10 (1), 1–25.
- (36) Nishimura, K.; Kobata, T.; Inada, H.; Shirota, Y. *J. Mater. Chem.* **1991**, 1 (5), 897–898.
- (37) Higuchi, A.; Ohnishi, K.; Nomura, S.; Inada, H.; Shirota, Y. *J. Mater. Chem.* **1992**, 2 (10), 1109.
- (38) Inada, H.; Shirota, Y. *J. Mater. Chem.* **1993**, 3, 319–320.
- (39) Kinoshita, M.; Kita, H.; Shirota, Y. *Adv. Funct. Mater.* **2002**, 12 (1112), 780–786.
- (40) Kimura, M.; Kuwano, S.; Sawaki, Y.; Fujikawa, H.; Noda, K.; Taga, Y.; Takagi, K. *J. Mater. Chem.* **2005**, 15, 2393–2398.

- (41) Geng, Y.; Katsis, D.; Culligan, S.; Ou, J.; Chen, S.; Rothberg, L. *Chem. Mater.* **2002**, *14* (1), 463–470.
- (42) Wang, S.; Oldham, W.; Hudack, R.; Bazan, G. *J. Am. Chem. Soc.* **2000**, *122* (24), 5695–5709.
- (43) Lebel, O.; Maris, T.; Perron, M.-E. Å. V.; Demers, E.; Wuest, J. D. *J. AM. CHEM. SOC* **2006**, *128* (32), 10372–10373.
- (44) Saenger, W. In *Principles of Nucleic Acid Structure*; Springer New York: New York, NY, 1984; pp 116–158.
- (45) Mignon, P.; Loverix, S.; Steyaert, J.; Geerlings, P. *Nucleic Acids Res.* **2005**, *33* (6), 1779–1789.
- (46) Shirota, Y.; Kageyama, H. *Chem. Rev.* **2007**, *107* (4), 953–1010.
- (47) Craig, D.; Royall, P.; Kett, V.; Hopton, M. *Int. J. Pharm.* **1999**, *179*, 179–207.
- (48) Hancock, B. C.; Zografis, G. *J. Pharm. Sci.* **1997**, *86* (1), 1–12.
- (49) Yu, L. *Adv. Drug Deliv. Rev.* **2016**, *100*, 3–9.
- (50) Shirota, Y. *J. Mater. Chem.* **2005**, *15* (1), 75–93.
- (51) Oyston, S.; Wang, C.; Hughes, G.; Batsanov, A. S.; Perepichka, I. F.; Bryce, M. R.; Ahn, J. H.; Pearson, C.; Petty, M. C. *J. Mater. Chem.* **2005**, *15* (1), 194–203.
- (52) Kido, J.; Hongawa, K.; Okuyama, K.; Nagai, K. *Appl. Phys. Lett.* **1993**, *63* (19), 2627–2629.
- (53) Zhou, X.; Pfeiffer, M.; Huang, J. S.; Blochwitz-Nimoth, J.; Qin, D. S.; Werner, A.; Drechsel, J.; Maennig, B.; Leo, K. *Appl. Phys. Lett.* **2002**, *81* (5), 922–924.
- (54) Naka, S.; Okada, H.; Onnagawa, H.; Tsutsui, T. *Appl. Phys. Lett.* **2000**, *76* (2), 197–199.
- (55) Jandke, M.; Strohriegel, P.; Berlab, S.; Werner, E.; Brutting, W. *Macromolecules* **1998**, *31* (19), 6434–6443.
- (56) Nunzi, J.-M. *Comptes Rendus Phys.* **2002**, *3* (4), 523–542.
- (57) Noda, T.; Shirota, Y. *J. Am. Chem. Soc.* **1998**, *120* (37), 9714–9715.
- (58) Palilis, L. C.; Mäkinen, A. J.; Uchida, M.; Kafafi, Z. H. *Appl. Phys. Lett.* **2003**, *82* (14), 2209–2211.
- (59) Zen, A.; Bilge, A.; Galbrecht, F.; Alle, R.; Meerholz, K.; Grenzer, J.; Neher, D.; Scherf, U.; Farrell, T. *J. Am. Chem. Soc.* **2006**, *128*, 3914–3915.
- (60) Chien, C.-T.; Lin, C.-C.; Watanabe, M.; Lin, Y.-D.; Chao, T.-H.; Chiang, T.; Huang, X.-H.; Wen, Y.-S.; Tu, C.-H.; Sun, C.-H.; Chow, T. J. *J. Mater. Chem.* **2012**, *22* (26), 13070–13075.

- (61) Waldauf, C.; Schilinsky, P.; Perisutti, M.; Hauch, J.; Brabec, C. J. *Adv. Mater.* **2003**, *15* (24), 2084–2088.
- (62) Sonntag, M.; Kreger, K.; Hanft, D.; Strohrriegl, P. *Chem. Mater.* **2005**, *17* (11), 3031–3039.
- (63) Adhikari, T.; Nunzi, J.-M.; Lebel, O. *Org. Electron.* **2017**, *48*, 230–240.
- (64) Adhikari, T.; Ghoshouni Rahami, Z.; Nunzi, J. M.; Lebel, O. *Org. Electron. physics, Mater. Appl.* **2016**, *34*, 146–156.
- (65) Adhikari, T.; Nunzi, J.-M.; Lebel, O. *Org. Electron.* **2017**, *49*, 382–392.
- (66) Adhikari, T.; Bobbara, S. R.; Nunzi, J.-M.; Lebel, O. *Org. Electron.* **2018**, *53*, 74–82.
- (67) Xue, J.; Uchida, S.; Rand, B. P.; Forrest, S. R. *Appl. Phys. Lett.* **2004**, *84* (16), 3013–3015.
- (68) Xue, J.; Rand, B. P.; Uchida, S.; Forrest, S. R. *Adv. Mater.* **2005**, *17* (1), 66–71.
- (69) Chu, C.-W.; Shao, Y.; Shrotriya, V.; Yang, Y. *Appl. Phys. Lett.* **2005**, *86* (24), 243506–243509.
- (70) Yoo, S.; Domercq, B.; Kippelen, B. *Appl. Phys. Lett.* **2004**, *85* (5427–5429).
- (71) Shirota, Y.; Kobata, T.; Noma, N. *Chem. Lett.* **1989**, *18* (7), 1145–1148.
- (72) Hong, Z. R.; Lee, C. S.; Lee, S. T.; Li, W. L.; Shirota, Y. *Appl. Phys. Lett.* **2002**, *81* (15), 2878–2880.
- (73) Dürr, H.; Bouas-Laurent, H. *Photochromism: Molecules and Systems*, 1st ed.; Elsevier: Amsterdam, 2003.
- (74) Utsumi, H.; Nagahama, D.; Nakano, H.; Shirota, Y. *J. Mater. Chem.* **2002**, *12* (9), 2612–2619.
- (75) Piskorz, K.; Dust, J. M.; Buncel, E.; Lebel, O.; Nunzi, J.-M. *New J. Chem.* **2017**, *41* (3), 940–947.
- (76) Mack, C. A. *Fundamental principles of optical lithography: the science of microfabrication*; Wiley: London, 2007.
- (77) Yoshiiwa, M.; Kageyama, H.; Shirota, Y.; Wakaya, F.; Gamo, K.; Takai, M. *Appl. Phys. Lett.* **1996**, *69* (17), 2605–2607.
- (78) Yang, D.; Chang, S. W.; Ober, C. K. *J. Mater. Chem.* **2006**, *16*, 1696–1696.
- (79) Chang, S. W.; Ayothi, R.; Bratton, D.; Yang, D.; Felix, N.; Cao, H. B.; Deng, H.; Ober, C. K. *J. Mater. Chem.* **2006**, *16* (15), 1470–1474.
- (80) Stanitski, C. *ChemCom: Chemistry in the Community*, 3rd ed.; Kendall/Hunt Publishing Co.: Dubuque, 1996.
- (81) Davis, M.; Davis, R. *Fundamentals of Chemical Reaction Engineering*, 1st ed.; McGraw-

- Hill Higher Education: New York, 2003.
- (82) Larhed, M.; Moberg, C.; Hallberg, A. *Acc. Chem. Res* **2002**, *35* (9), 717–727.
- (83) Ledoux, M.; Pham-Huu, C. *CATTECH* **2001**, *5* (4), 226–246.
- (84) Augustine, R.; Tanielyan, S.; Anderson, S.; Yang, H. *Chem. Commun.* **1999**, 1257–1258.
- (85) Mizuno, N.; Misono, M. *Chem. Rev.* **1998**, *98*, 199–217.
- (86) Kadish, K. M.; Smith, K. M.; Guillard, R. *The Porphyrin Handbook: Inorganic, organometallic and coordination chemistry*, 3rd ed.; Academic Press: San Diego, 2000.
- (87) Zhou, Q.-L. *Angew. Chemie Int. Ed.* **2016**, *55* (18), 5352–5353.
- (88) Robinet, L.; Corbeil, M.-C. *Studies in Conservation*. Taylor & Francis, Ltd. International Institute for Conservation of Historic and Artistic Works 2003, pp 23–40.
- (89) Mazaheri, L.; Bobbara, S.; Lebel, O.; Nunzi, J.-M. *Opt. Lett.* **2016**, *41* (13), 2958–2961.
- (90) Skoog, D. A.; West, D. M. *Principles of instrumental analysis*; Saunders College: Philadelphia, 1980.
- (91) Bain, G.; Berry, J. J. *Chem. Educ.* **2008**, *85* (4), 532–536.
- (92) Matthey, J. *Magnetic Susceptibility Balance Instruction Manual MSB Mk1*; Montreal, Qu, 2004.
- (93) Cozzi, P. G. *Chem. Soc. Rev.* **2004**, *33* (7), 410–421.
- (94) McNaught, A. D.; Wilkinson, A. *IUPAC Compendium of Chemical Terminology - Gold Book*; Blackwell Scientific Publications, 1997.
- (95) Baleizão, C.; Garcia, H. *Chem. Rev.* **2006**, *106*, 3987–4043.
- (96) Yoon, T.; Jacobsen, E. *Sciences.* **2003**, *299*, 1691–1693.
- (97) Venkataramanan, N. S.; Kuppuraj, G.; Rajagopal, S. *Coord. Chem. Rev.* **2005**, *249* (11–12), 1249–1268.
- (98) Atwood, D.; Harvey, M. J. *Chem. Rev.* **2001**, *101* (1), 37–52.
- (99) Larrow, J. F.; Jacobsen, E. N. In *Organometallics in Process Chemistry: Topics in Organometallic Chemistry*; Springer: Berlin, Heidelberg, 2004; pp 123–152.
- (100) Katsuki, T. *Chem. Soc. Rev.* **2004**, *33*, 437–444.
- (101) Jacobsen, E. N.; Zhang, W.; Muci, A. R.; Ecker, J. R.; Deng, L. *J. Am. Chem. Soc.* **1991**, *113* (18), 7063–7064.
- (102) Li, Z.; Conser, K. R.; Jacobsen, E. N. *J. Am. Chem. Soc.* **1993**, *115* (12), 5326–5327.

- (103) Martinez, L. E.; Leighton, J. L.; Carsten, D. H.; Jacobsen, E. N. *J. Am. Chem. Soc.* **1995**, *117* (21), 5897–5898.
- (104) Schaus, S.; Brånalt, J.; Jacobsen, E. N. *J. Org. Chem.* **1998**, *63* (2), 403–405.
- (105) Tokunaga, M.; Larrow, J. F.; Kakiuchi, F.; Jacobsen, E. N. *Science (80-.)*. **1997**, *277*, 936–938.
- (106) Sammis, G.; Jacobsen, E. N. *J. Am. Chem. Soc.* **2003**, *125* (15), 4442–4443.
- (107) Sigman, M.; Jacobsen, E. N. *J. Am. Chem. Soc.* **1998**, *120* (21), 5315–5316.
- (108) Tamura, Y.; Uchida, T.; Katsuki, T. *Tetrahedron Lett.* **2003**, *44* (16), 3301–3303.
- (109) Miller, J.; Jin, W.; Nguyen, S. T. *Angew. Chemie Int. Ed.* **2002**, *41* (16), 2953–2956.
- (110) Saito, B.; Katsuki, T. *Tetrahedron Lett.* **2001**, *42*, 3873–3876.
- (111) DiMauro, E. F.; Kozlowski, M. C. *Org. Lett.* **2001**, *3* (19), 3053–3056.
- (112) Cozzi, P. G. *Angew. Chemie Int. Ed.* **2003**, *42* (25), 2895–2898.
- (113) Belokon, Y.; North, M.; Parsons, T. *Org. Lett.* **2000**, *2* (11), 1617–1619.
- (114) Watanabe, A.; Uchida, T.; Ito, K.; Katsuki, T. *Tetrahedron Lett.* **2002**, *43* (25), 4481–4485.
- (115) Padwa, A.; Murphree, S. S. *Arc. Org. Chem.* **2006**, *3*, 6–33.
- (116) Zhang, W.; Loebach, J. L.; Wilson, S. R.; Jacobsen, E. N. *J. Am. Chem. Soc.* **1990**, *112* (7), 2801–2803.
- (117) Silva, A. R.; Wilson, K.; Whitwood, A. C.; Clark, J. H.; Freire, C. *Eur. J. Inorg. Chem.* **2006**, *6*, 1275–1283.
- (118) Zhang, W.; Jacobsen, E. N. *J. Org. Chem.* **1991**, *56* (7), 2296–2298.
- (119) Deng, L.; Jacobsen, E. N. *J. Org. Chem.* **1992**, *57* (15), 4320–4323.
- (120) Palucki, M.; Pospisil, P. J.; Zhang, W.; Jacobsen, E. N. *J. Am. Chem. Soc.* **1994**, *116* (20), 9333–9334.
- (121) Brandes, B. D.; Jacobsen, E. N. *J. Org. Chem.* **1994**, *59* (16), 4378–4380.
- (122) Paterson, I.; De Savi, C.; Tudge, M. *Org. Lett.* **2001**, *3* (20), 3149–3152.
- (123) Sinha, S.; Keinan, E. *J. Org. Chem.* **1997**, *62* (2), 377–386.
- (124) Sinha, A.; Sinha, S.; Sinha, S.; Keinan, E. *J. Org. Chem.* **1999**, *64* (7), 2381–2386.
- (125) Wipf, P.; Kim, Y.; Goldstein, D. M. *J. Am. Chem. Soc.* **1995**, *117* (45), 11106–11112.
- (126) Xiang, A. X.; Watson, D. A.; Ling, T.; Theodorakis, E. A. *J. Org. Chem.* **1998**, *63*, 6774–6775.

- (127) Hawkins, J. M.; Watson, T. J. N. *Angew. Chem. Int. Ed.* **2004**, *43* (25), 3224–3228.
- (128) *Asymmetric Catalysis on Industrial Scale: Challenges, Approaches and Solutions*; Blaser, H. U., Schmidt, E., Eds.; Wiley-VCH: Weinheim, 2004.
- (129) Leadbeater, N. E.; Marco, M. *Chem. Rev.* **2002**, *102* (10), 3217–3274.
- (130) Wan, J.-P.; Gan, S.-F.; Wu, J.-M.; Pan, Y. *Green Chem.* **2009**, *11*, 1633–1637.
- (131) Patil, S. V.; Patil, S. S.; Bobade, V. D. *Arab. Journal Chem.* **2016**, *9*, 515–521.
- (132) Darensbourg, D. J.; Frantz, E. B. *Inorg. Chem.* **2007**, *46*, 5967–5978.
- (133) Martínez, D.; Motevalli, M.; Watkinson, M. *Acta Crystallogr. Sect. C* **2002**, *58* (4), 258–260.
- (134) Chen, B.; Contreras, D. S.; Clancy, Y. L.; Fronczek, F. R. *Acta Crystallogr. Sect. E* **2004**, *60* (6), 732–734.
- (135) Bhattacharya, K.; Abtab, S.; Majee, M.; Endo, A.; Chaudhury, M. *Inorg. Chem* **2014**, *53*, 8287–8297.
- (136) Edulji, S.; Nguyen, S. *Organometallics* **2003**, *22* (17), 3374–3381.
- (137) Buckley, A. N.; Wilson, G. V. H.; Murray, K. S. *Chem. Commun.* **1969**, 718–719.
- (138) Resce, J. L.; Fanning, J. C.; Day, C. S.; Uhm, S. J.; Croisy, A. F.; Keefer, L. K. *Acta Crystallogr. Sect. C* **1987**, *43* (11), 2100–2104.
- (139) Wilkinson, G.; Gillard, R.; McCleverty, J. *Comprehensive Coordination Chemistry, Vol 2*; Pergamon Press, 1987.
- (140) Allen Annis, D.; Jacobsen, E. N. *J. Am. Chem. Soc.* **1999**, *121*, 4147–4154.
- (141) Yuan, W.-B.; Wang, H.-Y.; Du, J.-F.; Chen, S.-W.; Zhang, Q. *Acta Crystallogr. Sect. E* **2006**, *62* (12), 3504–3505.
- (142) Inba, P. J. K.; Annaraj, B.; Thalamuthu, S.; Neelakantan, M. A. *Bioinorg. Chem. Appl.* **2013**, 4398–4409.
- (143) Manfredotti, A. G.; Guastini, C.; IUCr. *Acta Crystallogr. Sect. C Cryst. Struct. Commun.* **1983**, *39* (7), 863–865.
- (144) Xie, H. *Acta Crystallogr. Sect. E* **2009**, *65*, 1577.
- (145) Shen, Y.-M.; Wang, W. *Acta Crystallogr. Sect. E* **2009**, *65*, 444.
- (146) Koopman, H.; Daams, J. *J. Rec. Trav. Chim. Pays-Bas* **1958**, *77* (3), 235–240.
- (147) Binnemans, K. In *Handbook on the Physics and Chemistry of Rare Earths*; 2005; Vol. 35, pp 107–272.

- (148) Bhattacharjee, S.; Yang, D.-A.; Ahn, W.-S. *Chem. Commun.* **2011**, 47, 3637–3639.
- (149) Bryant, B. E.; Fernelius, W. C.; Busch, D. H.; Stoufer, R. C.; Stratton, W. In *Inorganic Syntheses*; Wiley-Blackwell, 2007; pp 113–116.
- (150) Verma, P. N.; Sheikh, J. I.; Juneja, H. D. *World Appl. Sci. J.* **2011**, 14 (8), 1154–1157.
- (151) Vicente, J.; Chicote, M. T. *Coord. Chem. Rev.* **1999**, 193–195, 1143–1161.
- (152) Mehrotra, R. C. *Pure Appl. Chem* **1988**, 60 (8), 1349–1356.
- (153) Urbaniak, W.; Jurek, K.; Witt, K.; Gorączko, A. *Chemik* **2011**, 65 (4), 273–282.
- (154) Emsley, J. In *Complex Chemistry*; Springer Berlin Heidelberg: Berlin, Heidelberg, 1984; pp 147–191.
- (155) Marsh, A. In *NMR Spectroscopy in the Undergraduate Curriculum*; American Chemical Society: Washington, 2013; pp 205–210.
- (156) Reid, J. C.; Calvin, M. *J. Am. Chem. Soc.* **1950**, 72 (7), 2948–2952.
- (157) Barkley, L. B.; Levine, R. *J. Am. Chem. Soc.* **1951**, 73 (10), 4625–4627.
- (158) Barkley, L. B.; Levine, R. *J. Am. Chem. Soc.* **1953**, 75 (9), 2059–2063.
- (159) Park, J. D.; Brown, H. A.; Lacher, J. R. *J. Am. Chem. Soc.* **1953**, 75 (19), 4753–4756.
- (160) Ohta, K.; Yokoyama, M.; Kusabayashi, S.; Mikawa, H. *Mol. Cryst. Liq. Cryst.* **1981**, 69 (1–2), 131–142.
- (161) Ohta, K.; Akimoto, H.; Fujimoto, T.; Yamamoto, I. *J. Mater. Chem.* **1994**, 4 (1), 61–69.
- (162) Sprague, J. M.; Beckham, L. J.; Adkins, H. *J. Am. Chem. Soc.* **1934**, 56 (12), 2665–2668.
- (163) Adkins, H.; Rainey, J. *Org. Synth.* **1940**, 20, 6–11.
- (164) Furniss, B. S.; Hannaford, A. J.; Smith, P. W. G.; Tatchell, A. R. In *Vogel's Practical Organic Chemistry 5th Ed.*; 1989; pp 626–636.
- (165) Stary, J.; Liljenzin, J. *Critical Evaluation of Equilibrium Constants involving Acetylacetonates and its Metal Chelates*; 1982; Vol. 54.
- (166) Wanninger, S.; Lorenz, V.; Subhan, A.; Edelmann, F. T. *Chem. Soc. Rev.* **2015**, 44 (15), 4986–5002.
- (167) Pucci, D.; Crispini, A.; Mendiguchía, B. S.; Pirillo, S.; Ghedini, M.; Morelli, S.; De Bartolo, L. *Dalt. Trans.* **2013**, 42 (26), 9679–9687.
- (168) Deepthi, T. V.; Venugopalan, P. *Inorg. Chim. Acta* **2016**, 450, 243–250.
- (169) Pucci, D.; Bellini, T.; Crispini, A.; D'Agnano, I.; Liguori, P. F.; Garcia-Orduña, P.; Pirillo, S.; Valentini, A.; Zanchetta, G. *Medchemcomm* **2012**, 3 (4), 462–468.

- (170) Reddy, M.; Park, C. *Sci. Rep.* **2016**, *6* (1), 32306–32313.
- (171) Lamprey, H. *Ann. N. Y. Acad. Sci.* **1960**, *88* (2), 519–525.
- (172) Schoumacker, S.; Hamelin, O.; Pécaut, J.; Fontecave, M. *Inorg. Chem.* **2003**, *42* (24), 8110–8116.
- (173) Bellusci, A.; Barberio, G.; Crispini, A.; Ghedini, M.; La Deda, M.; Pucci, D. *Inorg. Chem.* **2005**, *44* (6), 1818–1825.
- (174) Liguori, P. F.; Valentini, A.; Palma, M.; Bellusci, A.; Bernardini, S.; Ghedini, M.; Panno, M. L.; Pettinari, C.; Marchetti, F.; Crispini, A.; Pucci, D. *Dalt. Trans.* **2010**, *39* (17), 4205–4212.
- (175) Shahabadi, N.; Falsafi, M.; Moghadam, N. H. *J. Photochem. Photobiol. B Biol.* **2013**, *122*, 45–51.
- (176) Valladolid, J.; Hortigüela, C.; Busto, N.; Espino, G.; Rodríguez, A. M.; Leal, J. M.; Jalón, F. A.; Manzano, B. R.; Carbayo, A.; García, B. *Dalt. Trans* **2014**, *43* (6), 2629–2645.
- (177) Bencini, A.; Vito, L. *Coord. Chem. Rev.* **2010**, *254*, 2096–2180.
- (178) Schilt, A. A.; Belcher, R.; Freiser, H. *Analytical Applications of 1,10-Phenanthroline and Related Compounds : International Series of Monographs in Analytical Chemistry*; Elsevier Science, 1969.
- (179) Luman, C. R.; Castellano, F. N. In *Comprehensive Coordination Chemistry II*; 2003; pp 25–39.
- (180) Brandt, W. W.; Dwyer, F. P.; Gyarfas, E. D. *Chem. Rev.* **1954**, *54* (6), 959–1017.
- (181) Sammes, P. G.; Yahioglu, G. *Chem. Soc. Rev.* **1994**, *23*, 327–334.
- (182) Accorsi, G.; Listorti, A.; Yoosaf, K.; Armaroli, N. *Chem. Soc. Rev.* **2009**, *38* (6), 1690–1700.
- (183) Riesgo, E. C.; Jin, X.; Thummel, R. P. *J. Org. Chem.* **1996**, *61*, 3017–3022.
- (184) Belser, P.; Bernhard, S.; Guerig, U. *Tetrahedron* **1996**, *52* (8), 2937–2944.
- (185) Gladiali, S.; Chelucci, G.; Mudadu, M. S.; Gastaut, M.-A.; Thummel, R. P. *J. Org. Chem.* **2001**, *66* (2), 400–405.
- (186) Bonacorso, H. G.; Andrighetto, R.; Krüger, N.; Martins, M. A. P.; Zanatta, N. *J. Braz. Chem. Soc.* **2011**, *22* (8), 1426–1438.
- (187) Case, F. H.; Catino, S.; Scholnick, F. *J. Org. Chem.* **1954**, *19* (1), 31–36.
- (188) Case, F. H.; Sasin, R. *J. Org. Chem.* **1955**, *20* (10), 1330–1336.
- (189) Case, F. H. *J. Org. Chem.* **1951**, *16* (6), 941–945.

- (190) Snyder, H. R.; Freier, H. E. *J. Am. Chem. Soc.* **1946**, 68 (7), 1320–1322.
- (191) Halcrow, B. E.; Kermack, W. O. *J. Chem. Soc.* **1946**, 155–157.
- (192) Antkowiak, R.; Antkowiak, Z. *Heterocycles* **1998**, 47 (2), 893–909.
- (193) Krishnan, S.; Kuhn, D. G.; Hamilton, G. A. *J. Am. Chem. Soc.* **1977**, 99 (24), 8121–8123.
- (194) Shen, Y.; Sullivan, B. P. *Inorg. Chem.* **1995**, 34 (25), 6235–6236.
- (195) Broomhead, J.; Dwyer, F. *Aust. J. Chem.* **1961**, 14 (2), 250–252.
- (196) Selvaganapathy, M.; Raman, N. *J Chem Biol Ther* **2016**, 1 (2), 406–423.
- (197) Villar-Garcia, I. J.; Abebe, A.; Chebude, Y. *Inorg. Chem. Comm.* **2012**, 19, 1–3.
- (198) Gomleksiz, M.; Alkan, C.; Erdem, B. *Bull. Chem. Soc. Ethiop.* **2013**, 27 (2), 212–220.
- (199) Hu, B.; Liu, Q.-Q.; Tao, T.; Zhang, K.; Geng, J.; Huang, W. *Inorg. Chim. Acta* **2013**, 394, 576–582.
- (200) Shaik, K. A.; Ahmed, A.; Reddy, B. S. *Int. J. Adv. Res. Chem. Sci.* **2014**, 1 (5), 2349–2403.
- (201) Amane, M. E.; Hamdani, H. E. *Int. J ChemTech Res.* **2014**, 6 (1), 465–473.
- (202) Bretonnière, Y.; Lebrun, C.; Mazzanti, M.; Pécaut, J. *Inorg. Chem.* **2000**, 39, 3499–3505.
- (203) Saitoh, Y.; Koizumi, T.-A.; Osakada, K.; Yamamoto, T. *Can. J. Chem.* **1997**, 75, 1336–1339.
- (204) Correa, A.; Martin, R. In *Encyclopedia of Reagents for Organic Synthesis*; John Wiley & Sons, Ltd: Chichester, UK, 2012.
- (205) Sauvage, J. P.; Dietrich-Buchecker, C. *Molecular Catenanes, Rotaxanes and Knots: A Journey Through the World of Molecular Topology*; Wiley-VCH: Weinheim, 1999.
- (206) Megiatto, J.; Schuster, D. *Org. Lett.* **2011**, 13 (7), 1808–1811.
- (207) Alder, J. F.; Das, B. C. *Analyst* **1977**, 102, 564–568.
- (208) Schoffers, E. *Eur. J. Org. Chem.* **2003**, No. 1145–1152.
- (209) Toshima, N.; Shiraishi, Y.; Teranishi, T.; Miyake, M.; Tominaga, T.; Watanabe, H.; Brijoux, W.; Bönnemann, H.; Schmid, G. *Appl. Organomet. Chem.* **2001**, 15 (3), 178–196.
- (210) Ahmed, Z.; Iftikhar, K. *Inorg. Chim. Acta* **2012**, 392, 165–176.
- (211) Yang, C.; Luo, J.; Ma, J.; Zhu, D.; Miao, L.; Zhang, Y.; Liang, L.; Lu, M. *Synth. Met.* **2012**, 162, 1097–1106.
- (212) Yan, B.; Gu, Y.-J. *Inorg. Chem. Comm.* **2013**, 34, 75–78.
- (213) Starosta, R.; Komarnicka, U. K.; Sobczyk, M.; Barys, M. *J. Lum.* **2012**, 132, 1842–1847.

- (214) Zhang, H.-G.; Tao, X.-T.; Chen, K.-S.; Yuan, C.-X.; Jiang, M.-H. *Synth. Met.* **2010**, *161*, 354–359.
- (215) Erkkila, K. E.; Odom, D. T.; Barton, J. K. *Chem. Rev.* **1999**, *99* (9), 2777–2796.
- (216) Tabassum, S.; Amir, S.; Arjmand, F.; Pettinari, C.; Marchetti, F.; Masciocchi, N.; Lupidi, G.; Pettinari, R. *Eur. J. Med. Chem.* **2013**, *60*, 216–232.
- (217) Yu, X.; Jin, X.; Tang, G.; Zhou, J.; Zhang, W.; Peng, D.; Hu, J.; Zhong, C. *European J. Org. Chem.* **2013**, *2013* (26), 5893–5901.
- (218) Armaroli, N.; De Cola, L.; Balzani, V.; Sauvage, J.-P.; Dietrich-Buchecker, C. O.; Kern, J.-M. *J. Chem. Soc. Faraday Trans.* **1992**, *88* (4), 553–556.
- (219) Lee, H. C.; Byeon, S. U.; Lukashev, A. *Opt. Lett.* **2012**, *37* (7), 1160–1162.
- (220) Parker, D.; Williams, J. A. G. *J. Chem. Soc. Dalt. Trans.* **1996**, No. 18, 3613–3628.
- (221) Leonard, J. P. In *Photochemistry and Photophysics of Coordination Compounds II*; 2007; pp 1–44.
- (222) Quici, S.; Cavazzini, M.; Marzanni, G.; Accorsi, G.; Armaroli, N.; Ventura, B.; Barigelletti, F. *Inorg. Chem.* **2005**, *44*, 529–537.
- (223) Xu, C. *Monatshefte für Chemie - Chem. Mon.* **2010**, *141* (6), 631–635.
- (224) Armelao, L.; Bottaro, G.; Quici, S.; Cavazzini, M.; Raffo, M. C.; Barigelletti, F.; Accorsi, G. *Chem. Comm.* **2007**, No. 28, 2911–2913.
- (225) Accorsi, G.; Armaroli, N.; Parisini, A.; Meneghetti, M.; Marega, R.; Prato, M.; Bonifazi, D. *Adv. Funct. Mater.* **2007**, *17* (15), 2975–2982.
- (226) Krennrich, D.; Knappe, R.; Henrich, B.; Wallenstein, R.; L’huillier, J. A. *Appl. Phys. B* **2008**, *92* (2), 165–174.
- (227) Zhao, Y.; Schwab, M. G.; Kiersnowski, A.; Pisula, W.; Baumgarten, M.; Chen, L.; Müllen, K.; Li, C. *J. Mater. Chem. C* **2016**, *4*, 4640–4646.
- (228) Zhang, H. .; Fu, L. .; Wang, S. .; Meng, Q. .; Yang, K. .; Ni, J. . *Mater. Lett.* **1999**, *38* (4), 260–264.
- (229) Liu, S.-W.; Lee, C.-C.; Su, W.-C.; Yuan, C.-H.; Shu, Y.-S.; Chang, W.-C.; Guo, J.-Y.; Chiu, C.-F.; Li, Y.-Z.; Su, T.-H.; Chen, K.-T.; Chang, P.-C.; Yeh, T.-H.; Liu, Y.-H. *ACS Appl. Mater. Interfaces* **2015**, *7* (17), 9262–9273.
- (230) Wong, H.-Y.; Lo, W.-S.; Chan, W. T. K.; Law, G.-L. *Inorg. Chem.* **2017**, *56* (9), 5135–5140.
- (231) Larionov, S. V; Bryleva, Y. A.; Glinskaya, L. A.; Plyusnin, V. F.; Kupryakov, A. S.; Agafontsev, A. M.; Tkachev, A. V; Bogomyakov, A. S.; Piryazev, D. A.; Korolkov, I. V. *Dalt. Trans.* **2017**, *46*, 11440–11450.

- (232) Oude Wolbers, M.; van Veggel, F.; Snellink-Ruël, B.; Hofstraat, J.; Geurts, F.; Reinhoudt, D. *J. Chem. Soc., Perkin Trans* **1998**, 2, 2141–2150.
- (233) Bellusci, A.; Barberio, G.; Crispini, A.; Ghedini, M.; Deda, L.; Pucci, D. *Inorg. Chem.* **2005**, 44, 1818–1825.
- (234) Khorasani-Motlagh, M.; Noroozifar, M.; Mirkazehi-Rigi, S. *Spectrochim. Acta Part A* **2011**, 79, 978–984.
- (235) Devi, R.; Priyanka; Chahar, S.; Khatkar, S. P.; Taxak, V. B.; Boora, P. *Inorg. Chim. Acta* **2018**, 471, 364–371.
- (236) Freund, C.; Porzio, W.; Giovanella, U.; Vignali, F.; Pasini, M.; Destri, S.; Mech, A.; Di Pietro, S.; Di Bari, L.; Mineo, P. *Inorg. Chem.* **2011**, 50 (12), 5417–5429.
- (237) Zucchi, G.; Murugesan, V.; Tondelier, D.; Aldakov, D.; Jeon, T.; Yang, F.; Thuéry, P.; Ephritikhine, M.; Geffroy, B. *Inorg. Chem.* **2011**, 50 (11), 4851–4856.
- (238) Romano, J. A.; Lukey, B. J.; Salem, H. *Chemical warfare agents: chemistry, pharmacology, toxicology, and therapeutics*; CRC Press, 2008.

Appendices

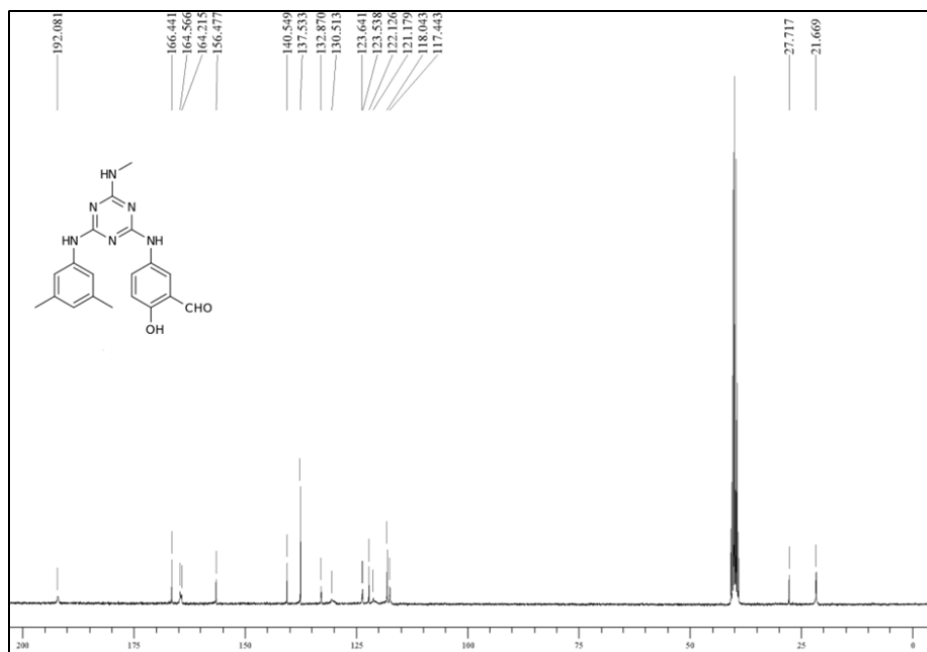
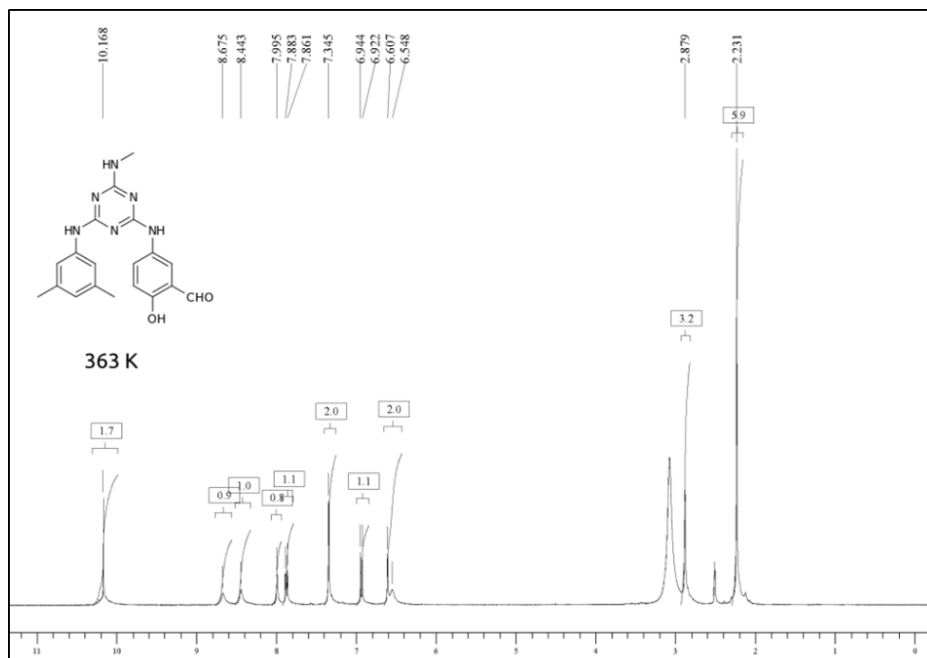
Appendix A: NMR Spectra

Appendix B: TGA Thermograms

Appendix C: DSC Thermograms

A. NMR Spectra

A.1 NMR Spectra for Salen Complexes Functionalized with Mexylaminotriazines



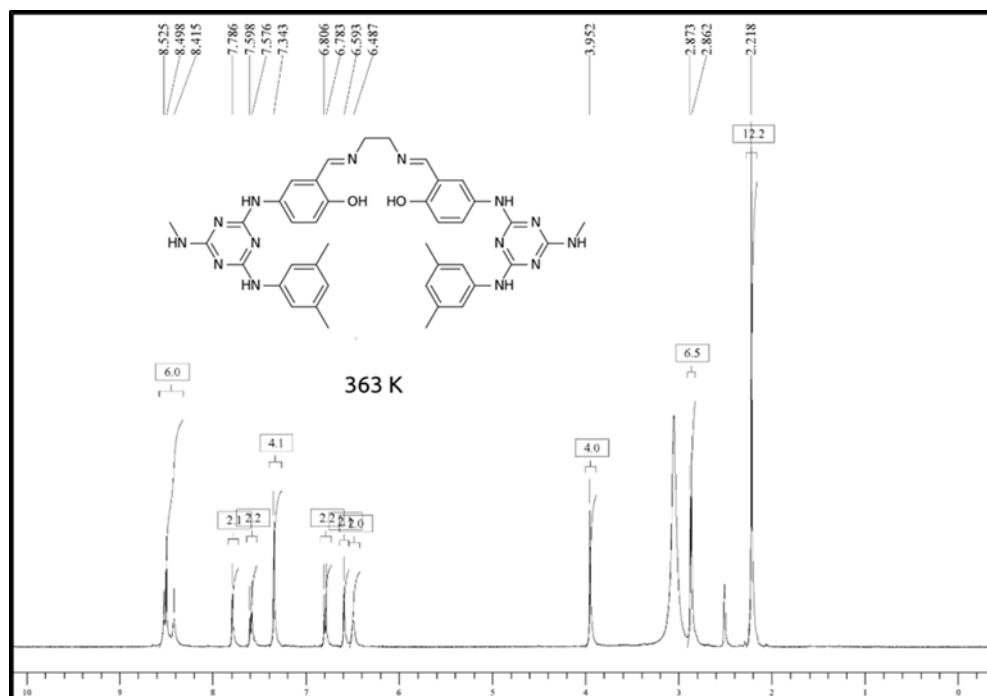


Figure 13: ^1H NMR of ligand **46a** in $\text{DMSO-}d_6$, 300 MHz at 363K.

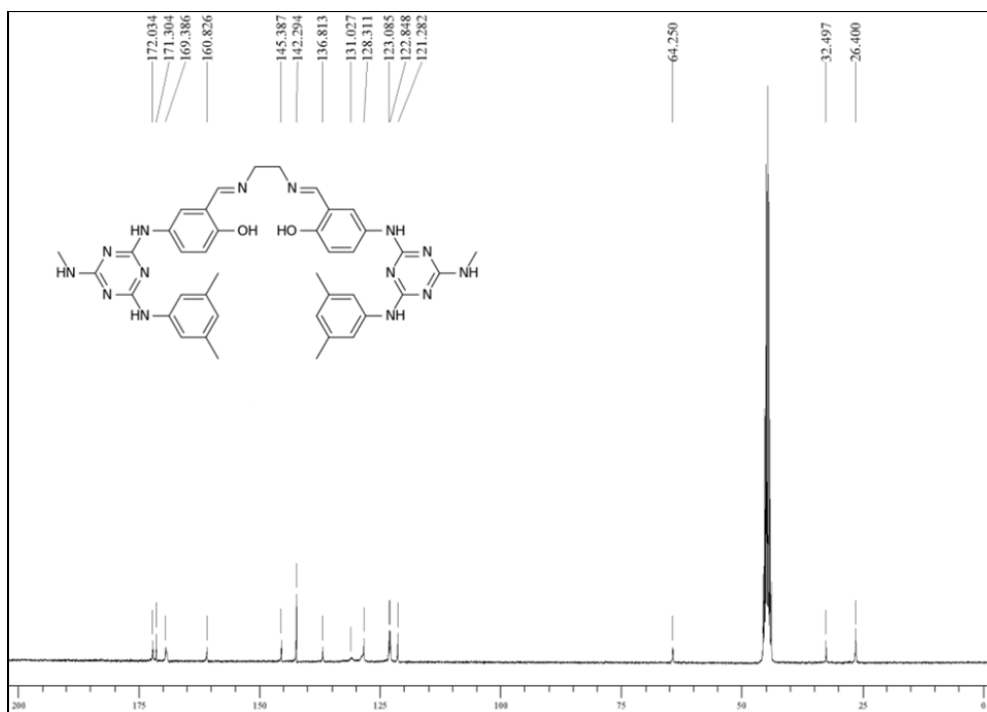


Figure 14: ^{13}C NMR of ligand **46a** in $\text{DMSO-}d_6$, 75 MHz.

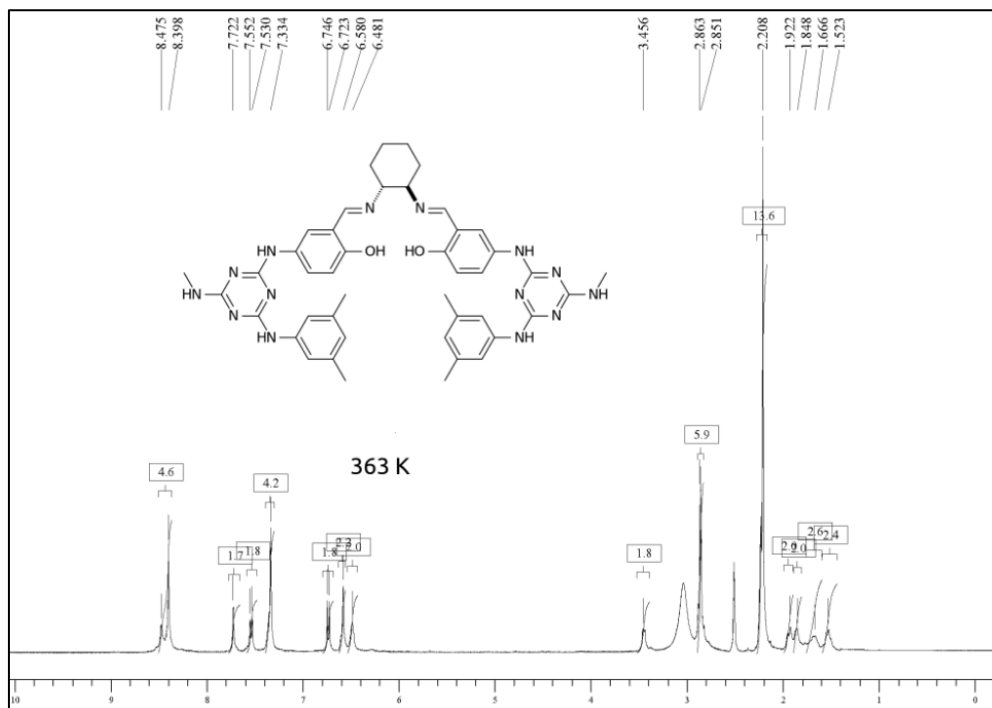


Figure 15: ^1H NMR of ligand **46b** in $\text{DMSO-}d_6$, 300 MHz at 363 K.

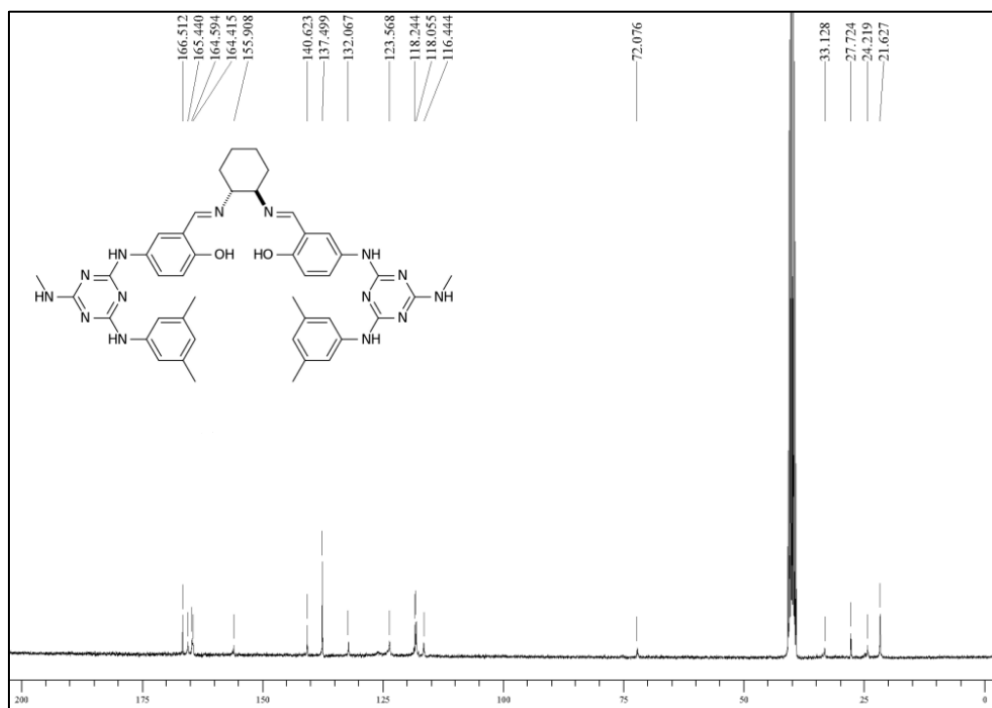


Figure 16: ^{13}C NMR of ligand **46b** in $\text{DMSO-}d_6$, 75 MHz.

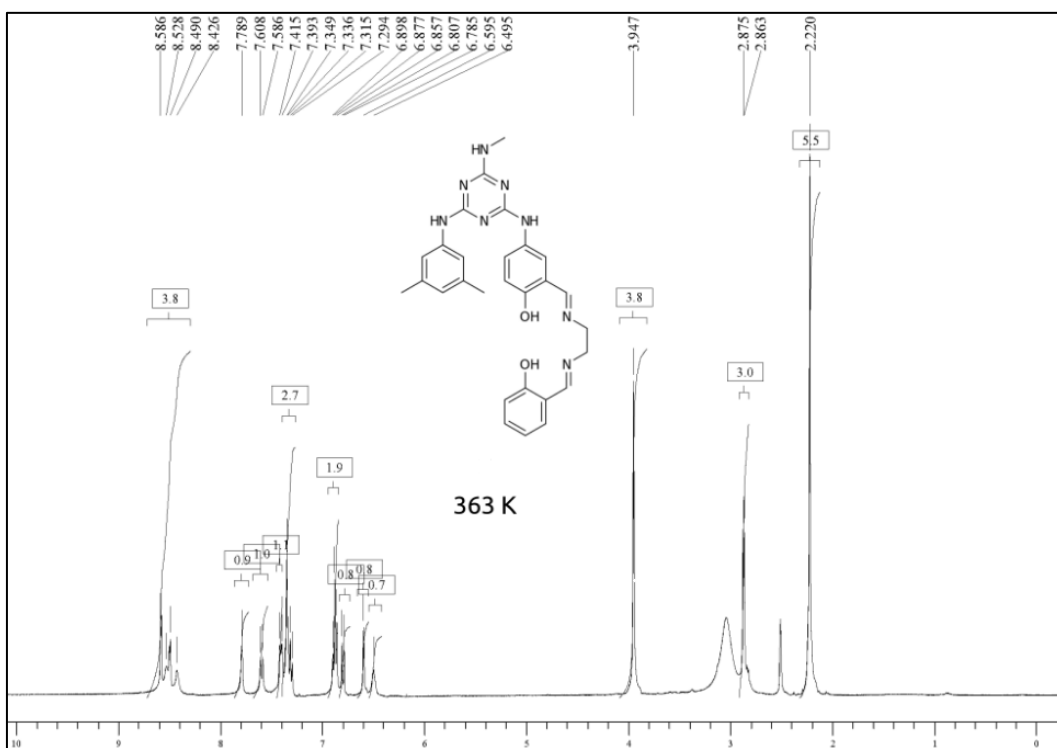


Figure 17: ¹H NMR of ligand **48a** in DMSO-*d*₆, 300 MHz at 363K.

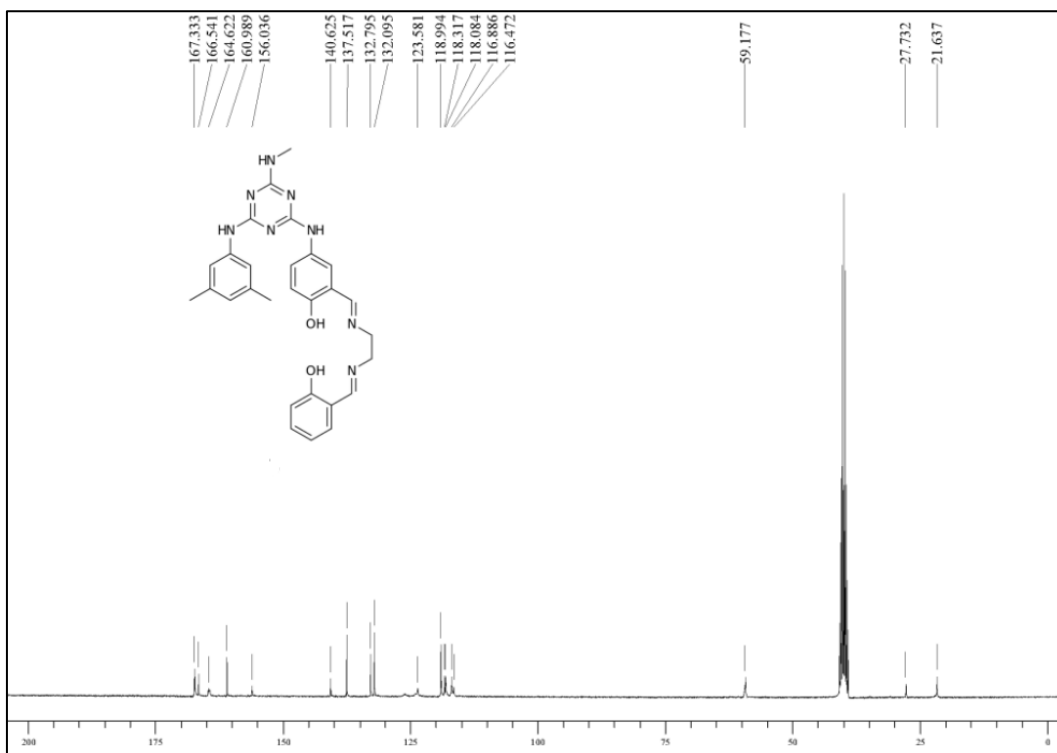


Figure 18: ¹³C NMR of ligand **48a** in DMSO-*d*₆, 75 MHz.

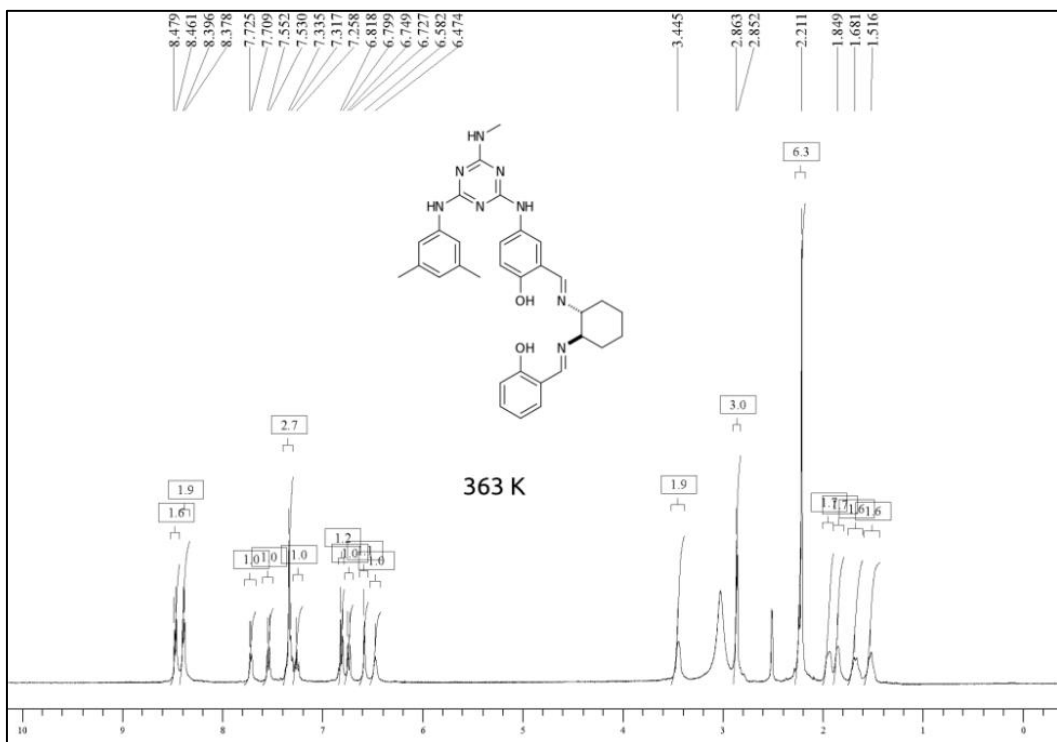


Figure 19: ¹H NMR of ligand **48b** in DMSO-*d*₆, 300 MHz at 363K.

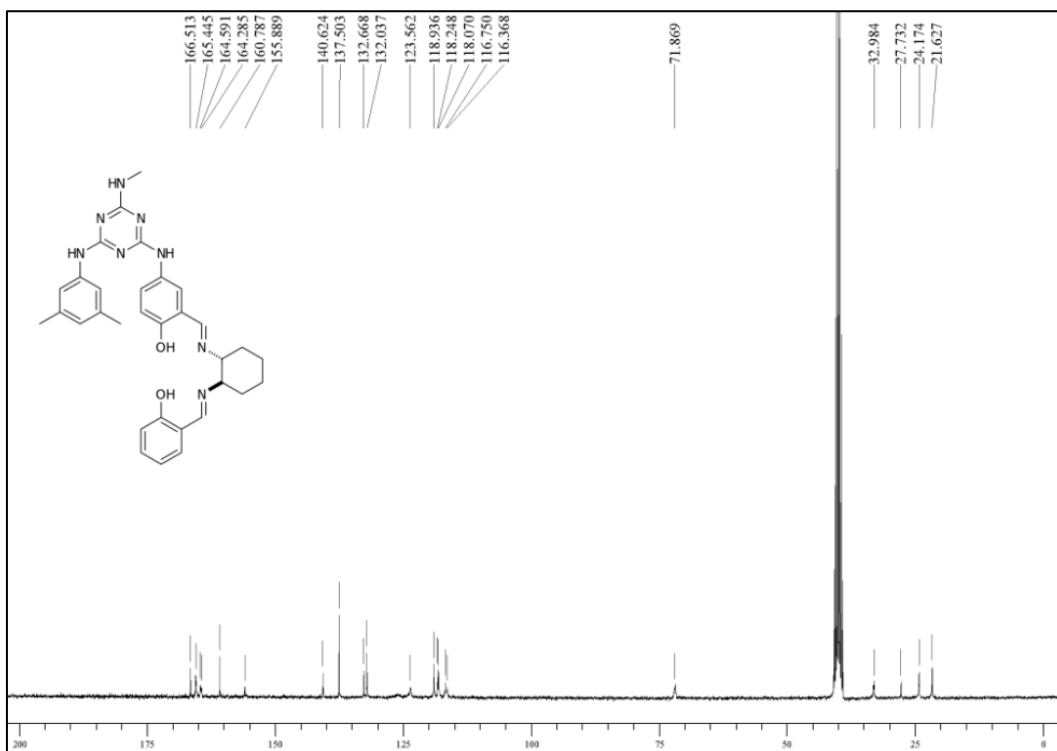


Figure 20: ¹³C NMR of ligand **48b** in DMSO-*d*₆, 75 MHz.

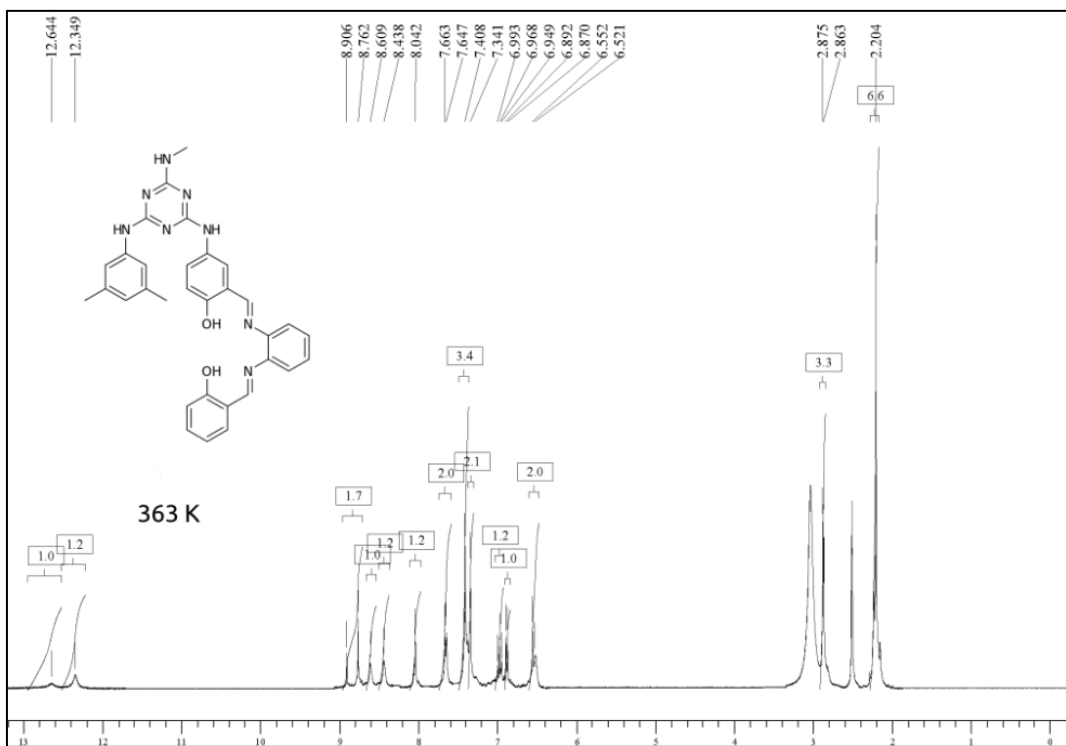


Figure 21: ^1H NMR of ligand **48c** in $\text{DMSO-}d_6$, 300 MHz at 363K.

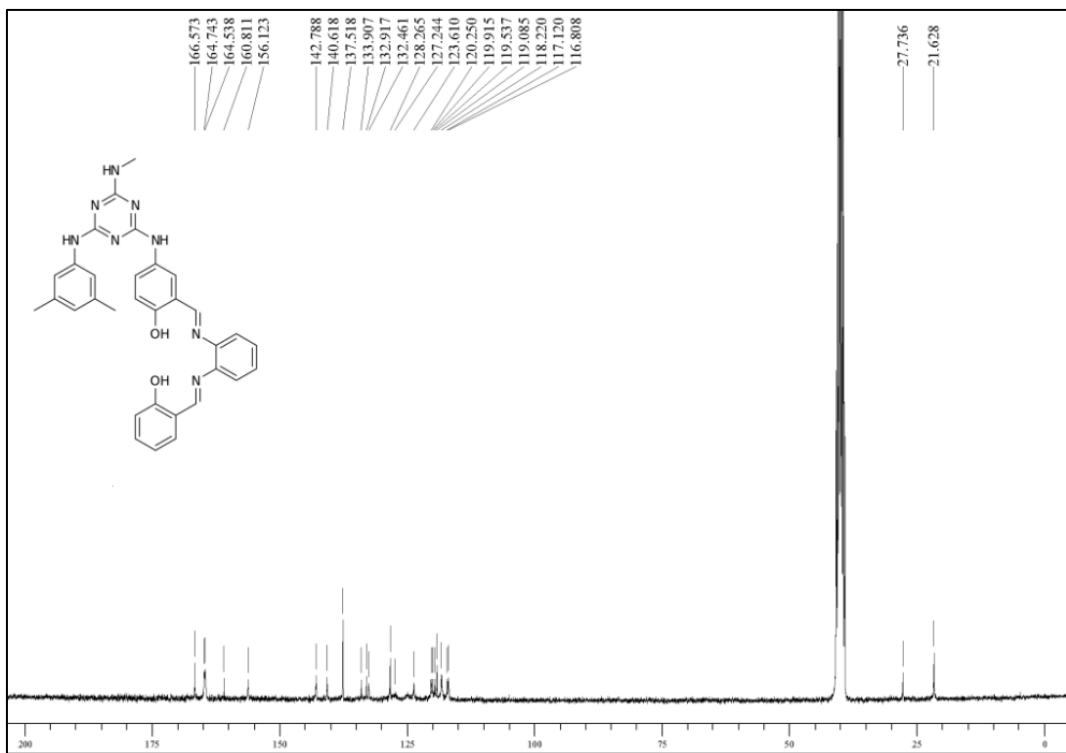


Figure 22: ^{13}C NMR of ligand **48c** in $\text{DMSO-}d_6$, 75 MHz.

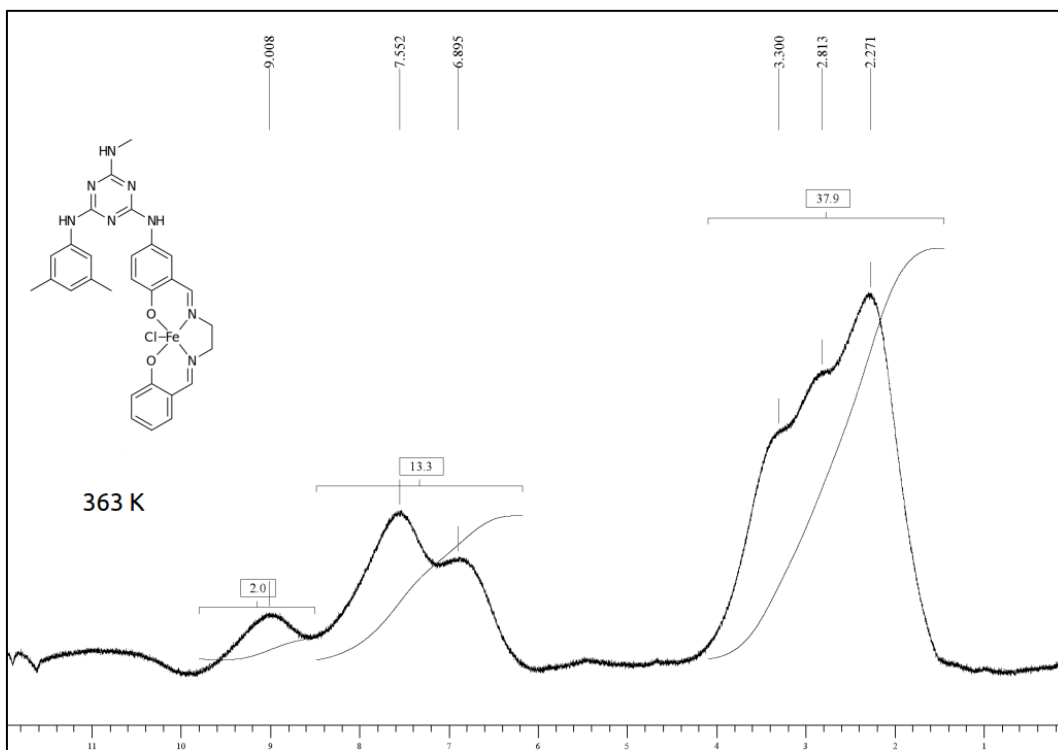


Figure 23: ^1H NMR of complex **48a•Fe(III)** in $\text{DMSO-}d_6$, 300 MHz at 363K.

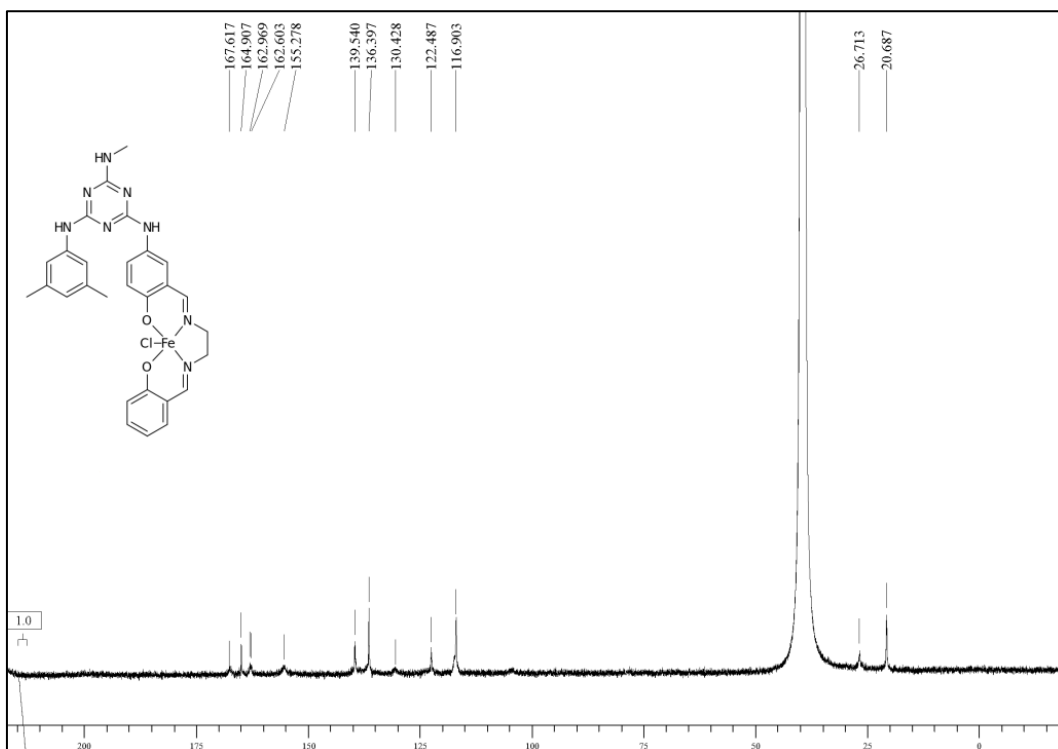


Figure 24: ^{13}C NMR of complex **48a•Fe(III)** in $\text{DMSO-}d_6$, 75 MHz.

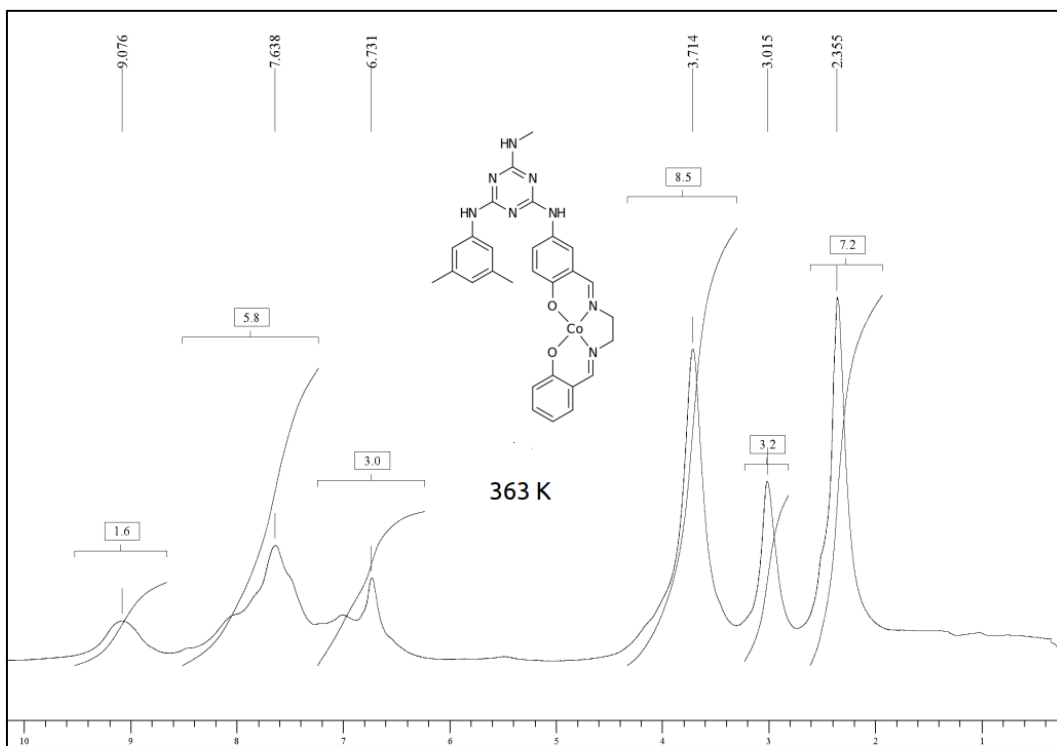


Figure 25: ^1H NMR of complex **48a•Co(II)** in $\text{DMSO-}d_6$, 300 MHz at 363K.

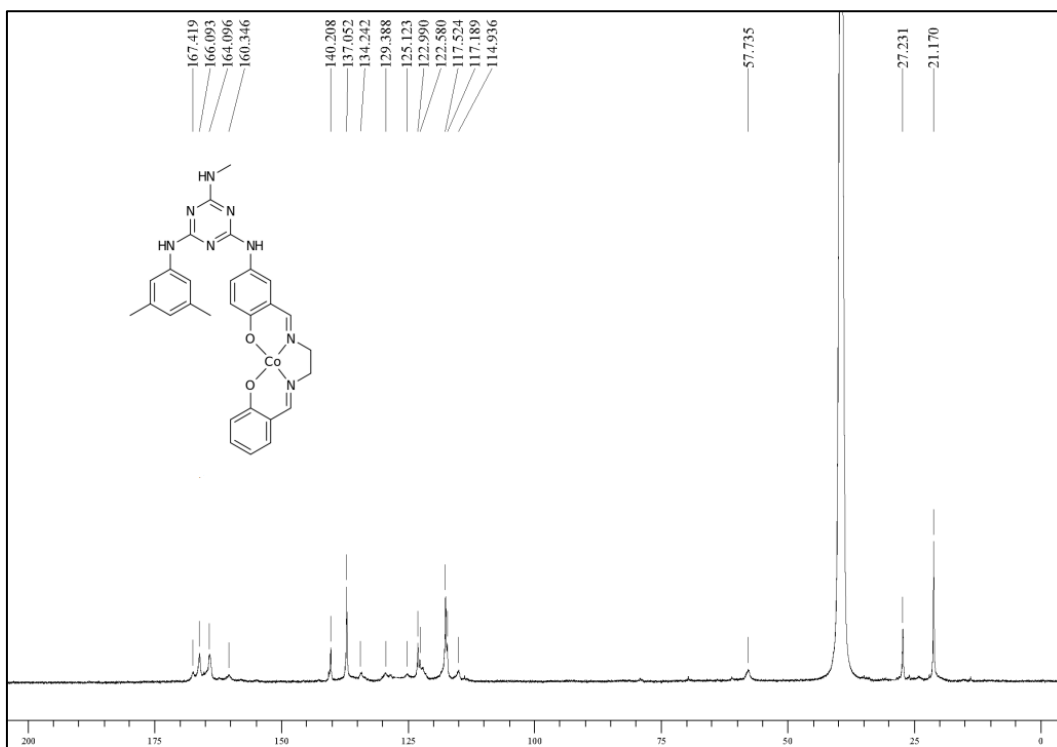


Figure 26: ^{13}C NMR of complex **48a•Co(II)** in $\text{DMSO-}d_6$, 75 MHz.

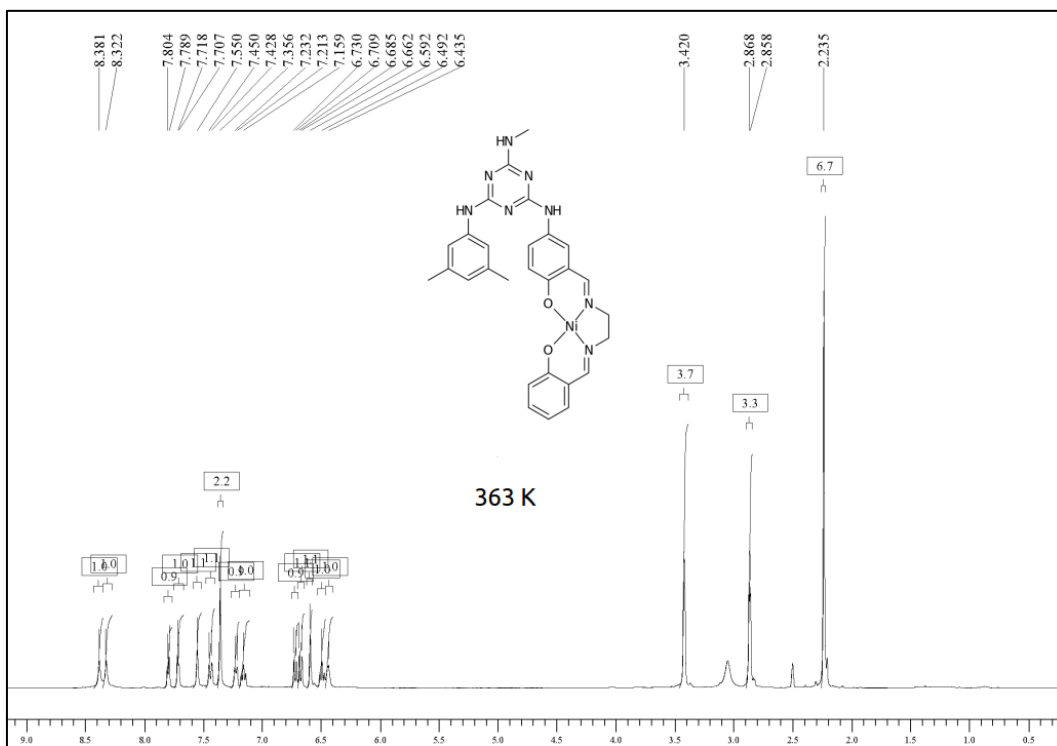


Figure 27: ^1H NMR of complex **48a•Ni(II)** in $\text{DMSO-}d_6$, 300 MHz at 363K.

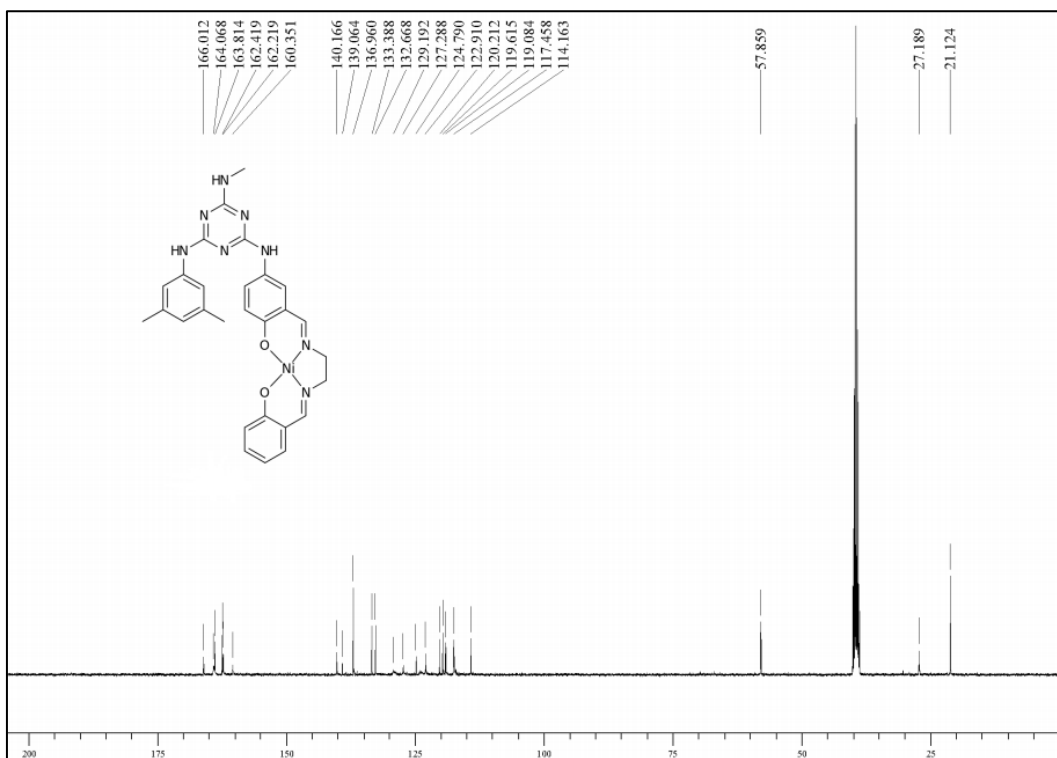


Figure 28: ^{13}C NMR of complex **48a•Ni(II)** in $\text{DMSO-}d_6$, 75 MHz.

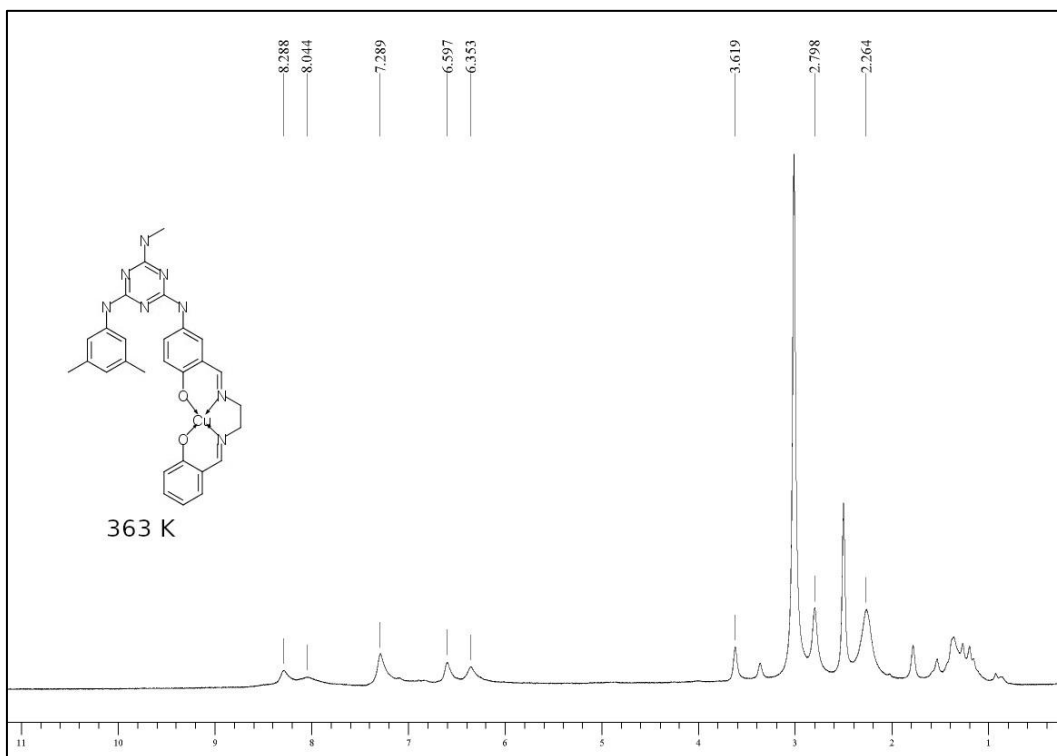


Figure 29: ¹H NMR of complex **48a**•Cu(II) in DMSO-*d*₆, 300 MHz at 363K.

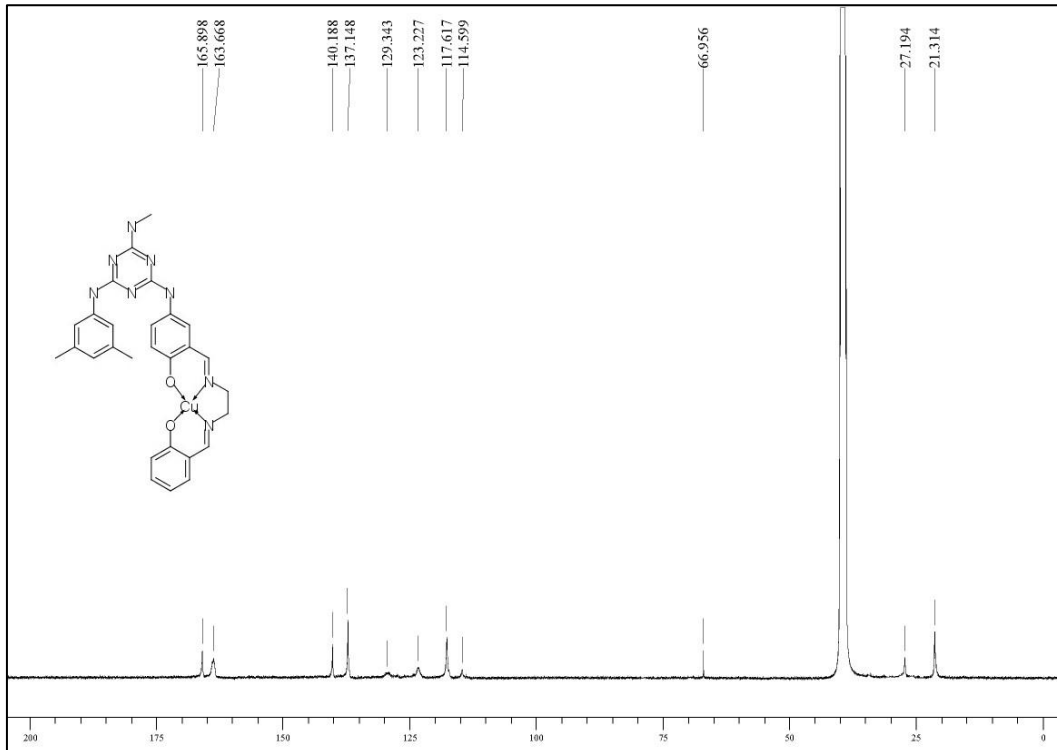


Figure 30: ¹³C NMR of complex **48a**•Cu(II) in DMSO-*d*₆, 75 MHz.

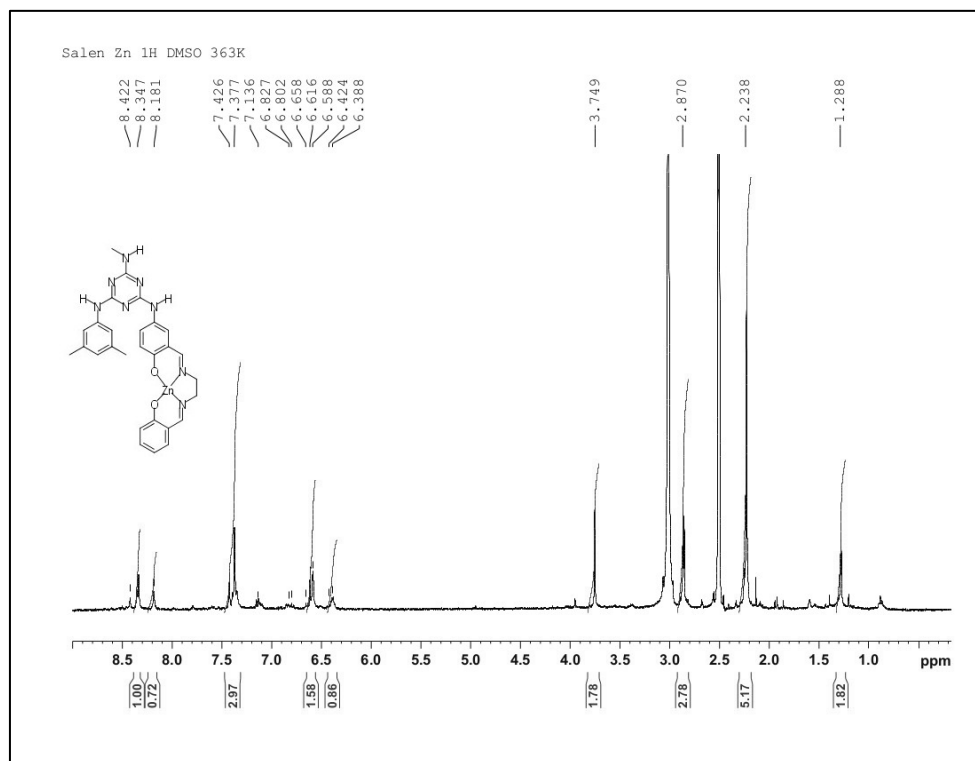


Figure 31: ^1H NMR of complex **48a**•Zn(II) in DMSO- d_6 , 300 MHz at 363K.

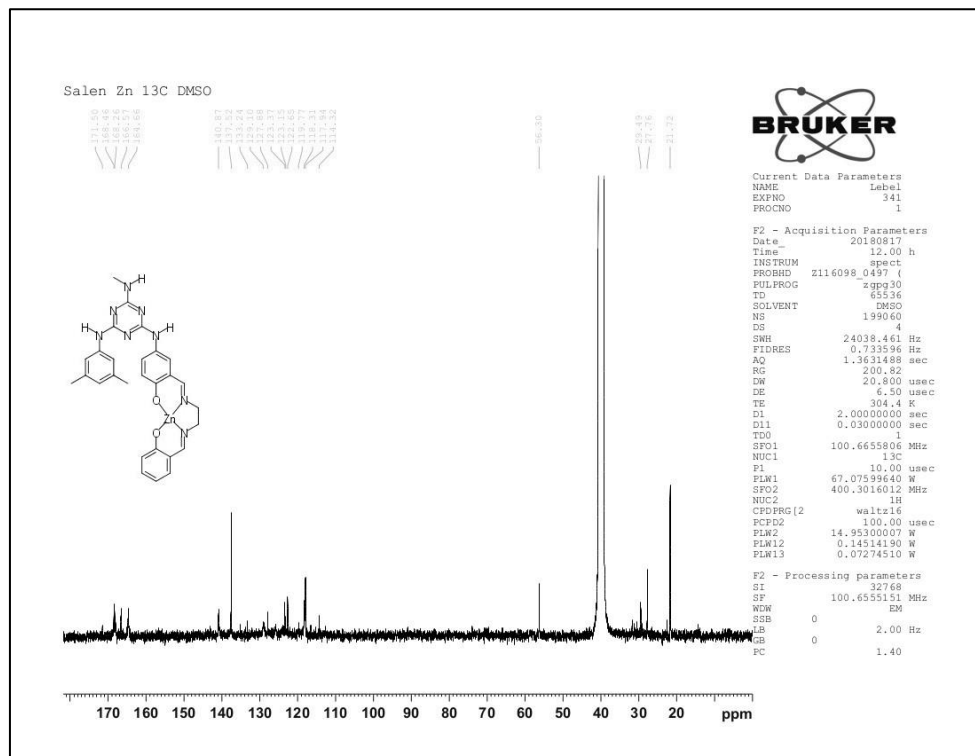


Figure 32: ^{13}C NMR of complex **48a**•Zn(II) in DMSO- d_6 , 75 MHz.

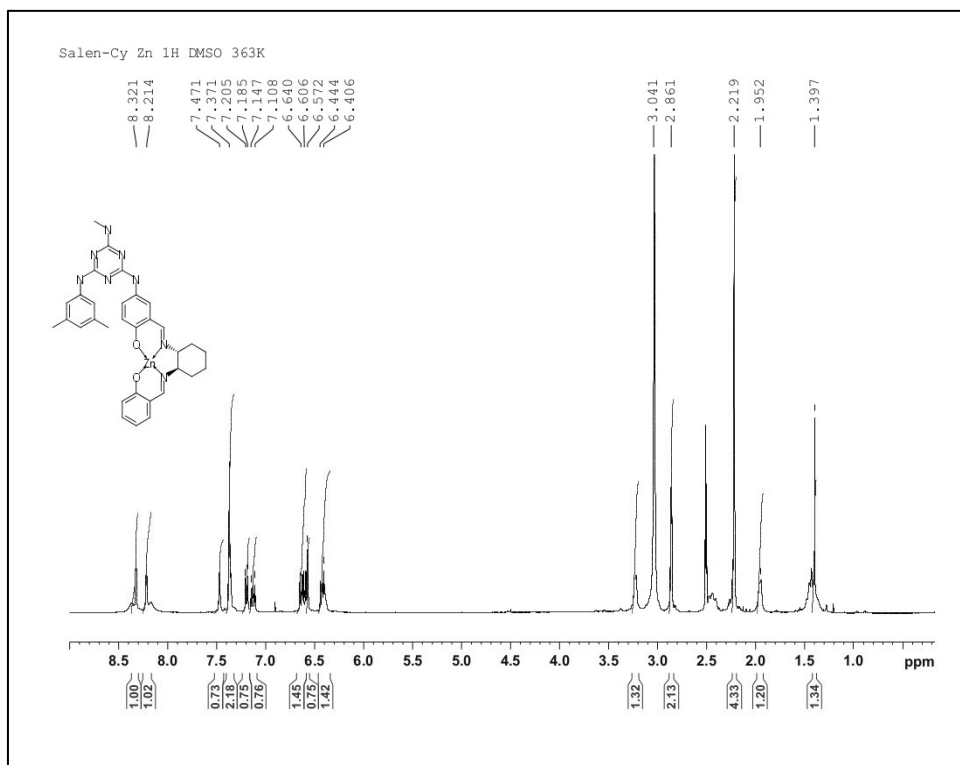


Figure 33: ^1H NMR of complex **48b•Zn(II)** in $\text{DMSO-}d_6$, 300 MHz at 363K.

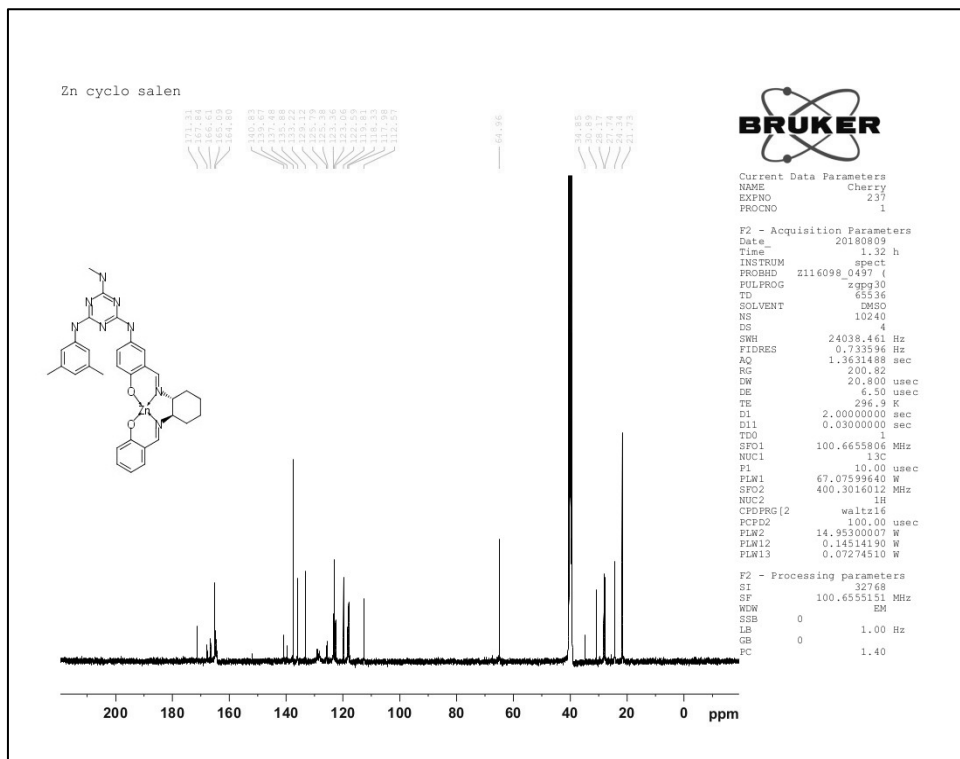


Figure 34: ^{13}C NMR of complex **48b•Zn(II)** in $\text{DMSO-}d_6$, 75 MHz.

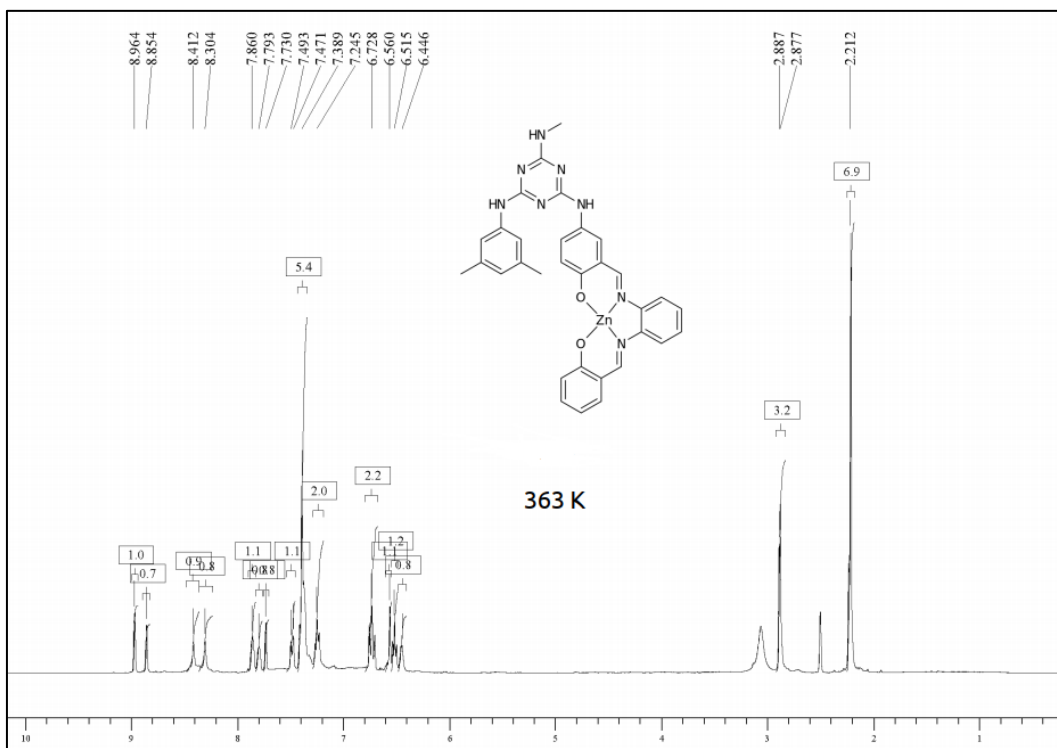


Figure 35: ^1H NMR of complex **48c•Zn(II)** in $\text{DMSO-}d_6$, 300 MHz at 363K.

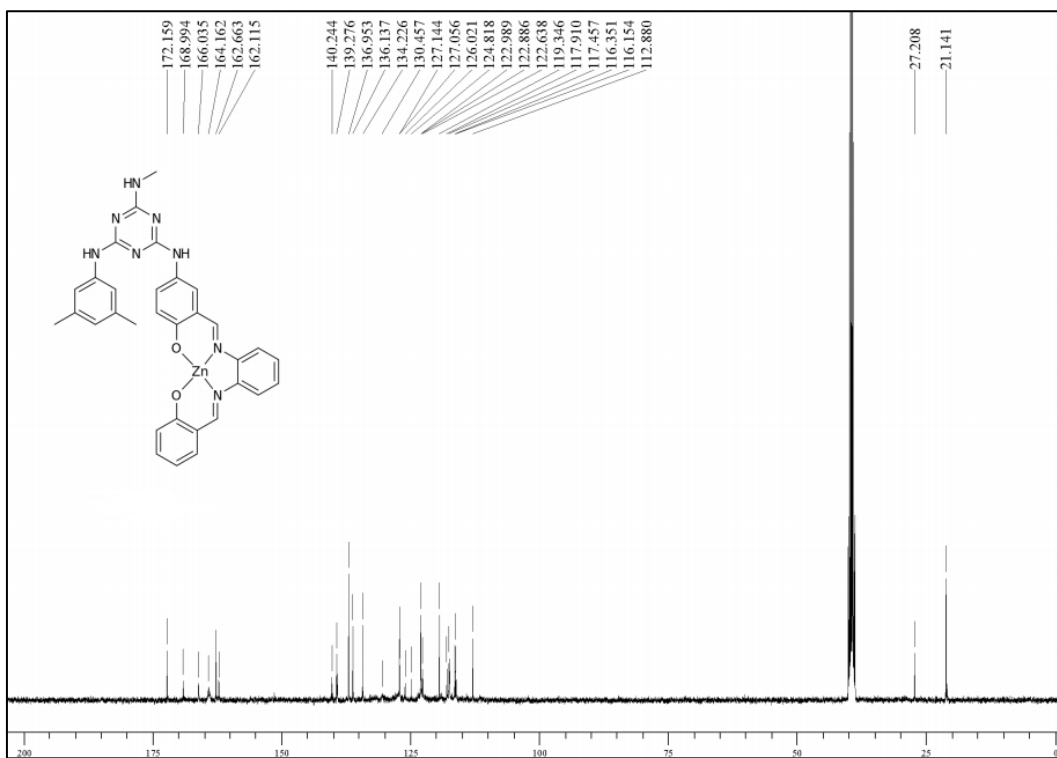


Figure 36: ^{13}C NMR of complex **48c•Zn(II)** in $\text{DMSO-}d_6$, 75 MHz.

A.2 NMR Spectra for Acetylacetonate Complexes Functionalized with Mexylaminotriazines

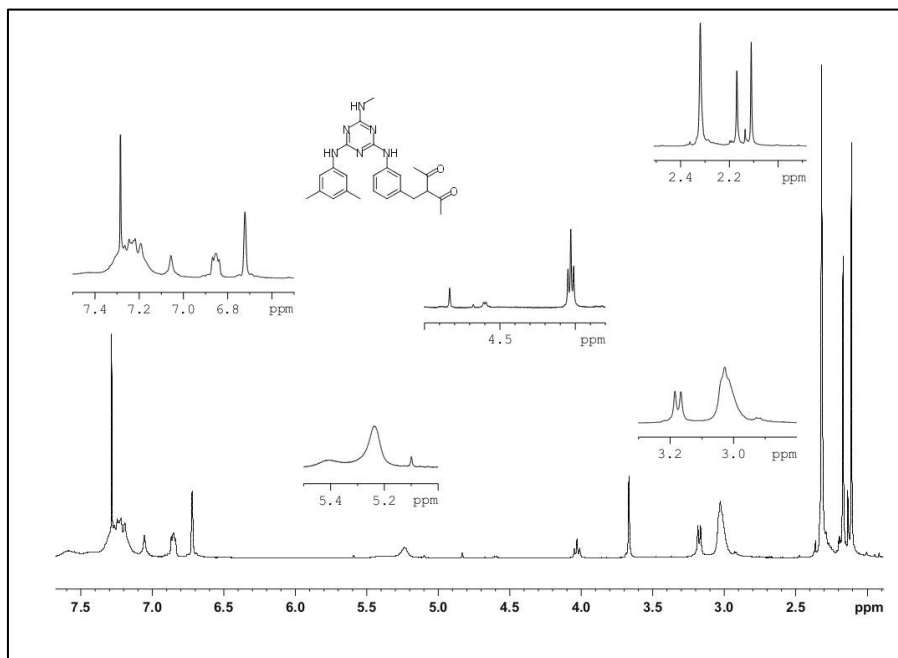


Figure 37: ^1H NMR of ligand **59** in $\text{DMSO-}d_6$, 300 MHz.

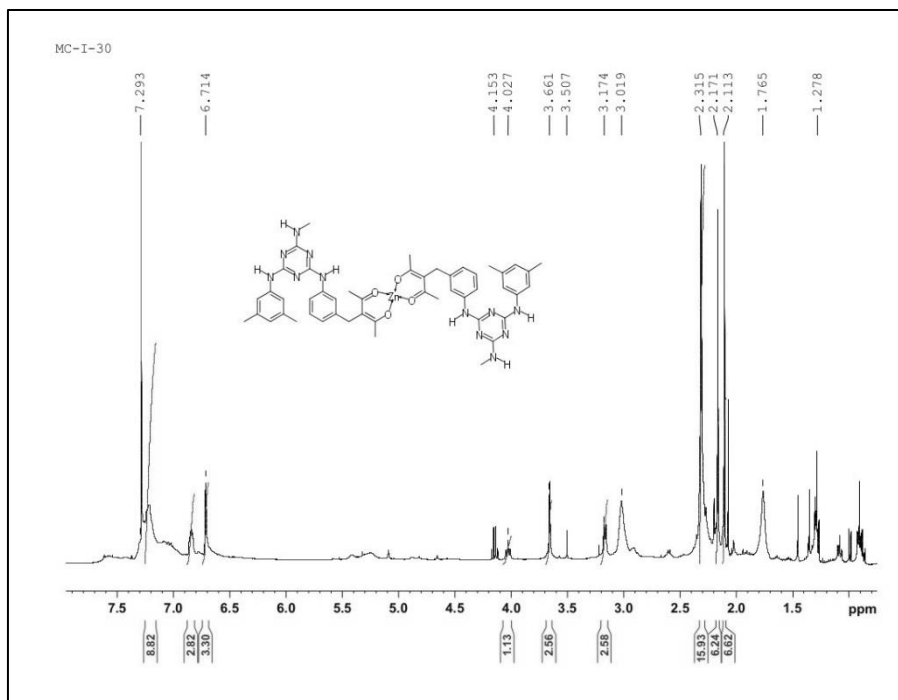


Figure 38: ^1H NMR of complex **59a·Zn(II)** in $\text{DMSO-}d_6$, 300 MHz.

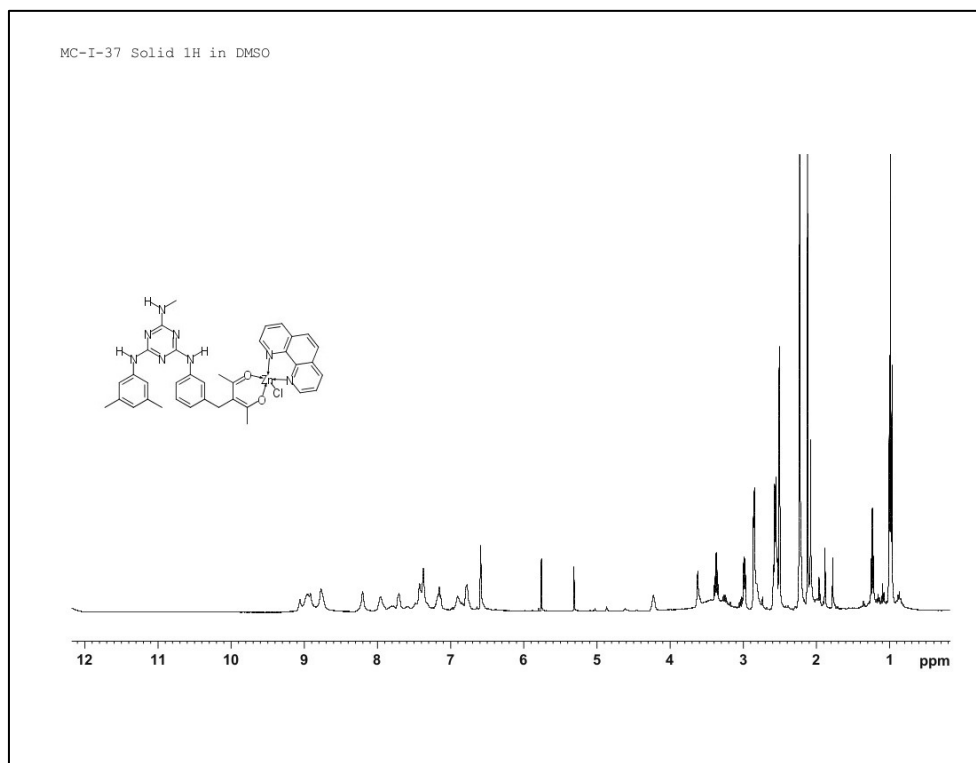


Figure 39: ¹H NMR of complex **59b**•Zn(II) in DMSO-*d*₆, 300 MHz.

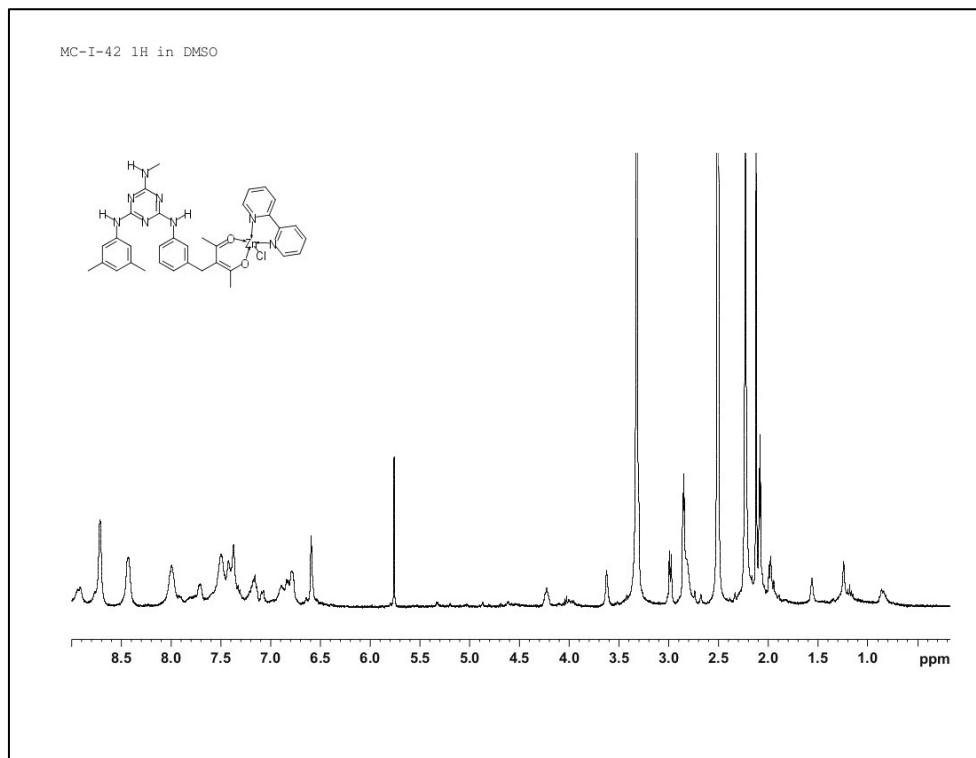


Figure 40: ¹H NMR of complex **59b**•Zn(II) in DMSO-*d*₆, 300 MHz.

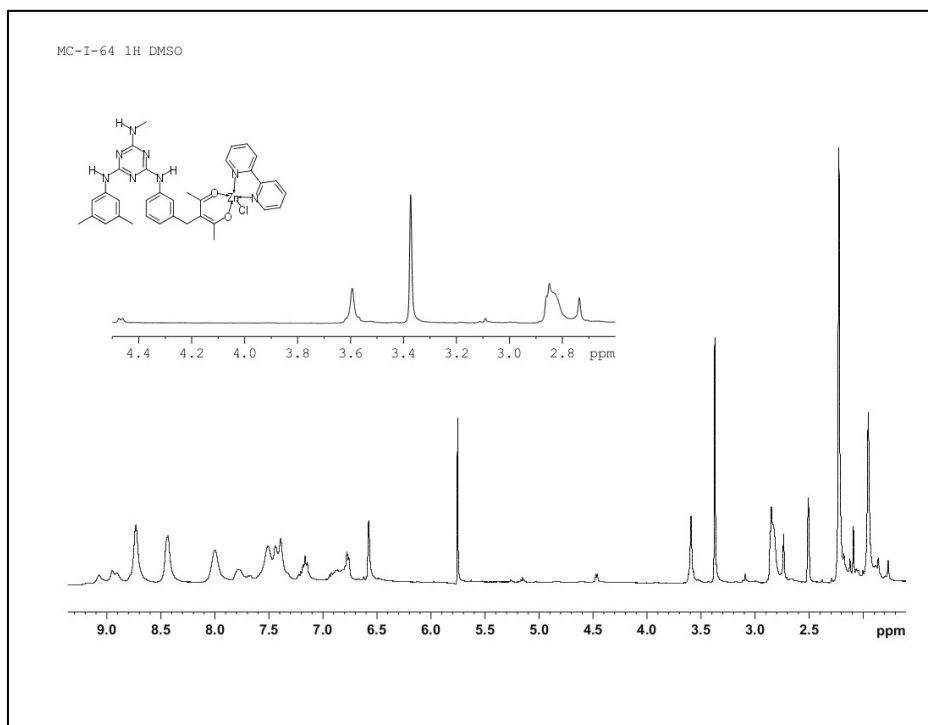


Figure 41: ¹H NMR spectrum of complex **56c•Zn(II)** in DMSO-*d*₆, 300 MHz, before purification by precipitation from water.

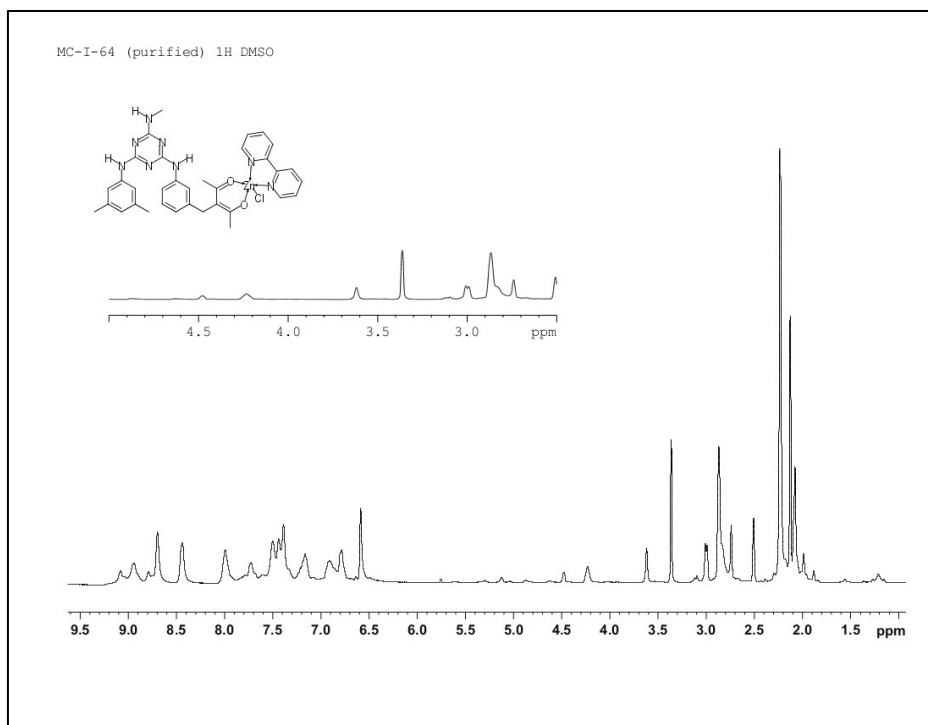


Figure 42: ¹H NMR of complex **59c•Zn(II)** in DMSO-*d*₆, 300 MHz, after purification by precipitating from water.

A.3 NMR Spectra for Phenanthroline Complexes Functionalized with Mexylaminotriazines

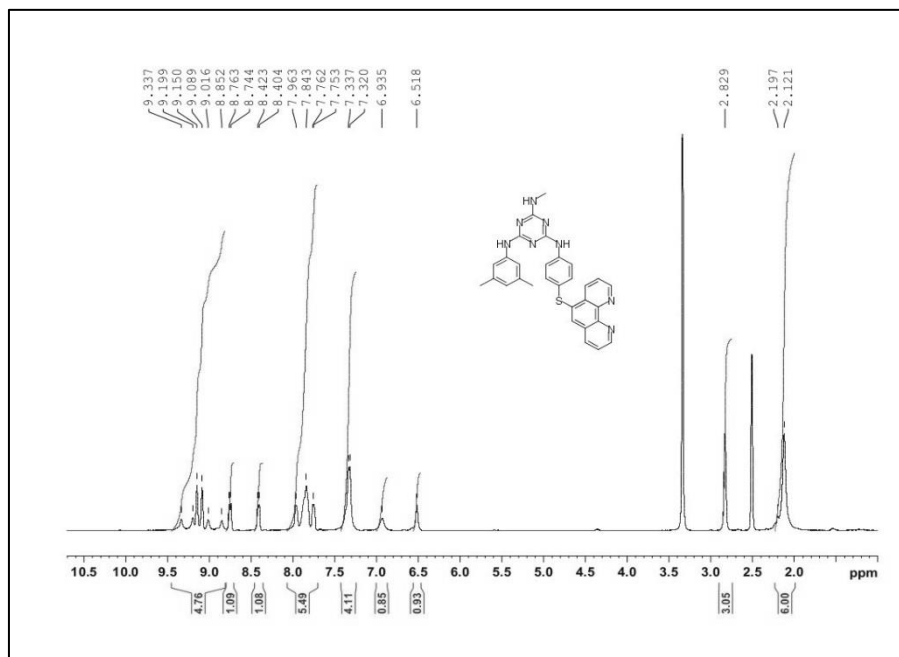
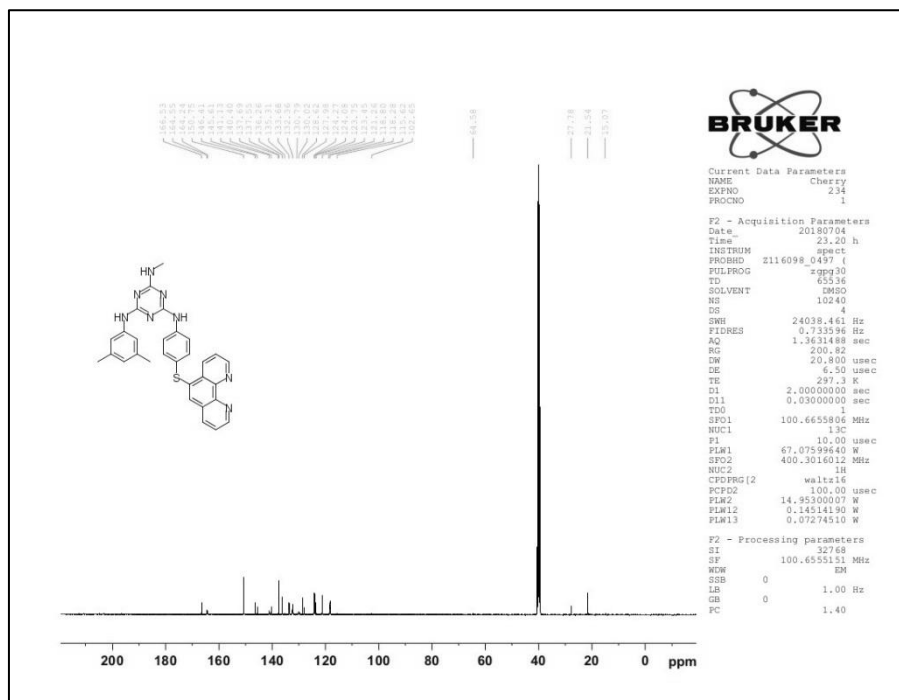


Figure 43: ¹H NMR of ligand **68** in DMSO-*d*₆, 300 MHz.



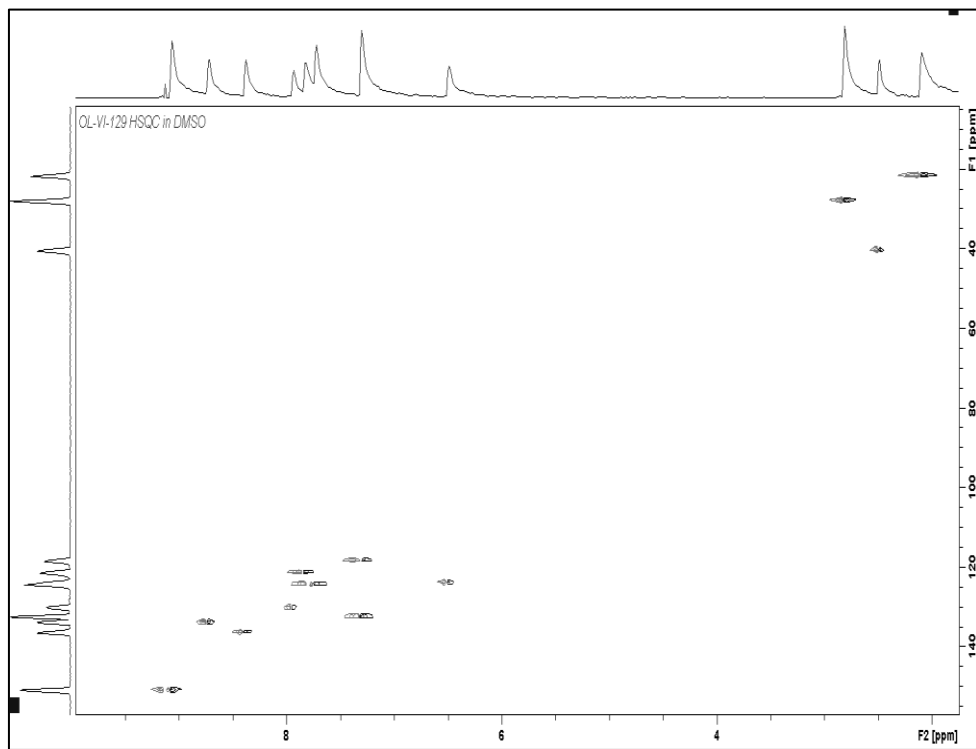


Figure 45: HSQC NMR of ligand **68** in DMSO-*d*₆.

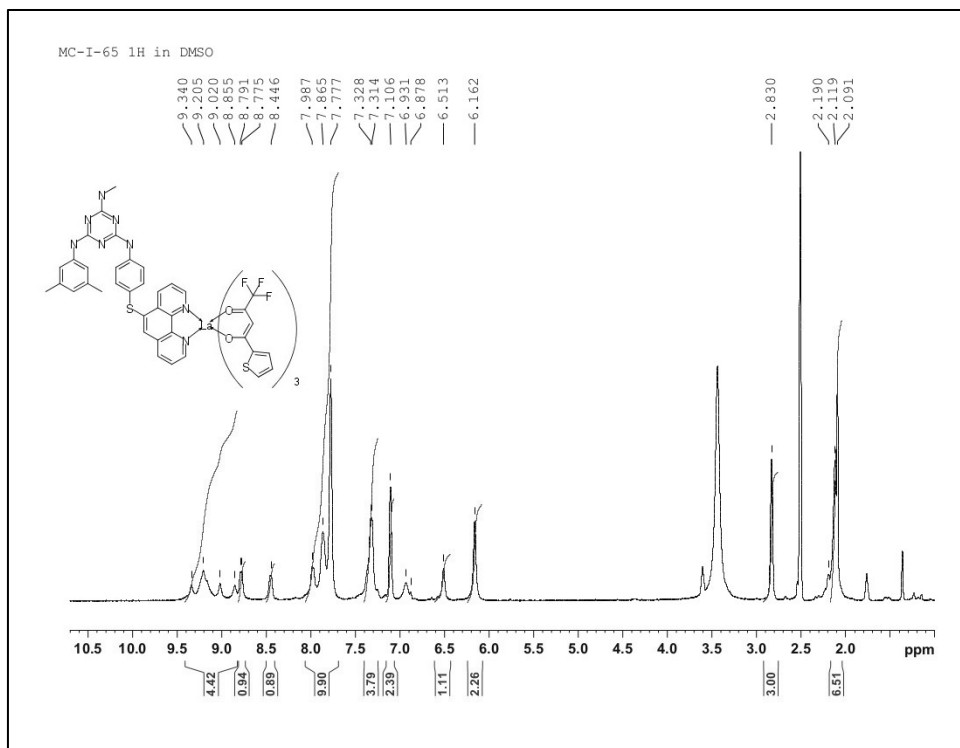


Figure 46: ¹H NMR of complex **68a•La(III)** in DMSO-*d*₆, 300 MHz.

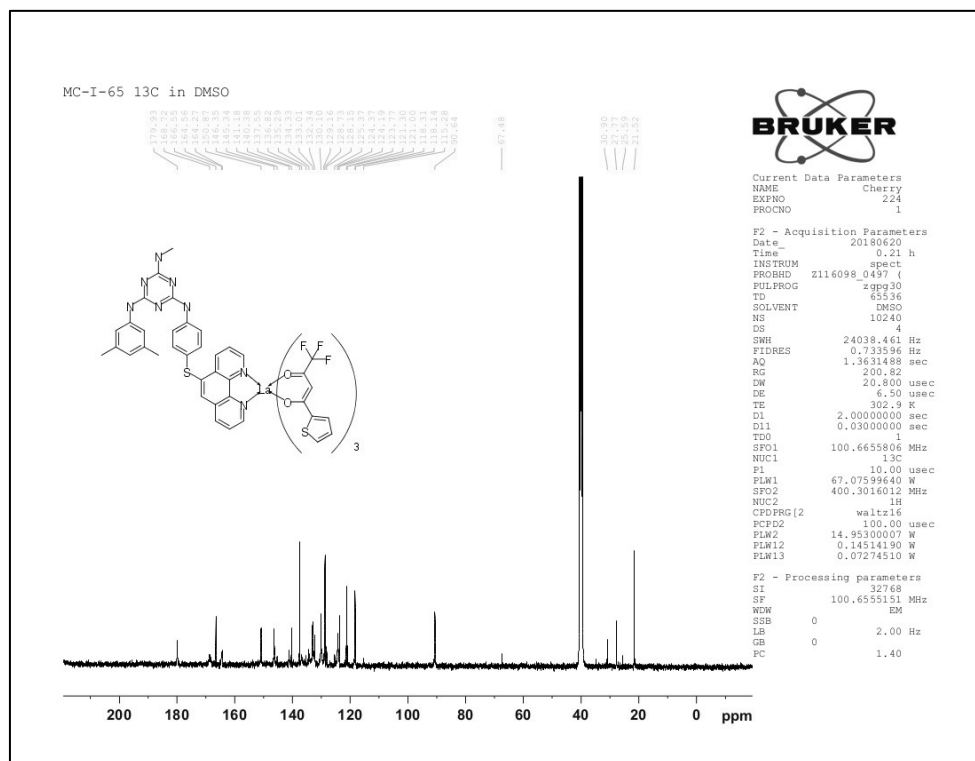


Figure 47: ^{13}C NMR of complex **68a**•La(III) in DMSO- d_6 , 75 MHz.

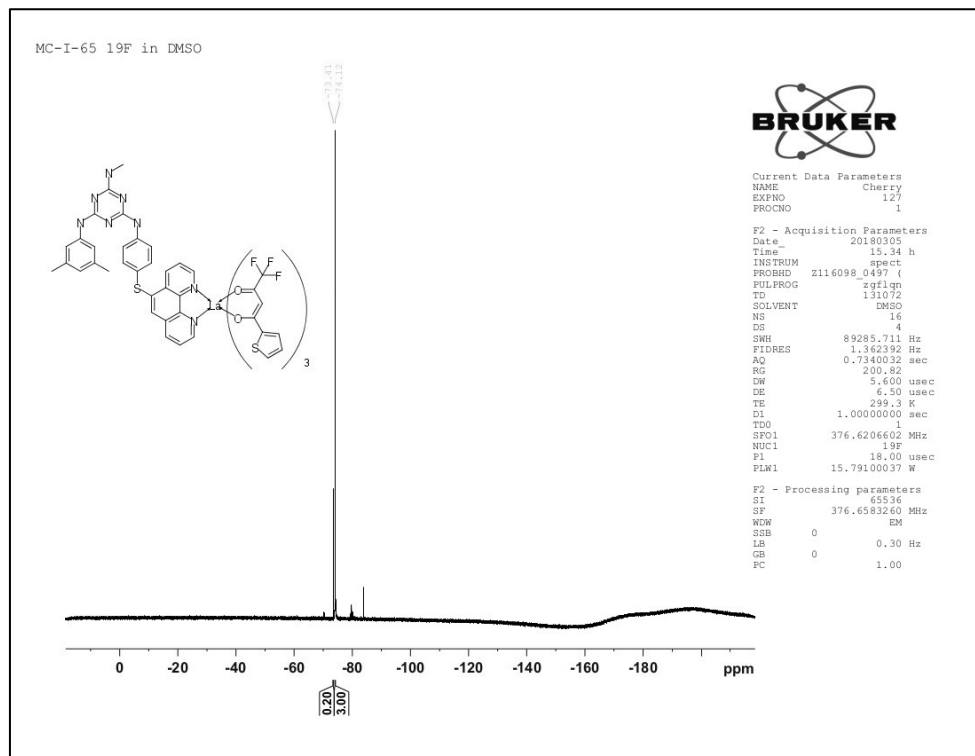


Figure 48: ^{19}F NMR of complex **68a**•La(III) in DMSO- d_6 , 376 MHz.

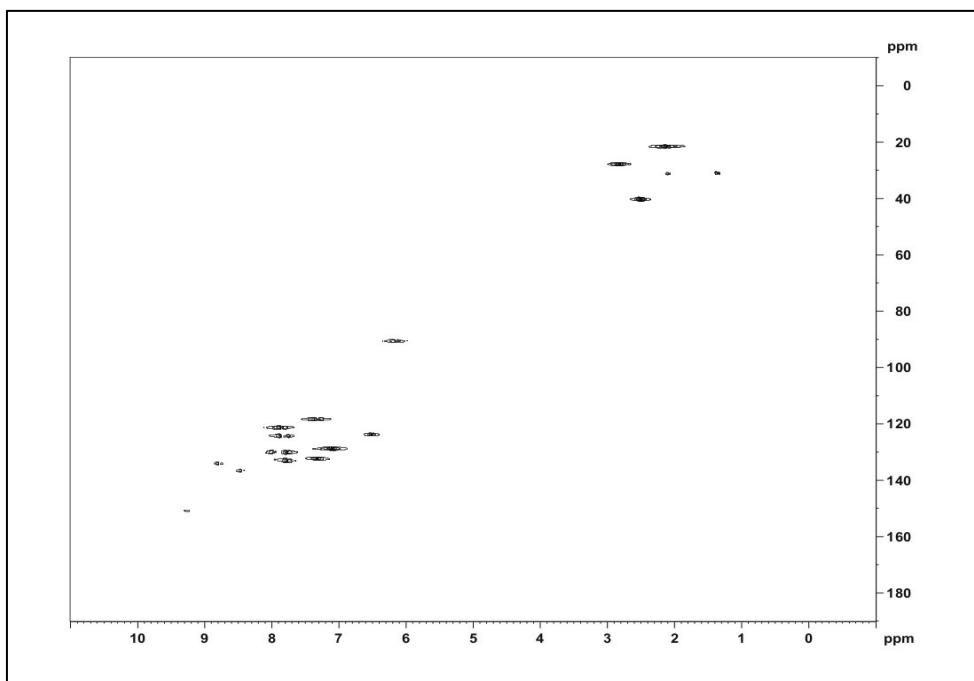


Figure 49: HSQC NMR of ligand **68a•La(III)** in DMSO-*d*₆.

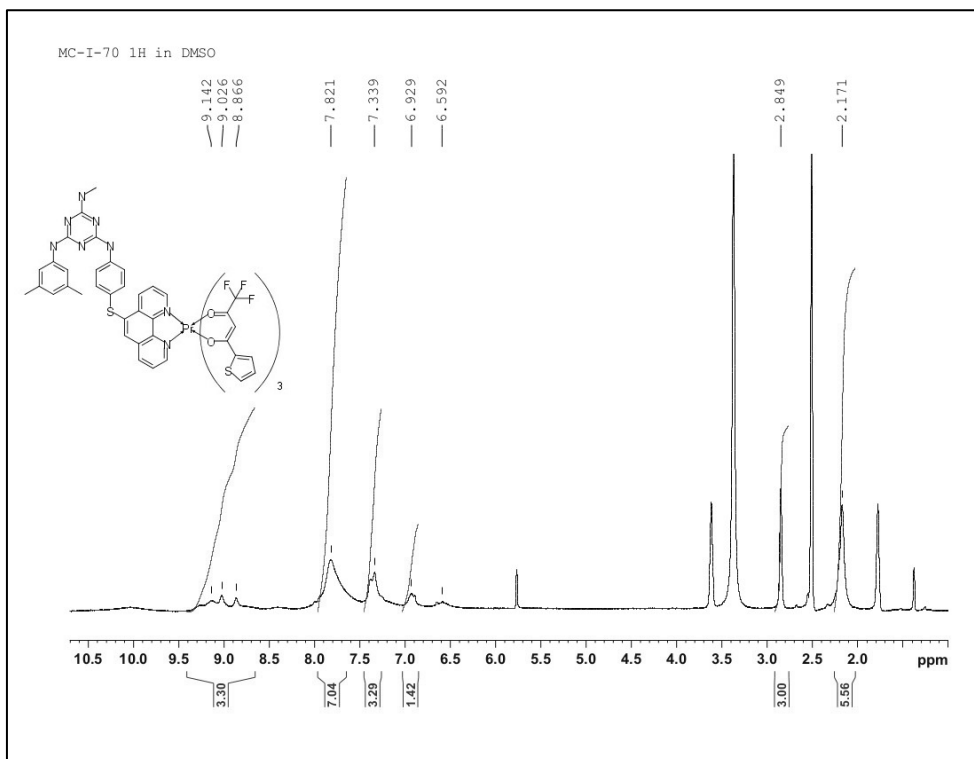


Figure 50: ¹H NMR of complex **68a•Pr(III)** in DMSO-*d*₆, 300 MHz.

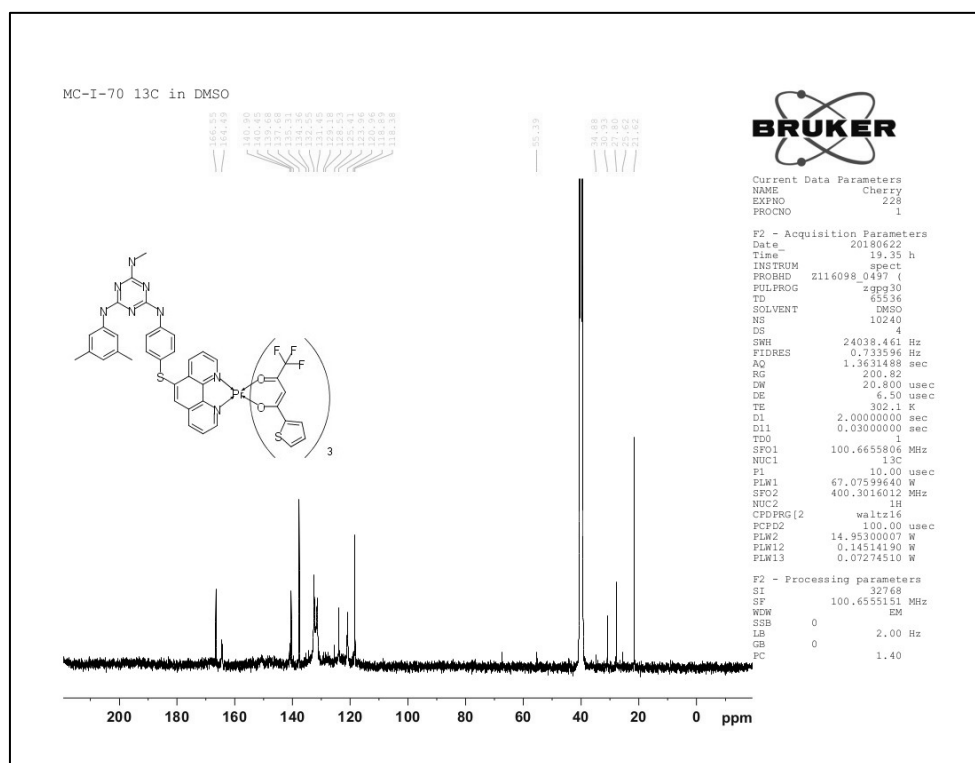


Figure 51: ^{13}C NMR of complex **68a•Pr(III)** in $\text{DMSO-}d_6$, 75 MHz.

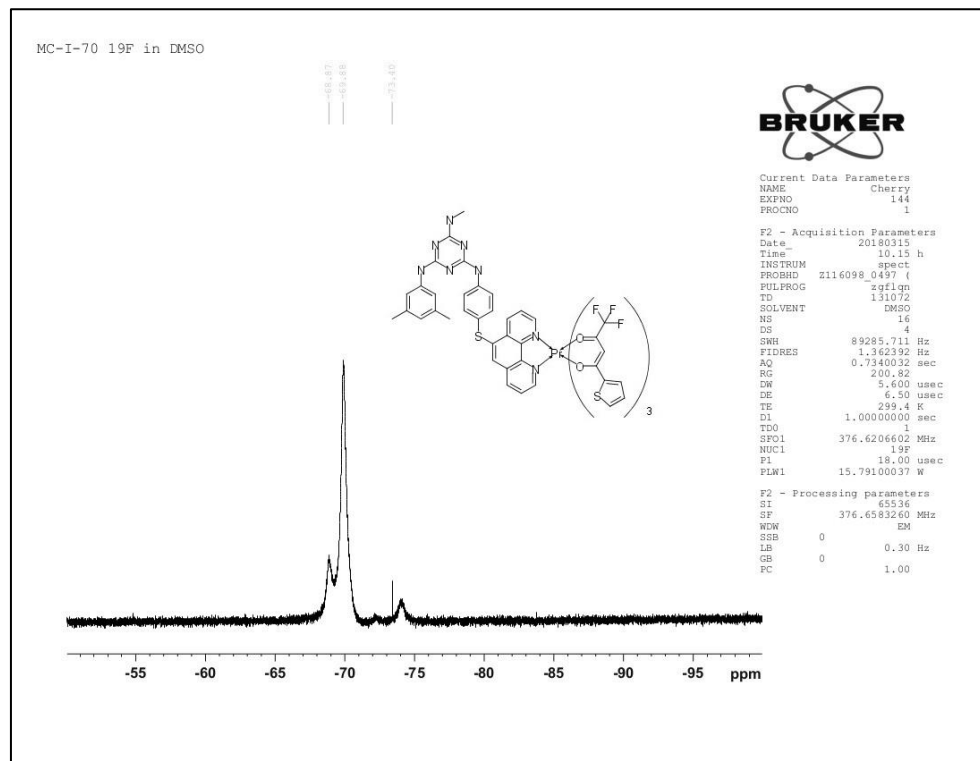


Figure 52: ^{19}F NMR of complex **68a•Pr(III)** in $\text{DMSO-}d_6$, 376 MHz.

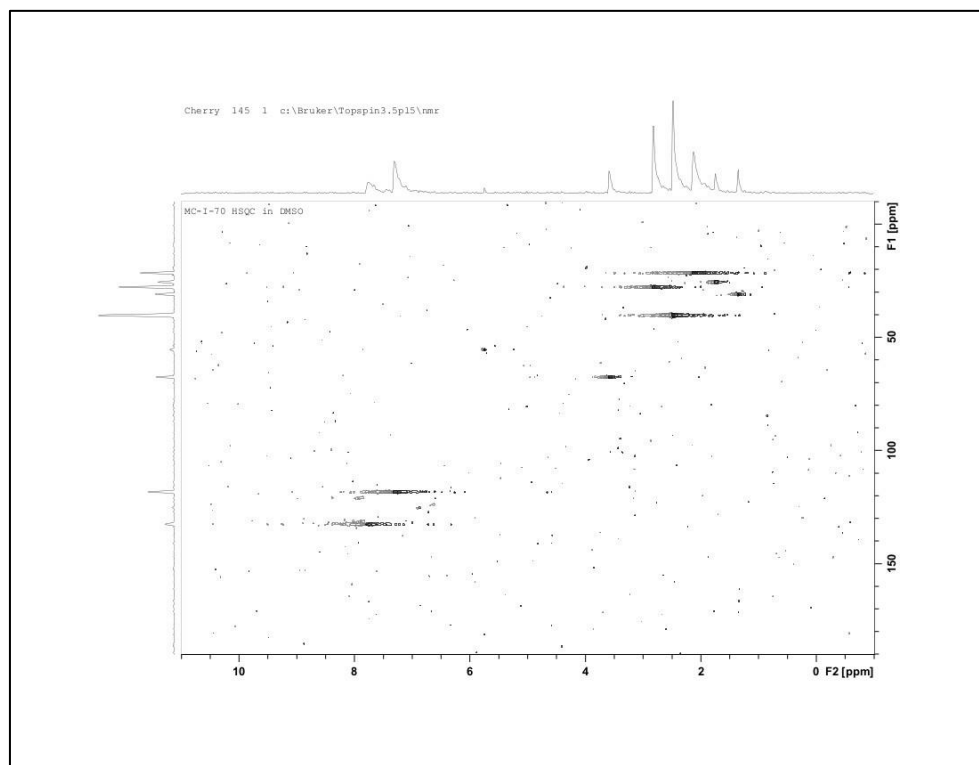


Figure 53: HSQC NMR of ligand **68a·Pr(III)** in DMSO-*d*₆.

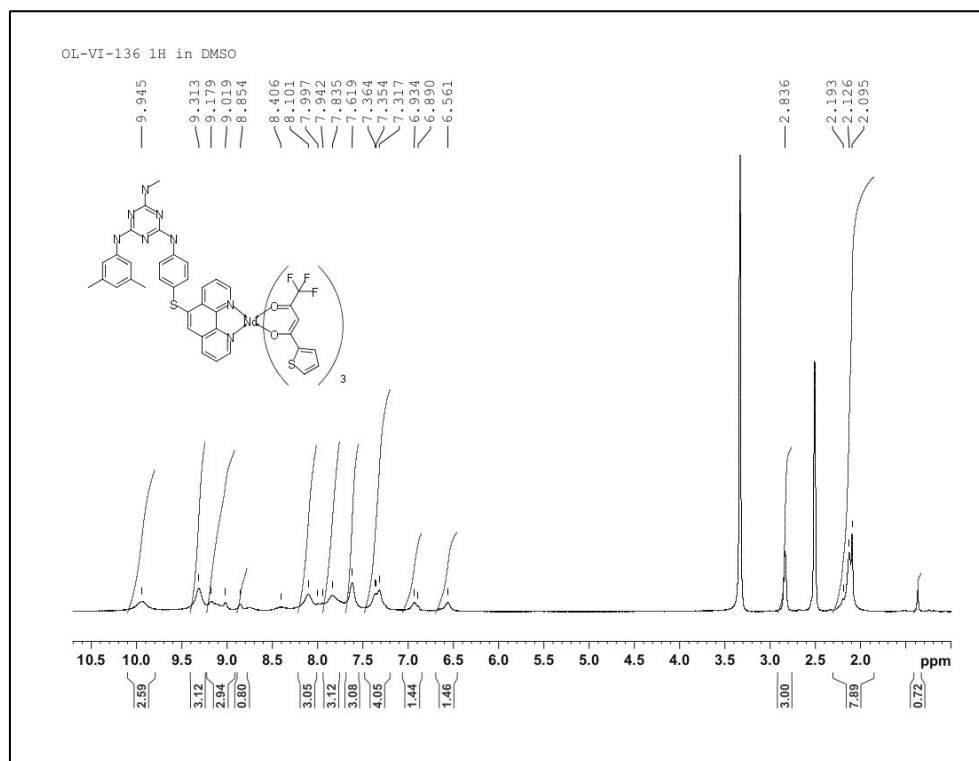


Figure 54: ¹H NMR of complex **68a·Nd(III)** in DMSO-*d*₆, 300 MHz.

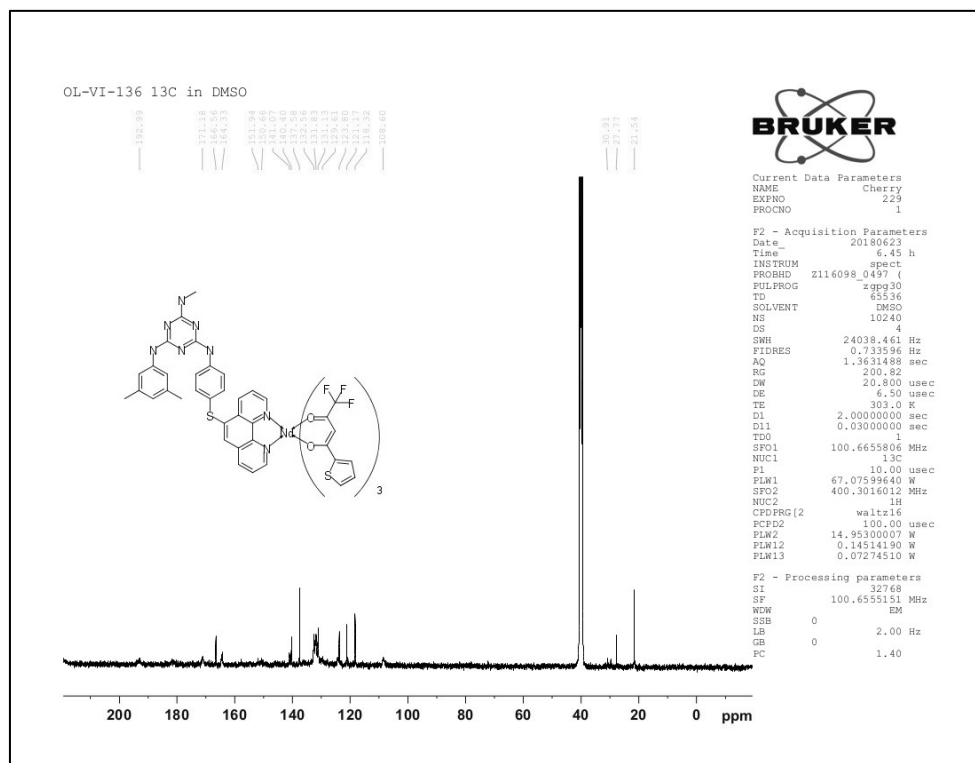


Figure 55: ^{13}C NMR of complex **68a**•Nd(III) in DMSO- d_6 , 75 MHz.

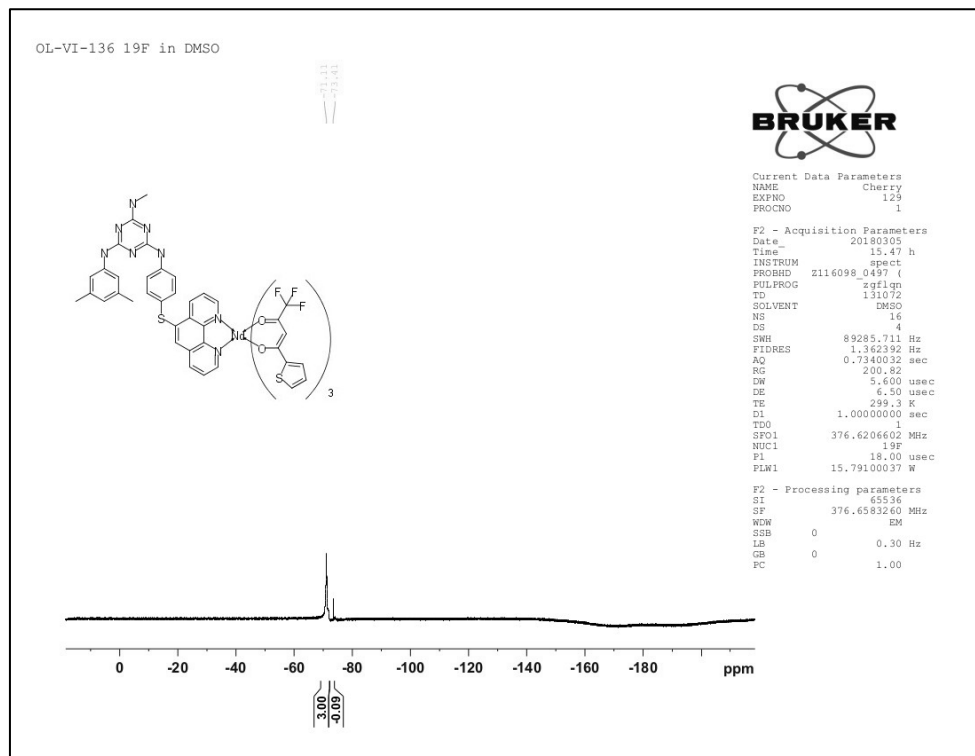


Figure 56: ^{19}F NMR of complex **68a**•Nd(III) in DMSO- d_6 , 376 MHz.

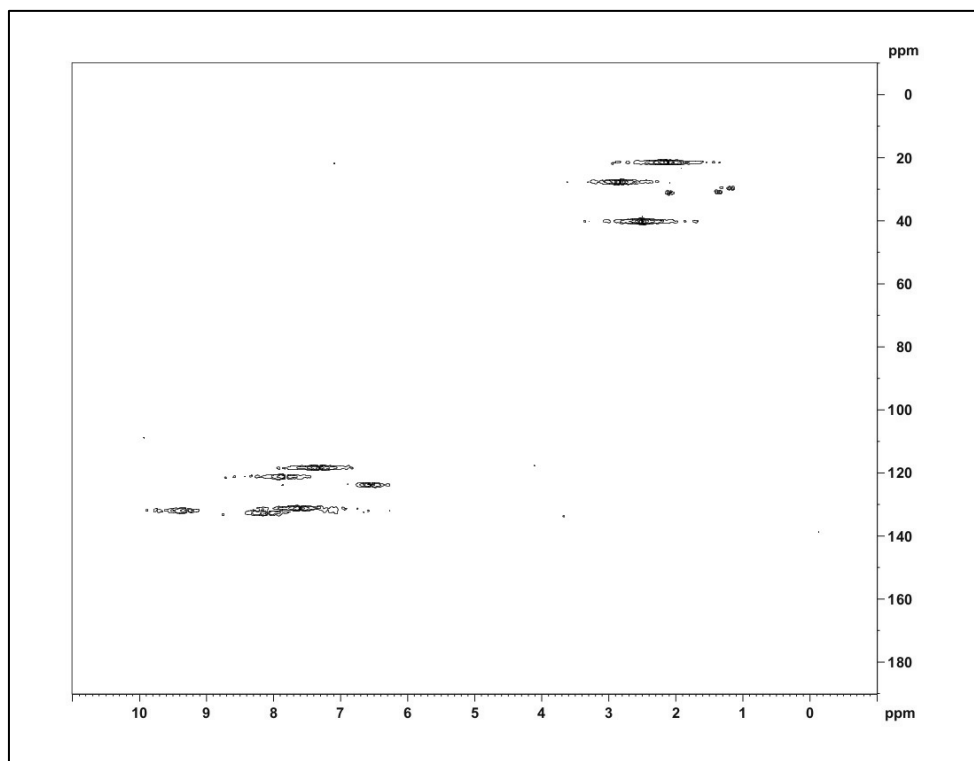


Figure 57: HSQC NMR of ligand **68a•Nd(III)** in DMSO-*d*₆.

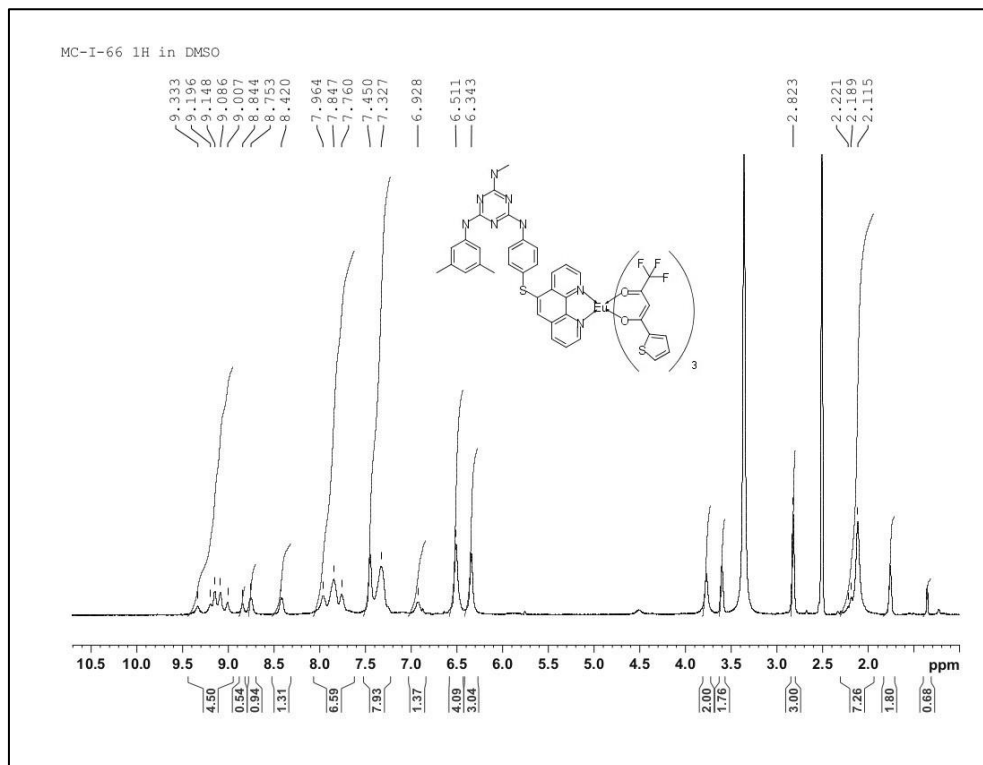


Figure 58: ¹H NMR of complex **68a•Eu(III)** in DMSO-*d*₆, 300 MHz.

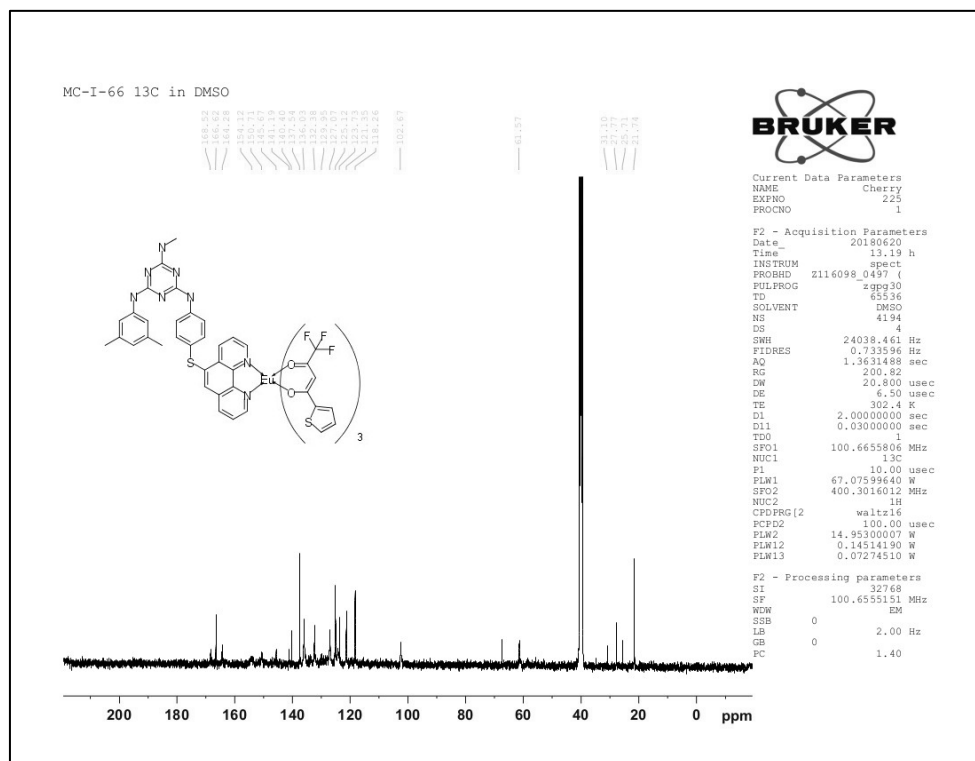


Figure 59: ^{13}C NMR of complex **68a**•Eu(III) in DMSO- d_6 , 75 MHz.

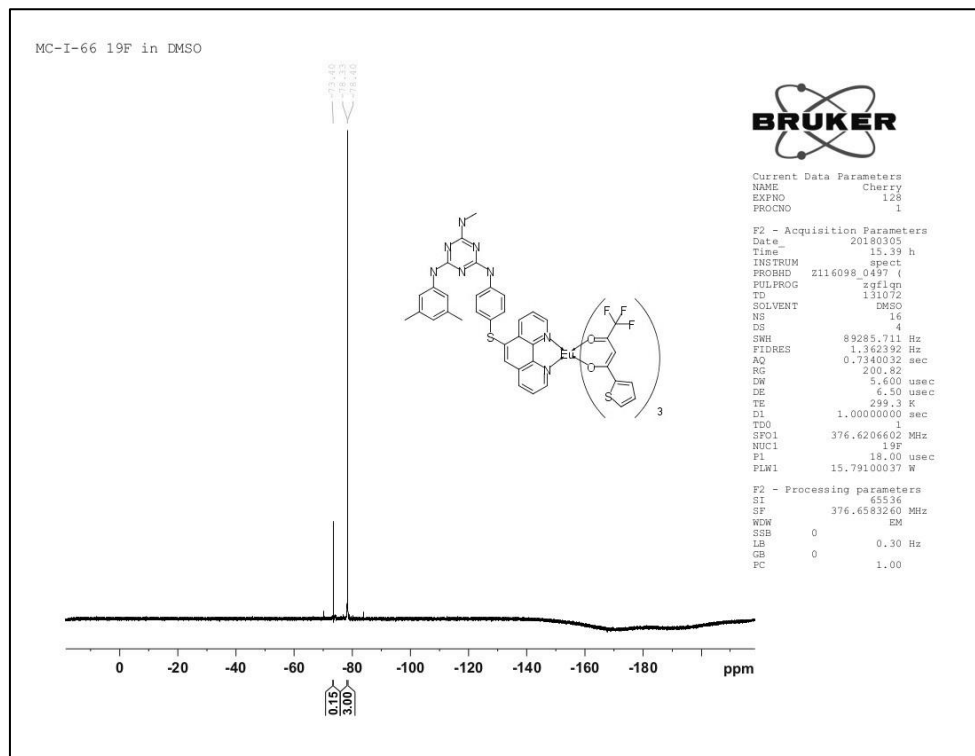


Figure 60: ^{19}F NMR of complex **68a**•Eu(III) in DMSO- d_6 , 376 MHz.

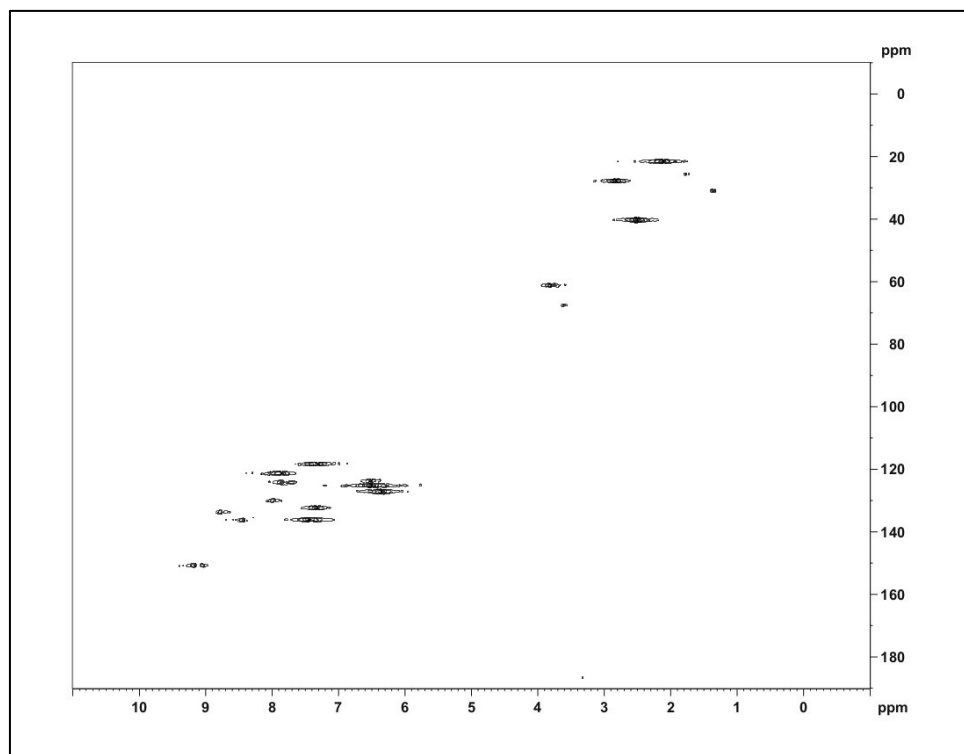


Figure 61: HSQC NMR of ligand **68a•Eu(III)** in DMSO-*d*₆.

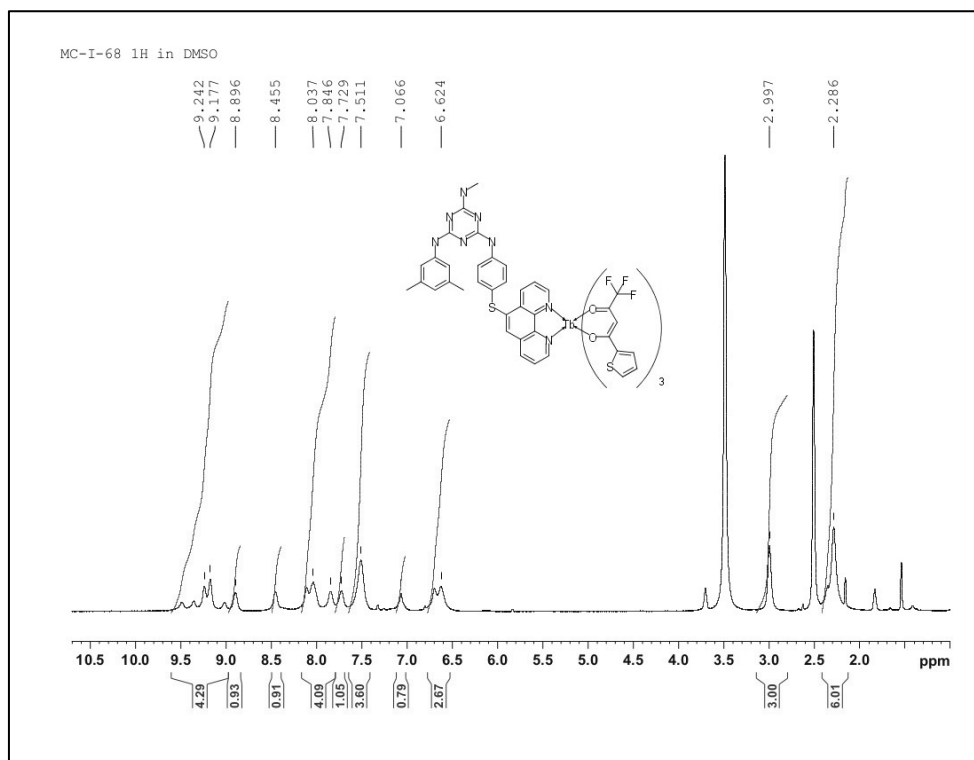


Figure 62: ¹H NMR of complex **68a•Tb(III)** in DMSO-*d*₆, 300 MHz.

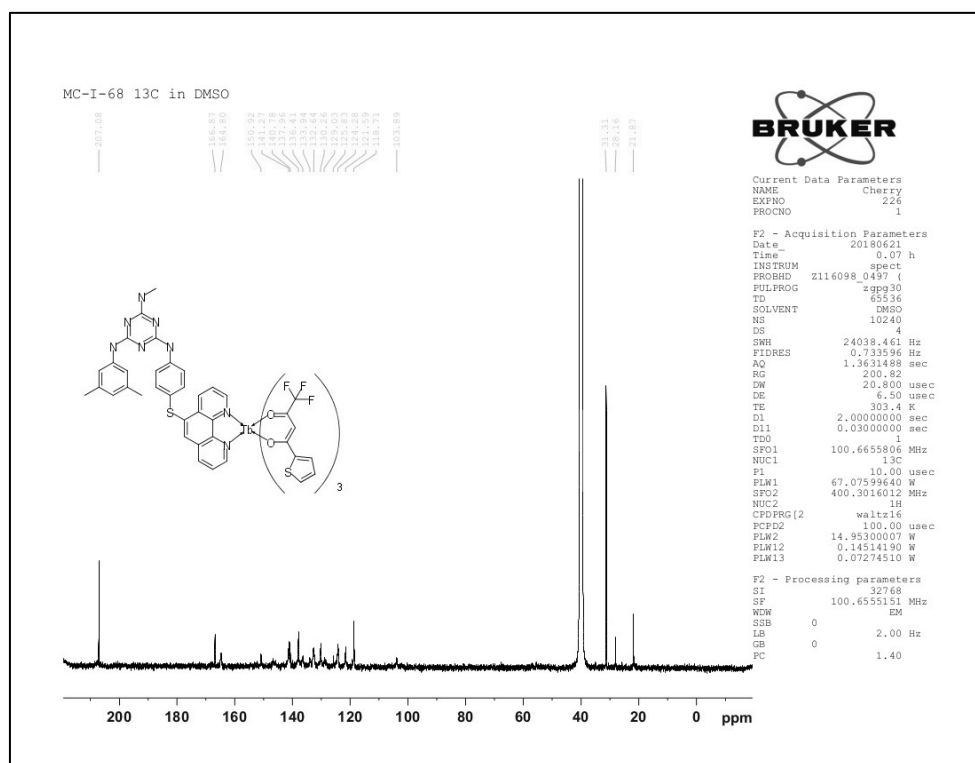


Figure 63: ^{13}C NMR of complex **68a•Tb(III)** in $\text{DMSO-}d_6$, 75 MHz.

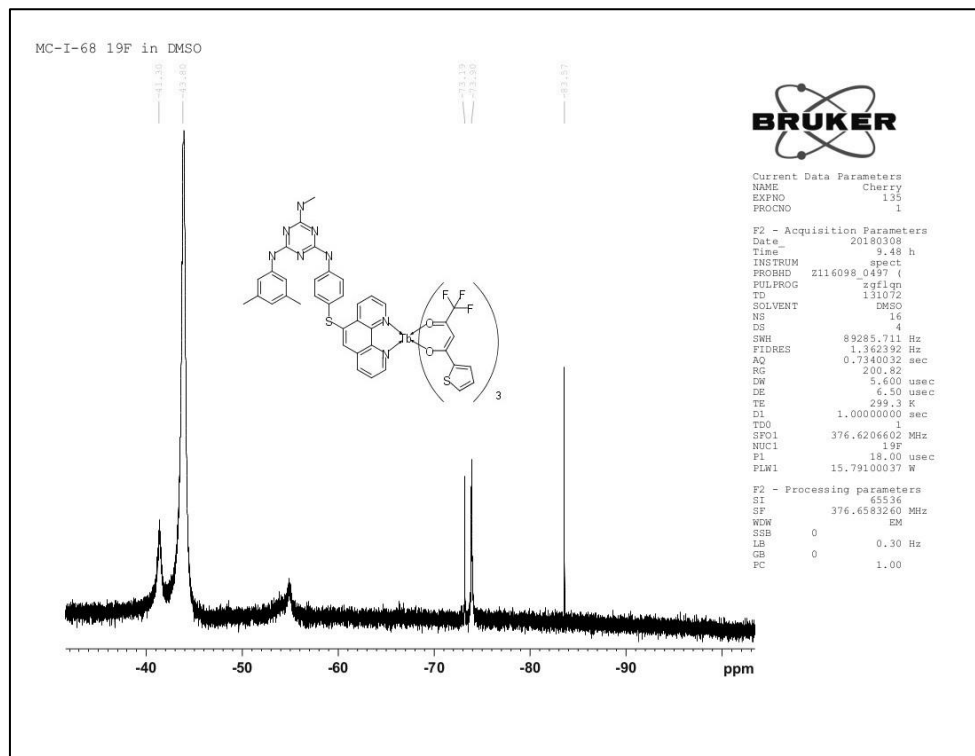


Figure 64: ^{19}F NMR of complex **68a•Tb(III)** in $\text{DMSO-}d_6$, 376 MHz.

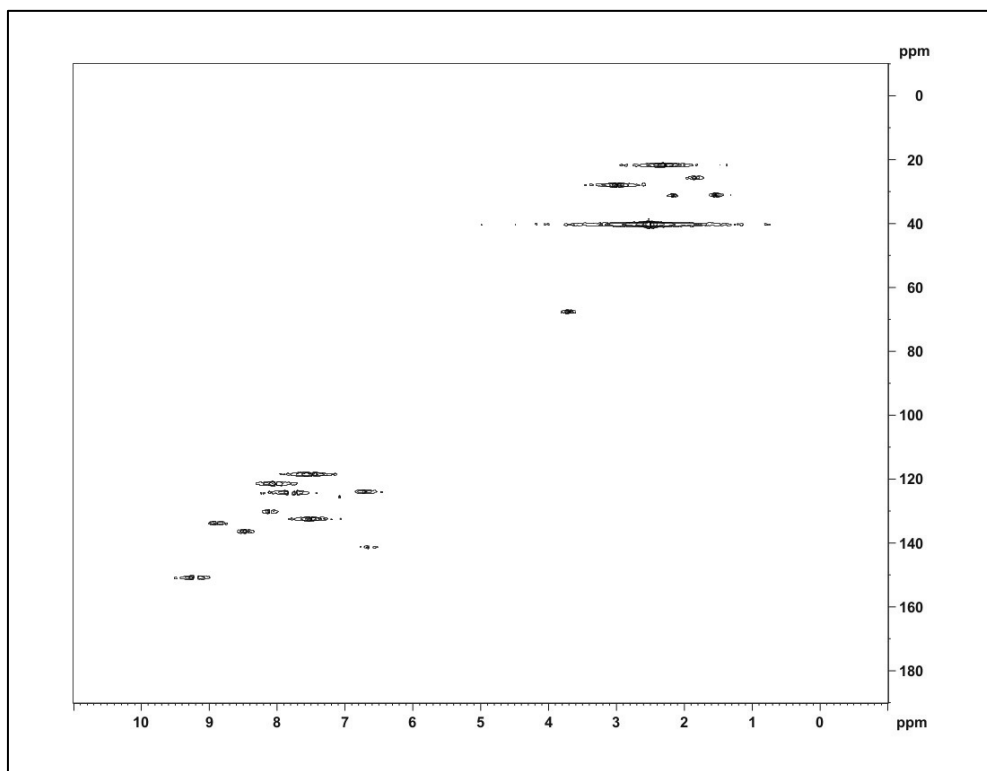


Figure 65: HSQC NMR of ligand **68a•Tb(III)** in DMSO-*d*₆.

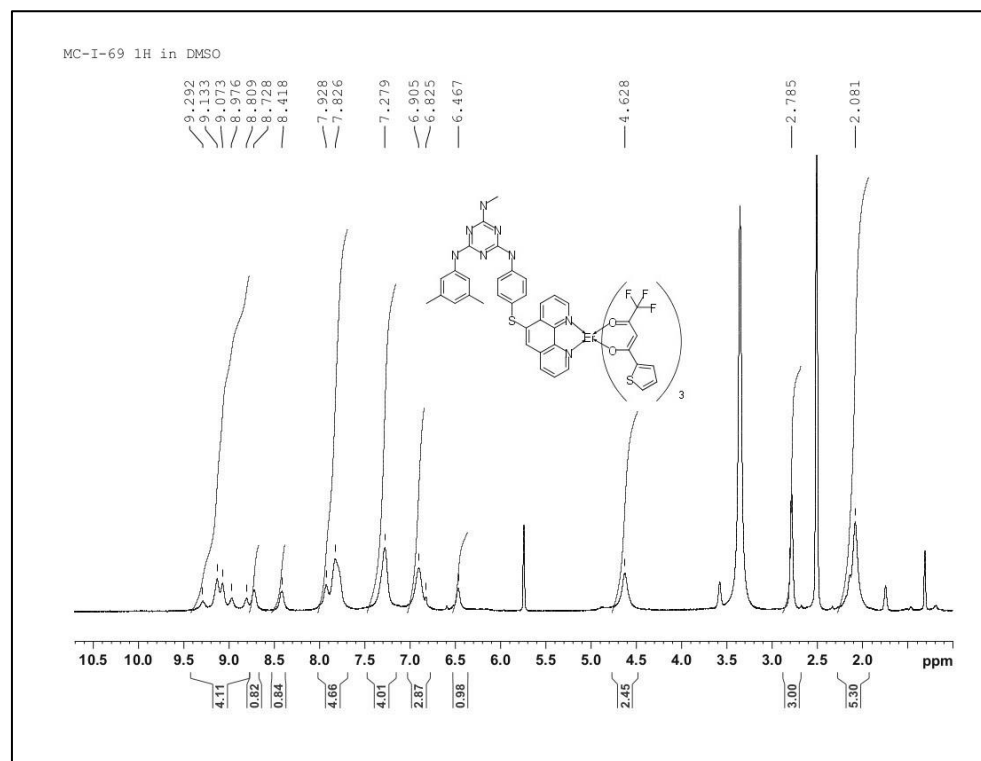


Figure 66: ¹H NMR of complex **68a•Er(III)** in DMSO-*d*₆, 300 MHz.

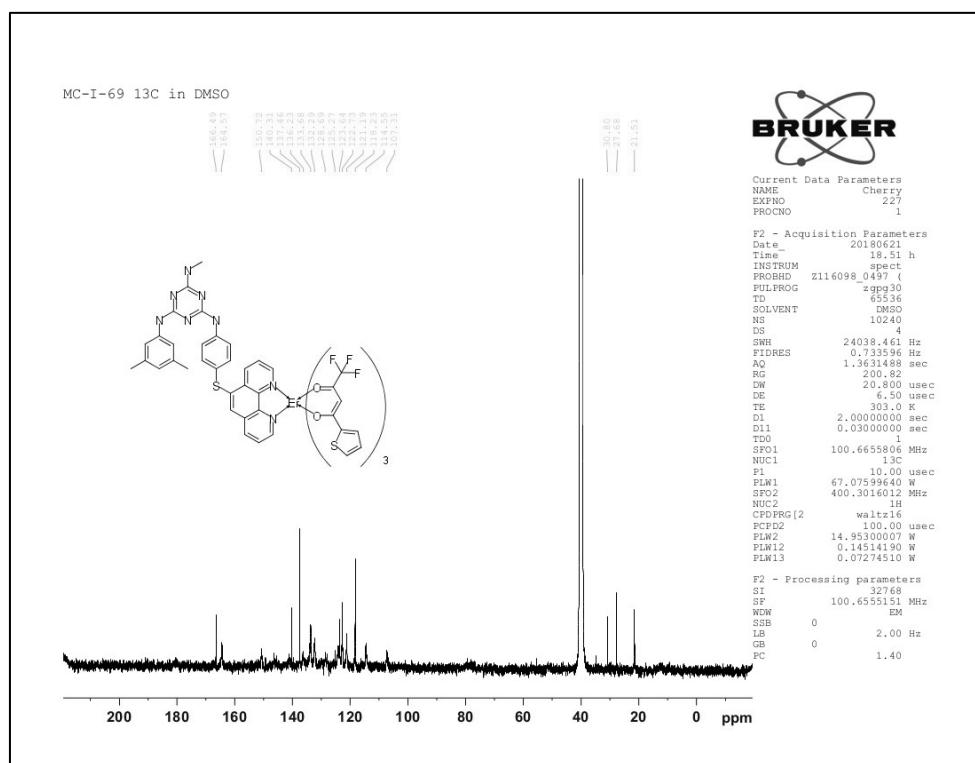


Figure 67: ^{13}C NMR of complex **68a•Er(III)** in $\text{DMSO-}d_6$, 75 MHz.

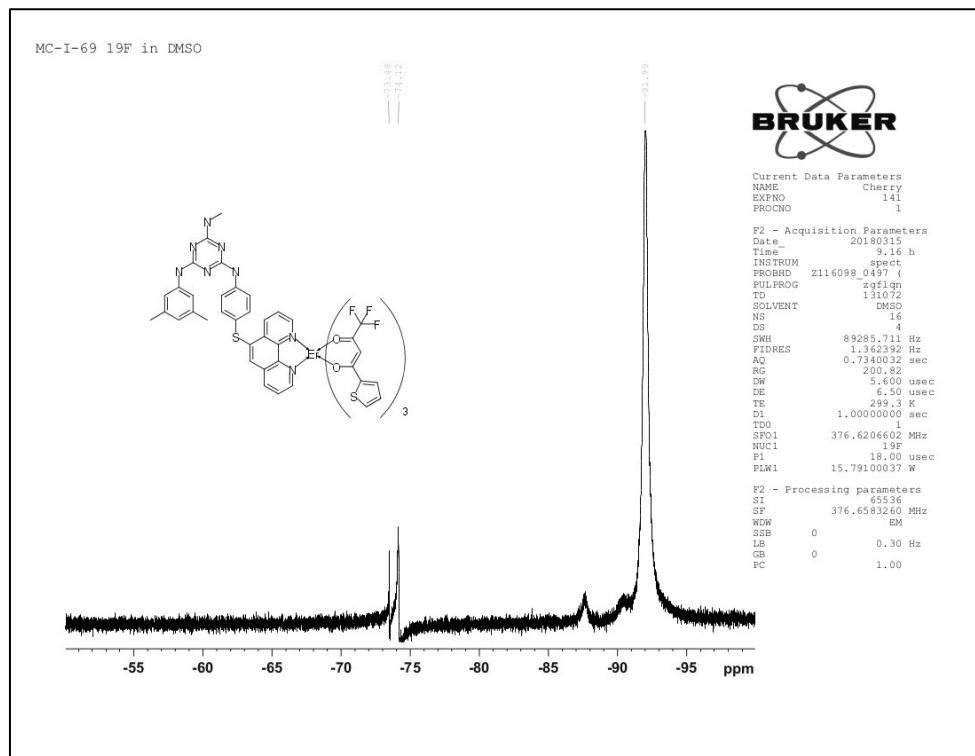


Figure 68: ^{19}F NMR of complex **68a•Er(III)** in $\text{DMSO-}d_6$, 376 MHz.

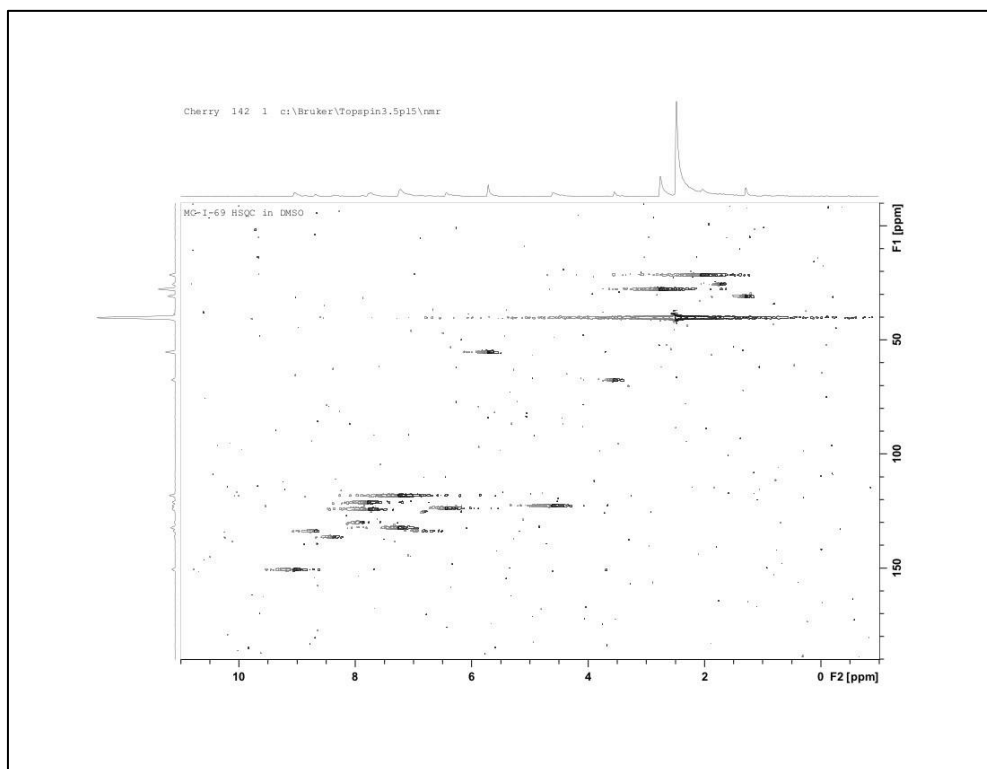


Figure 69: HSQC NMR of ligand **68a•Er(III)** in DMSO-*d*₆.

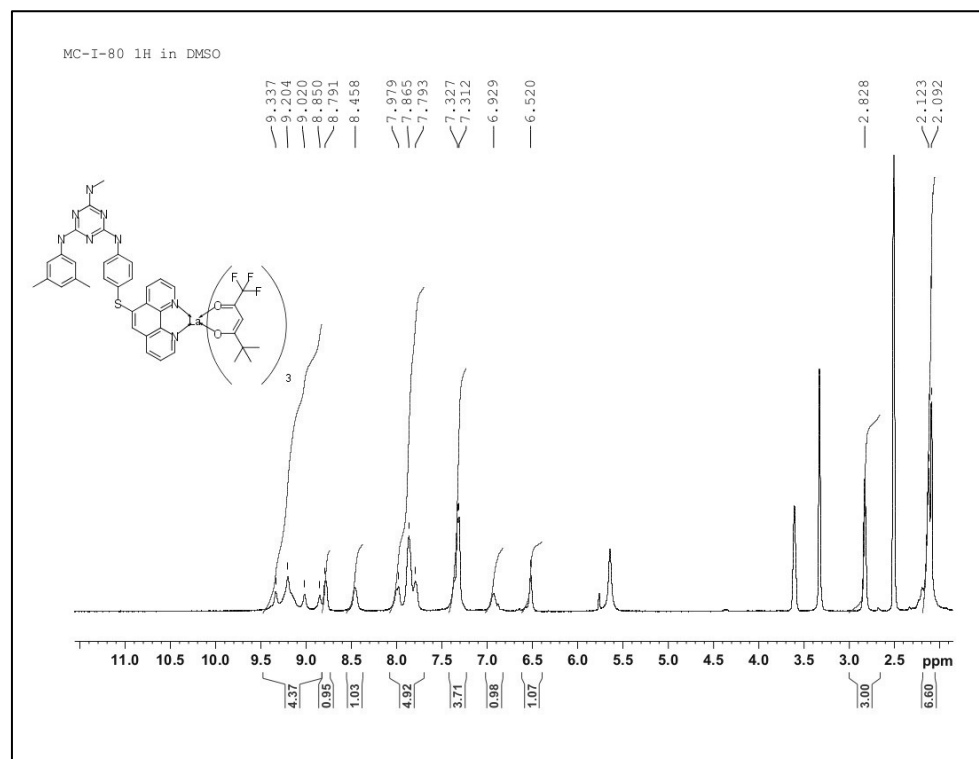


Figure 70: ¹H NMR of complex **68b•La(III)** in DMSO-*d*₆, 300 MHz.

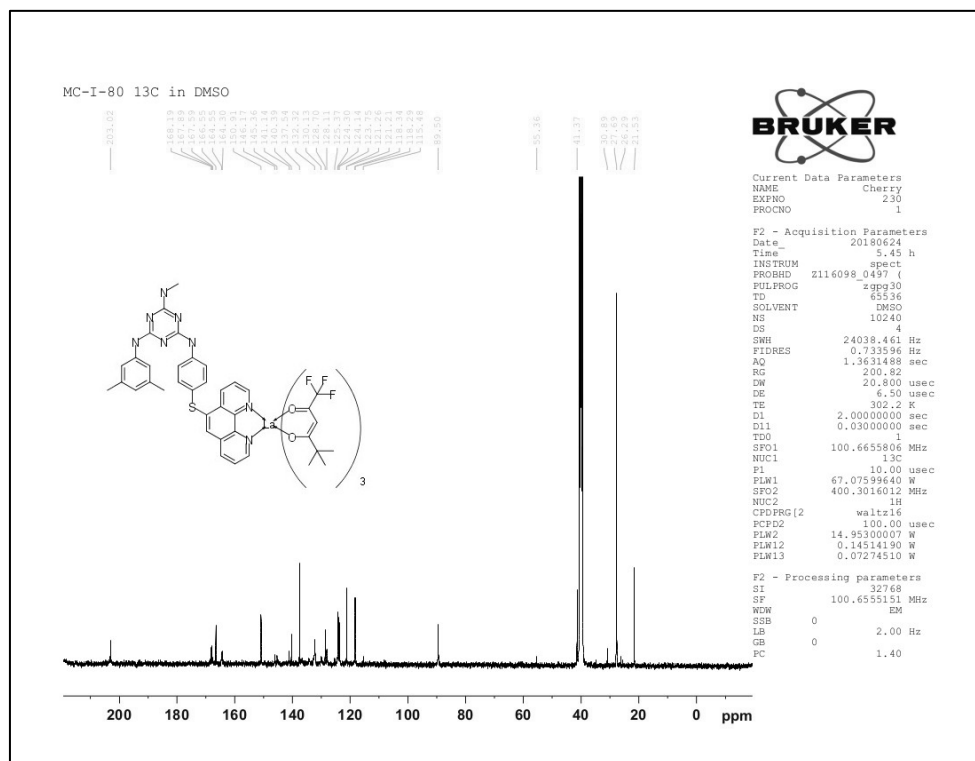


Figure 71: ^{13}C NMR of complex **68b•La(III)** in $\text{DMSO-}d_6$, 75 MHz.

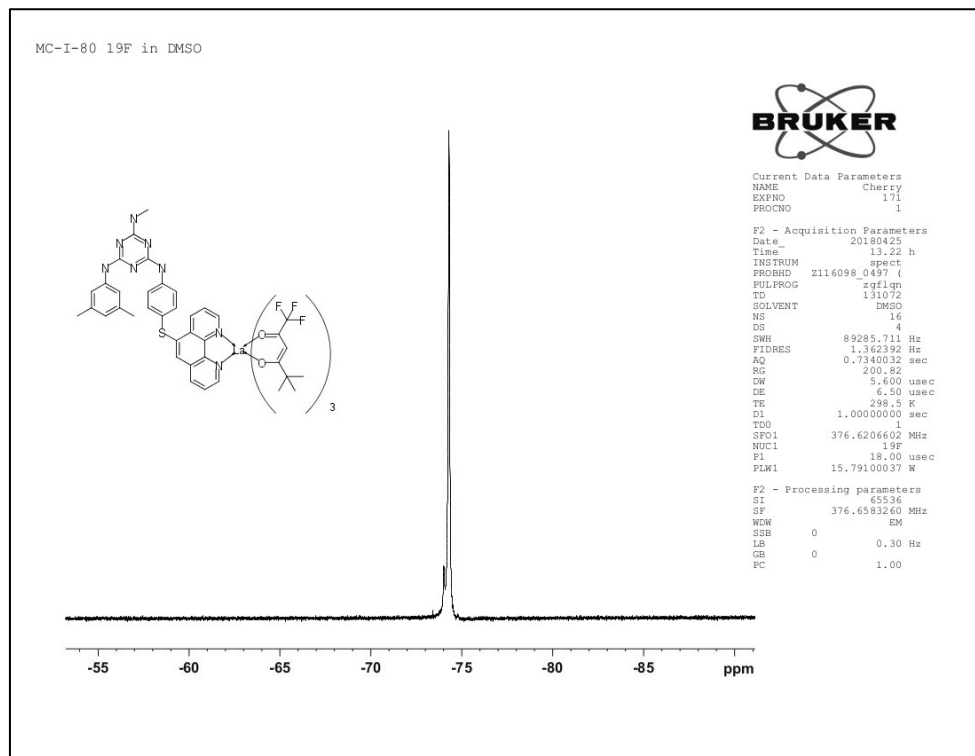


Figure 72: ^{19}F NMR of complex **68b•La(III)** in $\text{DMSO-}d_6$, 376 MHz.

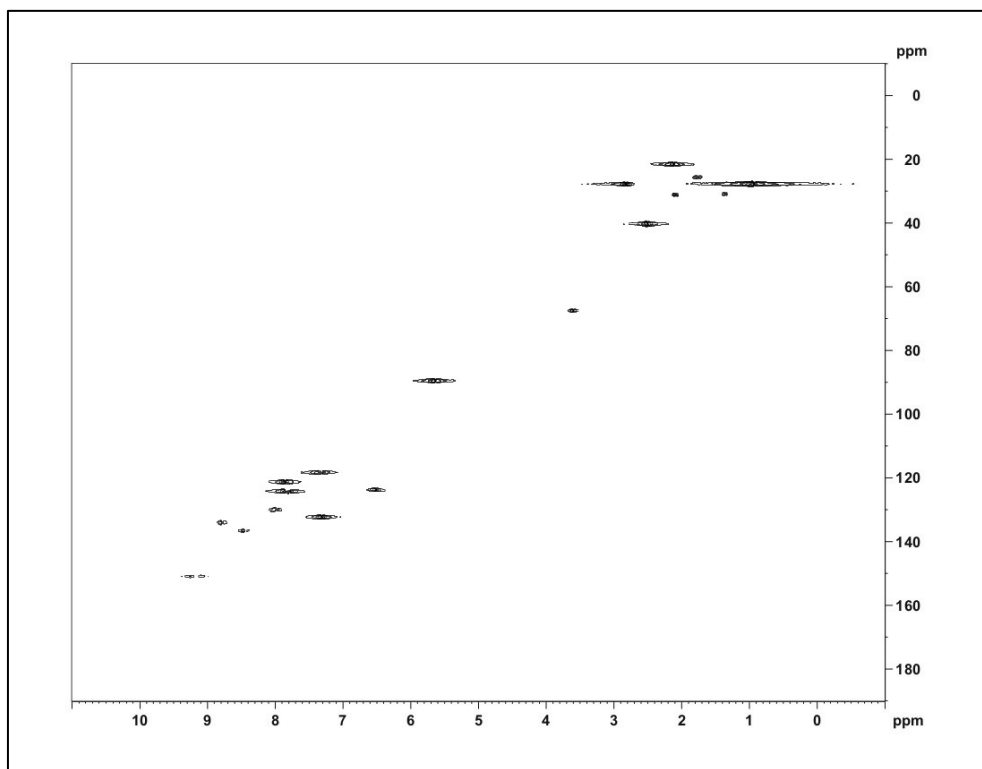


Figure 73: HSQC NMR of complex **68b•La(III)** in DMSO-*d*₆.

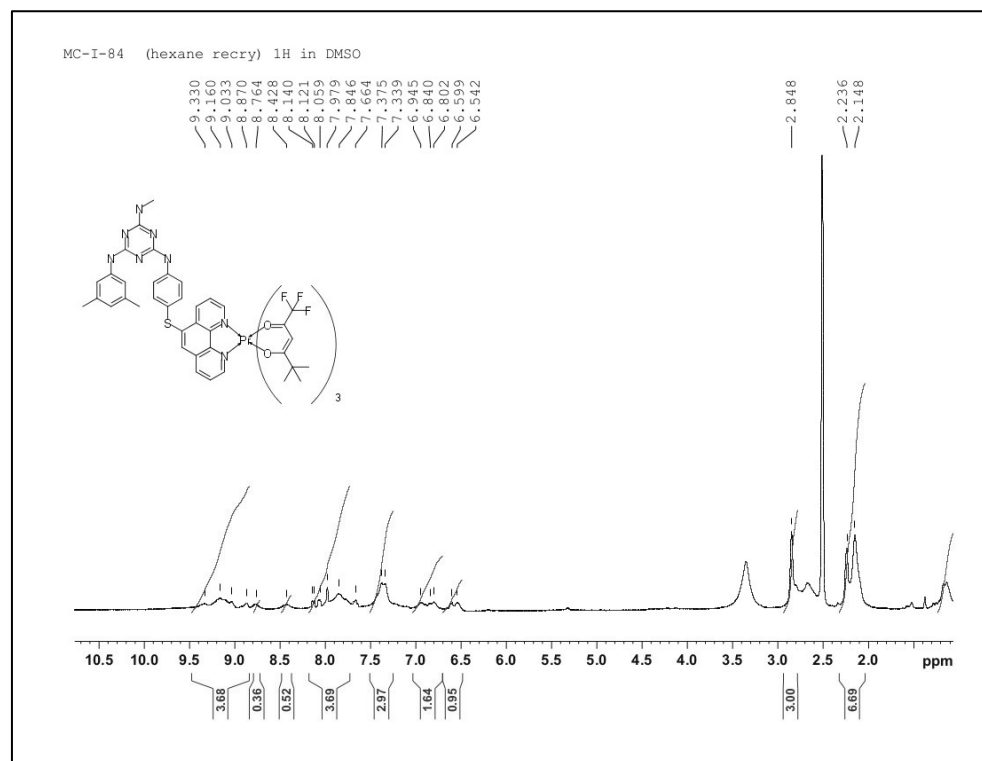


Figure 74: ¹H NMR of complex **68b•Pr(III)** in DMSO-*d*₆, 300 MHz.

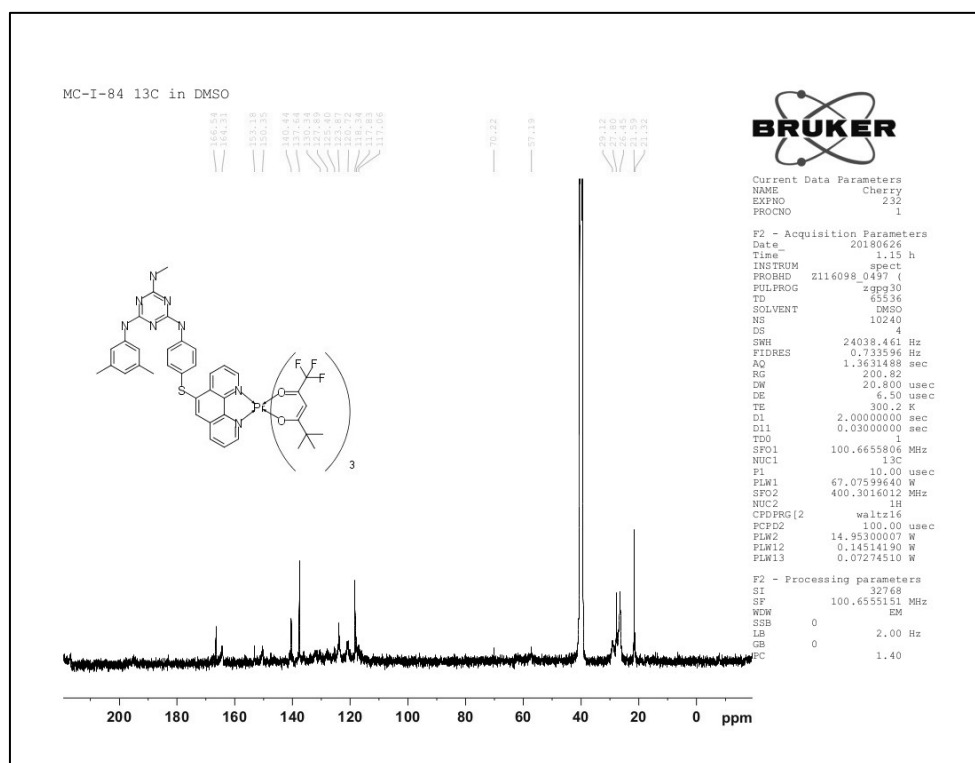


Figure 75: ¹³C NMR of complex **68b•Pr(III)** in DMSO-*d*₆, 75 MHz.

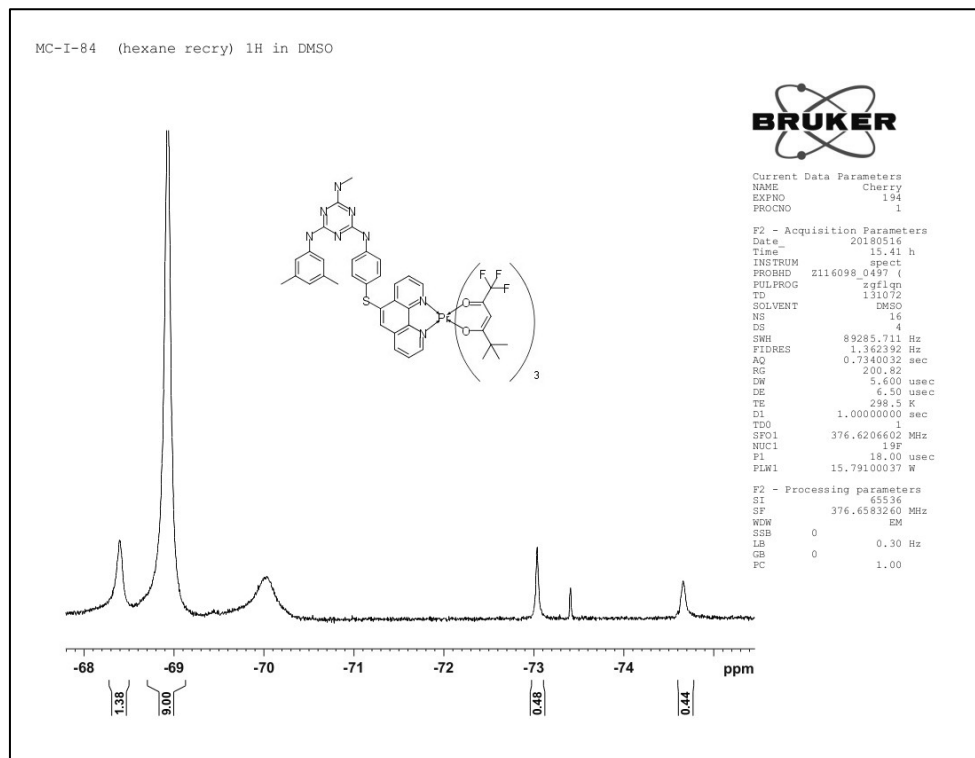


Figure 76: ¹⁹F NMR of complex **68b•Pr(III)** in DMSO-*d*₆, 376 MHz.

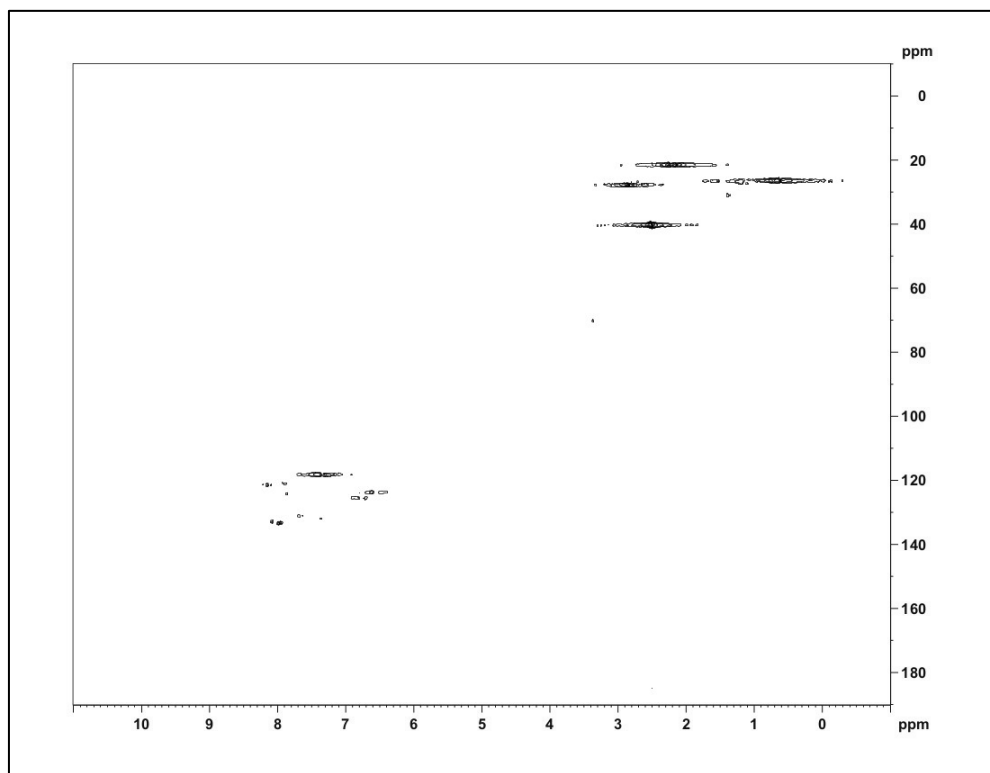


Figure 77: HSQC NMR of complex **68b•Pr(III)** in DMSO-*d*₆.

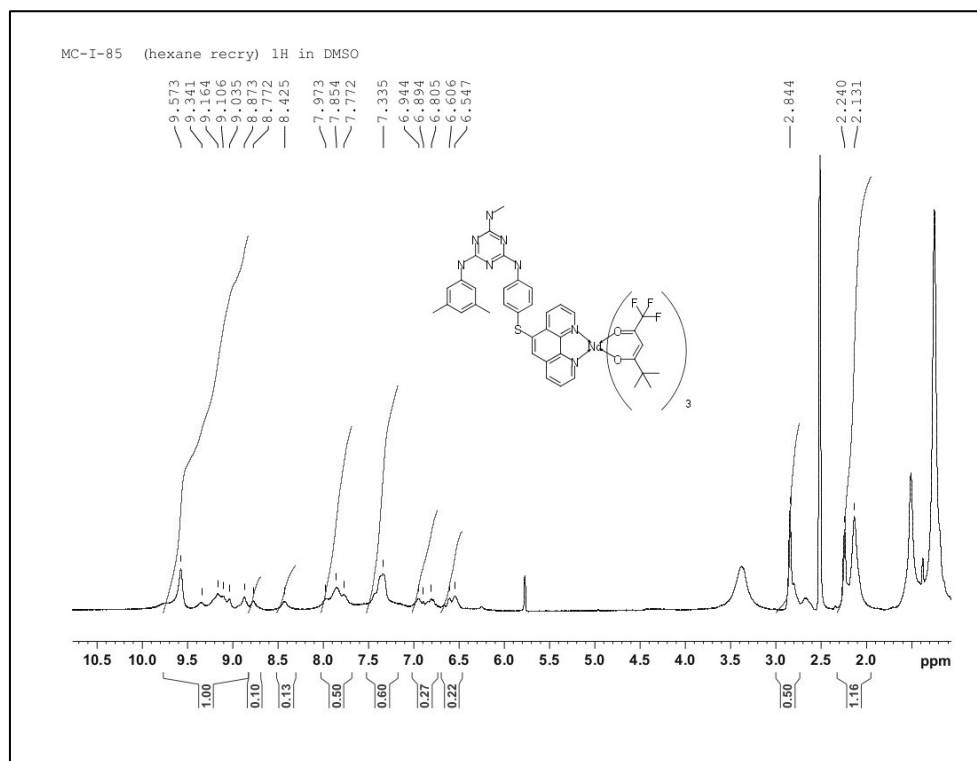


Figure 78: ¹H NMR of complex **68b•Nd(III)** in DMSO-*d*₆, 300 MHz.

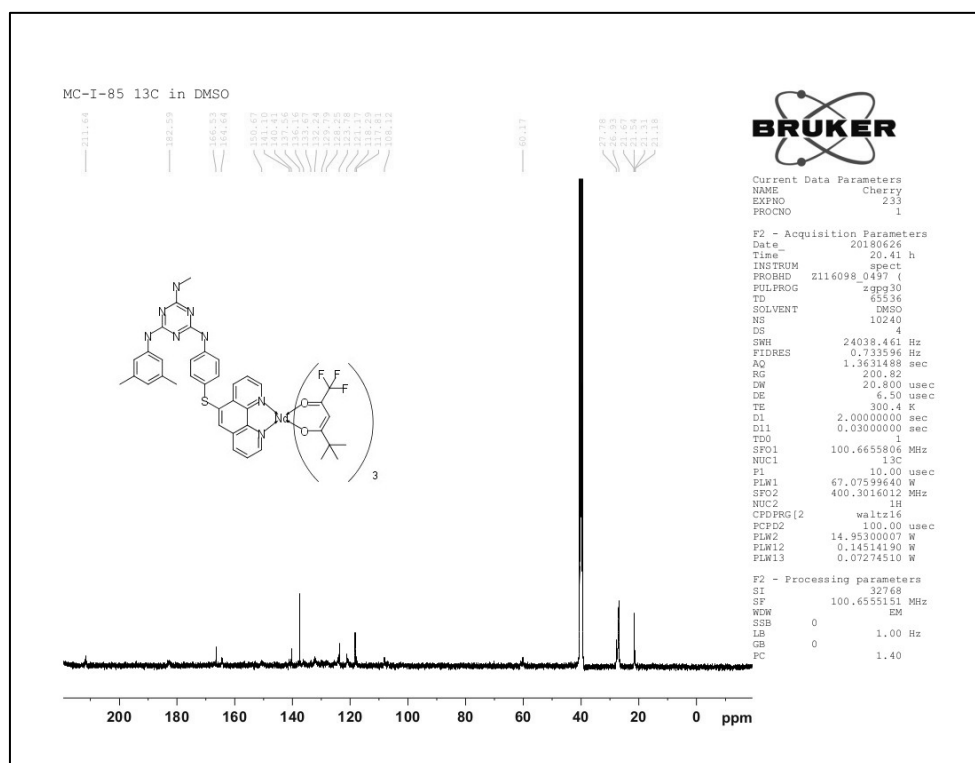


Figure 79: ^{13}C NMR of complex **68b**•Nd(III) in DMSO- d_6 , 75 MHz.

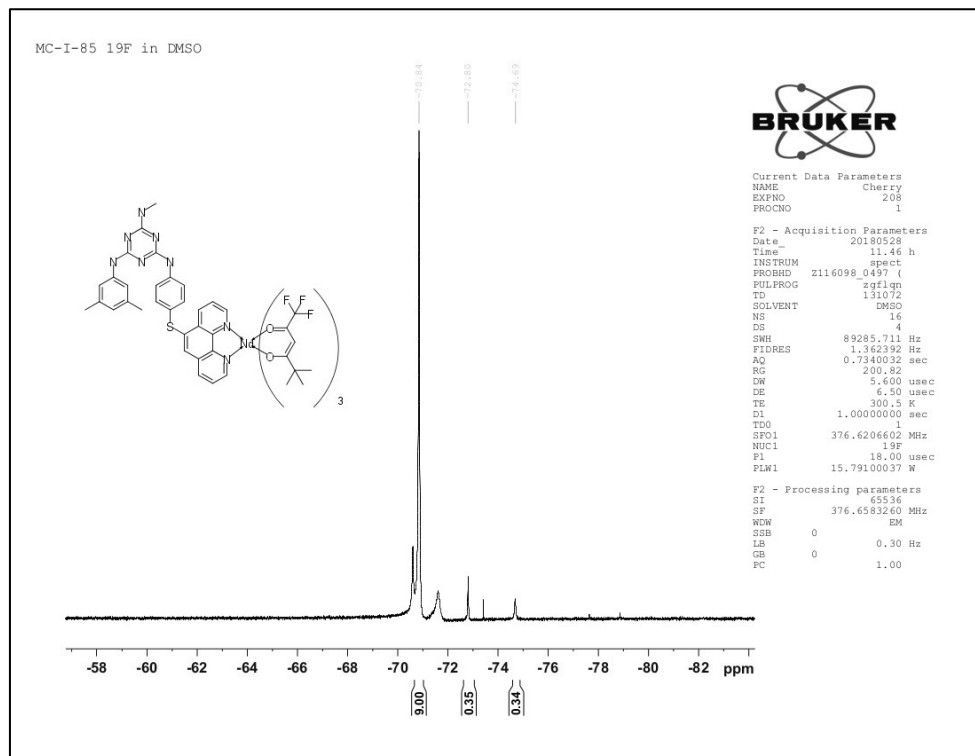


Figure 80: ^{19}F NMR of complex **68b**•Nd(III) in DMSO- d_6 , 376 MHz.

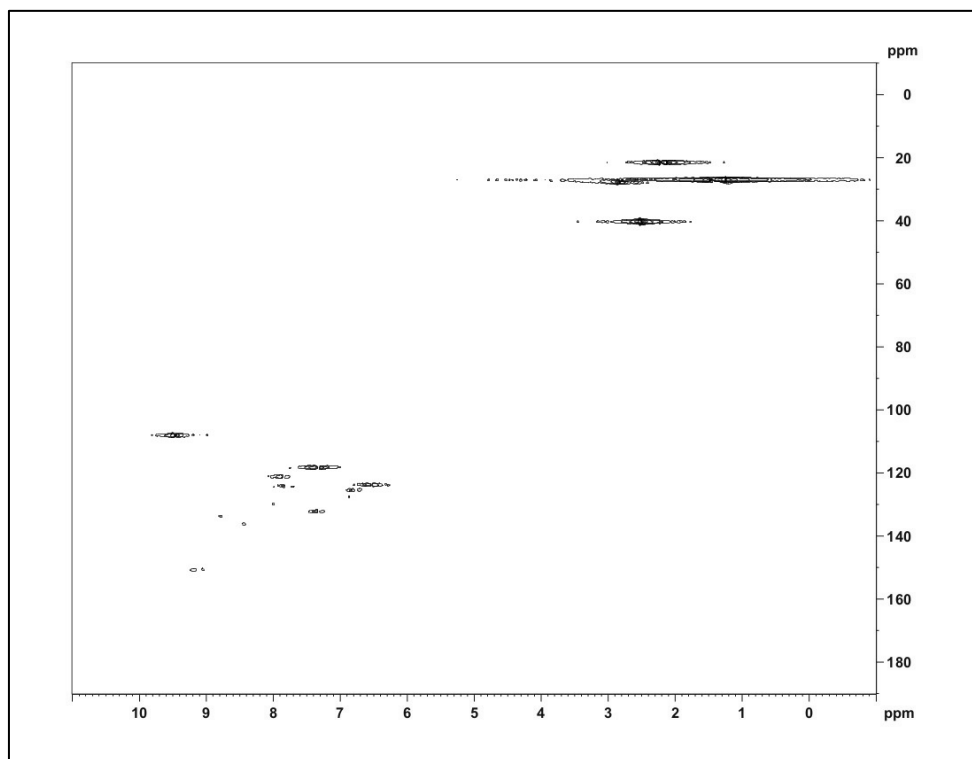


Figure 81: HSQC NMR of complex **68b•Nd(III)** in DMSO-*d*₆.

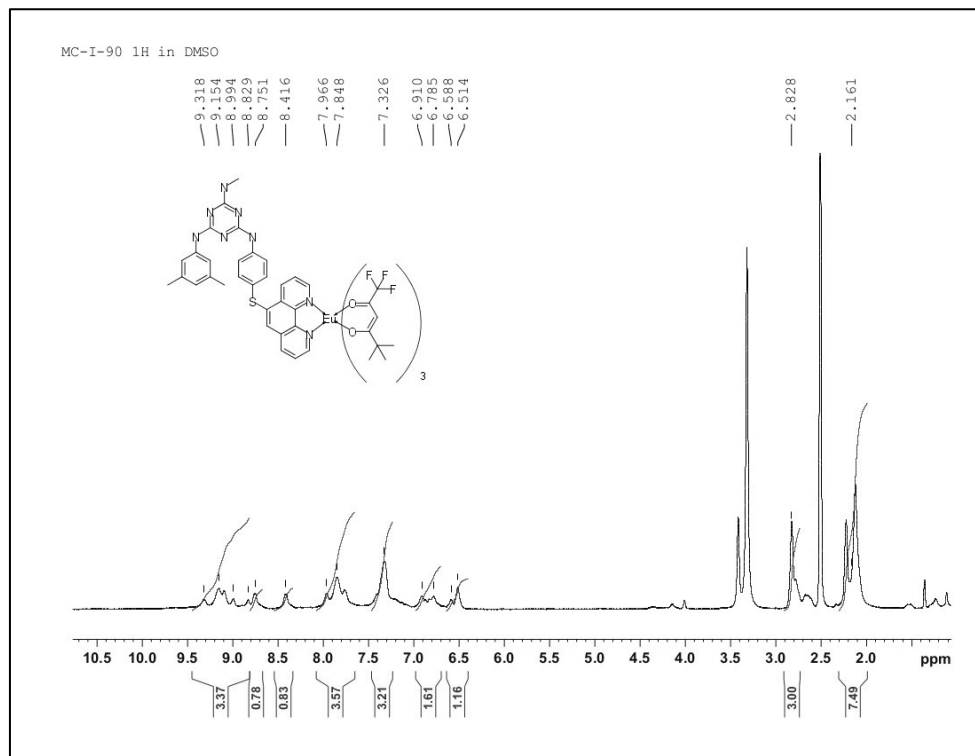


Figure 82: ¹H NMR of complex **68b•Eu(III)** in DMSO-*d*₆, 300 MHz.

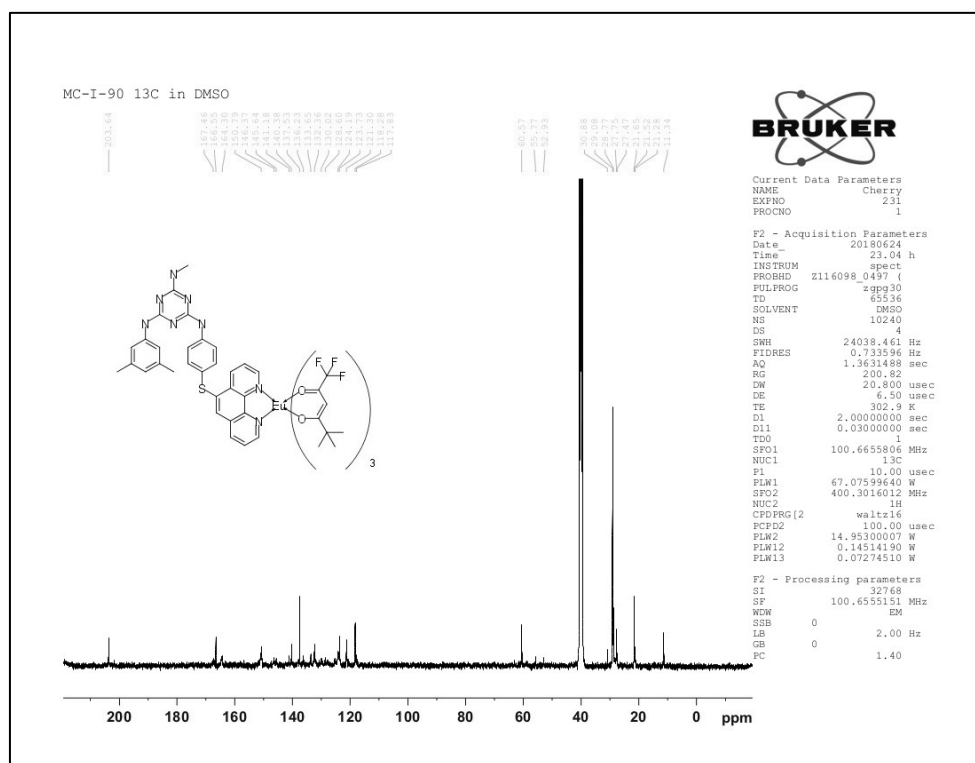


Figure 83: ^{13}C NMR of complex **68b•Eu(III)** in $\text{DMSO-}d_6$, 75 MHz.

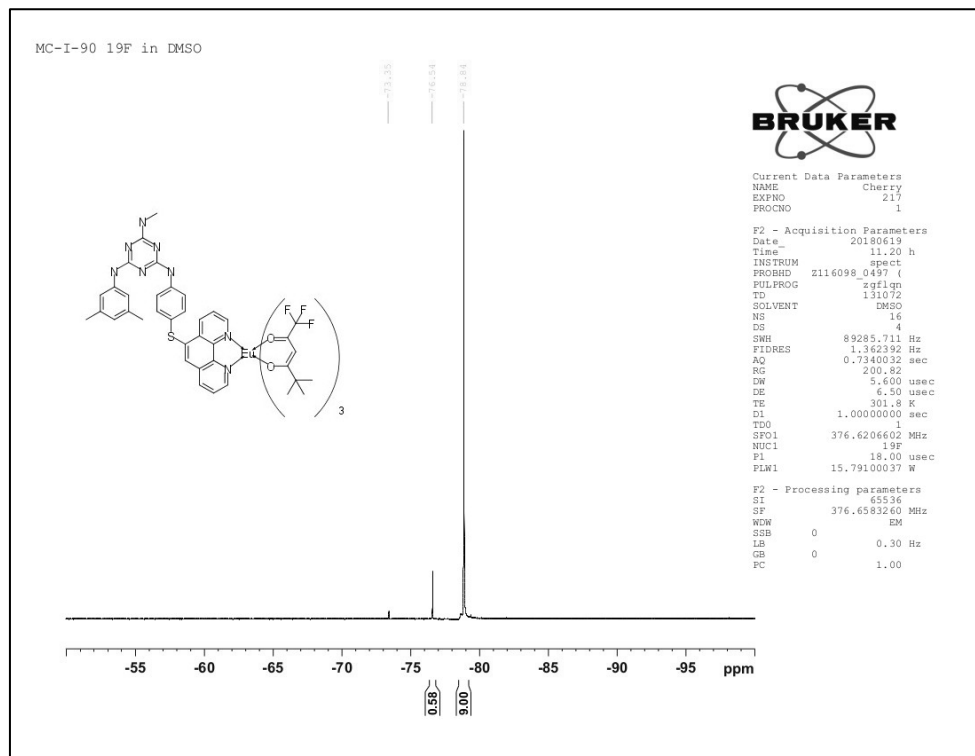


Figure 84: ^{19}F NMR of complex **68b•Eu(III)** in $\text{DMSO-}d_6$, 376 MHz.

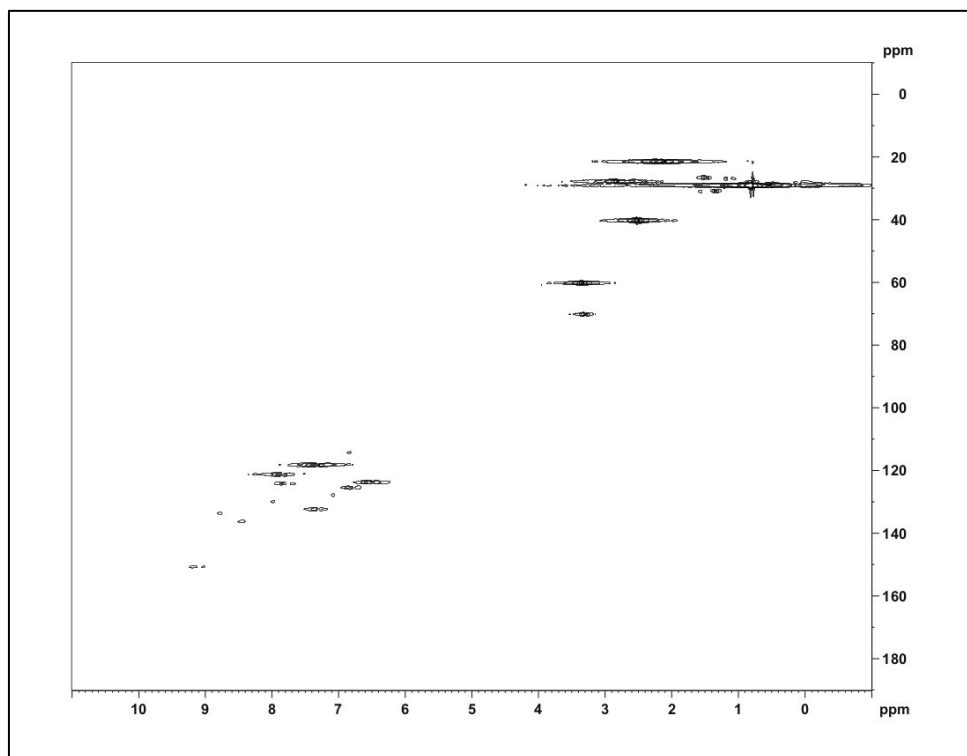


Figure 85: HSQC NMR of complex **68b•Eu(III)** in $\text{DMSO-}d_6$.

B. TGA Results

B.1 TGA Thermograms for Salen Complexes Functionalized with Mexylaminotriazines

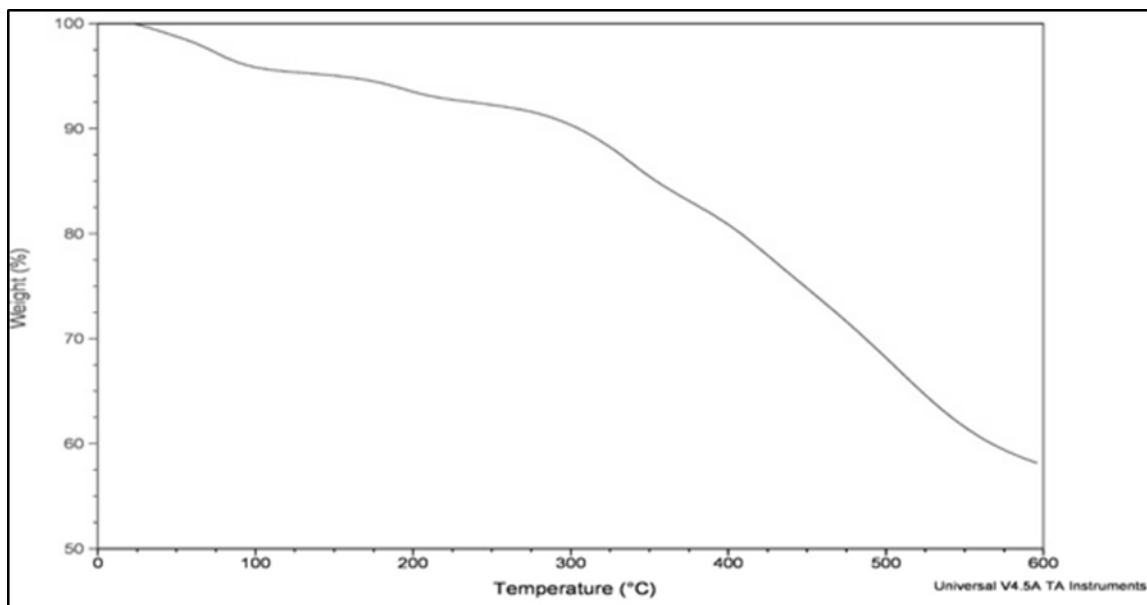


Figure 86: TGA thermogram for complex **48a•Mn(III)**.

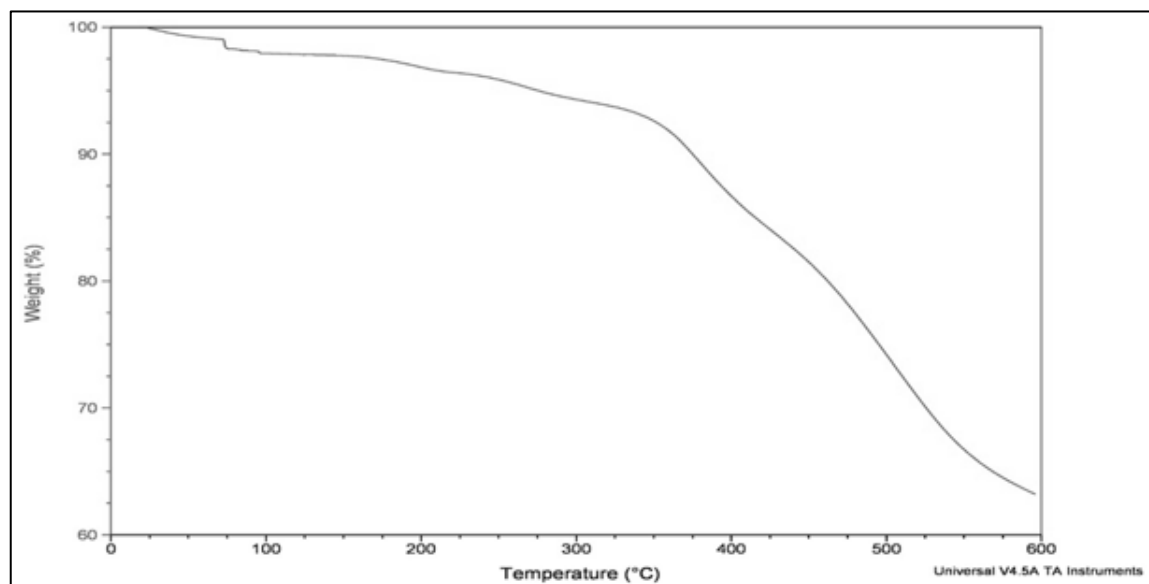


Figure 87: TGA thermogram for complex **48a•Fe(III)**.

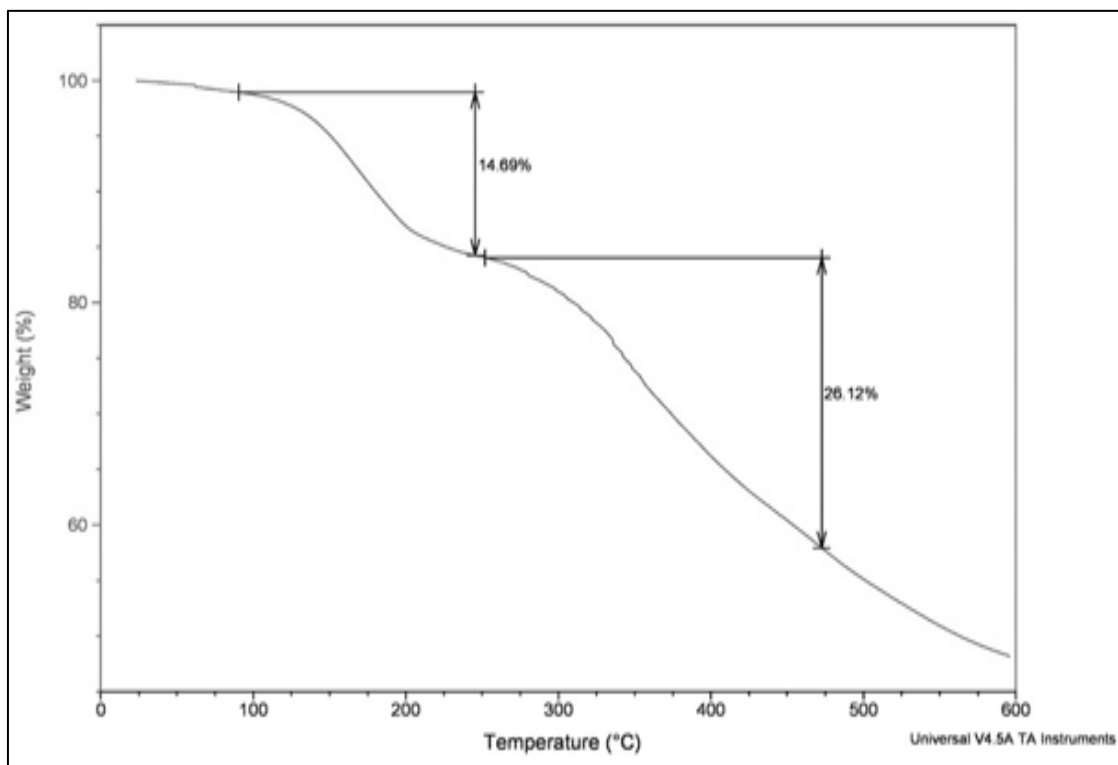


Figure 88: TGA thermogram for complex **48a•Co(II)**.

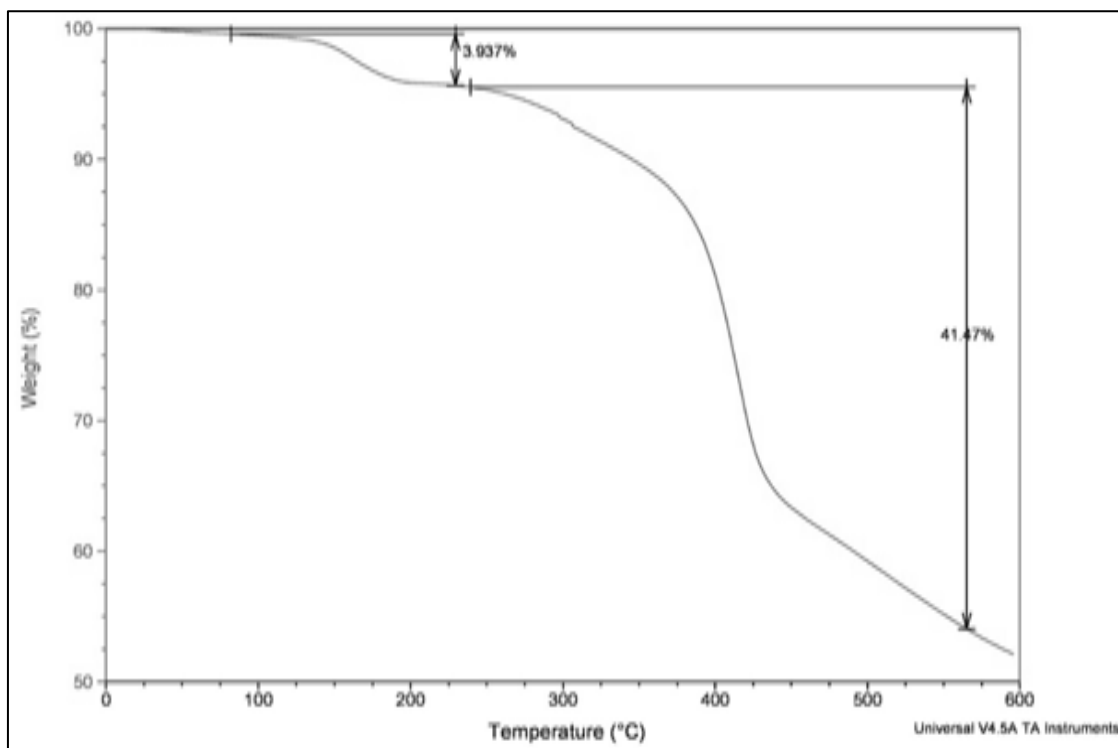


Figure 89: TGA thermogram for complex **48a•Ni(II)**.

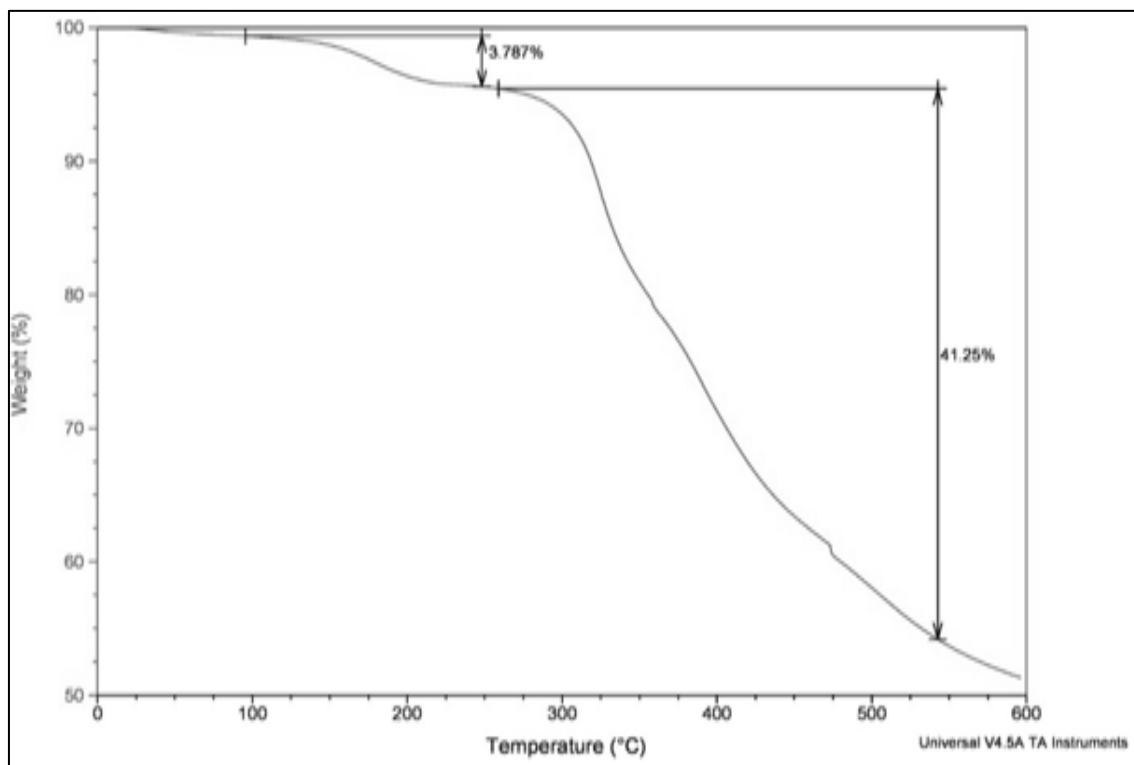


Figure 90: TGA thermogram for complex **48a•Cu(II)**.

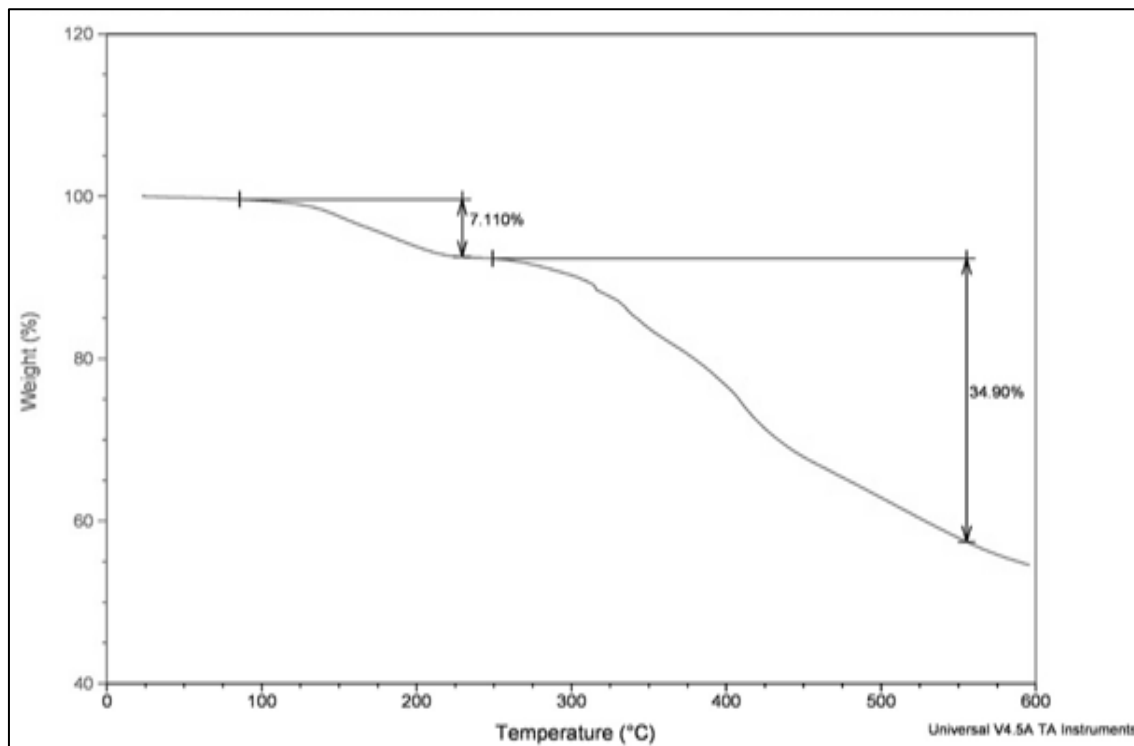


Figure 91: TGA thermogram for complex **48a•Zn(II)**.

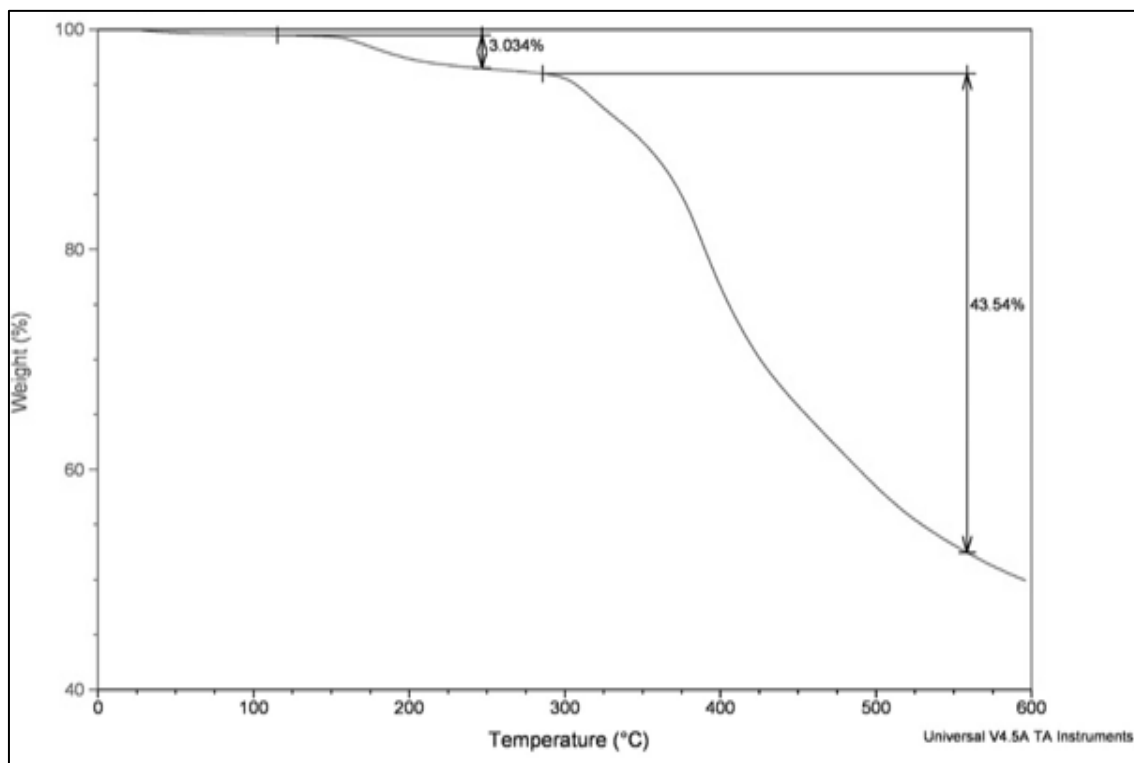


Figure 92: TGA thermogram for complex **48b•Zn(II)**.

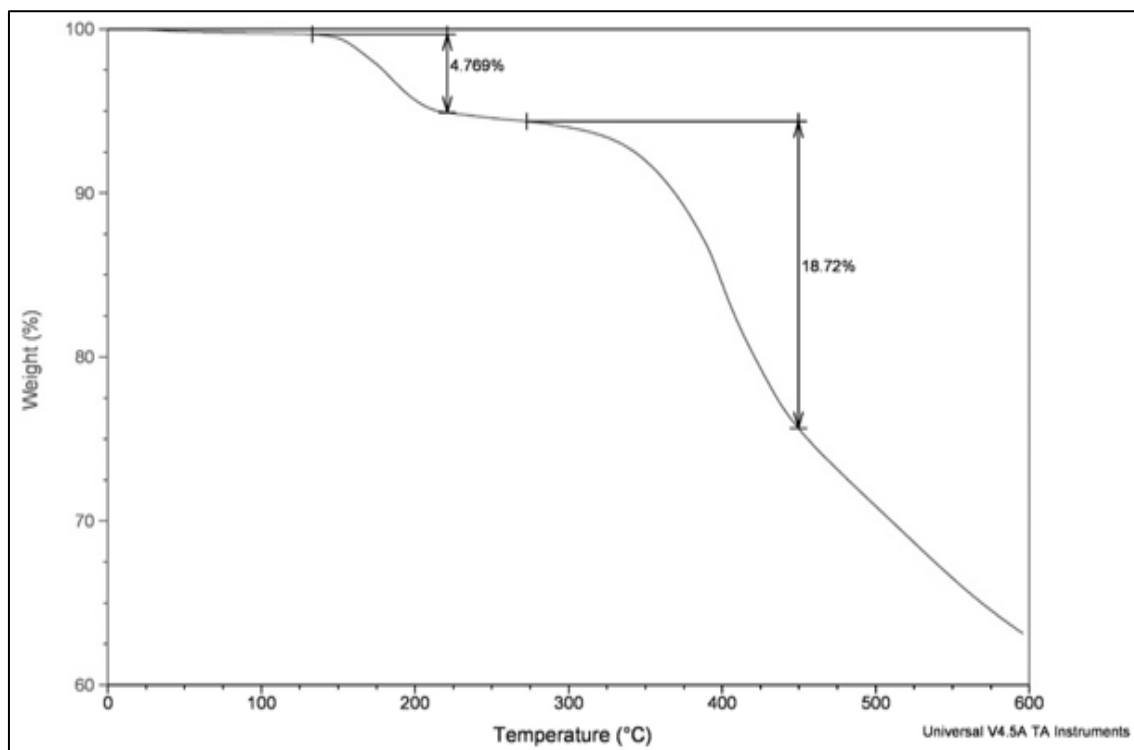


Figure 93: TGA thermogram for complex **48c•Zn(II)**.

B.2 TGA Thermograms for Acetylacetonate-Functionalized Mexylaminotriazine

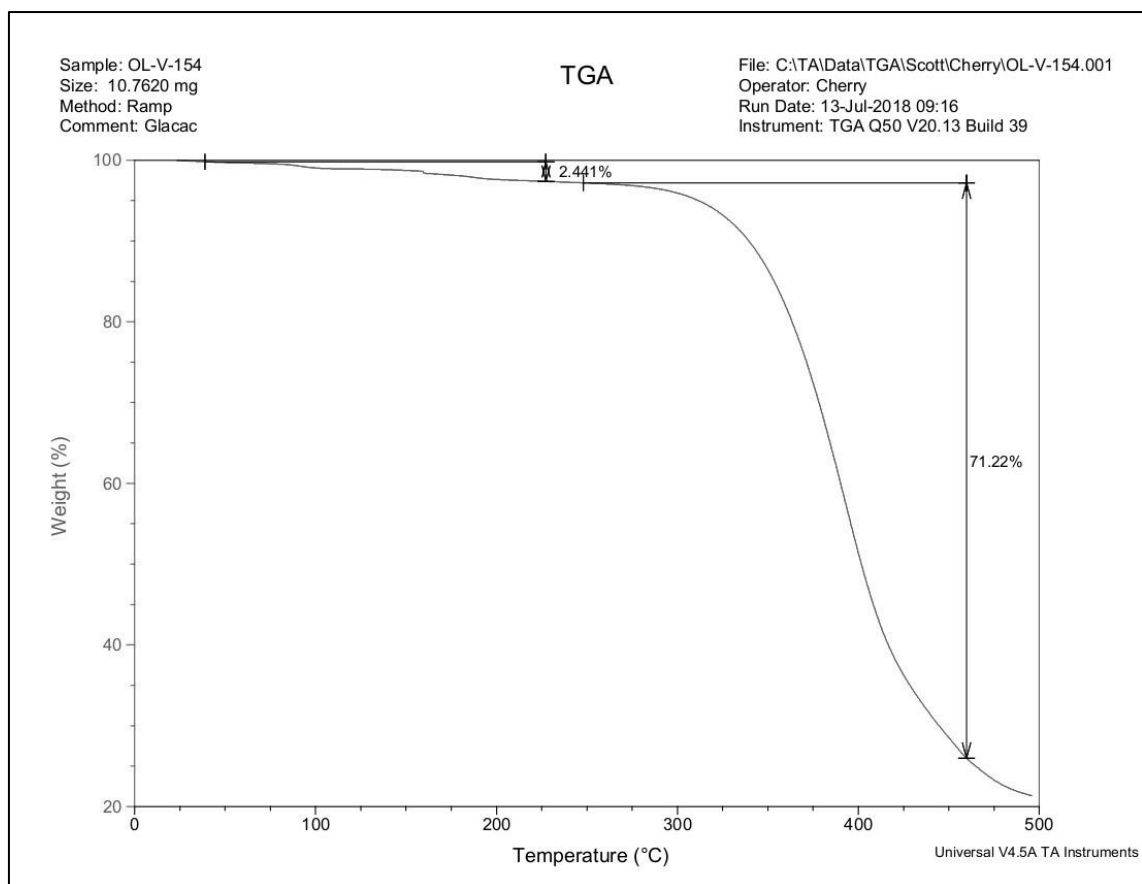


Figure 94: TGA thermogram for ligand **59**.

B.3 TGA Thermograms for Phenanthroline Complexes Functionalized with Mexylaminotriazine

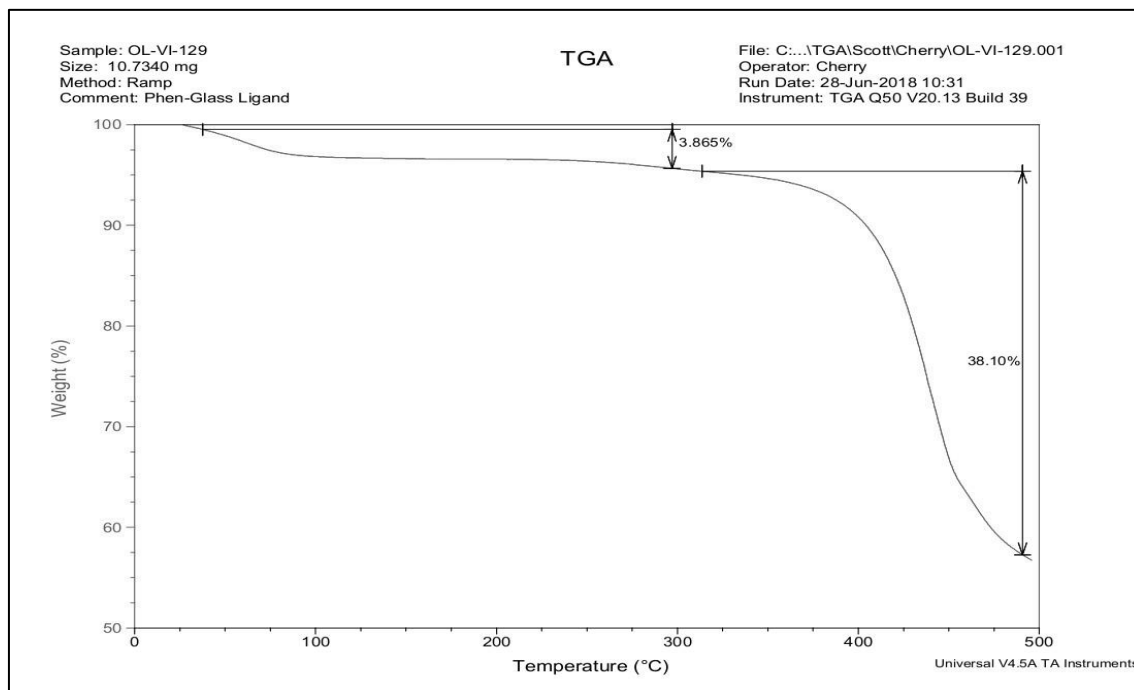


Figure 95: TGA thermogram of ligand **68**

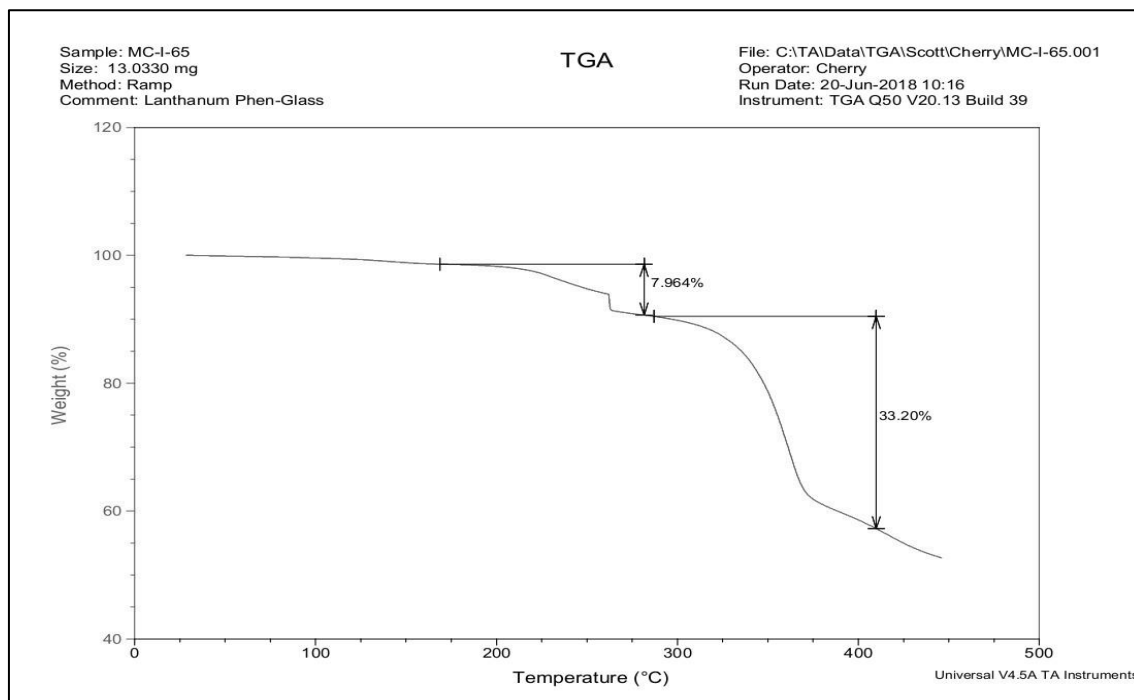


Figure 96: TGA thermogram for complex **68a•La(III)**.

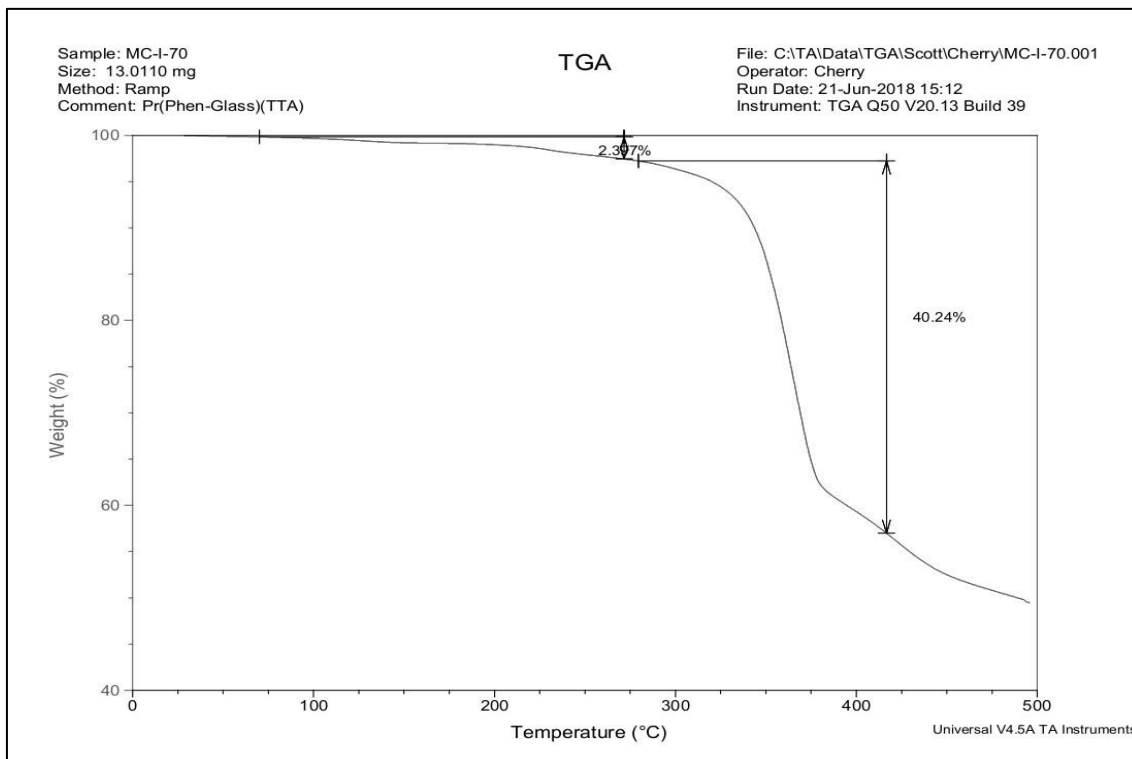


Figure 97: TGA thermogram for complex **68a•Pr(III)**.

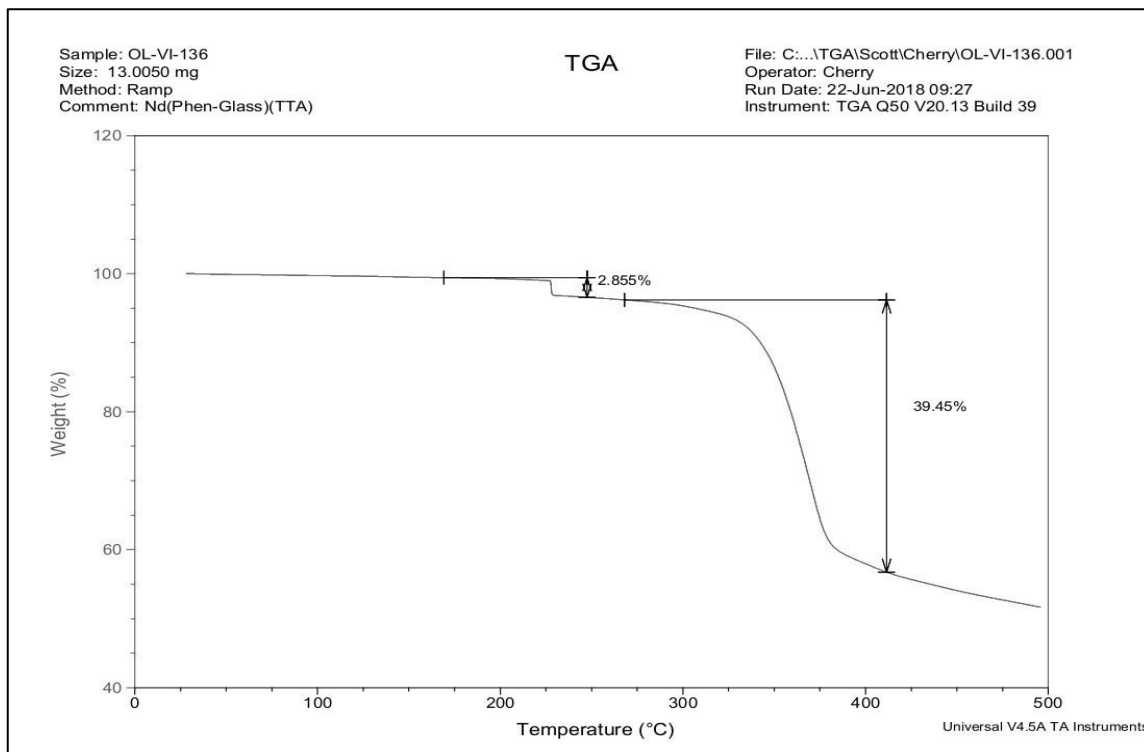


Figure 98: TGA thermogram for complex **68a•Nd(III)**.

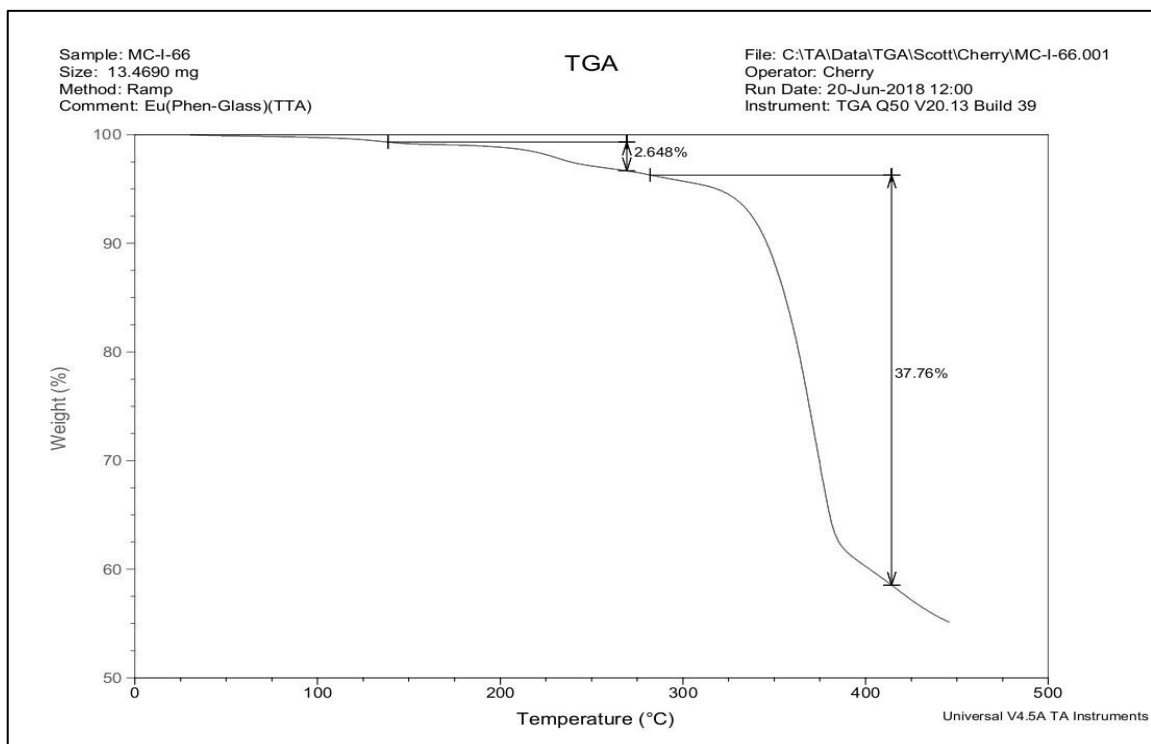


Figure 99: TGA thermogram for complex **68a•Eu(III)**.

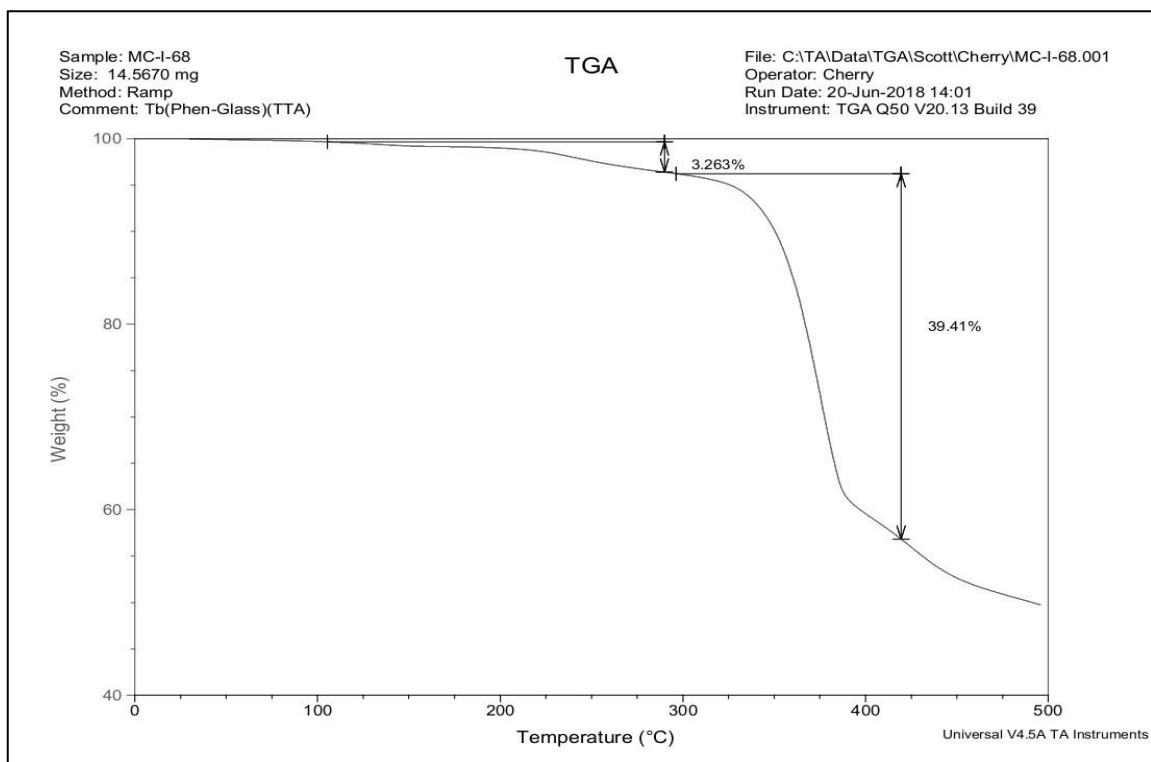


Figure 100: TGA thermogram for complex **68a•Tb(III)**.

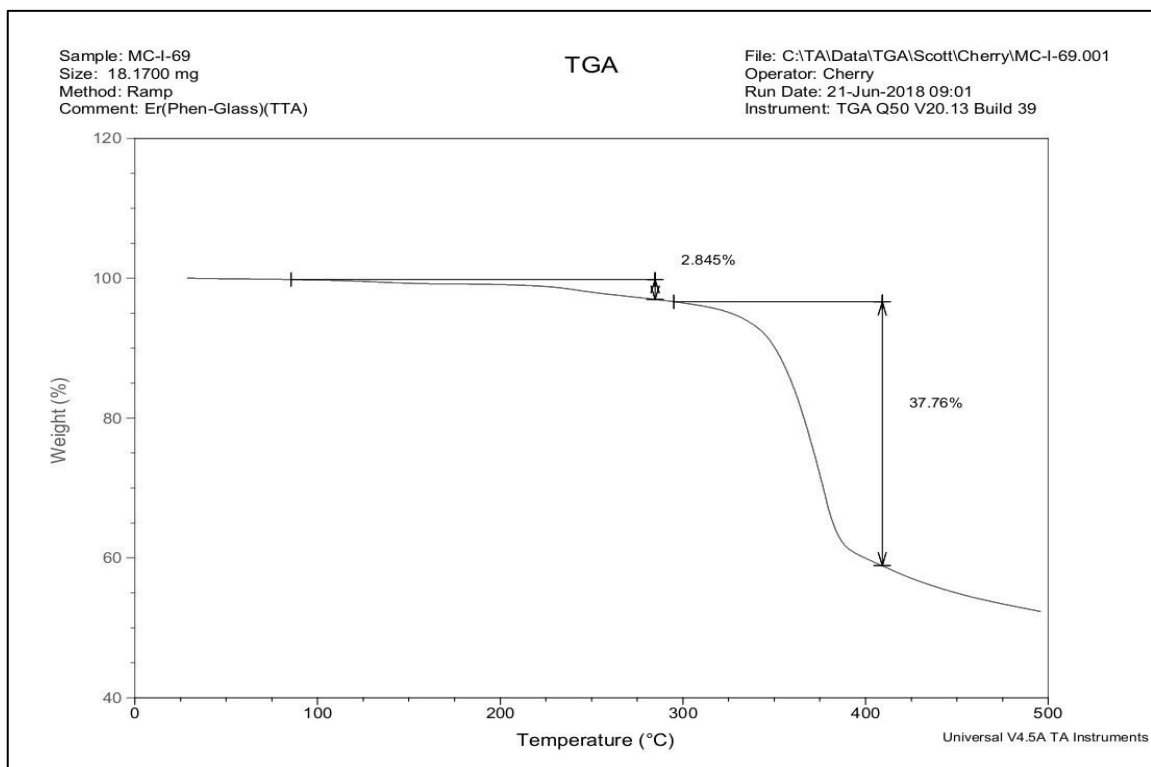


Figure 101: TGA thermogram for complex **68a•Er(III)**.

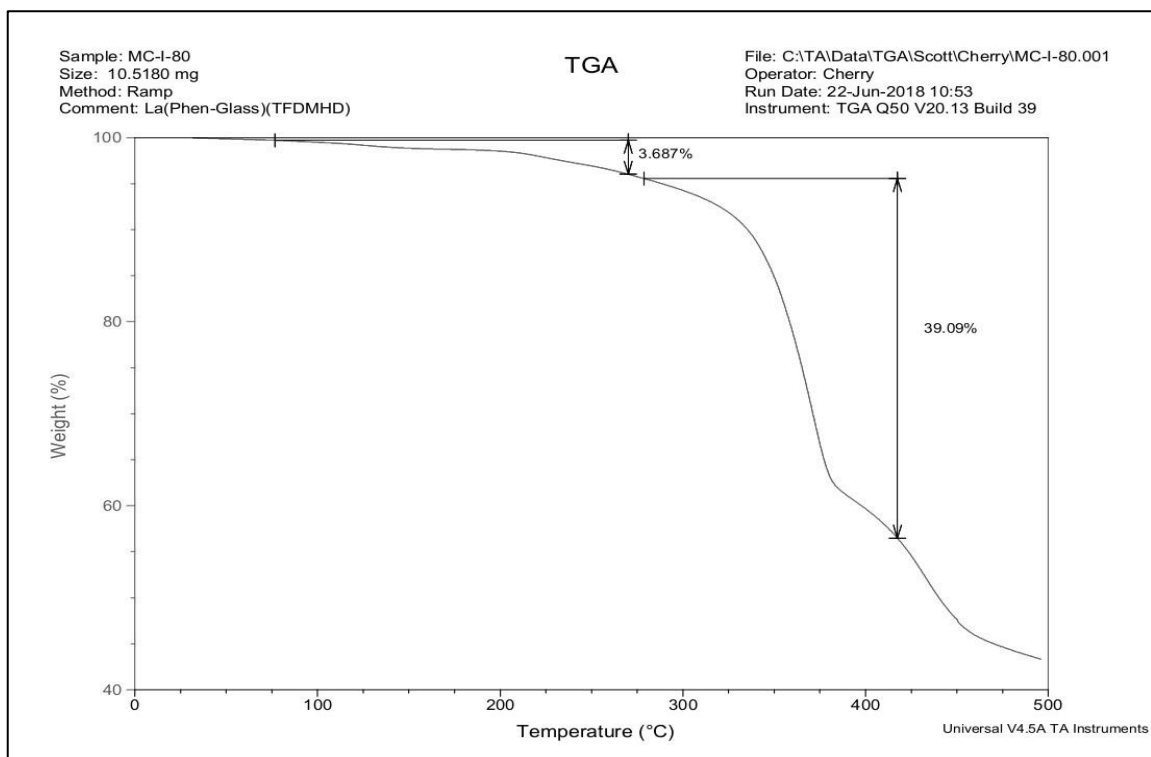


Figure 102: TGA thermogram for complex **68b•La(III)**.

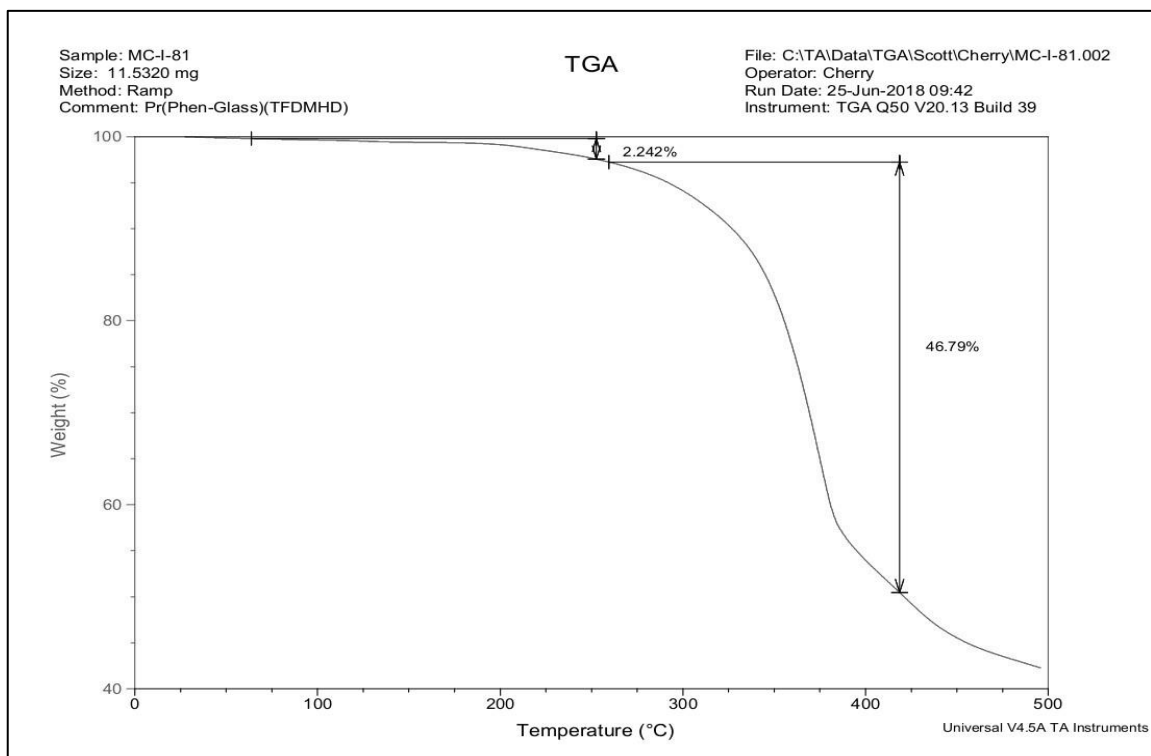


Figure 103: TGA thermogram for complex **68b•Pr(III)**.

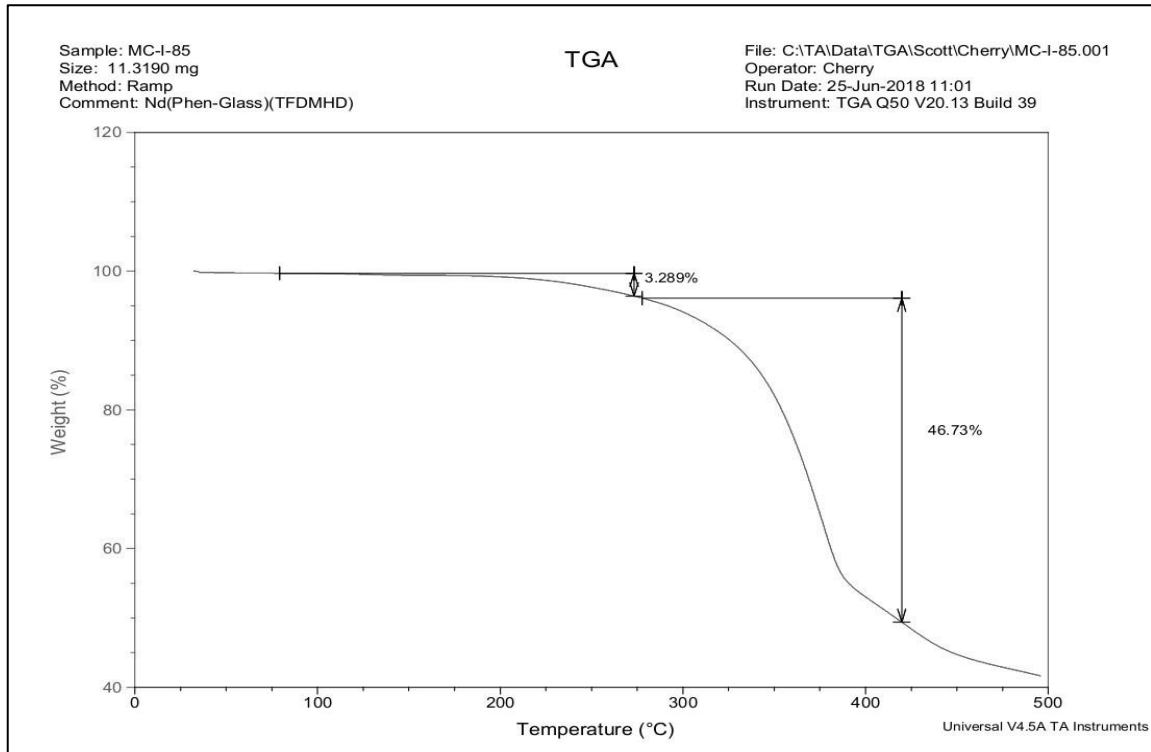


Figure 104: TGA thermogram for complex **68b•Nd(III)**.

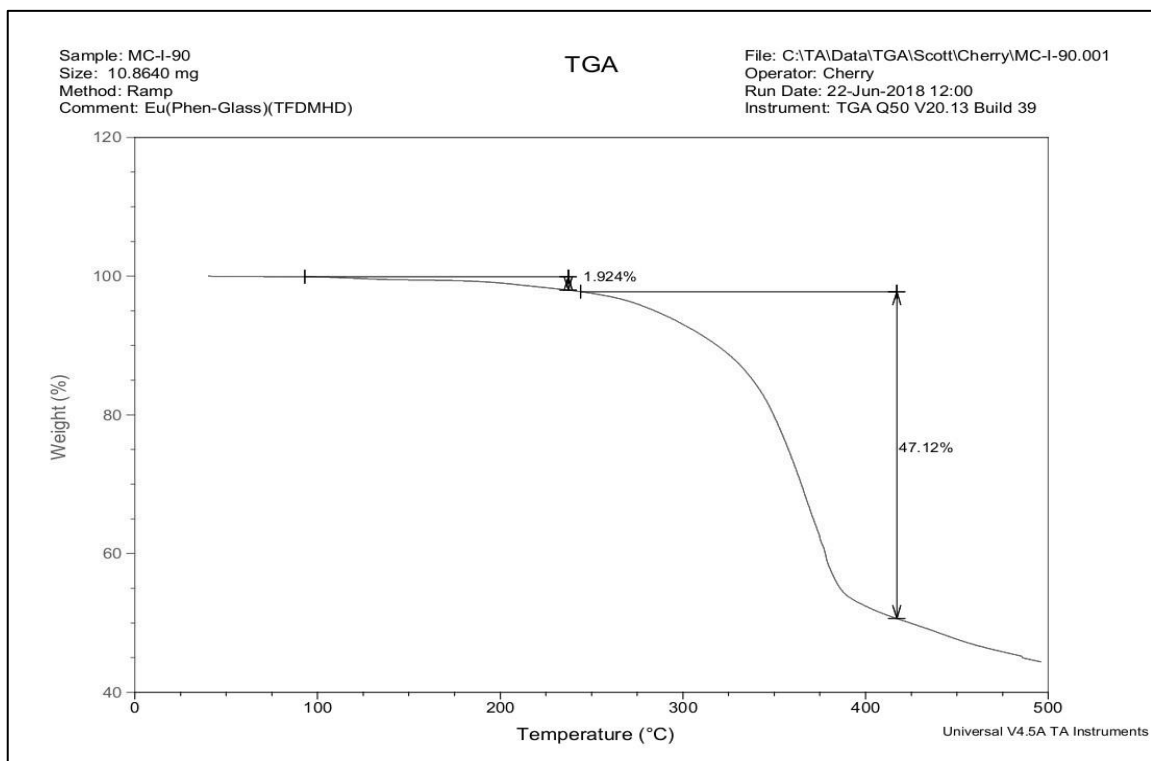


Figure 105: TGA thermogram for complex **68b•Eu(III)**.

C. DSC Results

C.1 DSC Thermograms for Salen Complexes Functionalized with Mexylaminotriazines

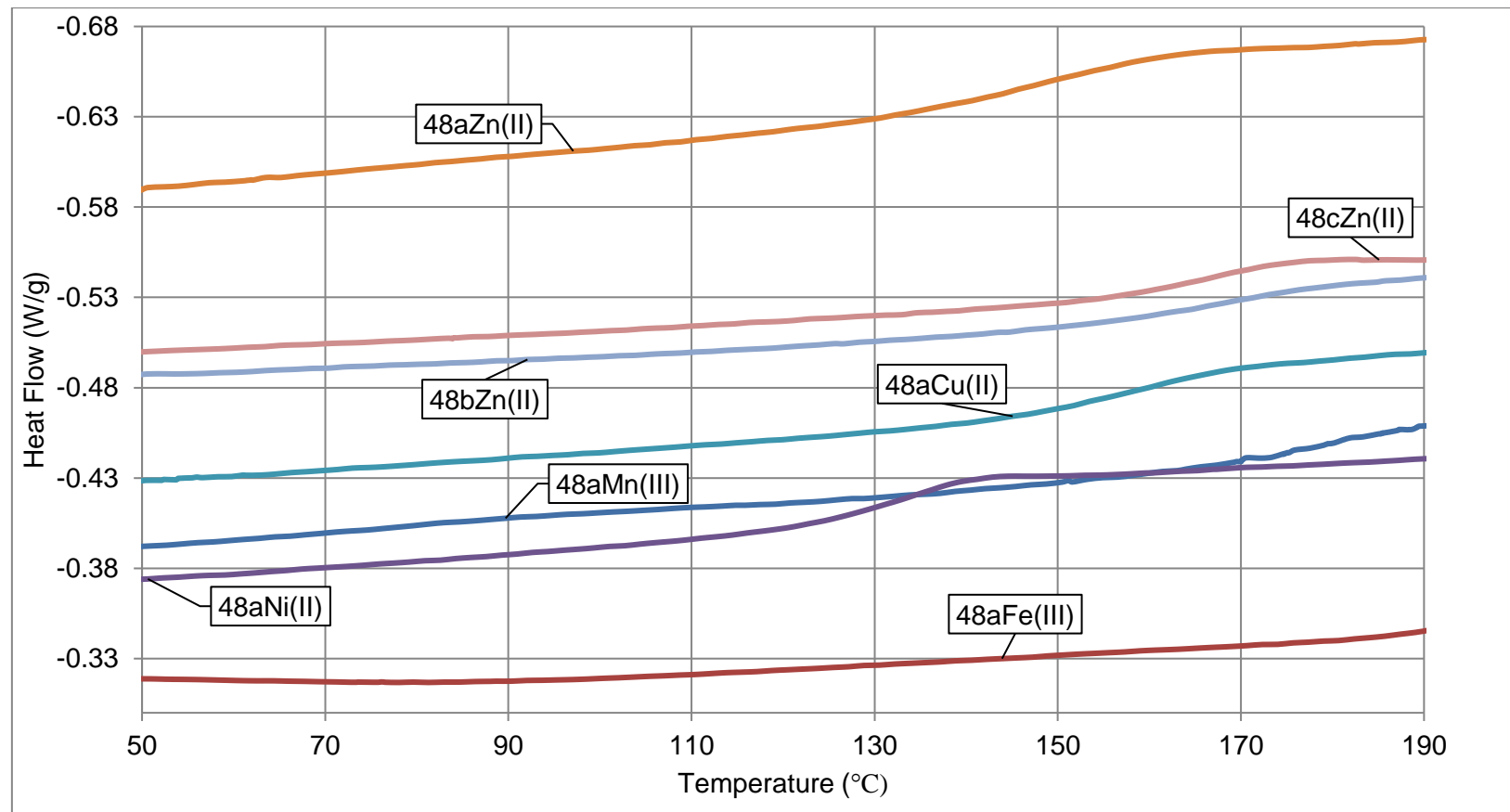


Figure 106: DSC thermograms of the synthesized mexylaminotriazine-functionalized salen complexes. For reference, the exotherm is oriented down in this chart.

C.2 DSC Thermograms for Acetylacetonate-Functionalized Mexylaminotriazine

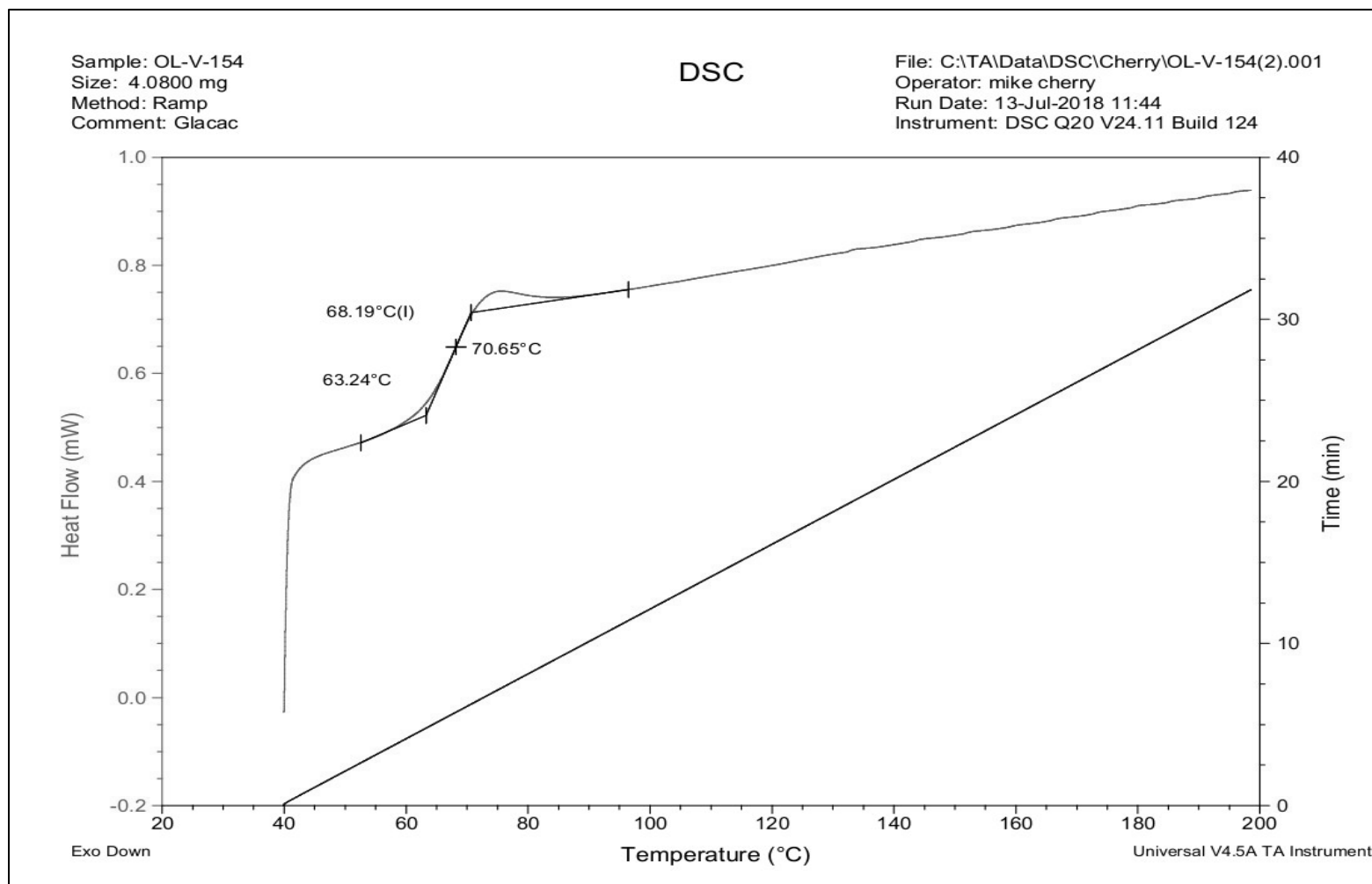


Figure 107: DSC thermogram for compound **58**.

C.3 DSC Thermograms for Phenanthroline Complexes Functionalized with Mexylaminotriazine

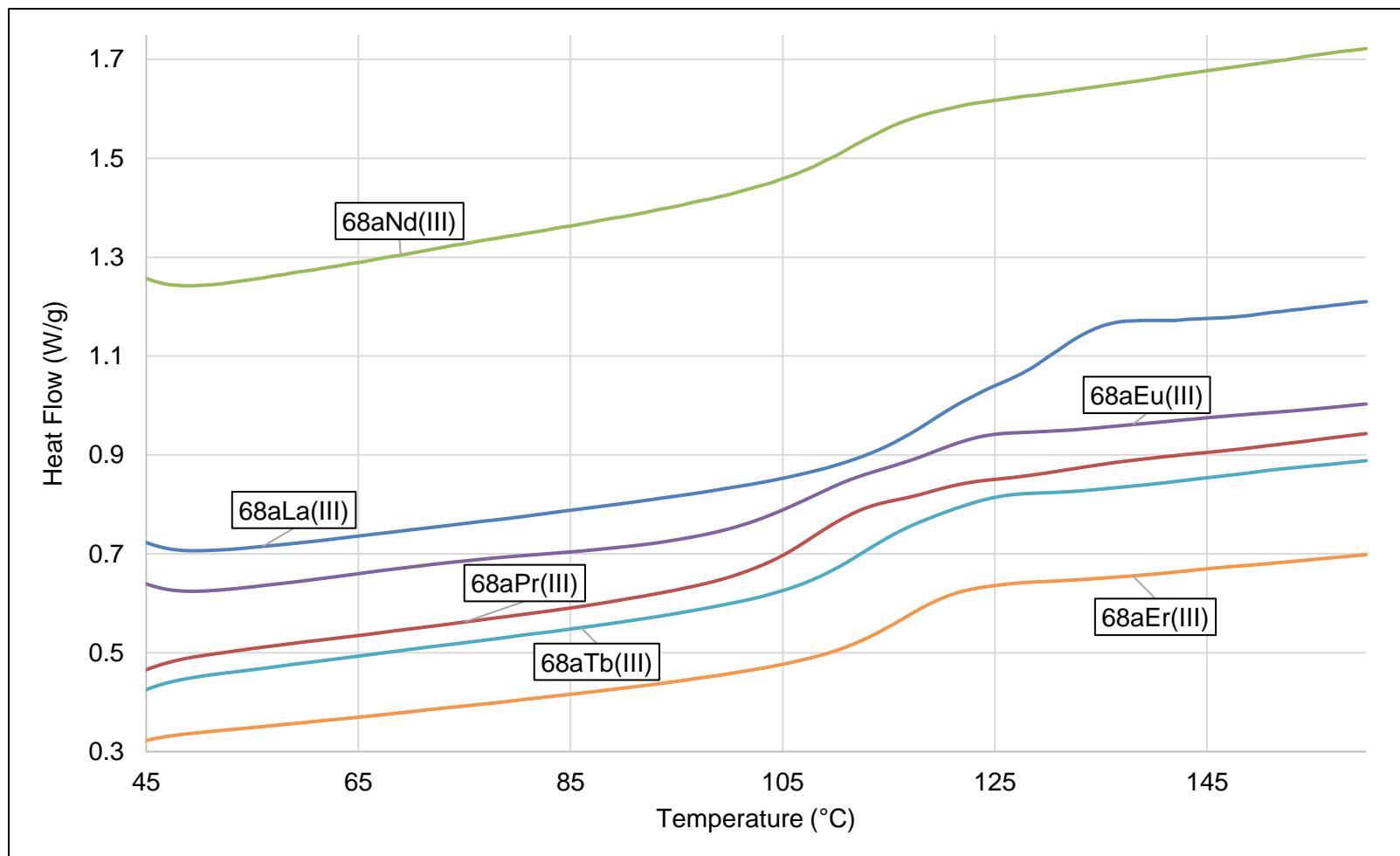


Figure 108: DSC thermograms of the synthesized mexylaminotriazine-functionalized phenanthroline complexes **68a**. For reference, the exotherm is oriented down in this chart.

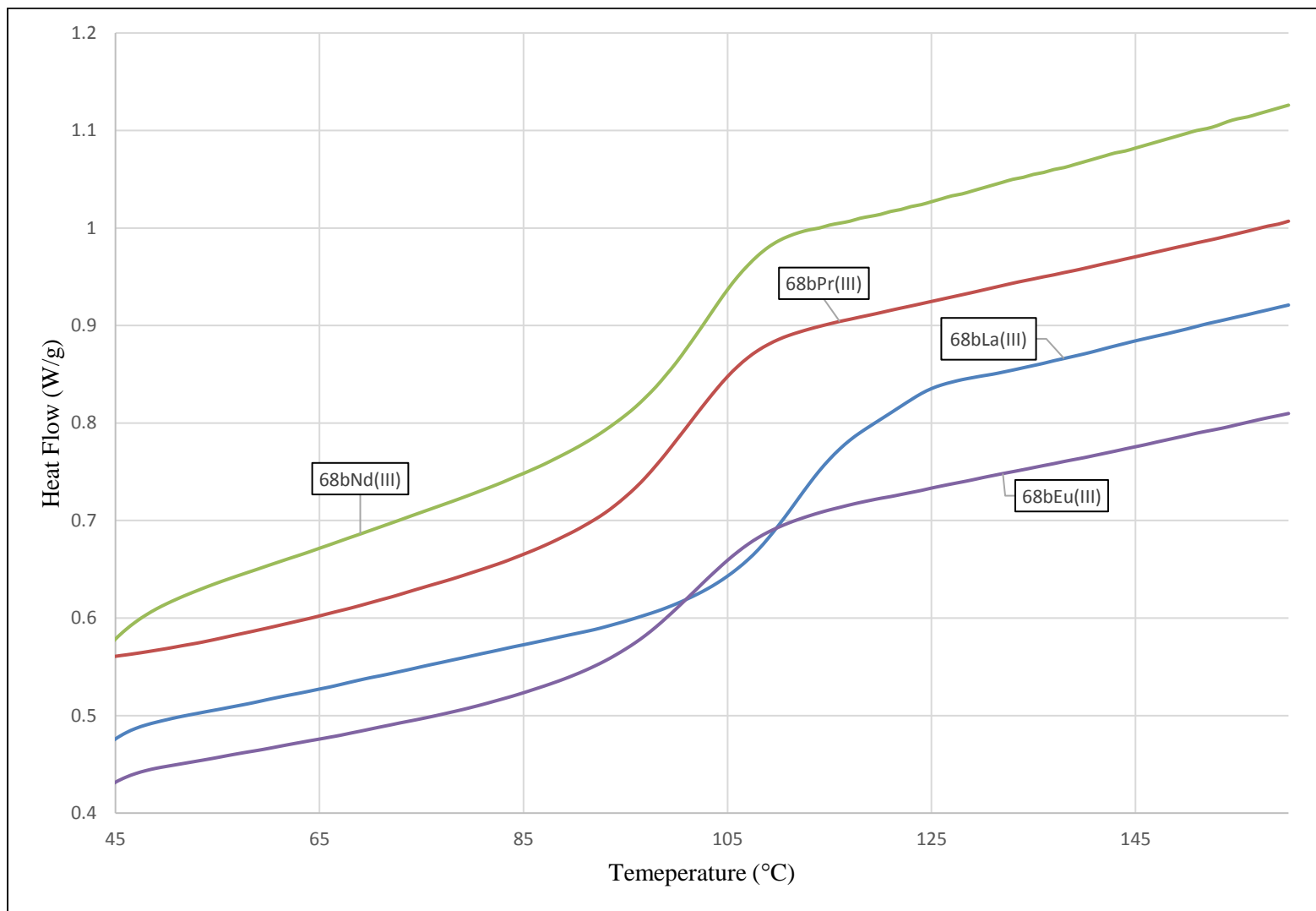


Figure 109: DSC thermograms of the synthesized mexylaminotriazine-functionalized phenanthroline complexes **68b**. For reference, the exotherm is oriented down in this chart.